Innovation Center of Molecular Diagnostics,
Beijing University of Chemical Technology

Volume 2 · Issue 4
November 2025

Innovative Medicines & Omics

ISSN: 3060-8910 (Print)
ISSN: 3060-8740 (Online)

ACCSCIENCE PUBLISHING

ACCSCIENCE PUBLISHING

Innovative Medicines & Omics

Print ISSN: 3060-8910
Online ISSN: 3060-8740

Innovative Medicines & Omics (IMO) aims to publish high-quality articles related to the discovery and development of innovative medicines through omics research in the field of human and animal health, for all the major therapeutic areas. The journal includes a variety of omics layers, such as genomics, proteomics, epigenomics metabolomics, lipidomics, peptidomics, metagenomics, microbiome, pharmacogenomics, toxicogenomics, etc., with the focus on disease etiology, prevention, treatment, prognosis and monitoring.

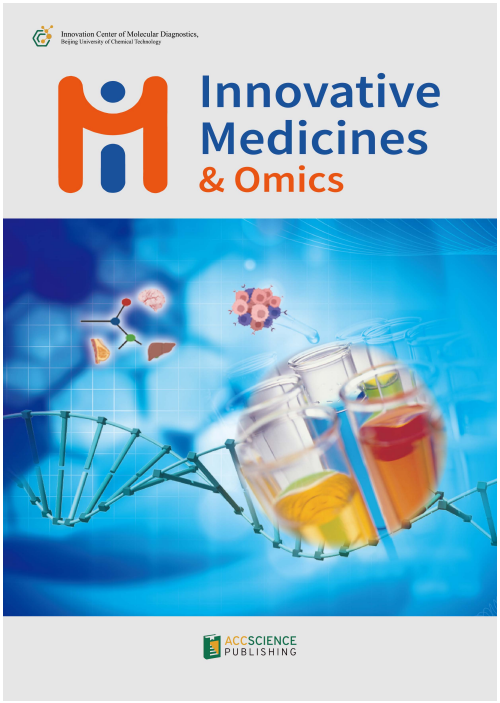

About the Publisher

AccScience Publishing is a publishing company based in Singapore. We publish a range of high-quality, open-access, peer-reviewed journals and books from a broad spectrum of disciplines.

Contact Us

Managing Editor
imo.office@accscience.sg

AccScience Publishing
9 Raffles Place, Republic Plaza 1 #06-00 Singapore 048619.

Volume 2 • Issue 4 • November 2025
ISSN 3060-8910 (print) ISSN 3060-8740 (online)

INNOVATIVE MEDICINES & OMICS

ACCSCIENCE PUBLISHING

Access Science Without Barriers

INNOVATIVE MEDICINES & OMICS

ISSN: 3060-8910 (print)
ISSN: 3060-8740 (online)

Editorial and Production Credits

Publisher: AccScience Publishing
Managing Editor: Ting Li
Production Editor: Sharmila Velapasamy
Article Layout and Typeset: Sinjore Technologies (India)

For all advertising queries, contact imo.office@accscience.sg.

Supplementary file

Supplementary files of articles can be obtained at https://accscience.com/journal/IMO/2/4.

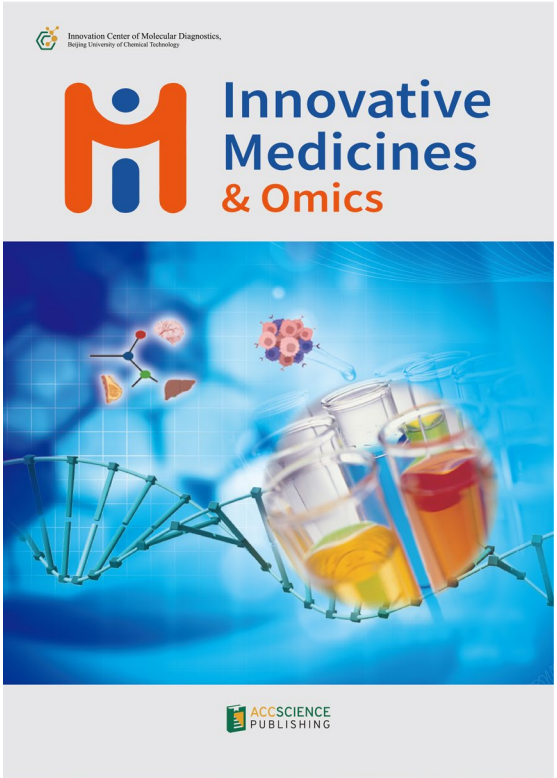

Disclaimer

AccScience Publishing is not liable to the statements, perspectives, and opinions contained in the publications. The appearance of advertisements in the journal shall not be construed as a warranty, endorsement, or approval of the products or services advertised and/or the safety thereof. AccScience Publishing disclaims responsibility for any injury to persons or property resulting from any ideas or products referred to in the publications or advertisements. AccScience Publishing remains neutral with regard to jurisdictional claims in published maps and institutional affiliations.

Innovative Medicines & Omics

Editorial Board

*Editorial Board Members as of November 19, 2025

ACCSCIENCE PUBLISHING

Volume 2 | Issue 4 | November 2025 | Page 1 – 101 |

Innovative Medicines & Omics

https://accscience.com/journal/IMO

CONTENTS

REVIEW ARTICLES

1 **No new needle in the COVID-19 therapeutic haystack: A COVID-19 therapeutics analysis**
Robert L. Martin

25 **Pathogenesis, diagnosis, treatment, and herbal interventions for rheumatoid arthritis: A review**
Brahmjot Singh, Kiranjot Kaur, Sukhmandeep Kaur, Kunal Mistry

PERSPECTIVE ARTICLE

36 **Nanotherapies: A potent treatment for neurodegenerative diseases**
Yihao Meng, Zhengwei Huang, Xuejuan Zhang

ORIGINAL RESEARCH ARTICLES

42 **Dominant and sustained mutations, deletions, and insertions in the Omicron coronavirus lineages JN.1, KP.3, LB.1, XEC, MC.1, and MV.1**
Asit Kumar Chakraborty

64 **Antidiarrheal activity assessment of *Operculina turpethum* stem extract and *in silico* analysis of its compounds**
Md. Abdullah Al Fahad, Md. Fahim Hasan, Md. Arman Islam, Nusrat Jahan, Md. Iqbal Ahmed

74 ***In silico* evaluation of ursodeoxycholic acid from *Jania rubens* and its analogs as potential anti-Alzheimer's agents**
Oluwafemi S. Aina, Owoyemi W. Elegbeleye, Nafisat O. Babamusa, Mujeeb O. Rofiu, Kafayat A. Owoseni-Fagbenro, Olubusayo F. Semire, Olasupo A. Idris, Luqman A. Adams, Oluwole B. Familoni

93 **Intramuscular progesterone and frozen embryo transfer outcomes: A multicenter prospective evaluation of the clinical relevance of serum progesterone monitoring**
Vipin Chandra, Matheus Roque, Kshitiz Murdia, Nitiz Murdia, Shashank V. Sanagoudar, Nagadeepti Naik, Shipra Nigam, Anjali Gahlan, Walmik Mistari, Isha Suwalka, Nihar Ranjan Bhoi, Ankita Saha, Korhan Cengiz, Saurav Mallik

ACCSCIENCE PUBLISHING

Innovative Medicines & Omics

REVIEW ARTICLE

No new needle in the COVID-19 therapeutic haystack: A COVID-19 therapeutics analysis

Robert L. Martin*

Independent Researcher, Loveladies, New Jersey, United States of America

Abstract

Despite nearly 5000 United States Food and Drug Administration (FDA)-tracked trials, no new FDA- or European Union-approved Coronavirus Disease 2019 (COVID-19) drug was discovered during the COVID-19 pandemic. Fortunately, drugs developed before the pandemic proved highly effective, particularly when used early in vaccinated patients. The most powerful treatments are antivirals targeting the spike structural protein and two non-structural proteins (NSPs), NSP5 (main protease [Mpro]) and NSP12 (RNA-directed RNA polymerase [RdRp]). Notably, two studies published before the pandemic and one shortly after its declaration had already identified these three key targets. New monoclonal antibodies were designed to block the spike protein from binding to the host cell. However, all such antibodies were eventually rendered ineffective by emerging viral variants. Several drugs previously used for Middle East respiratory syndrome, Ebola, respiratory syncytial virus, and other viruses work by disrupting the replication activity of Mpro and RdRp. Convalescent plasma, a treatment used since 1900, showed mixed results. For hyperinflammation, only three rheumatoid arthritis drugs and one glucocorticoid, also used in arthritis treatment, received approval. No new approaches were developed to treat blood clots or improve oxygenation. Despite a wartime-like focus and unprecedented research intensity, no respiratory illness, including COVID-19, has yet been cured. Using a personal database of 3050 therapeutic research papers, along with data from ClinicalTrials.gov and Google Scholar, this review examines approved, promising, and ineffective COVID-19 therapeutics. Potential candidates currently undergoing clinical trials are identified to highlight future therapeutic possibilities and guide ongoing research efforts.

Keywords: COVID-19; Therapeutics; Antivirals; Hyperinflammation

***Corresponding author:**
Robert L. Martin
(bobmartin08008@mac.com)

Citation: Martin RL. No new needle in the COVID-19 therapeutic haystack: A COVID-19 therapeutics analysis. *Innov Med Omics*. 2025;2(4):1-24.
doi: 10.36922/IMO025150020

Received: April 7, 2025

Revised: April 23, 2025

Accepted: May 8, 2025

Published online: July 15, 2025

1. Introduction

Although nearly 5000 clinical trials were tracked by the United States (US) Food and Drug Administration (FDA), no new FDA- or European Union (EU)-approved Coronavirus Disease 2019 (COVID-19) drug was developed during the COVID-19 pandemic. However, drugs developed before the pandemic proved highly effective, despite the eventual loss of efficacy of monoclonal antibodies due to emerging viral variants. Severe acute respiratory syndrome coronavirus 2 (SARS-CoV-2), the virus that causes COVID-19, affects all major organs through several mechanisms, as summarized in Table 1.

The seemingly simple question – "What will happen if I get COVID-19 and follow a treatment regimen?" – is impossible to answer definitively. The complex interplay of viral variants, vaccination history, comorbidities, prior infection, and available therapeutics creates enormous possible outcomes. However, the recommended therapeutic approach is relatively clear. Following vaccination, the first step is to reduce viral replication through the prompt use of antivirals – currently, Paxlovid is the best option for those eligible to take it. If the virus has already replicated explosively, subsequent therapeutic interventions to mitigate COVID-19 impacts are also fairly well established.

Therapeutics for COVID-19 is a technically complex field, involving discussions of the virus (SARS-CoV-2), the disease (COVID-19), therapeutic strategies, the immune system, and aspects of cellular biology.

Since the beginning of the pandemic, I have been summarizing COVID-19 research papers in a document titled "The Mouse That Roared" (R. L. Martin, unpublished report, 2025) – so named because SARS-CoV-2, a relatively mild virus, has caused profound societal impacts. The document spans approximately 21,000 pages and includes summaries of around 17,000 papers drawn from 2,250 sources. Each journal within a journal family was counted separately, e.g., 140 BMC journals were included. Most therapeutic papers were published in *Nature*, *Cell*, *Science*, *MDPI*, *Cureus*, *Journal of the American Medical Association*, *British Medical Journal*, *New England Journal of Medicine*, and *Proceedings of the National Academy of Sciences*, as well as other journals from Wiley Whiley, BMC, PLOS, the American Health Association, Sage, Frontiers, bioRxiv, medRxiv, preprints.org, SSRN, Research Square, and the Centers for Disease Control and Prevention (CDC). The document is organized into 32 chapters and nine appendices covering diverse topics, e.g., "Historical Perspective," "SARS-CoV-2," "COVID Disease Progression," "How People Behave," "Economics," "Vaccine Effectiveness," "Second Generation Vaccines," "Political and National COVID Responses," and "Preparing for the Next Pandemic." The "Therapeutics" chapter is the basis for this review.

2. Treatment/therapeutic strategy

The treatment/therapeutic strategy is summarized in the second bar beneath the disease progression diagram in Figure 1.

Therapeutic actions corresponding to the four treatment/therapeutic phases illustrated in Figure 1 are summarized in Table 2.

It is discouraging to note that:

(i) Many diseases, especially those that are rare, genetic, or complex, still lack definitive cures

(ii) No respiratory disease has ever been cured.

The US National Institute of Health (NIH) produced 72 versions of highly comprehensive COVID-19 treatment guidelines. These documents expanded from 90 pages to 278 pages within 12 months, eventually reaching 478 pages. The final version of the NIH COVID-19 treatment guidelines was released on February 29, 2024.

3. Therapeutic surge

During the pandemic, pharmaceutical companies and academic researchers pursued new therapeutics with World War II-like urgency and focus. Several websites tracked global therapeutic trials:

- No longer operational, the Global Coronavirus COVID-19 Clinical Trial Tracker listed 2533 trials as of December 31, 2020
- No longer being updated, the World Health Organization Treatment Tracker listed 4634 trials as of August 2023
- ClinicalTrials.gov (https://clinicaltrials.gov/) is still operational.

A 2021 study reported that many trials investigated the same drugs, but most were too small in sample size to draw definitive conclusions.[1] As will be shown, some of the therapeutics discussed in this review are supported by numerous studies, yet the results are often contradictory.

Table 1. Mechanisms of SARS-CoV-2 damage infection in major organs/systems

Organ/system	Direct viral damage	Hyperinflammation	Blood clots	Lack of oxygen	Other
Heart	✓	✓	✓	✓	Stress
Lungs	✓	✓	✓	✓	Scarring
Kidneys	✓	✓	✓	✓	Microvascular damage
Liver	✓	✓	✓	✓	COVID-19 drug injury
Pancreas	✓	✓	✓	✓	Increased triglycerides, reduced blood flow
Nervous system	✓	✓	✓	✓	Metabolic dysfunction

Abbreviation: SARS-CoV-2: Severe acute respiratory syndrome coronavirus 2.

For example, the Phase 3 trial for the Pfizer mRNA vaccine included 43,448 participants, whereas the initial Phase 3 trial for Paxlovid enrolled 2246 adult participants. A 2024 study summarized global COVID-19 clinical trials through April 23, 2023,[2] as shown in Figure 2.

Table 2. Treatment/therapeutic phases

Treatment/ therapeutic phase	Damage being addressed			
	Direct viral damage	Hyperinflammation	Blood clots	Lack of oxygen
Prevent infection	✓			
Suppress viral replication and inflammation	✓	✓	✓	
Suppress hyperinflammation		✓	✓	✓
Suppress organ damage			✓	✓

Table 3 summarizes data from ClinicalTrials.gov and therapeutic paper statistics from "The Mouse That Roared" (R. L. Martin, unpublished report, 2025), as of November 01, 2024. 1686 COVID-19 vaccine trials are excluded from this summary.

For perspective, there were 1107 FDA clinical trials for triple-negative breast cancer, 720 for the flu, 193 for RSV, and 18 for Addison's disease.

For high-impact therapeutics, Google Scholar was used to identify the paper with the most citations and/or perceived impact. However, this introduces a sample bias, as papers published in prestigious journals or those that are older tend to accumulate more citations. For example, among the 20 therapeutics referenced in this article, the most-cited papers for eight of them were published in the *New England Journal of Medicine*. Furthermore, many of the early, highly cited papers merely suggested that a therapy, such as probiotics, should be investigated or reported in preliminary trials with very small sample

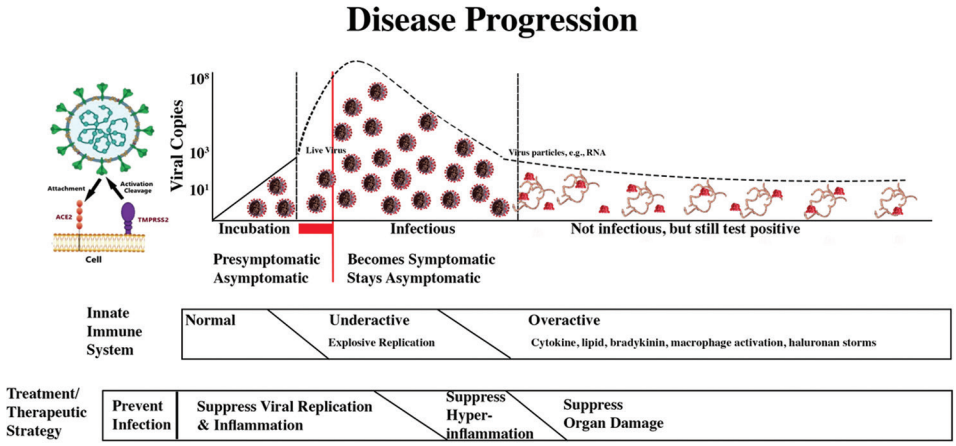

Figure 1. COVID-19 disease progression and treatment/therapeutic strategy. The image was created by the author using Photoshop. Abbreviations: ACE2: Angiotensin-converting enzyme 2; TMPRSS2: Transmembrane serine protease 2.

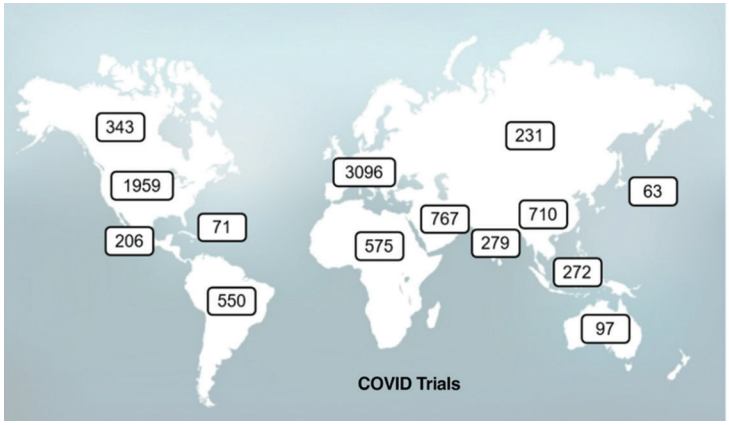

Region Name	Number of Studies
World	8,943
Africa	575
Central America	71
East Asia	710
Japan	63
Europe	3,096
Middle East	767
North America	2,399
Canada	343
Mexico	206
United States	1,959
North Asia	231
Pacifica	97
South America	550
South Asia	279
Southeast Asia	272

Figure 2. Global COVID-19 clinical trials as of April 23, 2023. Adapted from Meiraa *et al.*[2]

sizes. These papers are not strong indicators of therapeutic effectiveness.

Highly cited papers with actual therapeutic results were highlighted for two main reasons:

(i) They provide historical perspectives on the development of the therapeutic

(ii) Later papers often contributed little additional insight into the therapeutic impacts.

A therapeutic typically progresses through three trial phases and a regulatory review: Phase 1, which evaluates safety with a small group; Phase 2, assesses effectiveness in a larger group; Phase 3, confirms effectiveness and monitors adverse reactions in a large population.

Clinical trial costs and failure rates represent significant barriers to drug development. Cost estimates are presented in Figure 3, based on a 2014 report from the Office of the Assistant Secretary for Planning and Evaluation.[3] The report indicated that the likelihood of a drug successfully progressing through all phases of clinical trials and obtaining regulatory approval was only 12%.

Cost, success rates, and therapeutic differential advantage are key factors contributing to the low number of therapeutics approved by the FDA each year, as shown in Figure 4.

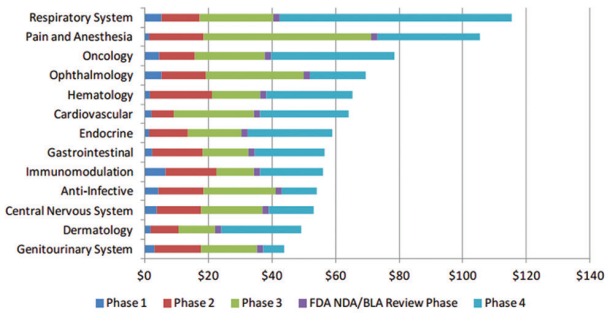

Figure 3. Clinical trial costs (in $ millions) in 2012. Reprinted from Sertkaya *et al.*[3]

An example of a drug that has not reached the market – potentially due to a "good enough" alternative, Paxlovid, is already available – is masitinib. A 2021 paper reported that masitinib (a main protease [Mpro] inhibitor) reduced SARS-CoV-2 viral load by more than 99% and lowered inflammatory cytokine levels in mice.[4] Since early 2023, the sponsoring pharmaceutical company has been attempting to recruit participants for a clinical trial.

4. Testing and targets

There are numerous potential COVID-19 therapeutic targets, including viral proteins, cytokines, immune system cells, and affected organs. Among these, viral proteins are excellent targets for COVID-19 therapeutic intervention. Antivirals, anti-inflammatory agents, and specialized therapeutics have been used as key strategies against these targets, as shown in Table 4.

4.1. "Squeakinstein"

Therapeutic testing typically begins with animal models. While COVID-19 has been reported in wild mice, their angiotensin-converting enzyme 2 (ACE2) receptors are not well-suited for binding SARS-CoV-2. In 2000,

Table 3. Statistics on global COVID-19 clinical trials data and therapeutic papers

ClinicalTrials.gov				Google Scholar	"The Mouse That Roared"
Total	Completed	Terminated	Results		
4855	2222	427	528	~3,000,000[a]	3065

Notes: [a]Google Scholar reported 5,500,000 papers for COVID-19. COVID-19 scholars reported 143,711, the NIH 374,733, and PubMed 53,165. Data from ClinicalTrials.gov, Google Scholar, and "The Mouse That Roared" (R. L. Martin, unpublished report, 2025), as of November 01, 2024.

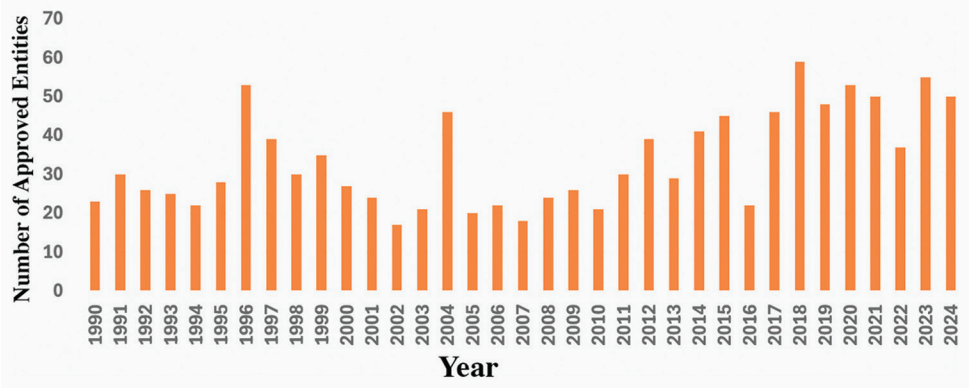

Figure 4. The United States Food and Drug Administration (FDA)-approved new molecular entities by year (new molecular entity vaccines and gene therapies are not included). The image was created by the author using Photoshop based on FDA data.

mice were genetically engineered to express human-like ACE2 receptors – hence "squeakinstein." More recently, advancements in genetic engineering have further refined these models – even enabling the development of mice suited for studying long COVID. A wide range of therapeutics has been tested on these genetically modified mice. In one example, researchers subjected mice to 3 months of swim training to evaluate how exercise might influence immune response.

Table 4. Therapeutic strategies targeting SARS-CoV-2 proteins

Proteins	Antivirals	Anti-inflammatory agents	Specialized therapeutics
Structural proteins			
S	✓	✓	
N	✓	✓	Heart, amyloidosis
M	✓	✓	
E	✓	✓	Kidney, lung
Non-structural proteins (NSP)			
NSP1	✓	✓	
NSP2			
NSP3 (PLpro)	✓		
NSP5 (Mpro)	✓	✓	
NSP6		✓	mRNA transport
NSP7	✓		
NSP8	✓		
NSP9	✓	✓	
NSP10	✓	✓	
NSP11			
NSP12 (RdRp)	✓		
NSP13	✓		
NSP14 (Exon)	✓	✓	
NSP15	✓	✓	
NSP16	✓	✓	
Accessory proteins			
ORF3a	✓	✓	Mitochondrial function
ORF3b		✓	
ORF3c			
ORF6		✓	
ORF7a	✓		
ORF7b	✓		
ORF8		✓	Cholesterol formation
ORF9b			
ORF9c			Mitochondrial function, heart cells, and cholesterol formation
ORF10		✓	

Abbreviations: Mpro: Main protease; PLpro: Papain-like protease; RdRP: RNA-dependent RNA polymerase; SARS-CoV-2: Severe acute respiratory syndrome coronavirus 2.

4.2. Article review in "The Mouse That Roared"

Figure 5 shows the distribution of all COVID-19 therapeutics papers covered in "The Mouse That Roared" (R. L. Martin, unpublished report, 2025) and highlights how many of them received FDA approval. Notably, 75% of the articles focused on antivirals.

5. Infection prevention

Infection prevention (prevent infection phase in Figure 1) article statistics from ClinicalTrials.gov, Google Scholar, and "The Mouse That Roared" (R. L. Martin, unpublished report, 2025) are presented in Table 5. In the table and subsequent similar tables, "Approved" refers to therapeutics that were approved at any point; some approvals were later withdrawn due to reduced effectiveness against emerging variants.

5.1. Approved therapeutics

The only currently FDA-approved COVID-19 therapeutic is Pemgarda. The company that manufactures Pemgarda reported the following Phase 3 trial results:

- An 84% relative reduction in infection risk through month 6
- A 64% reduction in the risk of symptomatic COVID-19 during months 7 – 12 in an immunocompetent adult population.

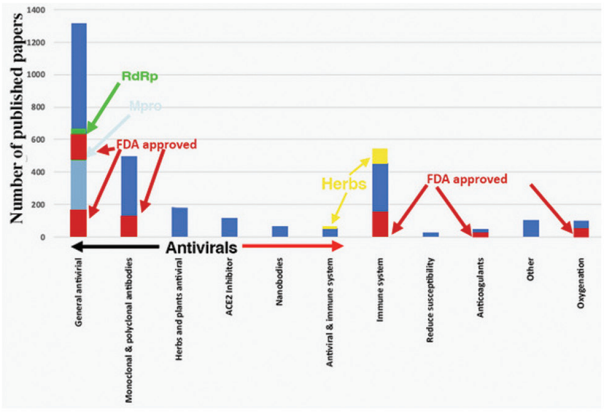

Figure 5. Distribution of COVID-19 therapeutic papers covered in "The Mouse That Roared" (R. L. Martin, unpublished report, 2025)
Abbreviations: ACE2: Angiotensin-converting enzyme 2; Mpro: Main protease; RdRP: RNA-dependent RNA polymerase.

Table 5. COVID-19 infection prevention therapeutics

Category	ClinicalTrials.gov			Google Scholar	"The Mouse That Roared"
	Total	Completed	Results		
Infection prevention[a]	326	145	53	-	-
Approved therapeutics					
Pemgarda	1	0	0	38	1
Promising therapeutics					
Nasal sprays	53	35	4	23,200	78
Probiotics	22	12	2	51,800	7
Limited-effectiveness therapeutics					
BCG vaccination	9	5	0	31,000	26
Vitamin D	89	52	4	1,370,000	49

Notes: [a]Some drugs here are also in treatment categories. Data from ClinicalTrials.gov, Google Scholar, and "The Mouse That Roared" (R. L. Martin, unpublished report, 2025), as of November 1, 2024. Abbreviation: BCG: Bacille Calmette-Guérin.

However, a 2024 bioRxiv preprint reported that viral variants KP.3.1.1 and XEC significantly impacted Pemgarda's neutralization rates.[5] These findings were later confirmed in subsequent articles.

5.2. Promising therapeutics

5.2.1. Nasal sprays

Since intramuscular COVID-19 vaccines offer limited protection in the upper respiratory tract, nasal sprays and gargles have been proposed as complementary therapeutic options. Notably, a nasal spray containing engineered llama nanobodies was shown to protect or even fully cure SARS-CoV-2-infected mice.

(a) Nasal spray or gargle containing 0.5 – 1% povidone-iodine

Several pre-pandemic studies reported that iodine-based nasal spray or gargle effectively eliminated viruses in the nose or mouth. A 2020 paper reported that all evaluated concentrations of nasal and oral antiseptics completely inactivated SARS-CoV-2 within 60 s.[6] A subsequent article from the same journal published in 2022 reported that povidone-iodine nasal spray resulted in an 8.57 times reduction in COVID-19 hospitalization or death rates.[7] Despite these findings, the NIH COVID-19 Treatment Guidelines remain silent on the use of nasal sprays.

5.2.2. Probiotics

A 2020 medRxiv preprint reported that, in an analysis of 327,720 United Kingdom participants, certain dietary supplements were associated with a reduced risk of SARS-CoV-2 infection.[8] Specifically, probiotics were linked to a 14% reduction in infection risk (95% confidence interval [CI]: 8 – 19%). Notably, "The Mouse That Roared" (R. L. Martin, unpublished report, 2025) did not include any articles reporting negative results for probiotics. Despite this, the NIH COVID-19 Treatment Guidelines do not mention probiotics.

5.3. Limited-effectiveness therapeutics

5.3.1. Bacille Calmette-Guérin (BCG) vaccination

The BCG vaccine, developed over 80 years ago for tuberculosis, is one of the most widely used vaccines globally. A 2020 paper proposed that BCG may stimulate "trained immunity" against respiratory infections.[9]

Early in the pandemic, African countries with extensive BCG vaccination had 65% of the COVID-19 case rates compared to neighboring countries with lower BCG vaccination coverage. However, a 2022 paper reported that these differences diminished over time and typically lost statistical significance.[10] Although a few subsequent studies noted minor protective effects, most found no significant benefit. The NIH COVID-19 Treatment Guidelines do not address BCD vaccination.

5.3.2. Vitamin D

Researchers assessed the preventive effects of Vitamins A, C, D, and K against COVID-19, with the majority of studies focusing on Vitamin D. Findings on its effectiveness varied widely. The NIH COVID-19 Treatment Guidelines concluded that there was insufficient evidence to recommend for or against the use of Vitamins C or D for the prevention of COVID-19.

6. Suppression of viral replication and inflammation

The key takeaway from this review is that infection prevention remains the highest priority. Once infected, therapeutics can help but generally have limited effectiveness (suppress viral replication and the inflammation phase in Figure 1). Figure 6 illustrates that promising antiviral targets were identified early in the pandemic.[11]

Table 6 summarizes antiviral article statistics from ClinicalTrials.gov, Google Scholar, and "The Mouse That Roared" (R. L. Martin, unpublished report, 2025). The table highlights therapeutics that receive detailed discussion in this review. As will become evident, nearly all antivirals target either the spike protein or two non-structural proteins – NSP5 (also known as Mpro or $3CL^{pro}$) and NSP12 (also known as RNA-directed RNA polymerase [RdRp]). Even though other structural proteins (e.g., nucleocapsid) and non-structural proteins (e.g., NSP1) represent viable

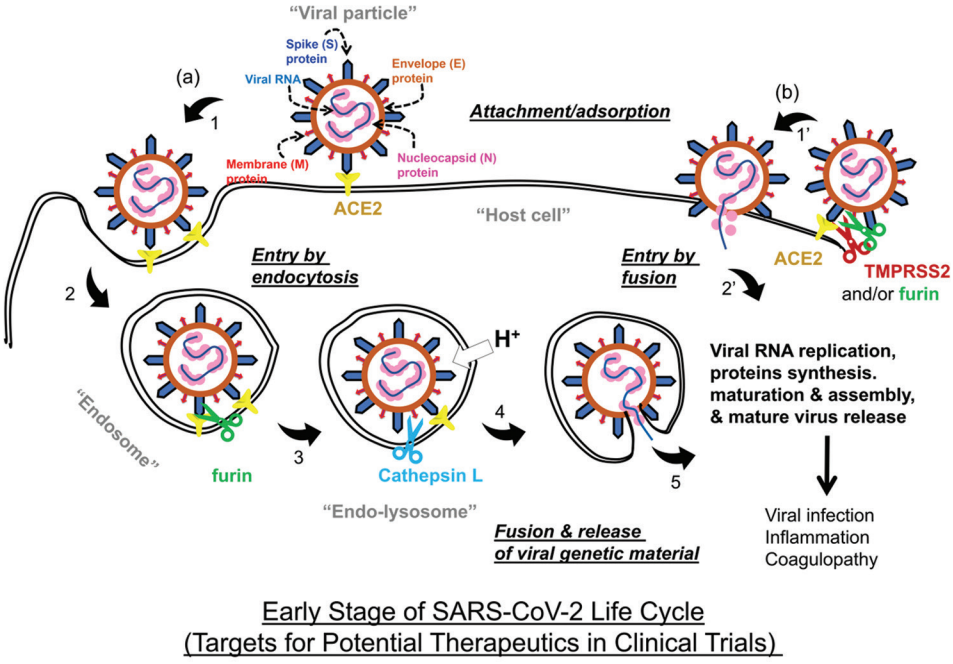

Figure 6. Early viral lifecycle and antiviral targets. Reprinted from Al-Horani *et al.*[11]
Abbreviations: ACE2: Angiotensin-converting enzyme 2; TMPRSS2: Transmembrane serine protease 2.

antiviral targets, few studies have investigated them, and no approved therapeutics have emerged targeting these proteins.

The three antiviral targets of approved COVID-19 drugs – spike proteins, NSP5 and NSP12 – were discovered early in 2020:

(i) A 2020 *Nature* paper[12] investigated drugs effective against other viruses, e.g., SARS-CoV-1, Middle East respiratory syndrome (MERS)-related coronavirus, and Ebola virus, and reported that remdesivir was likely to be effective against SARS-CoV-2
(ii) A 2020 *Science* paper[13] reported the development of an Mpro inhibitor
(iii) A 2020 *Nature* paper[14] identified the spike protein as an ideal target for vaccines and therapeutics.

6.1. Approved therapeutics

6.1.1. Monoclonal antibodies and nanobodies

Monoclonal antibodies and nanobodies bind to various targets, e.g., cancer cells or viral proteins, causing conformational changes. In the case of SARS-CoV-2, they bind to the spike protein, preventing it from attaching to the ACE2 receptor and entering host cells.

The FDA approved its first monoclonal antibody in 1986 for the prevention of kidney transplant rejection. According to a 2022 study,[15] 162 monoclonal antibodies had been approved worldwide as of June 30, 2022.

Monoclonal antibodies have been developed for a wide range of conditions, including transplants, cancers, sepsis, multiple sclerosis, arthritis, blood clotting disorders, stroke, bacterial infections, autoimmune diseases, respiratory syncytial virus (RSV) infections, degenerative myopia, diabetes, macular degeneration, and many obscure diseases. The influenza virus has no approved monoclonal antibody drugs because of its high mutation rate, though a 2024 study[16] reported a promising new approach for a flu-targeting monoclonal antibody. Its long-term effectiveness remains to be seen.

Monoclonal antibodies were initially highly effective against SARS-CoV-2; however, variants of concern significantly reduced their effectiveness over time. Figure 7 summarizes the timeline of monoclonal antibody approvals and when they were rendered ineffective by emerging viral variants.

Interestingly, a 2024 study reported that several non-neutralizing antibodies provided protection against SARS-CoV-2 in different animal models.[17]

The FDA-approved monoclonal antibodies were highly effective when administered early and were considered safe for use in pregnant women. Once taken, the FDA recommended delaying COVID-19 vaccination by 90 days, as monoclonal antibodies could interfere with the immune response to the vaccines. Effectiveness data for these antibodies are as follows:

Table 6. Statistics on antivirals in COVID-19 clinical trial data and therapeutic articles

Category	ClinicalTrials.gov			Google Scholar	"The Mouse That Roared"
	Total	Completed	Results		
Approved therapeutics					
Antiviral	736	304	102	3,200,000	2331
Spike protein monoclonal antibody[a]	99	39	18	24,400	497
Casirivimab/imdevimab[b]	25	8	11	6830	38
Sotrovimab[b]	24	9	10	5720	53
Tixagevimab/cilgavimab[b]	18	12	6	4230	39
Mpro				18,900	502
Paxlovid	45	14	7	9780	176
RdRp[c]				23,300	193
Molnupiravir[c]	20	7	5	11,000	107
Remdesivir[d]	108	51	26	41,200	73
Promising therapeutics					
Innate immunity					
Interferon	68	36	0	491,000	37
Other types					
ACE2	31	10	2	63,700	102
Simvastatin	4	1	0	16,900	8
Herbs (will be discussed later)	-	-	-	-	-
Limited-effectiveness therapeutics					
Renin-angiotensin system inhibitors	9	2	0	38,000	4
Convalescent plasma	175	87	30	42,300	48
Favipiravir	65	36	9	23,100	26

Notes: [a]There are 71 nanobodies that are reviewed in "The Mouse That Roared" but are not yet tested in United States Food and Drug Administration (FDA)-approved clinical trials. [b]Numerous papers discussed multiple monoclonal antibodies. [c]Numerous papers discussed RdRp therapeutics with other therapeutics, e.g., Paxlovid and monoclonal antibodies. [d]Twenty articles related to molnupiravir that are reviewed in "The Mouse That Roared" were co-studied with Paxlovid. Data sourced from ClinicalTrials.gov, Google Scholar, and "The Mouse That Roared" (R. L. Martin, unpublished report, 2025). Abbreviations: ACE2: Angiotensin-converting enzyme 2; Mpro: Main protease; RdRP: RNA-dependent RNA polymerase.

- Casirivimab with imdevimab: A 2022 study reported that among seronegative patients, 396 (24%) of 1633 patients receiving casirivimab and imdevimab died within 28 days, compared to 452 (30%) of 1520 patients receiving usual care (rate ratio [RR]: 0.79, 95% CI: 0.69 – 0.91).[18]

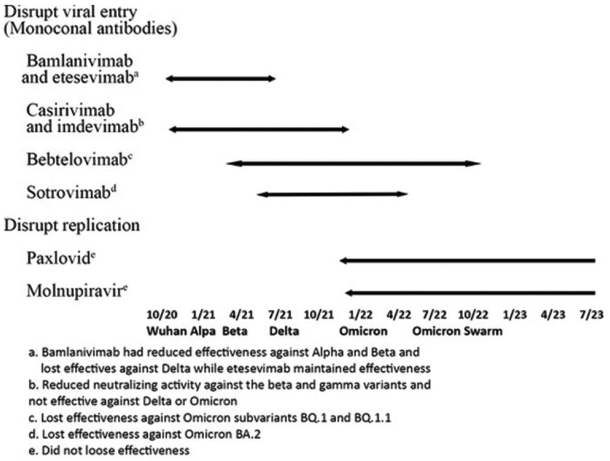

Figure 7. Timeline of monoclonal antibodies' effectiveness against Severe Acute Respiratory Syndrome Coronavirus 2 variants.
Notes: [a]Bamlanivimab has reduced effectiveness against alpha and beta variants and lost effectiveness against the delta variant, while etesevimab remains effective. [b]Reduced neutralizing activity against the beta and gamma variants, and not effective against delta and omicron variants. [c]Lost effectiveness against omicron subvariants BQ.1 and BQ.1.1. [d]Lost effectiveness against the omicron subvariant BA.2. [e]Did not lose effectiveness.

- Bamlanivimab in conjunction with etesevimab: A 2021 study reported that by day 29, 11 of 518 patients (2.1%) in the bamlanivimab–etesevimab group experienced COVID-19-related hospitalization or death, compared to 36 of 517 patients (7.0%) in the placebo group (absolute risk difference: −4.8 percentage points; 95% CI: −7.4 – −2.3; relative risk difference: 70%; $p<0.001$).[19] No deaths occurred in the bamlanivimab–etesevimab group, whereas 10 deaths occurred in the placebo group. Effectiveness was lost against Beta and Gamma variants.
- Sotrovimab: A 2021 study reported an 85% relative risk reduction in hospitalization or death (97.24% CI: 44 – 96%).[20] While it retained some effectiveness against Omicron BA.1 and BA.2, later Omicron subvariants rendered it ineffective.
- Evusheld (tixagevimab and cilgavimab): A 2022 study reported that follow-up at a median of 6 months showed a relative reduction in infection risk of 82.8% (95% CI: 65.8 – 91.4).[21] Although initially effective against Omicron BA.1 and BA.2, it was rendered ineffective by later Omicron subvariants. It was extensively used for infection protection.

The NIH COVID-19 Treatment Guidelines have noted that these monoclonal antibodies are no longer effective. At present, Llama, hamster, or ferret monoclonal antibodies and nanobodies have been developed to target:
(i) The neuropilin-1 binding domain

(ii) The furin/transmembrane serine protease 2 (TMPRSS2) cleavage site; and
(iii) Several structural and NSPs.

However, none of these candidates progressed to large-scale clinical trials.

(a) Inhibition of viral replication proteins

Several viral proteins and protein complexes are essential for viral replication. Figure 8 illustrates SARS-CoV-2 proteins, adopted from a *Cell* paper.[22]

(b) NSP 5/Mpro

The virus replicates by hijacking the host's replication machinery and materials. It produces two long polyproteins, ORF1a and ORF1b, which are cleaved into individual NSPs. This cleavage is initiated by the host's relatively inefficient enzymes and completed by two viral proteases. Mpro (NSP5) cleaves the ORF1a polyprotein, and its inhibition effectively halts viral replication. Likewise, inhibiting PLpro (NSP3) also disrupts viral replication. Currently, there are no approved drugs targeting PLpro.

6.1.2. Paxlovid

Paxlovid, which combines two drugs – nirmatrelvir and ritonavir – is the most effective FDA-approved COVID-19 antiviral. Nirmatrelvir, originally tested against MERS in 2012, inhibits Mpro by cleaving it. Ritonavir, although an antiviral used in acquired immunodeficiency syndrome (AIDS) treatment, is included primarily to boost nirmatrelvir's effectiveness. The FDA granted Paxlovid Emergency Use Authorization on December 21, 2021, and full approval on May 23, 2023. To date, no Mpro mutation has rendered it ineffective. China developed a Paxlovid analog, azvudine, and another Mpro drug, leritrelvir.

(a) Patient suitability

Paxlovid is not suitable for everyone because of potential drug interactions involving ritonavir. These interactions may occur with commonly prescribed medications, necessitating caution. The FDA Paxlovid Drug Interactions and the University of Liverpool Drug Interactions websites provide detailed assessments of these interactions. These resources categorize interactions based on clinical risk, including when Paxlovid should not be used, when it can be used with close monitoring, or when certain medications – such as simvastatin – must be paused before initiating treatment. Paxlovid is considered safe for use during pregnancy.

(b) Effectiveness against COVID-19

There have been numerous studies reporting varying results. A 2022 study presented the Phase 3 trial results in adults and reported:[23]

- An 89.1% reduction in hospitalization risk. No deaths occurred in the Paxlovid group, compared to 1% mortality in the placebo group
- Diarrhea was seen in 3.1% of participants taking Paxlovid, compared to 1.6% in the placebo group
- A strong bitter or metallic taste, later called Paxlovid mouth, was reported by 5.6% of participants taking Paxlovid. Sucking on sweets or using saccharin was found to help. Only 0.03% in the placebo group reported a similar taste.

A 2023 study highlighted the importance of early treatment.[24] It found that Paxlovid's effectiveness in preventing hospitalization or death differed greatly depending on how soon it was administered:

- Within 30 days of a positive test for SARS-CoV-2, effectiveness was 53.6% (95% CI: 6.6 – 77.0)

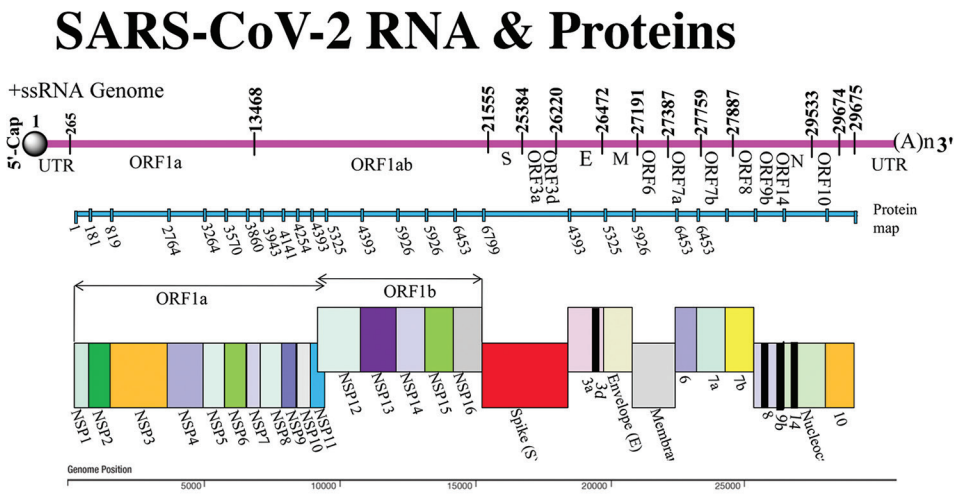

Figure 8. Severe Acute Respiratory Syndrome Coronavirus 2 proteins. Adopted from Yadav *et al.*[22]

- Within 5 days of symptom onset, effectiveness was 79.6% (95% CI: 33.9 – 93.8)
- On the 1st day of symptom onset, effectiveness was 89.6% (95% CI: 50.2 – 97.8).

According to NIH guidelines, treatment should begin promptly and within 5 days of the onset of symptoms.

(c) Viral rebound

Viral rebound occurs in 2 – 5% of individuals who take Paxlovid. The phenomenon is not well understood, and studies have reported widely differing results. According to the CDC,[25] among those with a virologic response by day 5, viral rebound was observed in 6.4 – 8.4% of Paxlovid recipients and 5.9 – 6.5% of placebo recipients during both the 2021 pre-Omicron and 2022 Omicron periods.

(d) Paxlovid underutilization

Due to cost concerns, fear of rebound, and side effects, Paxlovid remains significantly underutilized. A 2022 CDC report[26] found that among 699,848 adults aged 18 and older who were eligible for Paxlovid during April – August 2022, only 28.4% received a Paxlovid prescription within 5 days of their COVID-19 diagnosis. Furthermore, utilization was even lower among individuals in lower socioeconomic groups, despite government coverage of the medication during that time.

In October 2022, *The New York Times*[27] reported that Paxlovid was used by political affiliation and suggested that higher COVID-19 death rates in the red states may be linked to Paxlovid underutilization. Figure 9 summarizes US Department of Health and Human Services data on Paxlovid prescriptions in relation to the 2020 presidential election margin between Biden and Trump.

(e) NSP 12/RdRp

Unlike many viruses, including the influenza virus, SARS-CoV-2 has a replication mechanism that includes error correction, enhancing its replication fidelity. Two FDA-approved therapeutics target this process by interfering with the NSP12 (RdRp), a key component of the virus's replication complex:

(i) Remdesivir is an intravenous, hospital-administered therapeutic. It previously showed effectiveness against hepatitis C and RSV in 2009, Ebola in 2014, and Marburg virus disease in 2015. The FDA approved it for COVID-19 treatment on October 22, 2020

(ii) Lagevrio (molnupiravir) is a tablet therapeutic. It had previously shown effectiveness against influenza, Ebola, chikungunya, and various coronavirus-induced diseases, including MERS. The FDA approved it for COVID-19 use on December 23, 2021.

6.1.3. Remdesivir

A 2020 study reported remdesivir's effectiveness against COVID-19,[28] as shown in Table 7.

A 2024 study reported that remdesivir was associated with an absolute risk reduction of 6.4% and a relative risk reduction of 66% for all-cause hospitalization or death.[29] It is often taken with Paxlovid. To date, RdRp mutations have not yet disabled remdesivir's effectiveness.

Remdesivir can help keep patients alive for prolonged periods while they remain COVID-19 positive. However, extended infections provide an ideal environment for viral mutations. Five papers cited in "The Mouse That Roared" (R. L. Martin, unpublished report, 2025) reported that substantial viral mutations occurred in remdesivir-treated patients.

The NIH COVID-19 Treatment Guidelines recommend remdesivir for use within 7 days of symptom onset in a hospitalized setting, often in combination with other drugs. However, they recommend Paxlovid as the preferred option when appropriate.

6.1.4. Lagevrio (molnupiravir)

A 2021 study reported Lagevrio's effectiveness against COVID-19,[30] as summarized in Table 8.

A 2022 medRxiv preprint[31] reported a retrospective study of 92 million patients, of whom 11,270 received Paxlovid and 2374 received molnupiravir within 5 days of COVID-19 symptom onset. The results are summarized in Table 9.

Table 7. Remdesivir's effectiveness against COVID-19

Medication effectiveness measures	Remdesivir	Placebo
Recovery time (days)	10	15
Mortality by day 29 (%)	11.4	15.2
Serious adverse events (%)	24.6	31.6

Table 8. Lagevrio's (molnupiravir) effectiveness against COVID-19

Medication effectiveness measures	Molnupiravir	Placebo
Hospitalization or death by day 29 (%)	6.9	9.7
Serious adverse events (%)	30.4	31.6

Table 9. Molnupiravir's effectiveness against COVID-19

Medication effectiveness measures	Paxlovid		Molnupiravir	
	7 Days	30 Days	7 Days	30 Days
Symptoms (%)	2.31	5.87	3.75	8.21
Hospitalization (%)	0.44	0.77	0.84	1.39
Rebound[a] (%)	3.53	5.40	5.86	8.59

Note: [a]Patients with COVID-19 rebound had a significantly higher prevalence of underlying medical conditions than those without.

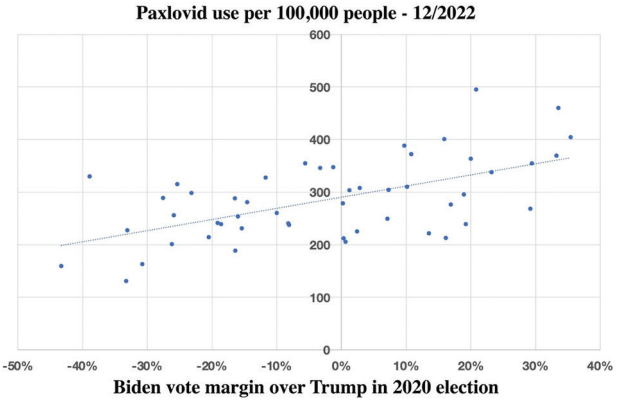

Figure 9. State-level Paxlovid usage rates by Biden–Trump vote margin in the 2020 presidential election. Graph created by the author using United States Department of Health and Human Services data.

All comprehensive studies reported greater effectiveness for Paxlovid. However, molnupiravir is suitable for a broader patient population. The NIH COVID-19 Treatment Guidelines recommended molnupiravir only when Paxlovid and remdesivir are not appropriate treatment options.

6.1.5. Mutations in SARS-CoV-2

A 2024 study reported that molnupiravir induced SARS-CoV-2 mutations,[32] as summarized in Figure 10.

Molnupiravir raised concerns about its potential to alter human DNA. However, the FDA reported that the post-treatment genotoxicity data imply a low risk of DNA damage. Nonetheless, the FDA issued the following precautions:

- Do not use in pregnant patients unless no alternative treatments are available and the potential benefits outweigh the risks
- Use effective contraception during molnupiravir treatment and for a period after completing the course
- Restrict use to adults aged 18 years and older.

6.2. Promising therapeutics

6.2.1. Interferon

The most discussed anti-inflammatory cytokines in the context of COVID-19 are interferons (IFNs). They "interfere" with viral replication to protect cells from infection. Although no approved IFN drugs are available for COVID-19 treatment, "The Mouse That Roared" (R. L. Martin, unpublished report, 2025) identified multiple potential drugs targeting IFNs, including IFN-beta (IFN-β), IFN-β1a, IFN-γ, IFN-λ2, and IFN-α16. A 2023 study reported that IFN-α2b reduced lung injury by 50% and decreased the odds of developing severe COVID-19 by a factor of five.[33]

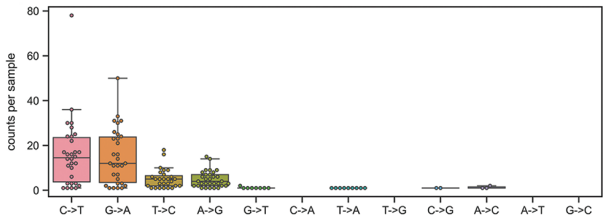

Figure 10. Molnupiravir-induced mutations in severe acute respiratory syndrome coronavirus 2. Reprinted from Gruber *et al.*[31]

The NIH COVID-19 Treatment Guidelines provided the following recommendations regarding IFN therapies:

- Recommended against the use of IFN-α or IFN-β for non-hospitalized patients with mild-to-moderate COVID-19, except in clinical trials
- Recommended against the use of IFN-α, except in a clinical trial, and IFN-β for hospitalized patients
- Made no recommendation for or against the use of IFN-λ.

While some IFN therapeutics showed early promise, none received FDA approval for the treatment of COVID-19.

6.2.2. ACE2 inhibitors

The primary way for SARS-CoV-2 to enter human cells is when its spike protein binds to a cell's ACE2 receptor, facilitating viral entry. Monoclonal antibodies interfere with this process by binding to the spike protein and blocking its interaction with ACE2 receptors. Several promising ACE2-based approaches were discussed in "The Mouse That Roared" (R. L. Martin, unpublished report, 2025), including:

(i) Biochemically altering ACE2 receptors to prevent spike protein binding
(ii) Reducing ACE2 receptor expression on host cells to limit viral entry points
(iii) Using ACE2 receptor-binding particles to pre-occupy receptors and block viral binding
(iv) Deploying ACE2 decoys – such as nanoparticles-bound, soluble, or inhaled forms – to bind and neutralize the spike protein before it can reach actual cells.

Although these strategies demonstrated excellent success rates across viral variants, little progress has been made in commercializing ACE2 inhibitors. The NIH COVID-19 Treatment Guidelines are currently silent on ACE2-based inhibitors.

6.2.3. Simvastatin

Many individuals take statins to manage cholesterol levels. Of the various statins tested, only simvastatin showed

a modest effect on COVID-19 outcomes in selected studies. A 2023 study evaluated simvastatin in critically ill COVID-19 patients.[34] Although the study ended early due to declining case numbers, the results indicated that simvastatin did not meet the pre-specified criteria for superiority compared to the control group.

6.2.4. Herbs

Table 10 summarizes the statistics of herbal therapeutic articles on COVID-19 collected from ClinicalTrials.gov, Google Scholar, and "The Mouse That Roared" (R. L. Martin, unpublished report, 2025).

Table 11 presents a breakdown of the herbs into various categories.

The February 2023 COVID-19 Treatment Guidelines (https://www.ncbi.nlm.nih.gov/books/NBK570371/pdf/Bookshelf_NBK570371.pdf) from China span 26 pages, with 10 pages dedicated to traditional Chinese medicines. These guidelines also included "Western" therapeutics, such as Paxlovid. In contrast, the NIH COVID-19 Treatment Guidelines mention herbs only in the context of potential medical contraindications. They note that while no herbal therapies are currently approved, many show promise.

6.3. Limited-effectiveness therapeutics

6.3.1. Renin-angiotensin system inhibitors

Given that the cytokine storm and the bradykinin storm result from disruption of the renin-angiotensin system, it is reasonable to speculate that preventing this disruption could serve as an effective antiviral strategy. However, four papers discussed in "The Mouse that Roared" (R. L. Martin, unpublished report, 2025) reported controversial results on this approach.

6.3.2. Convalescent plasma

Blood plasma is the yellowish liquid component of blood that suspends the blood cells and proteins throughout the body. The first Nobel Prize in Physiology and Medicine was awarded in 1901 to Emil von Behring for successfully using antibodies from the plasma of animals that had recovered from diphtheria to treat diphtheria patients.

Plasma therapy is believed to have reduced mortality by half during the 1918 Spanish Flu, especially when administered early. It was later used against measles in the 1930s, the Korean hemorrhagic fever in the 1950s, and has been one of the most effective treatments for Ebola.

In 2020, Arturo Casadevall, a Johns Hopkins Bloomberg Distinguished Professor of Molecular Microbiology and Immunology and the department chairman, led a strong advocacy campaign urging further investigation into COVID-19 plasma therapy.

(a) Conflicting results

Convalescent plasma trial results have been mixed. A 2023 study analyzed 19 trials and reported that the estimated mortality relative to placebo was 0.94 (95% CI: 0.81 – 1.08, p=0.33).[35]

The NIH COVID-19 Treatment Guidelines concluded that there is insufficient evidence to recommend either for or against the use of high-titer convalescent plasma in hospitalized or non-hospitalized immunocompromised patients.

6.3.3. Favipiravir

Favipiravir, though of uncertain effectiveness and not approved in the US, is used in Japan to treat influenza. For COVID-19, it was thought that favipiravir might inhibit

Table 10. Statistics on herbal therapeutic articles on COVID-19

Medication effectiveness measures	ClinicalTrials.gov			Google Scholar	"The Mouse That Roared"
	Total	Completed	Results		
Herbs	15	6	0	57,000	263
Traditional Chinese medicine[a]	21	7	0	447,000	53

Notes: [a]Included the total herb count; Data from ClinicalTrials.gov, Google Scholar, and "The Mouse That Roared" (R. L. Martin, unpublished report, 2025), as of November 01, 2024.

Table 11. Types of herbal therapeutics against COVID-19

Medication effectiveness measures	All	Herbs, excluding TCM			TCM		
		Antiviral	Mainly inflammation treatment	Antiviral and inflammation treatment	Antiviral	Treating mainly inflammation	Antiviral and inflammation treatment
Total	314	179	58	21	24	28	4
Mpro	45	36	-	1	8	-	0
RdRp	12	9	-	0	3	-	0

Note: Statistics from ClinicalTrials.gov, Google Scholar, and "The Mouse That Roared" (R. L. Martin, unpublished report, 2025), as of November 01, 2024.
Abbreviations: Mpro: Main protease; RdRp: RNA-directed RNA polymerase; TCM: Traditional Chinese medicine.

the viral RdRp and potentially disrupt the envelope and ORF7a proteins.

A 2020 study reported that among 35 patients treated with favipiravir and 45 control patients, the median viral clearance time was shorter with favipiravir – 4 days (interquartile range 2.5 – 9 days) versus 11 days (interquartile range 8 – 13 days).[36] The study also reported 91.43% improvements in chest computed tomography scans of favipiravir-treated patients, compared to 62.22% improvement in the control group. However, several clinical trials concluded that favipiravir did not significantly improve clinical outcomes, although it may offer some symptom relief in mild to moderate cases. The NIH COVID-19 Treatment Guidelines only referenced favipiravir in the context of one clinical trial that also included ivermectin.

6.4. Other antivirals with insufficient data to determine effectiveness

In addition to the antivirals already discussed, approximately 550 articles that address other parts of the viral lifecycle were reviewed in "The Mouse That Roared" (R. L. Martin, unpublished report, 2025). These therapeutics employed a wide range of mechanisms, such as utilizing amino acids, peptides, aptamers, short RNA, microRNA, ultraviolet light in lungs, and plasma-activated water, to disrupt viral biochemical processes – either by altering molecular shapes or damaging them through enzymes such as proteases or kinases. A significant number of therapeutics focused on interfering with the N-protein's glycans. Extensive drug and compound screening efforts were reported, with databases including, e.g., 350,000, 33,590, 22,000, 18,000, 6,710, 6,218, 2,100, 1,900, 1,796, and 850 candidates. These potential treatments were administered through diverse methods such as chewing gum, nasal spray, mouthwash, tablets, and injections.

The drug compounds and sources explored included: hydrogen sulfide compounds, sodium chloride, zinc oxide, cerium oxide, hydrophobic C60, copper, gold, silver, chlorine dioxide, copper ferrite, boron, nitric oxide, selenium, Vitamin B1 and B12 supplements, TMPRSS2 inhibitors, phosphatidic acid, nucleic acids, antiandrogens, human breast milk, pluripotent stem cells, earthworms, chewing gum, shark immune cells, mesenchymal stem cells, fungi, bacteria such as *Escherichia coli*, marine sponges, scorpion venom, IFNs, natural killer cells, sea cucumbers, mink lung epithelial cells, clustered regularly interspaced short palindromic repeats (CRISPR) technologies for identification or modification, cow's milk, monoclonal antibodies, coffee, bee venom, electric fields, mouthwash, purified immunoglobulin G, antiprotozoal agents, emetics, spider hemocytes, *Salamandra* species, sweet potato roots, oriental wasps, human defensins, bile acids, antibiotics, hen egg yolks, bovine herpesvirus, male contraceptives, cardiac imaging agents, and inhaled heparin.

Many drugs originally developed for other diseases showed some effectiveness against COVID-19. These diseases/symptoms include gas, leprosy, irritable bowel syndrome, tapeworm infections, epilepsy, gout, vaginal infections, hepatitis, AIDS, parasitic diseases, sleeping sickness, depression, anticonvulsant conditions, constipation, hyponatremia, overactive bladder, circadian rhythm disorders, cystinosis, influenza, fungal bacterial infections, macular degeneration, asthma, malaria, RSV, cardiac imaging conditions, ring-stage parasites, psychotic disorders, diuretic needs, kidney damage, human papillomavirus infection, bipolar disorder, schizophrenia, anxiety, migraines, tranquilizer use, high cholesterol, hepatitis C, pulmonary fibrosis, gallstones, liver disease, type I Gaucher disease, Fabry disease, anemia, hypovolemia, herpes, pancreatitis, reflux esophagitis, weight loss, hypertension, ectopic pregnancies, abnormal hemoglobin, allergies, hay fever, the common cold, rheumatoid arthritis, tachycardia, shortness of breath, pale skin, cold extremities, dark urine, jaundice, mitochondrial oxidative stress, lung transplantation, antiandrogen conditions, lactate-lowering needs, viral hemorrhagic fevers, throat and tonsils infections, ulcerative colitis, diabetic kidney disease, lupus, and methemoglobinemia.

7. Suppression of hyperinflammation

At the hyperinflammation stage (suppress hyperinflammation phase in Figure 1), the virus has replicated extensively and is now resulting in one of two outcomes:

(i) Mild-to-moderate COVID-19, which typically requires no further treatment
(ii) Severe COVID-19 may require hospitalization and carries a risk of death.

Long COVID can develop after either outcome, though it is more commonly associated with severe cases.

7.1. Inflammation

Inflammation is the body's natural response to injury or infection. Its purpose is to eliminate the cause of harm, remove damaged cells, and initiate healing. The inflammatory process involves:

(i) Recognition of harmful stimuli, such as physical injury or pathogens such as SARS-CoV-2
(ii) Release of signaling molecules, such as histamines and cytokines
(iii) Recruitment of immune cells – particularly white blood cells such as neutrophils and macrophages – to neutralize pathogens and remove cellular debris.

Hyperinflammation refers to excessive inflammation. In COVID-19, hyperinflammation can cause significant damage throughout the body, as shown in Figure 11, reprinted from a 2021 COVID article.[37]

7.1.1. Hyperinflammation causes

Hyperinflammation in COVID-19 has two primary causes:

(i) When SARS-CoV-2 binds to ACE2 receptors, it dysregulates the renin-angiotensin-aldosterone system, which plays important roles in controlling inflammation and blood pressure. Through a complex process, this dysregulation results in an overproduction of cytokines, which are small proteins that act as signaling molecules in the immune system. This excessive cytokine release is known as a cytokine storm. There are hundreds of cytokines, of which the most prominent pro-inflammatory cytokines are tumor necrosis factor-alpha (TNF-α), interleukin-1 (IL-1), IL-6, IL-17, IL-12, IL-23, and IFN-γ. Although cytokines work together to amplify inflammation and coordinate immune responses, their overproduction can lead to excessive inflammation and tissue damage, as seen in autoimmune diseases, cancers, infections, and physical damage.

(ii) The innate immune system's effector cells are damaged, releasing cytokines. This damage also promotes viral replication, as it generally takes 4 – 6 days before the adaptive immune system becomes fully activated.

If a patient reaches the point of hospitalization, their situation becomes critical. Hyperinflammation is especially difficult to treat because suppressing inflammation may impair the body's defense mechanisms, the underlying biology is highly complex and multifactorial, it is self-sustaining, there is significant individual variability in response, and the available treatments often carry side effects.

Numerous COVID-19 hyperinflammation drugs also target comorbidities frequently seen in COVID-19 patients, such as cancer, autoimmune diseases, obesity, diabetes, and gut microbiome imbalances. This overlap creates a complex interplay between the drugs' mechanisms and the observed clinical outcomes. The statistics on anti-inflammatory therapeutic articles for COVID-19 acquired from ClinicalTrials.gov, Google Scholar, and "The Mouse That Roared" (R. L. Martin, unpublished report, 2025) are shown in Table 12.

The two therapeutic approaches to hyperinflammation are:

(i) Address the cause, i.e., prevent inflammation by protecting the renin-angiotensin system and the innate immune system

(ii) Address the result, i.e., reduce inflammation.

Table 12. Statistics on anti-inflammatory therapeutic articles

Medication effectiveness measures	ClinicalTrials.gov			Google Scholar	"The Mouse That Roared"[a]
	Total	Completed	Results		
Prevent inflammation	241	97	22	214,000	457
Suppress inflammation					
Approved					
Tocilizumab	75	31	7	38,600	43
Anakinra	25	13	3	14,600	16
Baricitinib	27	8	3	13,400	24
Promising					
Corticosteroid	79	34	3	127,000	65
Dexamethasone	93	40	7	131,000	56
Spirulina	2	2	1	7,080	3
Metformin	9	2	1	42,600	24

Notes: [a]Many papers discussed several drugs; Statistics from ClinicalTrials.gov, Google Scholar, and "The Mouse That Roared" (R. L. Martin, unpublished report, 2025), as of November 1, 2024.

7.2. Inflammation prevention

No therapeutics to prevent inflammation have been approved for use.

7.2.1. Promising therapeutics

There are several promising therapeutics for preventing inflammation in COVID-19.

(a) Pro-inflammatory cytokine inhibition

Interleukins, the cytokines with primarily pro-inflammatory impacts, modulate the growth, differentiation, and activation of immune cells during inflammatory and immune responses. They stimulate immune cell recruitment and activation, increase vascular permeability, and induce fever – all of which are critical for fighting off invading pathogens. However, some ILs, such as IL-1, IL-4, IL-6, IL-10, IL-11, and IL-13, can have anti-inflammatory effects.

Despite its potential anti-inflammatory roles, IL-6 is frequently identified as a particularly pro-inflammatory IL in the context of COVID-19. A 2023 study reported that inhibiting IL-6 with Jusvinza reduced mortality to 10% in the treated group, compared to 60% in the untreated group.[38] Many traditional Chinese medicine therapies target IL-6 modulation.

Articles reviewed in "The Mouse That Roared" (R. L. Martin, unpublished report, 2025) addressed a broad range of ILs, such as IL-1Ra, IL-1β, IL-2C, IL-7, IL-17i, IL-18, IL-23, IL-23i, and IL-33. Meanwhile, the NIH COVID-19

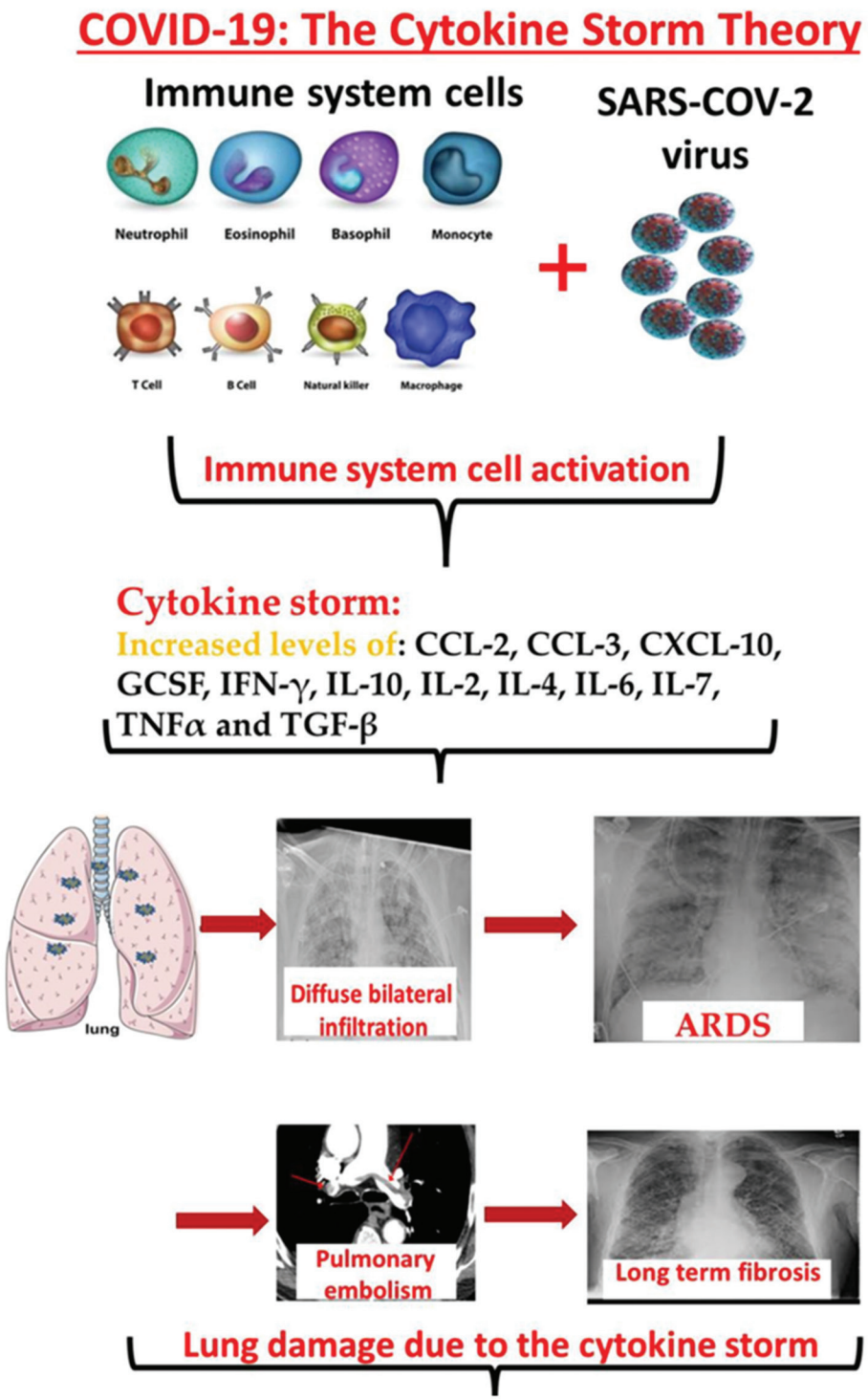

Figure 11. The cytokine storm theory in COVID-19. Reprinted from Venegas-Rodríguez *et al.*[37]
Abbreviations: ARDS: Acute respiratory distress syndrome; CCL: Chemokine (C-C motif) ligand; CXCL: Chemokine (C-X-C motif) ligand; GCSF: Granulocyte-colony stimulating factor; IFN: Interferon; IL: Interleukin; TNF: Tumor necrosis factor.

Treatment Guidelines address IL-6 suppression in hospitalized COVID-19 patients and recommend tocilizumab in combination with dexamethasone for certain cases.

(b) Effector cell protection

A few of the papers reviewed in "The Mouse That Roared" (R. L. Martin, unpublished report, 2025) discussed therapeutics aimed at reducing the inflammatory impacts on innate immune system effector cells. For example, macrophages were targeted with hydroxyl-polyamidoamine dendrimer-N-acetyl cysteine conjugate, natural killer cells were supported with 7DW8-5 glycolipid, TNF was modulated through nanochelating technology, neutrophils were addressed with sivelestat, and most importantly, neutrophil extracellular traps (NETs) were disrupted using thiocyanate and DNA proteases. In addition, a 2024 study reported that infusing cytotoxic T-cells led to viral elimination in patients, achieving more than 88% clearance in 4 days and more than 99% in 14 days.[39]

(c) Complement system enhancement

The complement system enhances the abilities of antibodies and phagocytic cells to ingest pathogens, promotes inflammation, and attacks the pathogen's cell membrane. It is dysregulated in COVID-19. A 2020 study reported that the Janus kinase (JAK)1/JAK2 inhibitor ruxolitinib helped normalize complement system activity.[40] The NIH COVID-19 Treatment Guidelines do not address the complement system.

7.2.2. Ineffective therapeutics

There are numerous ineffective therapeutics for preventing inflammation in COVID-19.

(a) Renin-angiotensin system inhibitors

A dysregulated renin-angiotensin system triggers the cytokine storm. ACE inhibitors, angiotensin receptor blockers, and direct renin inhibitors were trialed as potential treatments, but none reported encouraging results. In addition, certain blood pressure drugs interact with the renin-angiotensin system. The NIH COVID-19 Treatment Guidelines recommend that individuals already taking these drugs continue their use, but do not recommend initiating them specifically for COVID-19 treatment.

7.3. Hyperinflammation treatment

The approved and promising therapeutics for hyperinflammation treatment in COVID-19 are discussed in this section.

7.3.1. Approved therapeutics

Multiple medications have been used in treating hyperinflammation in COVID-19.

(a) Tocilizumab

Tocilizumab is a monoclonal antibody immunosuppressant that targets IL-6. Approved for use in Japan in 2008, it is primarily used to treat rheumatoid arthritis. It targets pro-inflammatory cytokines, including TNF-α, IL-6, IL-1, and IL-17, as well as immune cell surface receptors. The FDA granted tocilizumab Emergency Use Authorization for COVID-19 on December 21, 2022.

A 2021 study reported that eight clinical trials produced mixed outcomes.[41] Subsequent studies reported that tocilizumab:

(i) improved outcomes, including survival (36% vs. 26%)[42]

(ii) had no effect on disease severity or mortality.[43]

(b) Anakinra

Used to treat rheumatoid arthritis, anakinra is a recombinant, slightly modified version of a human IL-1 receptor antagonist. It targets pro-inflammatory cytokines, such as TNF-α, IL-6, IL-1, and IL-17, as well as immune cell surface receptors. Anakinra was first used for familial Mediterranean fever in 1998. The FDA granted it Emergency Use Authorization for COVID-19 on November 8, 2022, one year after the EU.

A 2021 paper summarized six clinical trials, reporting that anakinra showed a survival benefit when administered without dexamethasone (odds ratio [OR]: 0.23, 95% CI: 0.12 – 0.43), but not when given alongside dexamethasone (OR: 0.72, 95% CI: 0.37 – 1.41).[44] Other studies did not demonstrate strong effectiveness for anakinra.

(c) Baricitinib

Baricitinib was approved by the FDA for the treatment of rheumatoid arthritis in 2017. It blocks JAK enzymes, which are critical in the signaling pathways of several pro-inflammatory cytokines, such as IL-6 and IFN-γ. The FDA granted baricitinib Emergency Use Authorization for COVID-19 on May 10, 2022.

A 2020 study reported that patients receiving baricitinib had a median recovery time of seven days (95% CI: 6 – 8), compared to eight days (95% CI: 7 – 9) for controls.[45] Baricitinib also improved clinical status at day 15, with a 30% higher odds of improvement (OR: 1.3, 95% CI: 1.0 – 1.6). Among patients who were receiving high-flow oxygen or non-invasive ventilation at enrollment, the median recovery time was 10 days in the combination treatment group versus 18 days in controls (RR for recovery: 1.51, 95% CI: 1.10 – 2.08). The 28-day mortality was 5.1% in the combination group versus 7.8% in the control group.

The NIH COVID-19 Treatment Guidelines noted that the use of immunomodulators, such as dexamethasone,

JAK inhibitors (e.g., baricitinib and tofacitinib), IL-6 inhibitors (e.g., tocilizumab and sarilumab), TNF inhibitors (e.g., infliximab), and abatacept (also used for rheumatoid arthritis), to treat COVID-19 may increase the risk of infectious complications. However, when these therapies are used appropriately, the benefits outweigh the risks.

7.3.2. Promising therapeutics

The promising therapeutics include glucocorticoids, spirulina, and metformin.

(a) Glucocorticoids

Glucocorticoids are steroid hormones that exert diverse and potent immunosuppressive effects by downregulating pro-inflammatory cytokines, such as various ILs, and by blocking inflammatory signaling pathways.

Dexamethasone, the most frequently used glucocorticoid, was often administered in combination with antivirals. A 2020 study reported that in the dexamethasone group, the incidence of death was lower than that in the usual care group among patients receiving invasive mechanical ventilation (29.3% vs. 41.4%, RR: 0.64, 95% CI: 0.51 – 0.81) and among those receiving oxygen without invasive mechanical ventilation (23.3% vs. 26.2%, RR: 0.82, 95% CI: 0.72 – 0.94), but not among those who were not receiving support (17.8% vs. 14.0%, RR: 1.19, 95% CI: 0.92 – 1.55).[46]

Other studies reported mortality reductions of 42%, 33%, 32.2%, and 20% (in two separate papers). Nonetheless, dexamethasone use is not without risks. It has been associated with altered gut bacterial compositions and increased incidence of hyperglycemia in diabetic patients. The NIH COVID-19 Treatment Guidelines on dexamethasone noted:

(i) There is a lack of safety and efficacy data on dexamethasone use in outpatient COVID-19 patients, and it may cause harm in these cases
(ii) It should only be used if patients require supplemental oxygen, and should be used in combination with remdesivir.

(b) Spirulina

Spirulina is a type of bacteria that significantly reduces the levels of IL-6, TNF-α, IL-10, and IFN-gamma-induced protein 10. A 2024 study reported that spirulina supplementation was associated with reduced mortality risk in COVID-19 patients.[47] In non-intensive care unit (ICU) patients, the hazard ratio for mortality was 0.13 (95% CI: 0.02 – 0.97), whereas in ICU patients, the hazard ratio was 0.16 (95% CI: 0.05 – 0.48).

(c) Metformin

Clinical trials have reported that metformin reduces mortality by 0%, 40%, 50%, 80%, and 58% in hospitalization or death through 28 days. A June 2023, medRxiv preprint[48] reported that in a Phase 3, randomized, placebo-controlled, outpatient clinical trial, metformin use led to a 42% reduction in emergency room visits, hospitalizations, or death through 14 days, a 58% reduction in hospitalizations or death through 28 days, and a 42% reduction in the incidence of long COVID through 10 months. The NIH COVID-19 Treatment Guidelines noted that:

(i) There is insufficient evidence to recommend either for or against the use of metformin for the treatment of COVID-19 in non-hospitalized patients
(ii) The panel recommends against the use of metformin for the treatment of COVID-19 in hospitalized patients, except in a clinical trial
(iii) Patients with COVID-19 who are receiving metformin for an underlying condition should continue this therapy as directed by their health-care provider.

7.4. Other anti-inflammatory therapeutics with insufficient data to conclude effectiveness

There are 275 remaining anti-inflammatory articles from "The Mouse That Roared" (R. L. Martin, unpublished report, 2025) that have not yet been discussed. They addressed:

(i) Cytokines: IL-6 (main target), IL-2, TNF-α, IL-17, IL-23, IL-7, IFN-γ, TNFα, IL-1β, IL-18, transforming growth factor-β1, IFN-α, IFN-β, angiopoietin-2, and NACHT, LRR and PYD domains-containing protein 3
(ii) Effector cells: Macrophages, cytotoxic T cells, neutrophils, and mast cells
(iii) Kinases, enzymes that catalyze the transfer of a phosphate group from ATP to a specific molecule: JAK, casein kinase 2, TANK-binding kinase 1, and spleen tyrosine kinases
(iv) Miscellaneous targets: Transcription factors, genes that encode proteins that detect products of damaged cells and trigger an immune response, gasdermin D inhibitors, exosomes, adenine dinucleotide metabolism, and NETs.

These therapeutics encompass numerous ingredients or mechanisms: cluster of differentiation 24, N-protein antibodies, monoclonal antibodies for selected cytokines, IFNs, genes, CRISPR-modified T cells, stem cell transplants, hydrogen, immunoglobulins, molecules that induce cell death, bacteria, blood purification, plasma exchange, algae, synthetic angiotensin (1 – 7), angiotensin II type 1 receptor-biased ligand, low-dose radiation, low-intensity pulsed ultrasound, pharmacologic stress agents used in cardiac perfusion imaging studies, drugs to maintain

general anesthesia, hyperimmune plasma from sheep, mesenchymal stromal cells from many sources, injectable porous silicon particles, silver, selenium, lithium, sodium nitrate, hydrogen-rich water, cytotoxic T lymphocytes, cellular human amniotic fluid, degalactosylated bovine glycoproteins, activated protein C, Vitamin E, blood filter, and antioxidant enzymes.

These therapeutics address a wide array of diseases:

(i) Autoimmune diseases: Rheumatoid arthritis, ankylosing spondylitis, psoriasis (including plaque psoriasis), Crohn's disease, inflammatory bowel disease, ulcerative colitis, alopecia areata, multiple sclerosis, chronic immune thrombocytopenia, Behçet's disease, eczema, atopic dermatitis, seborrheic dermatitis, gout, and keratoconjunctivitis sicca associated with Sjögren's syndrome. Multiple human diseases, particularly immunosuppressive diseases, such as inflammatory bowel syndrome, are associated with inflammation. According to a 2024 study,[49] based on a 2013 national estimate, 2.7% of US adults were immunosuppressed due to health conditions or medication use. Certain autoimmune drugs are helpful in treating COVID-19 because they target cytokines, autoantibodies, and interfere with cell signaling pathways that drive inflammation.

(ii) Cancer: Bone marrow cancers, small cell lung cancer, leukemias (e.g., chronic myeloid leukemia, acute lymphoblastic leukemia, and chronic myelogenous leukemia), multiple myeloma, prostate cancer (including castration-resistant prostate cancer), high-risk primary or secondary myelofibrosis, testicular and ovarian cancers, glioblastoma multiforme, and myelodysplastic syndromes. Certain cancer drugs are helpful in treating COVID-19 because they target cytokines, exert strong anti-inflammatory effects, and reduce tumor burden, which in turn can decrease the release of pro-inflammatory mediators.

(iii) Other lung diseases: Chronic obstructive pulmonary disease, chronic bronchopulmonary disorders, idiopathic pulmonary fibrosis, acute lung injury, bleomycin lung injury, acute respiratory distress syndrome (ARDS), and tuberculosis.

(iv) Others: Abnormal blood lipid levels, acute pancreatitis, alcohol use disorder, Alzheimer's disease, amyotrophic lateral sclerosis, angina pectoris, chronic hepatitis, chronic kidney disease, diabetes, diabetic kidney disease, disseminated intravascular coagulation, epilepsy, gastroesophageal reflux disease, graft-versus-host disease, heart conditions, hemophagocytic lymphohistiocytosis, high blood pressure, hyperlipidemia, hypertriglyceridemia, lactobezoar, malaria, migraines, nausea, nephrotic syndrome, neuropathic pain, osteoporosis in postmenopausal women, peptic ulcer disease, prion diseases, depression, psychosis, anxiety, schizophrenia, sepsis, solid organ transplant, superficial mycoses, tapeworm infections, viscid or excessive mucus production, and Zollinger–Ellison syndrome.

8. Organ damage suppression

At the organ damage stage (Figure 1), the patient is critically ill, and no highly effective treatments are available. Table 13 summarizes statistics on studies that addressed two key areas of organ-specific treatment in COVID-19, data acquired from ClinicalTrials.gov, Google Scholar, and "The Mouse that Roared" (R. L. Martin, unpublished report, 2025).

8.1. Lungs

As previously noted, lung damage in COVID-19 patients can result from direct viral injury, inflammation, blood clots, and/or lack of oxygen. Oxygenation will be assessed in this section. Once again, timely intervention is the most important factor. The progression of oxygen treatments, from least to most intensive, includes:

(i) Conventional oxygen therapy
(ii) High-flow nasal cannula: Nasal delivery of an adjustable mixture of heated and humidified air and oxygen at rates that exceed spontaneous inspiratory flow
(iii) Mechanical ventilation
(iv) Extracorporeal membrane oxygenation (ECMO).

Table 13. Statistics on studies focusing on organ damage suppression in COVID-19

Medication effectiveness measures	ClinicalTrials.gov	Google Scholar	"The Mouse That Roared"
Lungs			
Approved therapeutics			
Oxygen	25	1,570,000	71
ECMO	3	40,800	52
Vilobelimab	1	446	6
Cardiovascular			
Approved therapeutics			
Anticoagulants[a]	-	-	54
Heparin	12	133,000	32

Notes: [a]Interpreting ClinicalTrials.gov searches must be done carefully. For example, these were the numbers of trials for different but highly related terms:
- "Anti-coagulant" or "anti coagulant": 34
- "Anti coagulant therapy": 31
- "Anti-coagulants": 1.

Statistics from ClinicalTrials.gov, Google Scholar, and "The Mouse That Roared" (R. L. Martin, unpublished report, 2025), as of December 01, 2024.
Abbreviation: ECMO: Extracorporeal membrane oxygenation.

8.1.1. ECMO

ECMO is a mechanically supported ventilation system used for severe COVID-19 respiratory failure. For COVID-19 patients, it is typically used for an average of 15 days, with an interquartile range of 8 – 17 days. ECMO has become the predominant form of mechanical ventilation in critical cases, with one meta-analysis reporting its use in 98.6% of such patients. It was cleared for COVID use by the FDA in February 2020.

A 2024 study reported that 54% of COVID-19 patients treated with ECMO experienced hemorrhagic complications.[50] Furthermore, despite the use of ECMO, some patients may still require lung transplantation. Figure 12 summarizes ECMO outcome statistics as reported in a 2025 *Journal of Clinical Medicine* paper.[51]

A 2023 study reported mortality rates for ARDS patients with and without ECMO treatment,[52] as summarized in Table 14.

The NIH COVID-19 Treatment Guidelines recommend starting treatment with high-flow nasal cannula oxygen, followed by non-invasive ventilation or intubation, and then progressing to mechanical ventilation. Although ECMO is referenced on 51 pages in the NIH guidelines regarding the use of other therapeutics, there is no explicit discussion or guidance regarding its direct use.

Table 14. Extracorporeal membrane oxygenation (ECMO) impacts on acute respiratory distress syndrome (ARDS) patient mortality

Characteristic	Follow-up	ECMO (%)	Conventional therapy (%)
ARDS-H1N1	6 months	37	53
ARDS	60 days	35	46
ARDS	60 days	34	47
ARDS	90 days	36	48
COVID ARDS	60 days	26	33
COVID ARDS	60 days	35	47

Note: Adopted from Burša *et al.*[51]

8.1.2. Vilobelimab

The monoclonal antibody vilobelimab was initially clinically trialed for septic shock in 2012. A 2022 study reported that all-cause mortality rate of COVID-19 at 28 days was 32% (95% CI: 25 – 39) in the vilobelimab group, compared to 42% (95% CI: 35 – 49) in the placebo group (hazard ratio: 0.73, 95% CI: 0.50 – 1.06; p=0.094).[53] The FDA granted Emergency Use Authorization for vilobelimab on April 04, 2023. The NIH COVID-19 Treatment Guidelines state that, although vilobelimab received a COVID-19 FDA Emergency Use Authorization, there is currently insufficient evidence to recommend either for or against its use in COVID-19.

8.1.3. Other unsuccessful oxygenation treatments

Studies reviewed in "The Mouse That Roared" (R. L. Martin, unpublished report, 2025) reported that other oxygenation treatments were clinically trialed but found to be ineffective. These included the use of hyperbaric chambers along with a cytokine therapeutic (erythropoietin), as well as repurposed drugs such as imatinib (a cancer treatment), methylthioninium chloride, and nebulized recombinant tissue plasminogen activator (commonly used for stroke).

8.2. Cardiovascular system

The cardiovascular system can be compromised by direct viral invasion, hyperinflammation, blood clots, and/or lack of oxygen. This section evaluates the management of blood clots. Well-known anti-coagulants, such as heparin, Xarelto, and aspirin, are employed to prevent or treat

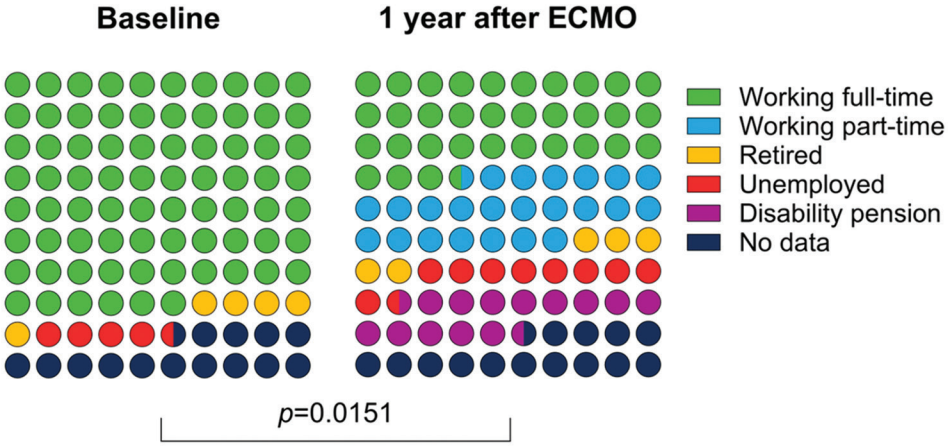

Figure 12. Distribution of extracorporeal membrane oxygenation outcomes. Reprinted from Staudacher *et al.*[50]

thrombosis. However, their use in COVID-19 requires caution, as anticoagulants can significantly increase the risk of bleeding.

In 2021, a study reported that the available evidence did not support the use of therapeutic-dose heparin for thrombosis prevention in critically ill COVID-19 patients.[54] While some benefit was observed in patients with severe comorbidities, the study emphasized the importance of proactive bleeding monitoring, noting that bleeding accounted for 3 – 6% of COVID-19-related deaths.

A 2024 study reported the relative risks and benefits of different heparin doses,[54] as summarized in Table 15.

Heparin received FDA approval for COVID-19-related use on September 17, 2020. The NIH COVID-19 Treatment Guidelines recommend its administration exclusively in hospital settings.

Another approach to mitigate clotting involves dissolving NETs**,** which are networks of extracellular fibers primarily composed of neutrophil DNA. Neutrophils, the immune system's first line of defense, traditionally function by engulfing pathogens and secreting antimicrobials. In 2004, a novel third mechanism was identified: the formation of NETs, which allow neutrophils to trap and kill extracellular pathogens. However, early in the COVID-19 pandemic, NETs were found to exacerbate inflammation and microvascular thrombosis, particularly in ARDS patients' lungs. Several drugs were shown to reduce NET formation, including colchicine, IL-1β blockers, and anakinra. The NIH COVID-19 Treatment Guidelines did not address NETs.

Other anticoagulation approaches discussed in the papers reviewed in "The Mouse that Roared" (R. L. Martin, unpublished report, 2025) lacked sufficient data for a clear assessment of their effectiveness. These included blood vessel dilation, antiplatelet therapies, plasma exchange, caplacizumab, and repurposed drugs used for conditions such as tapeworm (niclosamide), leprosy (clofazimine), multiple myeloma (bortezomib), and hypertension (bosentan). Two renal replacement therapies received FDA Emergency Use Authorization for COVID-19 but were later revoked.

Table 15. Heparin's effectiveness in COVID-19 patients by dosage

Medication effectiveness measures	Therapeutic dose compared to standard dose	Intermediate dose compared to therapeutic dose
VTE[a] risk	1.09 (0.58 – 2.02)	0.85 (0.52 – 1.38)
All-cause mortality	1.12 (0.75 – 1.67)	1.34 (0.83 – 2.17)
Bleeding risk	2.59 (1.87 – 3.57)	2.42 (1.58 – 3.70)

Notes: [a]Venous thromboembolism (VTE) is a condition in which a blood clot forms in a vein. VTE includes deep vein thrombosis (DVT) and pulmonary embolism. DVT occurs when a blood clot forms in a deep vein, usually in the lower leg, thigh, or pelvis. All data presented as odds ratio (95% CI). Table adopted from Chen *et al.*[54]

9. Popular but high-risk therapeutics

Some individuals tried certain therapeutics contrary to medical advice. A few of such therapeutics are listed in Table 16.

10. Future perspective

Presently available antivirals, when administered early and in conjunction with vaccination, have demonstrated considerable effectiveness in reducing the severity and progression of COVID-19. While the emergence of viral variants has rendered all monoclonal antibody therapies ineffective, the Mpro- and RdRp-targeting drugs have, to date, shown resilience to mutation. However, this resistance may not be permanent. Therefore, the proactive development of mutation-resistant antivirals remains a critical area of ongoing research. Notably, a wide range of Mpro-targeting therapeutics have been proposed, some of which claim inherent resistance to mutation and merit further investigation.

10.1. Future direction

Progress could be made by targeting NSPs, particularly NSP1 and the nucleocapsid protein. Inhibiting these proteins can effectively disrupt the virus's life cycle. Importantly, these proteins mutate less frequently than the spike protein.

10.2. Challenges

A major remaining therapeutic challenge in COVID-19 is hyperinflammation. While all approved drugs focus on

Table 16. Popular but high-risk therapeutics against COVID-19

Medication effectiveness measures	ClinicalTrials.gov			Google Scholar	"The Mouse That Roared"
	Total	Completed	Results		
Trump recommended					
Azithromycin	115	42	15	55,200	19
Hydroxychloroquine	237	85	29	64,200	32
Other					
Ivermectin	91	34	14	25,700	40

Note: Statistics from ClinicalTrials.gov, Google Scholar, and "The Mouse That Roared" (R. L. Martin, unpublished report, 2025), as of December 01, 2024.

Table 17. FDA-approved therapeutics against COVID-19

Therapeutics	Descriptions
Prevention	
mRNA vaccines	They are the most important drugs to prevent severe COVID-19 conditions.
Pemgarda	A monoclonal antibody for immunocompromised people. Originally, it showed 84% risk reduction through six months. However, its effectiveness is compromised by viral variants KP. 3.1.1 and XEC.
Suppression of viral replication and inflammation: Antivirals	
Monoclonal antibodies	Approximately 85% mortality reduction early in the COVID-19 pandemic. However, all but Pemgarda were eventually rendered ineffective by emerging variants.
Paxlovid	There are numerous assessments of its impact. One trial reported 89% mortality reduction among unvaccinated patients, in which 80% received Paxlovid and 20% received molnupiravir.
Remdesivir	It is often recommended in combination with another therapeutic and is the NIH's preferred option after Paxlovid. Administration must occur in a hospital setting.
Molnupiravir	It is an excellent alternative for patients who cannot administer Paxlovid.
Suppression of hyperinflammation: Anti-inflammatory agents	
Dexamethasone	None of these treatments is a magic bullet. Dexamethasone remains the most frequently used, followed by baricitinib. Recommendations for their use are quite complex, and remdesivir is often recommended alongside them.
Anakinra	
Baricitinib	
Tocilizumab	
Suppression of organ damage: Hypoxia	
ECMO	After other less aggressive oxygenation approaches have been attempted, ECMO is used. Early initiation of ECMO results in a 36% mortality rate compared to 58.9% with late initiation. Among patients receiving prolonged mechanical ventilation, one-year and five-year survival rates are 24.3% and 14.6%, respectively.
Vilobelimab	It is a monoclonal antibody that reduced 28-day mortality to 31.7%, compared to 41.6% in the placebo group.
Suppression of organ damage: Cardiovascular clotting	
Heparin	It must be used with extreme caution due to the risk of bleeding.

Abbreviations: ECMO: Extracorporeal membrane oxygenation; mRNA: Messenger RNA; NIH: National Institutes of Health.

mitigating its effects, none directly address its root causes. Moving forward, three promising strategies merit focused research and development:

(i) Prevent the dysregulation of the renin-angiotensin system
(ii) Protect the innate immune system from disruption by viral structural and NSPs
(iii) Target and inhibit highly inflammatory cytokines, particularly IL-6.

10.3. "Shoot for the Moon" program

Finally, a high-payoff strategy would be the development of antivirals targeting conserved regions of viruses, those that are stable across mutations and invariant among related coronaviruses. Furthermore, if such an antiviral completes the rigorous Phase 3 approval process for COVID-19, it may only require a Phase 2 trial for a related virus.

A proposed "Shoot for the Moon" program would support ambitious, long-range research aimed at developing broad-spectrum, pan-virus antivirals, especially against the most dangerous viral families, such as those that include Ebola and Marburg.

11. Conclusion

Even though there were 4,855 FDA-registered COVID-19 clinical trials through October 2024, no new therapeutics received FDA or EU approval during the pandemic. Fortunately, the pre-existing arsenal of therapeutics has proven effective, particularly when deployed early in the course of the disease. Table 17 summarizes all FDA-approved or FDA-cleared (in the case of ECMO) COVID-19 therapeutics.

Although the NIH is silent on the following promising therapeutics, they merit consideration. They have demonstrated positive impacts with minimal or no downsides, making them, in effect, Pascal's Wagers. These therapeutics are:

(i) Iodine nasal spray or gargle: Use before and after high-risk exposures.
(ii) Metformin: It also shows promise in cancer prevention.

(iii) Probiotics: While the evidence is less robust, they support gut health and may aid immune function with little risk involved.

Acknowledgments

None.

Funding

None.

Conflict of interest

The author declares no competing interests.

Author contributions

This is a single-authored article.

Ethics approval and consent to participate

Not applicable.

Consent for publication

Not applicable.

Availability of data

Data used in this work is available from the corresponding author upon reasonable request.

References

1. Pearson H. *How COVID Broke the Evidence Pipeline, Nature News;* 2021. Available from: https://www.nature.com/articles/d41586-021-01246-x
2. Meiraa DD, Zetuma AS, Casottia MC, *et al*. Bioinformatics and molecular biology tools for diagnosis, prevention, treatment and prognosis of COVID-19. *Heliyon*. 2024;10(14):e34393.

   doi: 10.1016/j.heliyon.2024.e34393
3. Sertkaya A, Birkenbach A, Berlind A, Eyraud J. *Examination of Clinical Trial Costs and Barriers for Drug Development, Assistant Secretary for Planning and Evaluation*; 2014. Available from: https://aspe.hhs.gov/reports/examination/clinical/trial/costs/barriers/drug/development/0
4. Drayman N, Demarco JK, Jones KA, *et al*. Masitinib is a broad coronavirus 3CL inhibitor that blocks replication of SARS-CoV-2. *Science*. 2021;373(6557):931-936.

   doi: 10.1126/science.abg5827
5. Yao T, Ma Z, Lan K, Guo Y, Liu L. *Neutralizing Activity and Viral Escape of Pemivibart by SARS-CoV-2 JN.1 Sublineages*. bioRxiv [Preprint]; 2024.

   doi: 10.1101/2024.11.08.622746
6. Pelletier JS, Tessema B, Frank S, Westover JB, Brown SM, Capriotti JA. Efficacy of povidone-iodine nasal and oral antiseptic preparations against severe acute respiratory syndrome-coronavirus 2 (SARS-CoV-2). *Ear Nose Throat J*. 2020;100(Suppl 2):192S-196S.

   doi: 10.1177/0145561320957237
7. Baxter AL, Schwartz KR, Johnson RW, *et al*. Rapid initiation of nasal saline irrigation to reduce severity in high-risk COVID+ outpatients. *Ear Nose Throat J*. 2022;103(Suppl 1):30S-39S.

   doi: 10.1177/014556132211237
8. Louca P, Murray B, Klaser K, *et al*. *Dietary Supplements During the COVID-19 Pandemic: Insights from 1.4M Users of the COVID Symptom Study App - a Longitudinal App-Based Community Survey*. medRxiv; 2020.

   doi: 10.1101/2020.11.27.20239087
9. Curtisa N, Sparrowd A, Ghebreyesuse TA, Netea MG. Considering BCG vaccination to reduce the impact of COVID-19. *Lancet*. 2020;395(10236):1545-1546.

   doi: 10.1016/S0140-6736(20)31025-4
10. Ledesma JR, Lurie P, Yorlets RR, Daly G, Chrysanthopoulou S, Lurie MN. Spurious early ecological association suggesting BCG vaccination effectiveness for COVID-19. *PLoS One*. 2022;17:e0274900.

    doi: 10.1371/journal.pone.0274900
11. Al-Horani RA, Kar S, Aliter KF. Potential anti-COVID-19 therapeutics that block the early stage of the viral life cycle: Structures, mechanisms, and clinical trials. *Int J Mol Sci*. 2020;21(15):5224.

    doi: 10.3390/ijms21155224
12. Wang M, Cao R, Zhang L, *et al*. Remdesivir and chloroquine effectively inhibit the recently emerged novel coronavirus (2019-nCoV) *in vitro*. *Cell Res*. 2020;30:269-271.

    doi: 10.1038/s41422-020-0282-0
13. Zhang L, Lin D, Sun X, *et al*. Crystal structure of SARS-CoV-2 main protease provides a basis for design of improved α-ketoamide inhibitors. *Science*. 2020;368(6489):409-412.

    doi: 10.1126/science.abb3405
14. Du L, He Y, Zhou Y, Liu S, Zheng BJ, Jiang S. The spike protein of SARS-CoV--a target for vaccine and therapeutic development. *Nat Rev Microbiol*. 2020;7:226-236.

    doi: 10.1038/nrmicro2090
15. Lyu X, Zhao Q, Hui J, *et al*. The global landscape of approved antibody therapies. *Antib Ther*. 2022;5(4):233-257.

    doi: 10.1093/abt/tbac021
16. Lederhofer J, Tsybovsky Y, Nguyen L, *et al*. Protective human monoclonal antibodies target conserved sites of vulnerability on the underside of influenza virus neuraminidase. *Immunity*. 2024;57(3):574-586.

doi: 10.1016/j.immuni.2024.02.003

17. Recovery Collaborative Group. Casirivimab and imdevimab in patients admitted to hospital with COVID-19 (RECOVERY): A randomized, controlled, open-label, platform trial. *Lancet*. 2022;399(10325):P665-P676.

18. Dougan M, Nirula A, Azizad M, *et al*. Bamlanivimab plus etesevimab in mild or moderate COVID-19. *N Engl J Med*. 2021;385:1382-1392.

doi: 10.1056/NEJMoa2102685

19. Gupta A, Gonzalez-Rojas Y, Juarez E, *et al*. Early treatment for COVID-19 with SARS-CoV-2 neutralizing antibody sotrovimab. *N Engl J Med*. 2021;385:1941-1950.

doi: 10.1056/NEJMoa2107934

20. Levin MJ, Ustianowski A, De Wit S, *et al*. Intramuscular AZD7442 (tixagevimab-cilgavimab) for prevention of COVID-19. *N Engl J Med*. 2022;386:2188-2200.

doi: 10.1056/NEJMoa2116620

21. Yadav R, Chaudhary JK, Jain N, *et al*. Role of structural and non-structural proteins and therapeutic targets for SARS-CoV-2 for COVID-19. *Cells*. 2021;1(4):821.

doi: 10.3390/cells10040821

22. Hammond J, Leister-Tebbe H, Gardner A, *et al*. Oral nirmatrelvir for high-risk, nonhospitalized adults with COVID-19. *N Engl J Med*. 2022;386:1397-1408.

doi: 10.1056/NEJMoa2118542

23. Lewnard JA, McLaughlin JM, Malden D, *et al*. Effectiveness of nirmatrelvir-ritonavir in preventing hospital admissions and deaths in people with COVID-19: A cohort study in a large US health-care system. *Lancet Infect Dis*. 2023;23(7):806-815.

doi: 10.1016/S1473-3099(23)00118-4

24. Smith DJ, Lambrou A, Patel P. SARS-CoV-2 rebound with and without use of COVID-19 oral antivirals. *MMW Morb Mortal Wkly Rep.* 2023;72(51):1357-1364.

doi: 10.15585/mmwr.mm7251a1

25. Shah MM, Joyce B, Plumb ID, *et al*. Paxlovid associated with decreased hospitalization rate among adults with COVID-19 - United States, April-September 2022. *Am J Transplant*. 2023;23(1):150-155.

doi: 10.1016/j.ajt.2022.12.004.CDC

26. Leonhardt D. *The Power of Paxlovid, NY Times*; 2022. Available from: https://www.nytimes.com/2022/10/07/briefing/covid-treatment-paxlovid.html

27. Beigel JH, Tomashek KM, Dodd LE, *et al*. Remdesivir for the treatment of COVID-19 - final report. *N Engl J Med*. 2020;383:1813-1826.

doi: 10.1056/NEJMoa2007764

28. Rajme-López S, Martinez-Guerra BA, Román-Montes CM, *et al*. Nirmatrelvir/ritonavir and remdesivir against symptomatic treatment in high-risk COVID-19 outpatients to prevent hospitalization or death during the Omicron era: A propensity score-matched study. *Ther Adv Infect Dis*. 2024;11.

doi: 1177/20499361241236582

29. Jayk Bernal A, Gomes Da Silva MM, Musungaie DB, *et al*. Molnupiravir for oral treatment of COVID-19 in nonhospitalized patients. *N Engl J Med*. 2022;386:509-520.

doi: 10.1056/NEJMoa2116044

30. Wang L, Berger NA, Davis PB, Kaelber DC, Volkow ND, Xu R. *COVID-19 Rebound after Paxlovid and Molnupiravir during January-June 2022*. medRxiv [Preprint]; 2022.

doi: 10.1101/2022.06.21.22276724

31. Gruber CEM, Tucci FG, Giombini E, *et al*. Molnupiravir increases SARS-CoV-2 genome diversity and complexity: A case-control cohort study. *J Med Virol*. 2024;96(5):e29642.

doi: 10.1002/jmv.29642

32. Kamyshnyi A, Koval H, Kobevko O, *et al*. Therapeutic effectiveness of interferon-α2b against COVID-19 with community-acquired pneumonia: The Ukrainian experience. *Int J Mol Sci*. 2023;24(8):6887.

doi: 10.3390/ijms24086887

33. REMAP-CAP Investigators, Hills TE, Lorenzi E, *et al*. The REMAP-CAP investigators, simvastatin in critically Ill patients with COVID-19. *N Engl J Med*. 2023;389:2341-2354.

doi: 10.1056/NEJMoa2309995

34. Mihalek N, Radovanović D, Barak O, Čolović P, Huber M, Erdoes G. Convalescent plasma and all-cause mortality of COVID-19 patients: Systematic review and meta-analysis. *Sci Rep.* 2023;13:12904.

doi: 10.1038/s41598-023-40009-8

35. Cai Q, Yang M, Liu D, *et al*. Experimental treatment with favipiravir for COVID-19: An open-label control study. *Engineering (Beijing)*. 2020;6(10):1192-1198.

doi: 10.1016/j.eng.2020.03.007

36. Basheer M, Saad E, Assy N. The cytokine storm in COVID-19: The strongest link to morbidity and mortality in the current epidemic. *COVID 2022.* 2022;2(5):540-552.

doi: 10.3390/covid2050040

37. Venegas-Rodríguez R, Serrano-Díaz A, Peña-Ruiz R, *et al*. Jusvinza, an anti-inflammatory drug derived from the human heat-shock protein 60, for critically ill COVID-19 patients. An observational study. *PLoS One*. 2023;18(2):e0281111.

doi: 10.1371/journal.pone.0281111

38. Grosso D, Wagner JL, O'Connor A, *et al*. Safety and feasibility of third-party cytotoxic T lymphocytes for high-risk patients with COVID-19. *Blood Adv*. 2024;8(15):4113-4124.

doi: 10.1182/bloodadvances.2024013344

39. Rosée FL, Bremer HC, Gehrke I, *et al*. The janus kinase 1/2 inhibitor ruxolitinib in COVID-19 with severe systemic hyperinflammation. *Nat Leuk*. 2020;34:1805-1815.

doi: 10.1038/s41375-020-0891-0

40. Mariette X, Hermine O, Tharaux PL, *et al*. Effectiveness of tocilizumab in patients hospitalized with COVID-19: A follow-up of the CORIMUNO-TOCI-1 randomized clinical trial. *JAMA Intern Med*. 2021;181(9):1241-1243.

doi: 10.1001/jamainternmed.2021.2209

41. Salama C, Han J, Yau L, *et al*. Tocilizumab in patients hospitalized with COVID-19 pneumonia. *N Engl J Med*. 2020;384(1):20-30.

doi: 10.1056/NEJMoa2030340

42. Stone JH, Frigault MJ, Serling-Boyd NJ, *et al*. Efficacy of tocilizumab in patients hospitalized with COVID-19. *N Engl J Med*. 2020;383(24):2333-2344.

doi: 10.1056/NEJMoa2028836

43. Kyriazopoulou E, Huet T, Cavalli G, *et al*. Effect of anakinra on mortality in patients with COVID-19: A systematic review and patient-level meta-analysis. *Lancet Rheumatol*. 2021;3(10):690-697.

doi: 10.1016/S2665-9913(21)00216-2

44. Kalil AC, Patterson TF, Mehta AK, *et al*. Baricitinib plus remdesivir for hospitalized adults with COVID-19. *N Engl J Med*. 2020;384(9):795-807.

doi: 10.1056/NEJMoa2031994

45. Recovery Collaborative Group, Horby P, Lim WS, *et al*. Dexamethasone in hospitalized patients with COVID-19. *N Engl J Med*. 2020;384(8):693-704.

doi: 10.1056/NEJMoa2021436

46. Aghasadeghi MR, Zaheri Birgani MA, Jamalimoghadamsiyahkali S, *et al*. Effect of high-dose Spirulina supplementation on hospitalized adults with COVID-19: A randomized controlled trial. *Front Immunol*. 2024;15:1332425.

doi: 10.3389/fimmu.2024.1332425

47. Bramante CT, Beckman KB, Mehta T, *et al*. *Metformin Reduces SARS-CoV-2 in a Phase 3 Randomized Placebo Controlled Clinical Trial*. medRxiv [Preprint]; 2023.

doi: 10.1101/2023.06.06.23290989

48. Martinson ML, Lapham J. Prevalence of immunosuppression among US adults. *JAMA*. 2024;33(10):880-882.

doi: 10.1001/jama.2023.28019

49. Feth M, Weaver N, Fanning RB, *et al*. Hemorrhage and thrombosis in COVID-19-patients supported with extracorporeal membrane oxygenation: An international study based on the COVID-19 critical care consortium. *BMC J Intensive Care*. 2024;12:18.

doi: 10.1186/s40560-024-00726-2

50. Staudacher DL, Felder M, Jäckel M, *et al*. Quality of life and mental health in COVID-ARDS survivors after V-V ECMO support: Results from the Freiburg ECMO outcome study (FEOS). *J Clin Med*. 2025;4(7):2206.

doi: 10.3390/jcm14072206

51. Burša F, Frelich M, Sklienka P, Jor O, Máca J. Long-term outcomes of extracorporeal life support in respiratory failure. *J Clin Med*. 2023;12(16):5196.

doi: 10.3390/jcm12165196

52. Vlaar APJ, Witzenrath M, Van Paassen P, *et al*. Anti-C5a antibody (vilobelimab) therapy for critically ill, invasively mechanically ventilated patients with COVID-19 (PANAMO): A multicenter, double-blind, randomized, placebo-controlled, phase 3 trial. *Lancet Respir Med*. 2022;12:1137-1146.

doi: 10.1016/S2213-2600(22)00297-1

53. REMAP-CAP Investigators, ACTIV-4a Investigators, ATTACC Investigators, *et al*. Therapeutic anticoagulation with heparin in critically Ill patients with COVID-19. *N Engl J Med*. 2021;385(9):777-789.

doi: 10.1056/NEJMoa2103417

54. Chen X, Zhang S, Liu H, *et al*. Effect of anticoagulation on the incidence of venous thromboembolism, major bleeding, and mortality among hospitalized COVID-19 patients: An updated meta-analysis. *Front Cardiovasc Med*. 2024;11:1381408.

doi: 10.3389/fcvm.2024.1381408

ACCSCIENCE PUBLISHING

Innovative Medicines & Omics

REVIEW ARTICLE

Pathogenesis, diagnosis, treatment, and herbal interventions for rheumatoid arthritis: A review

Brahmjot Singh*, Kiranjot Kaur, Sukhmandeep Kaur, and Kunal Mistry

Department of Pharmaceutical Sciences, Faculty of Life Sciences, Guru Nanak Dev University, Amritsar, Punjab, India

Abstract

Rheumatoid arthritis (RA) is a chronic autoimmune inflammatory disorder primarily targeting synovial joints, resulting in pain, stiffness, swelling, and progressive joint destruction. The disease is driven by proinflammatory cytokines such as interleukin (IL)-1β and IL-6, which promote synovial inflammation and cartilage degradation. RA affects not only the joints but also other organs, contributing to systemic complications such as cardiovascular disease, anemia, and osteoporosis. Despite the availability of disease-modifying antirheumatic drugs and biologics, their efficacy is often incomplete and frequently accompanied by adverse effects and high costs. This study presents a detailed overview of the etiology, pathogenesis, clinical manifestations, diagnostic strategies, and current treatment modalities of RA, emphasizing herbal medicine as a complementary approach. Botanicals with immunomodulatory and anti-inflammatory properties offer promising adjunctive benefits in RA management. Natural products such as *Curcuma longa*, *Aloe barbadensis*, and *Zingiber officinale* exhibit significant potential to reduce inflammation, modulate cytokine production, and improve patient outcomes. This review highlights the therapeutic promise of integrating herbal remedies with conventional pharmacological therapies, promoting a more holistic, effective, and safer management of RA.

Keywords: Rheumatoid arthritis; Autoimmune disease; Cytokines; Disease-modifying antirheumatic drug; Herbal medicine; Synovial inflammation

***Corresponding author:**
Brahmjot Singh
(brahmjot.pharma@gndu.ac.in)

Citation: Singh B, Kaur K, Kaur S, Mistry K. Pathogenesis, diagnosis, treatment, and herbal interventions for rheumatoid arthritis: A review. *Innov Med Omics*. 2025;2(4):25-35. doi: 10.36922/IMO025280031

Received: July 9, 2025

1st revised: August 13, 2025

2nd revised: August 15, 2025

Accepted: August 19, 2025

Published online: September 22, 2025

1. Introduction

Rheumatoid arthritis (RA) is a chronic, progressive autoimmune inflammatory disorder that primarily targets synovial joints. It also manifests systemically, affecting organs such as the lungs, heart, and eyes, leading to debilitating outcomes, including chronic pain, stiffness, joint deformities, reduced mobility, and a substantial decline in quality of life. Pathologically, RA involves persistent synovial inflammation driven by autoantibodies, T cell and B cell activation, and proinflammatory cytokines, notably interleukin (IL) 6 and tumor necrosis factor-alpha (TNF-α), resulting in cartilage and bone erosion.[1]

RA affects women 2–3 times more than men, with peak onset between the third and fifth decades of life.[2] Globally, RA is ranked among the leading causes of disability-adjusted life years due to musculoskeletal conditions. According to the Global Burden of Disease Study 2021, approximately 17.6 million people worldwide were living with

RA in 2020, and this number is projected to exceed 31 million by 2050 if current trends persist.[3] In India, recent systematic analyses estimate RA prevalence at 0.5–0.75%, with some urban and northern populations showing rates as high as 1%.[4,5]

Despite advances in therapeutics, including conventional disease-modifying antirheumatic drugs (DMARDs) and biologics, a significant proportion of RA patients continue to experience suboptimal disease control, adverse effects, or economic barriers to sustained treatment access.[6,7] These limitations underscore the growing interest in integrating complementary and alternative therapies, including herbal medicines, which offer immunomodulatory, anti-inflammatory, and antioxidant benefits with comparatively fewer side effects.[8]

Importantly, early diagnosis remains vital, as delayed intervention is associated with irreversible joint damage and systemic complications such as anemia, osteoporosis, cardiovascular disease, and increased mortality. The emergence of biomarkers such as rheumatoid factor (RF) and anti-cyclic citrullinated peptide antibodies (ACPA) has enhanced diagnostic accuracy, though challenges persist in early-stage and seronegative cases.[9]

A recent review by Kaur *et al.* also discloses the pathophysiology, diagnosis, and herbal medicine-based therapeutic implications of RA, emphasizing the role of phytoconstituents.[10] In contrast, this manuscript discusses major medicinal plants, rather than only their isolated phytoconstituents, and integrates detailed discussions on RA pathogenesis, diagnostic approaches, conventional pharmacological treatments, and herbal interventions. This broader scope aims to provide a comprehensive, clinically oriented perspective, particularly relevant for settings where whole-plant preparations are more accessible than purified compounds.

The present review not only provides a comprehensive examination of the pathogenesis, clinical features, and current treatment landscape of RA but also critically evaluates the therapeutic potential of herbal interventions as adjunctive or alternative strategies. In doing so, it aims to foster a more holistic and personalized approach to RA management.

2. Risk factors for RA

RA is a multifactorial autoimmune condition with a complex etiology involving genetic predisposition, epigenetic regulation, environmental exposures, socioeconomic and occupational influences, lifestyle behaviors, and nutritional status (Figure 1). Understanding these risk factors is critical for early diagnosis and for developing preventive strategies.

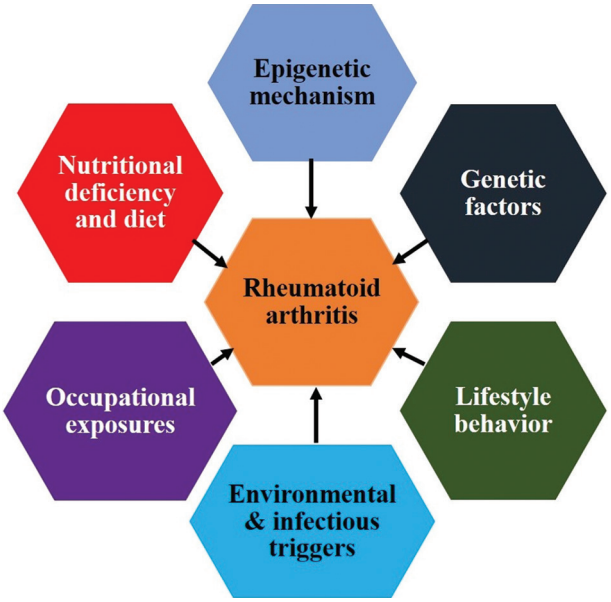

Figure 1. Various risk factors for rheumatoid arthritis

2.1. Genetic factors

Genetics plays a pivotal role in RA susceptibility. Monozygotic twins exhibit concordance rates between 9% and 15%, significantly higher than the 2–4% observed in dizygotic twins, confirming heritability. The *HLA-DRB1* gene within the major histocompatibility complex remains the most influential genetic locus, accounting for up to one-third of the genetic risk. Recent genome-wide association studies have identified over 100 RA-associated loci, with new candidate genes, such as *PTPN22*, *STAT4*, *IRF5*, and *CCR6*, linked to immune dysregulation and disease severity.[11]

2.2. Epigenetic mechanisms

Epigenetic modifications such as DNA methylation, histone modifications, and non-coding RNAs can influence RA development without altering DNA sequences. Environmental exposures such as smoking or poor diet can induce these epigenetic changes, thereby modulating gene expression relevant to RA onset.[12]

2.3. Environmental and infectious triggers

Pathogens, including *Porphyromonas gingivalis*, *Proteus mirabilis*, and *Mycoplasma*, have been linked to autoimmune activation in RA, potentially through mechanisms such as molecular mimicry and bystander activation. Chronic exposure to air pollutants, notably particulate matter (PM2.5), ozone, and nitrogen dioxide, is associated with heightened RA risk, especially in urban environments.[13]

2.4. Socioeconomic status

Lower socioeconomic status correlates with delayed RA diagnosis and poorer disease outcomes. Factors include limited health-care access, higher smoking rates, and poor nutritional habits. High socioeconomic status, conversely, is associated with early disease recognition and better management.[14]

2.5. Occupational exposures

Individuals working in industries with silica dust, organic solvents, or mineral oil exposure show significantly higher RA incidence. The chronic inhalation of silica particles stimulates immune responses via IL and TNF-α pathways, thereby triggering systemic inflammation.[15]

2.6. Lifestyle behaviors

Cigarette smoking remains the strongest modifiable risk factor. It promotes oxidative stress, citrullination, and *HLA-DRB1* shared epitope gene interactions, increasing susceptibility, especially to seropositive RA. Alcohol consumption presents conflicting findings; while excessive intake may exacerbate inflammation, moderate intake has been inversely associated with RA development in some populations.[16]

2.7. Nutritional deficiencies and diet

Vitamin D deficiency is implicated in RA pathogenesis due to its role in immune regulation. Recent trials suggest that long-term Vitamin D supplementation may reduce RA incidence by up to 40%. In addition, adherence to the Mediterranean diet—rich in olive oil, fish, and omega-3 fatty acids—has shown anti-inflammatory effects and protective potential against RA.[17] Conversely, Western diets high in sodium, saturated fats, and red meat are positively associated with systemic inflammation and RA risk.[18]

3. Pathophysiology of RA

RA is characterized by a cascade of aberrant immune events targeting synovial joints and progressing to systemic manifestations. The condition initiates with immune dysregulation involving antigen-presenting cells and T lymphocytes, leading to chronic synovitis and eventual destruction of cartilage and bone.[19]

3.1. Initiation and synovial inflammation

The disease begins when antigen-presenting dendritic cells capture autoantigens in genetically susceptible individuals. These dendritic cells mature and present peptides via major histocompatibility complex class II molecules to naïve $CD4^+$ T cells in lymphoid tissue, driving differentiation into T helper (Th) 1 and Th17 subsets, which secrete proinflammatory cytokines such as interferon-γ, IL-17, and TNF-α. These cytokines recruit additional immune cells, amplify inflammation, and mediate endothelial activation.[20,21]

3.2. Synovial hyperplasia and pannus formation

Activated T cells, along with B cells and macrophages, infiltrate the synovial membrane, triggering fibroblast-like synoviocytes to proliferate and form the pannus, a granulation tissue that invades cartilage and bone. Fibroblast-like synoviocytes secrete matrix metalloproteinases (MMPs) and inflammatory cytokines (IL-6, IL-15, and IL-18), further accelerating cartilage degradation.[22]

3.3. Role of cytokines

Cytokines are pivotal in sustaining chronic inflammation (Table 1). TNF-α and IL-1β drive leukocyte recruitment, osteoclast activation, and systemic effects such as fever and cachexia. IL-6 amplifies B cell differentiation and acute-phase responses, whereas IL-17, secreted by Th17 cells, enhances neutrophil recruitment and angiogenesis within the synovium. These cytokines act synergistically, promoting joint destruction.[23]

3.4. Contributions of immune cells

B cells produce RF and ACPA, initiating immune complex formation and complement activation. They also act as antigen-presenting cells and release pro-osteoclastogenic cytokines like receptor activator of nuclear factor-κB ligand, facilitating bone erosion.[24] Macrophages in the synovium are major producers of TNF-α, IL-1, and IL-6; their density correlates with disease activity.[25] Osteoclasts differentiate under the influence of receptor activator of nuclear factor-κB and TNF-α and are responsible for bone resorption at the cartilage-bone interface.[26]

3.5. Systemic effects and extra-articular manifestations

The systemic release of cytokines contributes to the development of anemia of chronic disease, fatigue,

Table 1. Various cytokines in the pathophysiology of rheumatoid arthritis

Key cytokines	Roles in rheumatoid arthritis
TNF-α	Synovial inflammation, joint destruction
IL-1	Enhances osteoclastogenesis, cartilage damage
IL-6	Acute-phase response, B-cell maturation
IL-17	Neutrophil recruitment, angiogenesis
IL-12/IL-23	Promotes Th1 and Th17 responses

Abbreviations: IL: Interleukin; Th: T helper; TNF: Tumor necrosis factor

osteoporosis, atherosclerosis, and depression. Common extra-articular features include rheumatoid nodules, interstitial lung disease, vasculitis, and pericarditis.[27]

4. Diagnosis of RA

Early and accurate diagnosis of RA is critical to reducing irreversible joint damage, preserving function, and improving long-term outcomes. Diagnostic protocols rely on a multifaceted clinical-laboratory-imaging approach and internationally accepted classification criteria.

4.1. Clinical assessment

Patients often present with symmetrical joint pain, morning stiffness lasting over 30 min, fatigue, fever, and generalized malaise. A high index of suspicion is essential, particularly when patients show polyarticular involvement of small joints like those of the hands and feet. Studies report that early diagnosis and intervention can prevent long-term disability in over 90% of RA patients.[28]

4.2. Laboratory tests

RF and ACPA are critical serological markers. While RF lacks specificity, ACPA has over 95% specificity, making it a key diagnostic biomarker.[29] C-reactive protein (CRP) and erythrocyte sedimentation rate are used to assess systemic inflammation. Elevated levels correlate with disease activity and prognosis.[30]

Recent advances have included novel autoantibodies such as anti-carbamylated protein antibodies, which may offer added sensitivity in seronegative RA cases.[31]

4.3. Imaging techniques

Ultrasound is widely used for both diagnosis and disease monitoring. Power Doppler ultrasound detects active synovitis and neovascularization; grayscale imaging identifies joint effusion and bone erosions. It is cost-effective and non-invasive but operator-dependent.[32]

Magnetic resonance imaging is highly sensitive in early RA and can detect synovial hypertrophy, bone marrow edema, and early erosions before they appear on X-ray. However, limitations include high cost and limited availability.[33] X-rays remain a standard tool for documenting joint space narrowing, periarticular osteopenia, and bony erosions, but lack sensitivity in early disease.[34]

4.4. The 2010 American College of Rheumatology/ European League Against Rheumatism classification criteria

The 2010 American College of Rheumatology/European League Against Rheumatism classification criteria[35] provide a scoring system out of 10 based on joint involvement (up to five points), serology (RF and ACPA; up to three points), acute-phase reactants (CRP and erythrocyte sedimentation rate; one point), and symptom duration ≥6 weeks (1 point).

A score of more than six is required for RA classification, provided other differential diagnoses such as lupus, psoriatic arthritis, and infection are ruled out.

4.5. Recent diagnostic enhancements

Artificial intelligence-driven algorithms are emerging to automate joint scoring in radiographic and ultrasound imaging.[36] Biomarker panels using multiplex platforms now aim to improve sensitivity in early or seronegative RA cases.[37]

5. Treatment of RA

The therapeutic goal in RA is to induce remission or, at a minimum, achieve low disease activity within the first 6 months of diagnosis to prevent irreversible joint deformity, disability, and systemic complications. Studies have shown that 80% of inadequately treated patients develop joint deformities, and 40% become disabled within 10 years.

Historically, RA management followed a step-wise approach: Starting with non-steroidal anti-inflammatory drugs (NSAIDs) and escalating to DMARDs as the disease progressed. This delayed strategy resulted in poor long-term outcomes.[38] The current Treat-to-Target paradigm, endorsed by the American College of Rheumatology and the European League Against Rheumatism, emphasizes early initiation of DMARDs and regular monitoring to adjust therapy promptly.[39]

5.1. Pharmacological treatments

5.1.1. NSAIDs

NSAIDs provide symptomatic relief from pain and stiffness but do not prevent joint damage. Common agents include ibuprofen, naproxen, diclofenac, and celecoxib. Cyclooxygenase (COX)-2 inhibitors (e.g., celecoxib) offer reduced gastrointestinal toxicity. NSAIDs are best used for initial symptom control while awaiting the effect of slower-acting DMARDs.[40]

5.1.2. Glucocorticoids

Glucocorticoids such as prednisone are effective for short-term symptom control and bridging therapy. However, long-term use is associated with osteoporosis, diabetes, and hypertension. Tapering is recommended as DMARDs take effect.[41]

5.1.3. Conventional synthetic DMARDs

Methotrexate is the first-line anchor drug. It inhibits dihydrofolate reductase, limiting lymphocyte proliferation. Folic acid coadministration reduces adverse effects. Methotrexate monotherapy is effective for most early RA cases.[42] Hydroxychloroquine, an antimalarial agent, modulates antigen presentation and inhibits monocyte cytokine secretion, reducing Th17-related cytokines.[43] In addition, sulfasalazine interferes with cytokine production (IL-8, monocyte chemoattractant protein), though mechanisms remain unclear. They are often combined with methotrexate in dual or triple therapy.[44] Leflunomide inhibits pyrimidine synthesis, suppressing T cell proliferation. However, it can be hepatotoxic and teratogenic.[45] Combination conventional synthetic DMARD therapy is more effective than monotherapy for moderate-to-severe RA.

5.1.4. Biological DMARDs

Biologics target specific immune pathways and are reserved for moderate-to-severe RA unresponsive to conventional synthetic DMARDs. TNF-α inhibitors (e.g., infliximab, adalimumab, and etanercept) block inflammation mediators and slow radiographic progression.[46] IL-6 inhibitors (e.g., tocilizumab) inhibit IL-6 signaling, reducing joint damage and systemic symptoms.[47] B cell depletion agents (e.g., rituximab) target $CD20^+$ B cells to reduce autoantibody production,[48] whereas T cell co-stimulation blockers (e.g., abatacept) inhibit CD28-CD80/86 signaling to prevent T cell activation.[49]

Recent biologics, although effective, are expensive and associated with immunosuppression risks, including tuberculosis and reactivation of latent infections.

5.1.5. Targeted synthetic DMARDs

Targeted synthetic DMARDs include Janus kinase inhibitors, such as tofacitinib and baricitinib, which block intracellular cytokine signaling. They offer oral convenience but may increase the risk of herpes zoster and thromboembolic events.[50]

5.2. Non-pharmacological approaches

A comprehensive RA management plan includes physical therapy to maintain joint mobility, occupational therapy for assistive device training, patient education to promote adherence, and dietary interventions, such as omega-3 fatty acids, for anti-inflammatory benefits.[51] Exercise and lifestyle modification significantly reduce fatigue and improve physical function.

6. Role of herbal and plant-based therapies in the management of RA

The limitations of conventional therapies such as NSAIDs and DMARDs—including partial symptom relief, long-term toxicity, and economic burden—have catalyzed global interest in complementary and alternative medicine. Among these, herbal plants (Table 2) offer anti-inflammatory, antioxidant, and immunomodulatory effects, making them promising candidates for adjunctive RA management.

6.1. *Curcuma longa* (Turmeric)

Curcumin, the active polyphenol in turmeric, has demonstrated potent inhibition of nuclear factor kappa B (NF-Kb) activation, suppression of COX-2 expression, and decreased production of prostaglandin E2 and IL-6, all key mediators in RA pathogenesis. In a collagen-induced arthritis (CIA) rat model, curcumin reduced arthritic scores in a dose-dependent manner, with the 110 mg/kg group showing the greatest anti-inflammatory benefit.[52]

6.2. *Aloe barbadensis* (Aloe vera)

Aloe demonstrates immunosuppressive, anti-inflammatory, and regenerative properties. It modulates mast cell activity, reduces TNF-α, and enhances fibroblast-mediated tissue repair. In animal studies, aloe extract led to a 50% reduction in synovial pouch vascularity, suggesting its potential in mitigating synovial inflammation.[53]

6.3. *Zingiber officinale* (Ginger)

Ginger contains gingerols and shogaols, which inhibit both prostaglandin and leukotriene biosynthesis. Diarylheptanoids in ginger have been shown to suppress 5-lipoxygenase, reducing inflammatory mediator production. Clinical trials have demonstrated its capacity to relieve joint pain and decrease markers of systemic inflammation.[54]

6.4. *Ginkgo biloba*

Ginkgo exerts its anti-RA effects through inhibition of mitogen-activated protein kinase/c-Jun N-terminal kinase and Wnt5a pathways, promoting apoptosis of synovial fibroblasts and reducing levels of MMP-3, IL-1β, IL-6, and TNF-α. This confirmed its efficacy in CIA mouse models by demonstrating reduced joint swelling and improved cartilage integrity.[55]

6.5. *Camellia sinensis* (Green tea)

Epigallocatechin-3-gallate, the active flavonoid in green tea, blocks NF-κB and TNF-α signaling pathways. It

Table 2. Herbal and plant-based therapies for rheumatoid arthritis

Plant name	Active components	Mechanism of action	Observed effects	References
Curcuma longa (Turmeric)	Curcumin	Inhibits NF-κB, COX-2, IL-6, and prostaglandin 2	Reduced arthritis score and inflammation in the CIA model	51
Aloe barbadensis (Aloe vera)	Polysaccharides, glycoproteins	Decreases TNF-α, modulates mast cells, and enhances repair	A 50% reduction in synovial vascularity in animal models	52
Zingiber officinale (Ginger)	Gingerols, shogaols	Inhibits prostaglandin and leukotriene biosynthesis	Reduced joint pain and inflammatory markers	53
Ginkgo biloba	Ginkgolides, flavonoids	Inhibits mitogen-activated protein kinase/c-Jun N-terminal kinase, Wnt5a; reduces IL-6, MMP-3	Decreased synovitis and improved cartilage	54
Camellia sinensis (Green tea)	Epigallocatechin-3-gallate	Inhibits NF-κB, TNF-α; antioxidant	Reduced leukocyte infiltration in joints	55
Crocus sativus (Saffron)	Crocin	Suppresses TNF-α, IL-1β	Decreased joint swelling and hyperplasia	56
Cannabis sativa	Cannabidiol, tetrahydrocannabinol	Cannabinoid receptor 2 agonist; reduces immune activation	Anti-inflammatory and analgesic effects	57
Arnica montana	Helenalin	Inhibits nitric oxide, TNF-α, and IL-6	Reduced oxidative stress and inflammation	58
Jatropha gossypifolia	Flavonoids	Inhibits lipid peroxidation and reactive oxygen species	Reduced paw edema in animal models	59
Nigella sativa (Black seed)	Thymoquinone	Inhibits IL-6 and TNF-α	A 45% reduction in arthritic score	60
Withania somnifera (Ashwagandha)	Withanolides	Modulates TNF-α, IL-1β; boosts regulatory T cells	A 36% reduction in paw swelling	61
Boswellia serrata	Boswellic acids	Inhibits 5-lipoxygenase, Th17 activity	A>30% reduction in joint stiffness	62
Perilla frutescens (Shiso)	Rosmarinic acid	Inhibits NF-κB, reduces IL-6, IL-1β	Improved cartilage, reduced inflammation	63
Tribulus terrestris	Saponins, Protodioscin	Inhibits COX and lipoxygenase enzymes	Reduced edema and histopathology score	64
Tinospora cordifolia (Guduchi)	Tinosporide, berberine-like alkaloids	Modulates Th1/Th2, reduces TNF-α	Lower arthritis score and oxidative stress	65
Sigesbeckia orientalis	Darutoside	Reduces MMP-9, angiogenesis, and immune infiltration	Reduced joint damage and stiffness	66
Uncaria tomentosa (Cat's Claw)	Oxindole alkaloids	Inhibits TNF-α, MMP-9; antioxidant	Reduced fatigue, improved pain scores	67

Abbreviations: COX: Cyclooxygenase; IL: Interleukin; MMP: Matrix metalloproteinase; NF-κB: Nuclear factor kappa B; Th: T helper cells; TNF: Tumor necrosis factor.

reduces leukocyte recruitment to inflamed joints and has shown positive outcomes in both *in vivo* and *in vitro* arthritic models.[56]

6.6. *Crocus sativus* (Saffron)

Crocin, a carotenoid in saffron, significantly reduces serum TNF-α and IL-1 levels. Recent pre-clinical evidence indicates its efficacy in reducing ankle joint swelling and synovial hyperplasia, particularly in combination with methotrexate.[57]

6.7. *Cannabis sativa*

Phytocannabinoids such as cannabidiol and tetrahydrocannabinol exhibit anti-inflammatory and analgesic activity through CB2 receptor agonism, reducing immune cell activation and pain perception. A recent scoping review emphasized its potential for symptom control, though regulatory and psychotropic concerns remain.[58]

6.8. *Arnica montana*

Arnica's helenalin component exhibits anti-inflammatory activity by inhibiting nitric oxide synthesis, TNF-α, and IL-6. It has shown efficacy in CIA models by reducing oxidative stress and joint inflammation.[59]

6.9. *Jatropha gossypifolia*

The latex of this plant, rich in flavonoids, has been found to reduce paw edema and joint inflammation in carrageenan

and Freund's adjuvant-induced arthritis models, possibly via modulation of lipid peroxidation and reactive oxygen species.[60]

6.10. *Nigella sativa* (Black seed)

A review highlighted *N. sativa* as a potent herb due to its thymoquinone content, which reduces synovial inflammation by inhibiting IL-6 and TNF-α pathways. Its immunoregulatory effects were evident in pre-clinical models of RA, where black seed oil decreased arthritic score and joint stiffness by 45%.[61]

6.11. *Withania somnifera* (Ashwagandha)

Recent findings affirm ashwagandha's role as a TNF-α and IL-1β modulator, with adaptogenic effects that reduce systemic inflammation. A 2024 study reported a 36% reduction in paw swelling in CIA rats, with enhanced T-regulatory cell activity.[62]

6.12. *Boswellia serrata* (Indian frankincense)

Boswellic acids inhibit 5-lipoxygenase and modulate Th17 cell proliferation. A 2024 randomized controlled trial showed that *Boswellia* supplementation reduced joint stiffness and morning pain in RA patients by over 30% within 6 weeks.[63]

6.13. *Perilla frutescens* (Shiso)

P. frutescens, commonly known as shiso, is a medicinal herb native to East Asia and widely used in Korean and Japanese traditional medicine. Its leaves are rich in rosmarinic acid, a phenolic compound with strong anti-inflammatory activity. Studies have shown that *Perilla* extract can downregulate TNF-α, IL-6, and IL-1β by inhibiting the NF-κB signaling pathway, leading to reduced synovial inflammation in collagen-induced arthritic animal models. Its dual antioxidant and immunomodulatory action supports cartilage preservation and alleviation of joint stiffness.[64]

6.14. *Tribulus terrestris*

T. terrestris, a traditional Ayurvedic herb, is rich in saponins and protodioscin, which have shown potent anti-arthritic effects in experimental models. It exerts its effects by downregulating COX and lipoxygenase enzymes, thereby reducing leukocyte infiltration and oxidative damage in joint tissues. Animal studies have documented improvements in joint swelling, paw edema, and histopathological scores following treatment, suggesting its potential as a cost-effective, adjunct therapy for RA.[65]

6.15. *Tinospora cordifolia* (Guduchi)

Guduchi, or *T. cordifolia*, is one of the most studied Ayurvedic immunomodulators. Its active constituents, such as tinosporide and berberine-like alkaloids, have been shown to modulate Th1/Th2 balance, reduce TNF-α and IL-6, and enhance macrophage phagocytic activity. In adjuvant-induced arthritis models, guduchi reduced paw thickness, arthritis scores, and oxidative stress markers. Its safety and adaptogenic properties make it a popular supplement in integrative RA care in India.[66]

6.16. *Sigesbeckia orientalis*

Used in traditional Chinese medicine to "dispel wind-dampness," *S. orientalis* has recently attracted scientific attention for its antirheumatic properties. Darutoside, its main active compound, reduces synovial inflammation, angiogenesis, and immune cell infiltration. Animal studies confirmed significant reductions in joint stiffness, MMP-9 activity, and bone erosion, positioning it as a botanical with both anti-inflammatory and chondroprotective benefits.[67]

6.17. *Uncaria tomentosa* (Cat's claw)

Native to South America, *U. tomentosa* has long been used for inflammatory conditions. It contains oxindole alkaloids, which inhibit TNF-α, MMP-9, and suppress leukocyte migration. Clinical studies in RA patients report improved pain scores and reduced fatigue. It also has antioxidant effects, aiding in the reduction of reactive oxygen species and nitric oxide levels in joint tissues.[68,69]

7. Conclusion

RA remains a complex autoimmune disorder requiring multifaceted therapeutic strategies encompassing early diagnosis, immunological understanding, and tailored interventions. While conventional treatments such as DMARDs, biologics, and Janus kinase inhibitors have significantly advanced disease control, they remain limited due to high costs, side effects, and incomplete remission in many patients. Recent integrative approaches, particularly the exploration of herbal and plant-based therapies, have revealed promising anti-inflammatory, immunomodulatory, and chondroprotective effects from compounds such as curcumin, gingerols, thymoquinone, Boswellic acids, epigallocatechin-3-gallate, and cannabidiol, among others. Emerging botanicals—such as *P. frutescens*, *T. cordifolia*, *S. orientalis*, and *Centella asiatica*—modulate novel molecular targets, including NF-κB, COX/lipoxygenase, mitogen-activated protein kinases, and cytokine signaling, suggesting a potential paradigm shift toward adjunctive phytomedicine. Future perspectives call for well-powered, randomized clinical trials, herbal formulation standardization, biomarker-guided therapy selection, and regulatory integration to ensure efficacy and safety. Combining evidence-based phytotherapy with conventional regimens may usher in

a more holistic, personalized, and sustainable model for RA management, especially in resource-limited settings and for patients with multidrug intolerance or incomplete response.

Acknowledgments

None.

Funding

None.

Conflict of interest

The authors declare that they have no competing interests.

Author contributions

Conceptualization: Brahmjot Singh
Data curation: Kiranjot Kaur
Formal analysis: Kiranjot Kaur, Sukhmandeep Kaur, Kunal Mistry
Methodology: Brahmjot Singh
Project administration: Sukhmandeep Kaur
Supervision: Brahmjot Singh
Visualization: Kunal Mistry
Writing–original draft: Brahmjot Singh
Writing–review & editing: Kiranjot Kaur, Kunal Mistry

Ethics approval and consent to participate

Not applicable.

Consent for publication

Not applicable.

Availability of data

Not applicable.

References

1. Smolen JS, Aletaha D, McInnes IB. Rheumatoid arthritis. *Lancet*. 2016;388(10055):2023-2038.

   doi: 10.1016/S0140-6736(16)30173-8

2. Tanaka, Y. A review of upadacitinib in rheumatoid arthritis. *Mod Rheumatol*. 2020;30(5):779-787.

   doi: 10.1080/14397595.2020.1782049

3. Black RJ, Cross M, Haile LM, *et al*. Global, regional, and national burden of rheumatoid arthritis, 1990-2020, and projections to 2050: A systematic analysis of the global burden of disease study 2021. *Lancet Rheumatol*. 2023;5(10):e594-e610.

   doi: 10.1016/S2665-9913(23)00211-4

4. Radu AF, Bungau SG. Management of rheumatoid arthritis: An overview. *Cells*. 2021;10(11):2857.

   doi: 10.3390/cells10112857

5. Garg R, Garg A. The research trends and scientometric assessment of rheumatoid arthritis in India during 2016-2021. *Curr Rheumatol Rev*. 2023;19(1):26-35.

   doi: 10.2174/1573397118666220804162313

6. Putrik P, Ramiro S, Kvien TK, *et al*. Inequities in access to biologic and synthetic DMARDs across 46 European countries. *Ann Rheum Dis*. 2014;73(1):198-206.

   doi: 10.1136/annrheumdis-2012-202603

7. Smolen JS, Landewé RBM, Bergstra SA, *et al*. EULAR recommendations for the management of rheumatoid arthritis with synthetic and biological disease-modifying antirheumatic drugs: 2022 update. *Ann Rheum Dis*. 2023;82(1):3-18.

   doi: 10.1136/ard-2022-223356corr1

8. Ashiq K, Ashiq S, Mobashar A, *et al*. An updated review on rheumatoid arthritis (RA): Epidemiology, pathophysiology, diagnosis, and the current approaches for its treatment. *Sudan J Med Sci*. 2023;18:539-551.

   doi: 10.18502/sjms.v18i4.14742

9. Singh JA, Saag KG, Bridges SL, *et al*. 2015 American College of Rheumatology guideline for the treatment of rheumatoid arthritis. *Arthritis Rheumatol*. 2016;68(1):1-26.

   doi: 10.1002/art.39480

10. Kaur C, Mishra Y, Kumar R, *et al*. Pathophysiology, diagnosis, and herbal medicine-based therapeutic implication of rheumatoid arthritis: An overview. *Inflammopharmacology*. 2024;32(3):1705-1720.

    doi: 10.1007/s10787-024-01445-8

11. Kurkó J, Besenyei T, Laki J, Glant TT, Mikecz K, Szekanecz Z. Genetics of rheumatoid arthritis - a comprehensive review. *Clin Rev Allergy Immunol*. 2013;45:170-179.

    doi: 10.1007/s12016-012-8346-7

12. Danieli MG, Casciaro M, Paladini A, *et al*. Exposome: Epigenetics and autoimmune diseases. *Autoimmun Rev*. 2024;23:103584.

    doi: 10.1016/j.autrev.2024.103584

13. Venetsanopoulou AI, Alamanos Y, Voulgari PV, Drosos AA. Epidemiology and risk factors for rheumatoid arthritis development. *Mediterr J Rheumato*l. 2023;34(4):404-413.

    doi: 10.31138/mjr.301223.eaf

14. Molina E, Del Rincon I, Restrepo JF, Battafarano DF, Escalante A. Association of socioeconomic status with treatment delays, disease activity, joint damage, and disability in rheumatoid arthritis. *Arthritis Care Res (Hoboken)*. 2015;67(7):940-946.

    doi: 10.1002/acr.22542

15. Cooper GS, Miller FW, Germolec DR. Occupational exposures and autoimmune diseases. *Int Immunopharmacol*. 2002;2(2-3):303-313.

doi: 10.1016/s1567-5769(01)00181-3

16. Novella-Navarro M, Plasencia-Rodríguez C, Nuño L, Balsa A. Risk factors for developing rheumatoid arthritis in patients with undifferentiated arthritis and inflammatory arthralgia. *Front Med (Lausanne)*. 2021;8:668898.

doi: 10.3389/fmed.2021.668898

17. Heidari B, Hajian-Tilaki K, Babaei M. Vitamin D deficiency and rheumatoid arthritis: Epidemiological, immunological, clinical and therapeutic aspects. *Mediterr J Rheumatol*. 2019;30(2):94-102.

doi: 10.31138/mjr.30.2.94

18. Philippou E, Nikiphorou E. Are we really what we eat? Nutrition and its role in the onset of rheumatoid arthritis. *Autoimmun Rev*. 2018;17(11):1074-1077.

doi: 10.1016/j.autrev.2018.05.009

19. Khan S, Mohan K, Muzammil S, Alam MA, Khayyam KU. Current prospects in rheumatoid arthritis: Pathophysiology, genetics, and treatments. *Recent Adv Antiinfect Drug Discov*. 2024;19(1):36-55.

doi: 10.2174/2772434418666230406083149

20. Sweeney SE, Firestein GS. Rheumatoid arthritis: Regulation of synovial inflammation. *Int J Biochem Cell Biol*. 2004;36(3):372-378.

doi: 10.1016/s1357-2725(03)00259-0

21. Wehr P, Purvis H, Law SC, Thomas R. Dendritic cells, T cells and their interaction in rheumatoid arthritis. *Clin Exp Immunol*. 2019;196(1):12-27.

doi: 10.1111/cei.13256

22. Makkar R, Sehgal A, Singh S, *et al*. Current trends in epigenetic, cellular and molecular pathways in management of rheumatoid arthritis. *Inflammopharmacology*. 2023;31(4):1577-1588.

doi: 10.1007/s10787-023-01262-5

23. Koper-Lenkiewicz OM, Sutkowska K, Wawrusiewicz-Kurylonek N, Kowalewska E, Matowicka-Karna J. Proinflammatory cytokines (IL-1, -6, -8, -15, -17, -18, -23, TNF-α) single nucleotide polymorphisms in rheumatoid arthritis-a literature review. *Int J Mol Sci*. 2022;23(4):2106.

doi: 10.3390/ijms23042106

24. Mishra AP, Kumar R, Harilal S, Nigam M, Datta D, Singh S. Emerging landscape of *in vitro* models for assessing rheumatoid arthritis management. *ACS Pharmacol Transl Sci*. 2024;7(8):2280-2305.

doi: 10.1021/acsptsci.4c00260

25. Wu D, Huang Y, Zhao J, *et al*. Synovial macrophages drive severe joint destruction in established rheumatoid arthritis. *Sci Rep*. 2025;15(1):12111.

doi: 10.1038/s41598-025-93784-x

26. Takeshita A, Nishida K, Yoshida A, *et al*. RANKL expression in chondrocytes and its promotion by lymphotoxin-α in the course of cartilage destruction during rheumatoid arthritis. *PLoS One*. 2021;16(7):e0254268.

doi: 10.1371/journal.pone.0254268

27. Bonfiglioli KR, de Medeiros Ribeiro AC, Carnieletto AP, *et al*. Extra-articular manifestations of rheumatoid arthritis remain a major challenge: Data from a large, multi-centric cohort. *Adv Rheumatol*. 2023;63:34.

doi: 10.1186/s42358-023-00318-y

28. Trivedi J. Clinical presentation and diagnosis of rheumatoid arthritis. *Ann Clin Med Case Rep*. 2024;13(18):1-7.

29. Iyengar KP, Vaish A, Nune A. Anti-cyclic citrullinated peptide antibody (ACPA) and rheumatoid arthritis: Clinical relevance. *J Clin Orthop Trauma*. 2022;24:101729.

doi: 10.1016/j.jcot.2021.101729

30. Alharthi AH, Al-Shehri SHA, Albarqi MAA, *et al*. Laboratory markers of inflammation: CRP and ESR in clinical practice. *J Int Crisis Risk Commun Res*. 2024;7(S8):2376.

doi: 10.63278/jicrcr.vi.1233

31. Van Delft MA, Verheul MK, Burgers LE, *et al*. The anti-CarP antibody response is of overall low avidity despite extensive isotype switching. *Ann Rheum Dis*. 2020;79(1):63.

32. Cho MJ, Chai JW, Kim DH, Kim HJ, Seo J. Ultrasonographic differential diagnosis of medial elbow pain. *Ultrasonography*. 2024;43(5):299-213.

doi: 10.14366/usg.24102

33. Weaver JS, Omar I, Mar W, Kauser AS, Mlady GW, Taljanovic M. Magnetic resonance imaging of rheumatological diseases. *Pol J Radiol*. 2022;87(1):93-112.

doi: 10.5114/pjr.2022.113390

34. Sambri A, Spinnato P, Tedeschi S, *et al*. Bone and joint infections: The role of imaging in tailoring diagnosis to improve patients' care. *J Pers Med*. 2021;11(12):1317.

doi: 10.3390/jpm11121317

35. De Stefano L, Cassione EB, Sakellariou G, *et al*. Tender joints in early autoantibody-negative rheumatoid arthritis: Should they be included in the scoring of joint involvement of the 2010 ACR/EULAR classification criteria? *Semin Arthritis Rheum*. 2025;55:152637.

doi: 10.1016/j.semarthrit.2025.152637

36. Bird A, Oakden-Rayner L, McMaster C, *et al*. Artificial intelligence and the future of radiographic scoring in rheumatoid arthritis: A viewpoint. *Arthritis Res Ther*. 2022;24(1):268.

doi: 10.1186/s13075-022-02972-x

37. Perera J, Delrosso CA, Nerviani A, Pitzalis C. Clinical phenotypes, serological biomarkers, and synovial features defining seropositive and seronegative rheumatoid arthritis: A literature review. *Cells*. 2024;13(9):743.

doi: 10.3390/cells13090743

38. Gupta R, Sharma R. Advancement in the management of rheumatoid arthritis. *RPS Pharmacol Rep.* 2023;2(1):rqad005.

doi: 10.1093/rpsppr/rqad005

39. Vlad AL, Popazu C, Lescai AM, Voinescu DC, Baltă AAȘ. Where do we stand in the management of rheumatoid arthritis ahead of EULAR/ACR 2025? *Clin Pract*. 2025;15(6):103.

doi: 10.3390/clinpract15060103

40. Lin Y, Chen Y, Deng R, *et al*. Delivery of neutrophil membrane encapsulated non-steroidal anti-inflammatory drugs by degradable biopolymer microneedle patch for rheumatoid arthritis therapy. *Nano Today*. 2023;49:101791.

doi: 10.1016/j.nantod.2023.101791

41. Krause D, Mai A, Klaassen-Mielke R, *et al*. The efficacy of short-term bridging strategies with high- and low-dose prednisolone on radiographic and clinical outcomes in active early rheumatoid arthritis: A double-blind, randomized, placebo-controlled trial. *Arthritis Rheumatol*. 2022;74(10):1628-1637.

doi: 10.1002/art.42245

42. Sherbini AA. *Investigating Methotrexate Associated Adverse Events in Patients with Rheumatoid Arthritis [dissertation]*. Manchester: Univ Manchester; 2023. Available from: https://www.proquest.com/openview/c9b2ccfabc0d5c80e9cb918769f5f359/1?pq-origsite=gscholar&cbl=2026366&diss=y [Last accessed on 2025 Sep 05].

43. Krueger J, Santinon F, Kazanova A, *et al*. Hydroxychloroquine (HCQ) decreases the benefit of anti-PD-1 immune checkpoint blockade in tumor immunotherapy. *PLoS One*. 2021;16(6):e0251731.

doi: 10.1371/journal.pone.0251731

44. Shams S, Martinez JM, Dawson JR, *et al*. The therapeutic landscape of rheumatoid arthritis: Current state and future directions. *Front Pharmacol*. 2021;12:680043.

doi: 10.3389/fphar.2021.680043

45. Pulungan Y, Saputra AK, Purnamasari D, Wijayanti N, Sari LR. Conventional synthetic disease-modifying antirheumatic drugs (csDMARD) in rheumatoid arthritis during pregnancy and lactation: A review. *Indones J Pharmacol Ther*. 2022;3(1):1-7.

doi: 10.22146/ijpther.3297

46. Dar E, Abbas M, Nazir S, Abbas M. Novel management, cure and complications-control of rheumatoid arthritis with traditional and modern remedies: A review. *Pharm Chem J*. 2024;58(1):1-9.

doi: 10.1007/s11094-024-03238-3

47. Taylor PC, Feist E, Pope JE, *et al*. What have we learnt from the inhibition of IL-6 in RA and what are the clinical opportunities for patient outcomes? *Ther Adv Musculoskelet Dis*. 2024;16:1-19.

doi: 10.1177/1759720X241283340

48. Alghazali T, Saleh RO, Uthirapathy S, *et al*. Rheumatoid arthritis unmasked: The power of B cell depletion therapy. *Mol Biol Rep.* 2025;52(1):254.

doi: 10.1007/s11033-025-10366-w

49. Meng Q, Liu H, Liu J, Pang Y, Liu Q. Advances in immunotherapy modalities for atherosclerosis. *Front Pharmacol*. 2023;13:1079185.

doi: 10.3389/fphar.2022.1079185

50. Tanaka Y, Luo Y, O'Shea JJ, Nakayamada S. Janus kinase-targeting therapies in rheumatology: A mechanisms-based approach. *Nat Rev Rheumatol*. 2022;18(3):133-145.

doi: 10.1038/s41584-021-00726-8

51. Franchinotti R, Moler M, Paulenas E, Saura JP, Andreu MF. Non-pharmacological interventions for feeding disorders in pediatrics: A scoping review. *Occup Ther Health Care*. 2024;38(1):1-35.

doi: 10.1080/07380577.2024.2401732

52. Makuch S, Więcek K, Woźniak M. The immunomodulatory and anti-inflammatory effect of curcumin on immune cell populations, cytokines, and *in vivo* models of rheumatoid arthritis. *Pharmaceuticals (Basel)*. 2021;14(4):309.

doi: 10.3390/ph14040309

53. Rahman T, Jahan R, Chowdhury AR, Rahmatullah M. Potential therapeutic benefits of *Aloe barbadensis* in treatment of rheumatoid arthritis. *J Autoimmune Dis Rheumatol*. 2014;2(1):35-44.

doi: 10.12970/2310-9874.2014.02.01.6

54. Maryam H, Azhar S, Akhtar MN, *et al*. Role of bioactive components of ginger in management of osteoarthritis: A review. *Int J Food Prop.* 2023;26(1):1903-1913.

doi: 10.1080/10942912.2023.2236811

55. Xie C, Jiang J, Liu J, Yuan G, Zhao Z. Ginkgolide B attenuates collagen-induced rheumatoid arthritis and regulates fibroblast-like synoviocytes-mediated apoptosis and inflammation. *Ann Transl Med*. 2020;8(22):1497.

doi: 10.21037/atm-20-6420

56. Mokra, D, Joskova, M, Mokry, J. Therapeutic effects of green tea polyphenol (−)-Epigallocatechin-3-gallate (EGCG) in

relation to molecular pathways controlling inflammation, oxidative stress, and apoptosis. *Int J Mol Sci*. 2022;24(1):340.

doi: 10.3390/ijms24010340

57. Chrastina, M, Dráfi, F, Pružinská, K, *et al*. *Crocus sativus* L. extract (saffron) effectively reduces arthritic and inflammatory parameters in monotherapy and in combination with methotrexate in adjuvant arthritis. *Nutrients*. 2023;15(19):4108.

doi: 10.3390/nu15194108

58. Da Nóbrega Marinho AM, da Silva Neto RWG. Anti-inflammatory effects of cannabinoids. *BrJP.* 2023;6:31-37.

doi: 10.5935/2595-0118.20230010-en

59. Sharma S, Arif M, Nirala RK, Gupta R, Thakur SC. Cumulative therapeutic effects of phytochemicals in *Arnica montana* flower extract alleviated collagen-induced arthritis: Inhibition of both pro-inflammatory mediators and oxidative stress. *J Sci Food Agric*. 2016;96(5):1500-1510.

doi: 10.1002/jsfa.7252

60. Ahmed AS, Chopde CT, Kashmiri ZN. Assessment of anti-inflammatory and anti-arthritis activity of *Jatropha gossypifolia* in rats. *Int J Pharm Pharm Sci.* 2015;7(1):258-260.

61. Wahab S, Alsayari A. Potential pharmacological applications of *Nigella* seeds with a focus on *Nigella sativa* and its constituents against chronic inflammatory diseases: Progress and future opportunities. *Plants (Basel)*. 2023;12(22):3829.

doi: 10.3390/plants12223829

62. Haque MT, Rahman, N, Faruk MO, *et al*. Potential of analgesic and anti-inflammatory activity of *Withania somnifera* Linn. leaves. *Asian J Res Med Pharm Sci*. 2025;14(3):117-125.

doi: 10.9734/ajrimps/2025/v14i3324

63. Ansari P, Reberio AD, Ansari NJ, *et al*. Therapeutic potential of medicinal plants and their phytoconstituents in diabetes, cancer, infections, cardiovascular diseases, inflammation and gastrointestinal disorders. *Biomedicines*. 2025;13(2):454.

doi: 10.3390/biomedicines13020454

64. Kim N, Kim SY, Kim SW, *et al*. Efficacy of *Perilla frutescens* (L.) Britton var. frutescens extract on mild knee joint pain: A randomized controlled trial. *Front Pharmacol.* 2023;14:1114410.

doi: 10.3389/fphar.2023.1114410

65. Park YJ, Cho YR, Oh JS, Ahn EK. Effects of *Tribulus terrestris* on monosodium iodoacetate-induced osteoarthritis pain in rats. *Mol Med Rep.* 2017;16(4):5303-5311.

doi: 10.3892/mmr.2017.7296

66. Prasad S, Kulshreshtha A, Lall R, Gupta SC. Inflammation and ROS in arthritis: Management by Ayurvedic medicinal plants. *Food Funct*. 2021;12(18):8227-8247.

doi: 10.1039/D1FO01078F

67. Linghu KG, Xiong SH, Zhao GD, *et al*. *Sigesbeckia orientalis* L. extract alleviated the collagen type II-induced arthritis through inhibiting multi-target-mediated synovial hyperplasia and inflammation. *Front Pharmacol*. 2020;11:547913.

doi: 10.3389/fphar.2020.547913

68. Arado GM, Amatto PPG, Marins, M, *et al*. Anti-inflammatory and/or immunomodulatory activities of *Uncaria tomentosa* (cat's claw) extracts: A systematic review and meta-analysis of *in vivo* studies. *Front Pharmacol*. 2024;15:1378408.

doi: 10.3389/fphar.2024.1378408

69. Coelho LJ, do Nascimento GNL. Anti-inflammatory and diuretic activity of *Uncaria tomentosa* (cat's claw): Systematic review. *Rev Cereus*. 2020;12(2):119-129.

doi: 10.18605/2175-7275/cereus.v12n2p119-129

ACCSCIENCE PUBLISHING

Innovative Medicines & Omics

PERSPECTIVE ARTICLE

Nanotherapies: A potent treatment for neurodegenerative diseases

Yihao Meng, Zhengwei Huang*, and Xuejuan Zhang*

Department of Pharmaceutics, College of Pharmacy, Jinan University, Guangzhou, Guangdong, China

Abstract

It is generally reported that neurodegenerative diseases, including Alzheimer's disease and Parkinson's disease, pose severe threats to global public health. Traditional therapies for neurodegenerative diseases exhibit low drug delivery efficiency due to the restrictive nature of the blood–brain barrier. Fortunately, nanomedicines can effectively overcome blood–brain barrier through mechanisms such as intercellular penetration and receptor targeting, which have advantages such as controlled release, reduced toxicity, and enhanced efficacy. In this paper, we summarize the latest research progress based on the types of nanomaterials, administration approach, and implications, with the aim of providing insights for optimizing the research and development of nanomedicines for neurodegenerative diseases.

Keywords: Nanotherapy; Neurodegenerative diseases; Drug delivery; Targeted delivery

***Corresponding authors:**
Zhengwei Huang (huangzhengw@jnu.edu.cn)
Xuejuan Zhang (zhanghongdou0223@126.com)

Citation: Meng Y, Huang Z, Zhang X. Nanotherapies: A potent treatment for neurodegenerative diseases. *Innov Med Omics*. 2025;2(4):36-41. doi: 10.36922/IMO025360044

Received: September 2, 2025

Revised: October 12, 2025

Accepted: October 27, 2025

Published online: November 14, 2025

1. Background

Neurodegenerative diseases represent the most prevalent disorders affecting the central nervous system (CNS), with key examples including Alzheimer's disease (AD), Parkinson's disease (PD), Huntington's disease, frontotemporal dementia, and amyotrophic lateral sclerosis (ALS). These diseases cause problems related to movement disorders or mental functional disorders and greatly aggravate patients' quality of life.[1,2] Specifically, AD already impacts more than 55 million people globally, a number that has been projected to reach 78 million by 2030. Based on the 2019 estimates by the World Health Organization, 850,000 people are affected by PD worldwide.[3] Amid the accelerated global aging, populations worldwide face substantial burdens from the rising costs associated with neurodegenerative diseases.

Despite rapid advancements in medical technology, effective therapeutic strategies for most neurodegenerative diseases remain unavailable in clinical practice. For instance, donepezil, aducanumab, rivastigmine, memantine, and galantamine for AD, and *L*-3,4-dihydroxyphenylalanine (L-DOPA) for PD, merely delay disease progression, rather than providing a cure. Delivery of therapeutics to the CNS is limited by the blood–brain barrier (BBB; Figure 1), which acts like a two-edged sword: while it protects brain tissues, it further imposes restrictions on the access of a range of therapeutics into the CNS.[4] It is worth mentioning that almost all macromolecular drugs and over 98% of small-molecule drugs fail to traverse the BBB.[5] Hence, identifying effective approaches to cross the BBB are crucial for improving the delivery efficiency of therapeutics in neurodegenerative disease treatment.

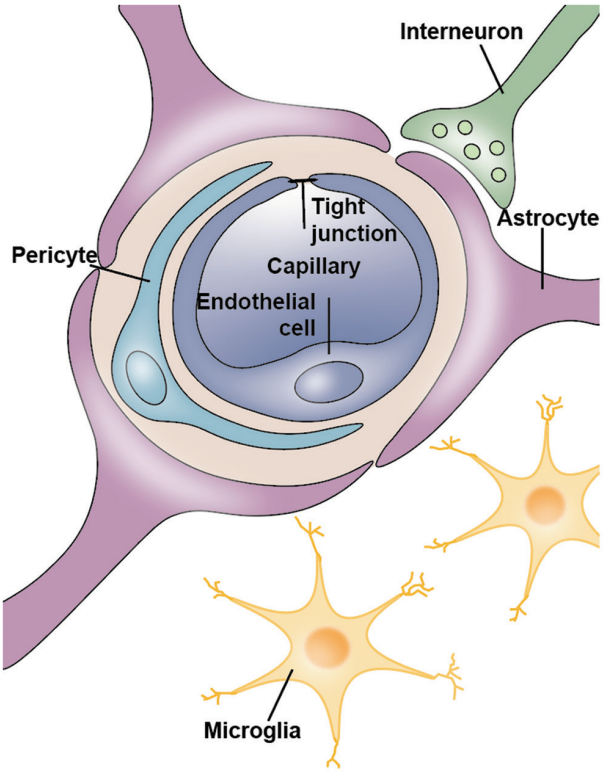

Figure 1. Schematic diagram of blood–brain barrier. Adapted from Cui *et al.*[6] with modifications.

Nanoparticles (NPs) emerge as a promising solution. With diameters varying from 1 nm to 100 nm, NPs possess distinct advantages such as the ability to encapsulate drugs, enable minimal dosage requirements, enhance drug stability, achieve controlled or sustained release, and reduce toxic side effects.[7-9] Most importantly, through intercellular penetration and receptor targeting effects, NPs can traverse the BBB. More precisely, NPs with sufficiently small particle sizes can utilize the intercellular spaces between tight junctions for intercellular penetration.[10] Receptor targeting is achieved by attaching specific ligands to NPs' surfaces, enabling receptor-mediated endocytosis of the NPs. Subsequently, the NPs undergo transcytosis across endothelial cells, allowing them to traverse the BBB.[8] Given these unique features, nano-delivery systems facilitate drug delivery across the BBB and enhance CNS targeting efficiency, offering new prospects for neurodegenerative diseases.[4] Until now, various nano-systems have been applied in neurodegenerative diseases, including solid lipid NPs (SLNPs), liposomes, gold NP, non-polymeric micelles, dendrimers, lipoplex, polymeric micelle, nanotubes, polymeric NP, quantum dots, and magnetic NP (Figure 2).[9]

At the forefront of nanotechnology development, this perspective aims to summarize the current status of

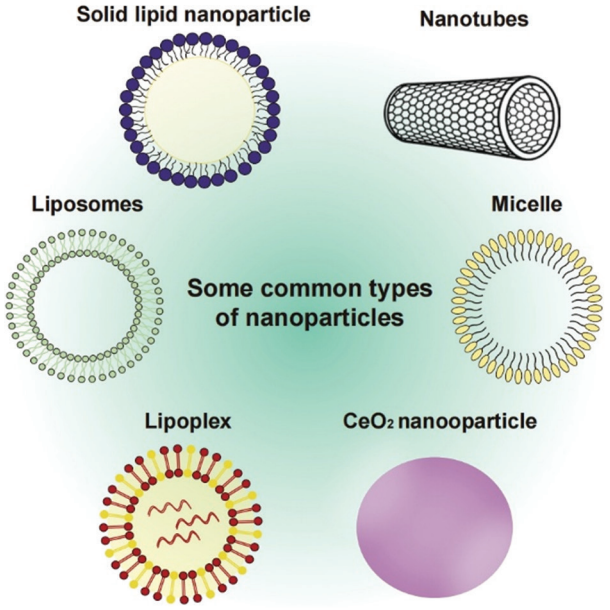

Figure 2. Some common types of nanoparticles. Adapted from Akhtar *et al.*[9] with modifications.

the field. For a better, logical presentation, we focus on three dimensions: types of nanomaterials, administration routes, and their implications, highlighting recent research progress and offering insights into addressing key challenges in the use of NPs for neurodegenerative disease treatment.

2. Classification by nanomaterials

Currently, various nanomaterials are used to treat neurodegenerative diseases, each with unique merits in drug delivery and efficacy by virtue of their structural differences.

Lipid-based nanocarriers mainly include liposomes and SLNPs.[11] Liposomes are spherical structures made up of one or more bilayers, which consist of phospholipids of natural or synthetic origin.[12] Lipid-based nanocarriers are among the safest and most promising platforms for neurodegenerative disease therapy due to their biocompatibility, structural flexibility, and ability to deliver targeted compounds across the BBB while specifically homing to brain cells.[13] Recent research has demonstrated the potential of transferrin-modified liposomes linked to vitamin B12 as a therapeutic for AD. The formulation targets both neuronal cells and the BBB, effectively slowing the aggregation of amyloid-beta (Aβ) fibrils, demonstrating considerable promise for AD treatment.[11] Notably, SLNPs offer distinct advantages, including the capacity to traverse physiological barriers and enhance drug bioavailability without requiring high doses. These particles can direct

active compounds to intended targets, significantly reducing toxicity to surrounding tissues while protecting payloads from chemical and enzymatic degradation. Preclinical studies have shown that functionalized SLNPs loaded with nicotinamide can improve cognitive function in AD animal models by decreasing tau hyperphosphorylation. Furthermore, SLNPs encapsulating rivastigmine tartrate have been designed to enhance intranasal delivery into the brain for AD treatment.[11] In a nutshell, lipid-based nanocarrier systems have shown positive properties, including sustained drug release profiles, improved CNS bioavailability, and enhanced therapeutic efficacy.[14]

Polymeric NPs have been integrated into clinical practice for several decades, demonstrating their long-standing application potential.[7] These solid particles consist of organic colloidal NPs fabricated from polymeric, natural, or synthetic materials. There is no doubt that poly(D,L-lactide-co-glycolide) (PLGA) and chitosan are the most widely used in AD treatment.[11] PLGA NPs exhibit excellent biocompatibility and biodegradability, rendering them ideal for the regulated release of therapeutic molecules. These NPs are capable of encapsulating drugs or other therapeutics, and further support the targeted delivery of these payloads to the brain. Chitosan NPs, obtained from chitin, which is recognized for its favorable biocompatibility and low toxicity, have also been investigated for their application potential in AD therapy. Chitosan NPs are capable of encapsulating drugs or therapeutic agents, thereby enabling targeted drug delivery to specific sites.[8] However, polymer-based nanomedicines are not without limitations. Some polymers (like polyquaternium polymers) may cause toxicity or inflammation, raising regulatory concerns.[15]

3. Categorization by administration approach

The administration route of NPs is key to determining their biodistribution patterns, brain deposition, and influences the effectiveness of nanotherapeutic interventions.

For the treatment of neurodegenerative diseases, oral administration is widely recognized as a preferred route due to its safety, high patient adherence, and convenience. Nevertheless, a major challenge persists: many therapeutic agents are prone to degradation in the gastrointestinal tract and have difficulty crossing the gastrointestinal mucosal barrier, which in turn leads to low systemic bioavailability.[16] A key concern for pharmaceutical researchers has long been identifying strategies to preserve drug stability while boosting drug absorption in the gastrointestinal environment. Multiple studies have confirmed that lipid NPs (LNPs) exhibit strong competence to encapsulate diverse bioactive agents (including RNA, DNA, small-molecule drugs, and proteins) and protect them against enzymatic degradation in the body. Beyond protection, LNPs also facilitate drug transit across gastrointestinal physiological barriers through diverse transport mechanisms, significantly boosting the absorption of oral drugs. Furthermore, functionalizing LNP surfaces with specific targeting ligands enables precise delivery to diseased brain cells or tissues, making LNPs promising oral drug delivery systems for neurodegenerative disease.[17]

Injection is commonly used for targeting nanomedicines to the CNS, particularly in cases of neuroinflammation with impaired BBB.[18] The core merit of intravenous delivery is the rapid onset and complete bioavailability of drugs even with low doses, while avoiding first-pass metabolism. A study demonstrated that a single intravenous injection of reactive oxygen species-responsive NPs enabled targeted drug release within affected brain regions, concurrently activated autophagy, attenuated neuroinflammation, markedly reduced Aβ burden, and reversed cognitive deficits in a mouse model of AD.[19] However, this approach may induce systemic infections while showing weak efficacy in drug targeting.[18,19]

Compared with conventional oral or intravenous administration, intranasal administration boasts multiple advantages, including non-invasiveness, ease of administration, patient acceptability, and the competence to traverse the BBB for direct drug delivery into the CNS. These features make it a compelling choice compared to invasive approaches such as injection and oral therapy.[8,9] For instance, PLGA NPs loaded with lamotrigine attained higher brain concentrations and superior efficacy in animal models compared to oral delivery. In addition, advanced formulations including polyethylene glycol (PEG)-modified chitosan-lipid nanocapsules or carbon nanotubes have shown significant potential for nasal drug administration, further enhancing therapeutic results. When combined with nanotechnology and biomaterials, intranasal drug delivery technology offers a novel non-invasive therapeutic strategy for neurodegenerative diseases (and other fields), highlighting substantial potential for clinical application.[20]

4. Categorization by implication

Owing to the complexity of brain function, treating neurodegenerative diseases has long posed a major challenge. Nevertheless, owing to the ongoing rapid advancements in the fields of nanomaterials and nanotechnology, these nanoscale materials are expected to offer long-term therapeutic hope.

As one of the most prevalent neurodegenerative diseases, AD is a progressive and irreversible nervous

system disorder. Currently, no effective therapeutic approaches exist to alleviate symptoms of AD or achieve a cure.[6] Inhibiting or blocking the pathogenic mechanism by NPs is a key strategy to treating AD.[21] For instance, gold NPs (AuNPs) functionalized by tryptophan-proline-methionine can alleviate oxidative stress, as well as regulate behavior and the cholinergic system, thereby enhancing neuroprotective efficacy in AD model mice.[22] Guo *et al.*[23] illustrated that multifunctional selenium quantum dots not only effectively inhibited Aβ aggregation but also alleviated oxidative stress and restored mitochondrial function. In addition, Yang *et al.*[24] showed that fucoxanthin-loaded PLGA-PEG NPs penetrate the BBB and release fucoxanthin in a sustained manner, preventing cognitive impairment in AD model mice induced by Aβ with higher efficacy than free fucoxanthin.[25] These results indicate that NPs may serve as a suitable therapeutic strategy against AD. Nonetheless, critical issues such as the *in vivo* metabolism of metal ions and their potential toxicity require consideration.[19]

PD is characterized by abnormal basal ganglia function, which leads to the aberrant build-up of Lewy bodies within the substantia nigra and the decrease of dopaminergic neuronal populations.[26] Currently, levodopa preparations serve as the primary therapy for PD, but they provide only modest symptom relief, do not halt disease progression, lack long-term efficacy, and are associated with a high incidence of side effects.[6,19] NPs have shown promise in overcoming these limitations: Mn_3O_4 NPs effectively lowered α-syn levels in the cerebrospinal fluid of PD model mice, enhanced the cognitive abilities, and showed favorable biodegradability. AuNPs counteracted PD symptoms caused by reserpine in C57BL/6 mice and reduced reserpine-induced neuronal apoptosis. These results highlight NPs' potential as a promising therapeutic option for PD.[19]

In addition, advanced nanotherapeutic attempts for Huntington's disease include nanotechnology-optimized adeno-associated virus vector-mediated gene editing. In the treatment for ALS, lactoferrin-modified LNPs facilitated the transport of riluzole across the BBB through interaction with lactoferrin receptors expressed on brain endothelial cells.[27]

However, research on some neurodegenerative diseases remains scarce, such as progressive supranuclear palsy and spinocerebellar ataxia. We are anticipating to see the related research in the near future.

5. Conclusion and indication

Nanotherapy, as an innovative strategy to overcome the treatment challenges of neurodegenerative diseases, has been extensively validated for its ability to bypass the limitations of traditional drug delivery while enhancing the accuracy and safety of therapies.[28] Particularly, it has shown remarkable potential in the treatment of diseases such as AD and PD.[7]

Based on the research progress discussed above, this perspective outlines the implications for the development of nanomedicines as follows. First, the biocompatibility of nanomaterials and the safety of encapsulated drugs are the core prerequisites for clinical transformation, in which case it is necessary to assess the stability of long-term efficacy and safety of NPs.[29] Second, studies have confirmed that non-invasive approaches, such as intranasal administration, offer advantages including the ability to cross the BBB.[4,30] Thus, the process of their translation from fundamental research to clinical practice should be accelerated. On the other hand, the feasibility of emerging approaches such as transdermal and inhalation administration should be explored to build a diversified administration system. Third, current nanotherapy research primarily targets high-incidence neurodegenerative diseases, while rare and orphan conditions receive comparatively little attention. Moving forward, it is necessary to strengthen research on these conditions and broaden the application of nanomedicines to more neurodegenerative diseases.

With continuous innovation and the resolution of current challenges, NPs have the potential to revolutionize the treatment field of neurodegenerative diseases in the coming decades.[30] We look forward to the successful introduction of safe and effective nanomedicine products in the near future, offering new therapeutic hope to patients worldwide.

Acknowledgments

None.

Funding

This work was supported by the Natural Science Foundation of Guangdong Province under Grant No. 2025A1515010639.

Conflict of interest

The authors declare they have no competing interests.

Author contributions

Conceptualization: Yihao Meng
Writing–original draft: Yihao Meng
Writing–review & editing: Zhengwei Huang, Xuejuan Zhang

Ethics approval and consent to participate

Not applicable.

Consent for publication

Not applicable.

Availability of data

Not applicable.

References

1. Biswas A, Hivare P, Solanki R, Gupta S, Bhatia D. Applications of bionanomaterials in neurodegenerative diseases. *Mater Adv*. 2025;6(12):3785-3804.

   doi: 10.1039/D4MA01215A

2. Rafe MR. Drug delivery for neurodegenerative diseases is a problem, but lipid nanocarriers could provide the answer. *Nanotheranostics*. 2024;8(1):90-99.

   doi: 10.7150/ntno.88849

3. Jiang Q, Liu J, Huang S, *et al*. Antiageing strategy for neurodegenerative diseases: From mechanisms to clinical advances. *Signal Transduct Target Ther*. 2025;10:76.

   doi: 10.1038/s41392-025-02145-7

4. Luo Q, Yang J, Yang M, *et al*. Utilization of nanotechnology to surmount the blood-brain barrier in disorders of the central nervous system. *Mater Today Bio*. 2025;31:101457.

   doi: 10.1016/j.mtbio.2025.101457

5. Lamptey RNL, Chaulagain B, Trivedi R, Gothwal A, Layek B, Singh J. A review of the common neurodegenerative disorders: Current therapeutic approaches and the potential role of nanotherapeutics. *Int J Mol Sci*. 2022;23(3):1851.

   doi: 10.3390/ijms23031851

6. Cui W, Fu W, Zhang T, Zhou R, Zhang T, Lin Y. Application of nanomaterials in neurodegenerative diseases. In: Lin Y, Zhou R, editors. *Advances in Nanomaterials-Based Cell Biology Research*. Berlin: Springer; 2021. p. 87-110.

   doi: 10.1007/978-981-16-2666-1_3

7. López-Espinosa J, Park P, Holcomb M, Godin B, Villapol S. Nanotechnology-driven therapies for neurodegenerative diseases: A comprehensive review. *Ther Deliv*. 2024;15(12):997-1024.

   doi: 10.1080/20415990.2024.2401307

8. Dong N, Ali-Khiavi P, Ghavamikia N, *et al*. Nanomedicine in the treatment of Alzheimer's disease: Bypassing the blood-brain barrier with cutting-edge nanotechnology. *Neurol Sci*. 2025;46(4):1489-1507.

   doi: 10.1007/s10072-024-07871-4

9. Akhtar A, Andleeb A, Waris TS, *et al*. Neurodegenerative diseases and effective drug delivery: A review of challenges and novel therapeutics. *J Control Release*. 2021;330:1152-1167.

   doi: 10.1016/j.jconrel.2020.11.021

10. Saeedi M, Eslamifar M, Khezri K, Dizaj SM. Applications of nanotechnology in drug delivery to the central nervous system. *Biomed Pharmacother*. 2019;111:666-675.

    doi: 10.1016/j.biopha.2018.12.133

11. Puranik N, Yadav D, Song M. Advancements in the application of nanomedicine in Alzheimer's disease: A therapeutic perspective. *Int J Mol Sci*. 2023;24(18):14044.

    doi: 10.3390/ijms241814044

12. Andrade S, Ramalho MJ, Loureiro JA, Pereira MC. Transferrin-functionalized liposomes loaded with vitamin VB12 for Alzheimer's disease therapy. *Int J Pharm*. 2022;626:122167.

    doi: 10.1016/j.ijpharm.2022.122167

13. Rafieezadeh D, Sabeti G, Khalaji A, Mohammadi H. Advances in nanotechnology for targeted drug delivery in neurodegenerative diseases. *Am J Neurodegener Dis*. 2025;14(2):51-57.

    doi: 10.62347/QHVI3317

14. Witika BA, Poka MS, Demana PH, *et al*. Lipid-based nanocarriers for neurological disorders: A review of the state-of-the-art and therapeutic success to date. *Pharmaceutics*. 2022;14(4):836.

    doi: 10.3390/pharmaceutics14040836

15. Hansen AMB, Poulsen R, Von Gersdorff Jørgensen L, Hansen M. Polyquaternium polymers cause inflammatory response and alterations of the lipidome in *Danio rerio* larvae. *J Hazard Mater Lett*. 2024;5:100095.

    doi: 10.1016/j.hazl.2023.100095

16. Lou J, Duan H, Qin Q, *et al*. Advances in oral drug delivery systems: Challenges and opportunities. *Pharmaceutics*. 2023;15(2):484.

    doi: 10.3390/pharmaceutics15020484

17. Zou Y, Zhang J, Chen L, Xu Q, Yao S, Chen H. Targeting neuroinflammation in central nervous system diseases by oral delivery of lipid nanoparticles. *Pharmaceutics*. 2025;17(3):388.

    doi: 10.3390/pharmaceutics17030388

18. Chenthamara D, Subramaniam S, Ramakrishnan SG, *et al*. Therapeutic efficacy of nanoparticles and routes of administration. *Biomater Res*. 2019;23:20.

    doi: 10.1186/s40824-019-0166-x

19. Duan L, Li X, Ji R, *et al*. Nanoparticle-based drug delivery systems: An inspiring therapeutic strategy for neurodegenerative diseases. *Polymers (Basel)*. 2023;15(9):2196.

    doi: 10.3390/polym15092196

20. Wu X, Zang R, Qiu Y, *et al*. Intranasal drug delivery technology in the treatment of central nervous system

diseases: Challenges, advances, and future research directions. *Pharmaceutics*. 2025;17(6):775.

doi: 10.3390/pharmaceutics17060775

21. Passeri E, Elkhoury K, Morsink M, *et al*. Alzheimer's disease: Treatment strategies and their limitations. *Int J Mol Sci*. 2022;23(22):13954.

doi: 10.3390/ijms232213954

22. Georgeous J, AlSawaftah N, Abuwatfa WH, Husseini GA. Review of gold nanoparticles: Synthesis, properties, shapes, cellular uptake, targeting, release mechanisms and applications in drug delivery and therapy. *Pharmaceutics*. 2024;16(10):1332.

doi: 10.3390/pharmaceutics16101332

23. Guo X, Lie Q, Liu Y, *et al*. Multifunctional selenium quantum dots for the treatment of Alzheimer's disease by reducing Aβ-neurotoxicity and oxidative stress and alleviate neuroinflammation. *ACS Appl Mater Interfaces*. 2021;13(26):30261-30273.

doi: 10.1021/acsami.1c00690

24. Yang M, Jin L, Wu Z, *et al*. PLGA-PEG nanoparticles facilitate *in vivo* anti-Alzheimer's effects of fucoxanthin, a marine carotenoid derived from edible brown algae. *J Agric Food Chem*. 2021;69(34):9764-9777.

doi: 10.1021/acs.jafc.1c00569

25. Zhang X, Hu H, Li Q, *et al*. Cascade-targeting multifunctional nanochaperone remodels brain microenvironment for synergistic therapy of Alzheimer's disease. *Nano Today*. 2024;55:102168.

doi: 10.1016/j.nantod.2024.102168

26. Emamzadeh FN, Surguchov A. Parkinson's disease: Biomarkers, treatment, and risk factors. *Front Neurosci*. 2018;12:612.

doi: 10.3389/fnins.2018.00612

27. Teixeira MI, Lopes CM, Gonçalves H, *et al*. Formulation, characterization, and cytotoxicity evaluation of lactoferrin functionalized lipid nanoparticles for riluzole delivery to the brain. *Pharmaceutics*. 2022;14(1):185.

doi: 10.3390/pharmaceutics14010185

28. Shukla R, Srivastava V, Sethi A, Ruwali M. Nanomaterial-based drug delivery systems as tools for targeted therapy of neurodegenerative diseases. In: Yadav AK, Shukla R, Flora SJS, editors. *Nanomedical Drug Delivery for Neurodegenerative Diseases*. Ch. 15. United States: Academic Press; 2022. p. 243-259.

doi: 10.1016/B978-0-323-85544-0.00003-4

29. Zakharova L, Gaynanova G, Vasilieva E, *et al*. Recent nanoscale carriers for therapy of Alzheimer's disease: Current strategies and perspectives. *Curr Med Chem*. 2023;30(33):3743-3774.

doi: 10.2174/0929867330666221115103513

30. Vashist A, Manickam P, Raymond AD, *et al*. Recent advances in nanotherapeutics for neurological disorders. *ACS Appl Bio Mater*. 2023;6(7):2614-2621.

doi: 10.1021/acsabm.3c00254

ACCSCIENCE PUBLISHING

Innovative Medicines & Omics

ORIGINAL RESEARCH ARTICLE

Dominant and sustained mutations, deletions, and insertions in the Omicron coronavirus lineages JN.1, KP.3, LB.1, XEC, MC.1, and MV.1

Asit Kumar Chakraborty*

Department of Biochemistry and Biotechnology, Faculty of Oriental Institute of Science and Technology, Vidyasagar University, Midnapore, West Bengal, India

Abstract

The JN.1 Omicron coronaviruses possess a unique 16MPLF spike insertion that compensates for deletions at positions 24LPP, 31S, 69HV, 145Y, 211N, and V483 in the spike protein. These viruses also exhibit a 3576SGF deletion in the open reading frame (ORF)1ab protein, 26–49 nucleotide deletions in the 3′-untranslated region (UTR), and a 31ERS amino acid deletion in the N protein. In an ongoing analysis of JN.1 lineages, an N30 deletion in the spike was detected. This N30 deletion was found in many subvariants, suggesting viral instability and low penetration. SWISS-MODEL analysis revealed that the 30N deletion mutants exhibit a more compact and symmetrical three-dimensional spike structure. The modeling was performed using templates 7nc8.1.A (88.8% similarity) and 8x4h.1.A (99.07% similarity). In the resulting models, His440 was positioned as the first amino acid to interact with the angiotensin-converting enzyme receptor (ACE). However, the JN.1-derived 8y5j.1.A template showed a flattened trimeric spike with protruding residues engaging the receptor. Moreover, a T44I mutation in the nsp2 ribonucleic acid topoisomerase (XLQ96433), a potential drug target, was identified. The T224I ORF1ab mutation occurred in ~300 subvariants. Further analysis identified several important mutations in the ORF1ab polyprotein. The mutations T19I, S50L, V127F, G339H, K356T, S371F, S373P, S375F, R403S, K417N, V455H, G446S, N460K, S477K, Q493E, and Y505H were identified in the spike protein of JN.1 lineages. Moreover, the mutations P13L, Q229K, and S413R in N protein, A63T in M protein, T223I in ORF3a, and F19L in ORF7b protein were observed within the newly studied JN.1 lineage. A 26-nucleotide deletion in the 3′-UTR was highly prevalent (99%), while a 49-nucleotide deletion was observed less frequently. In addition, mutations in the accessory proteins (A68V in XEC.2, H144Q in XEC.3, and G71R in XEC.5) were found, suggesting that recent mutations are clustered in the NH_2-terminus of the spike protein.

Keywords: Sustained mutations; Omicron coronaviruses; KP.3.1.1; XEC.1; Spike insertion

***Corresponding author:**
Asit Kumar Chakraborty
(chakraakc@gmail.com)

Citation: Chakraborty AK. Dominant and sustained mutations, deletions, and insertions in the Omicron coronavirus lineages JN.1, KP.3, LB.1, XEC, MC.1, and MV.1. *Innov Med Omics*. 2025;2(4):42-63. doi: 10.36922/IMO025080014

Received: February 21, 2025

Revised: March 18, 2025

Accepted: April 9, 2025

Published online: August 18, 2025

1. Introduction

The severe acute respiratory syndrome coronavirus 2 (SARS-CoV-2) Alpha, Beta, and Delta variants caused millions of deaths in the world between 2020 and 2025.[1,2] At present, six different coronavirus strains are known to infect humans: HCoV-229E (229E), HCoV-OC43 (OC43), SARS-CoV-2 (COVID-19), HCoV-NL63 (NL63),

HCoV-HKU1 (HKU1), and middle east respiratory syndrome coronavirus.[3] COVID-19 has two unique polyproteins (open reading frame [ORF]1a and ORF1b), an antigenic spike protein (S), and small regulatory proteins such as ORF3a, ORF7a, ORF8, and ORF10. The ORF1ab generates 16 functional peptides proteolytically: nsp1 (1–180 amino acid [aa]), nsp2 (181–818aa), nsp3 (819–2763aa), nsp4 (2764–3263aa), nsp5 (3264–3569aa), nsp6 (3570–3859aa), nsp7 (3860–3942aa), nsp8 (3943–4140aa), nsp9 (4141– 4253aa), nsp10 (4265–4392aa), nsp11 (4393–4400aa), nsp12 (4401–5324aa), nsp13 (5325–5925aa), nsp14 (5926–6462aa), nsp15 (6453–6798aa), and nsp16 (6799–7096aa).[4] It was clearly demonstrated through a multi-alignment approach that nsp2 is a ribonucleic acid (RNA) topoisomerase, which is a target for vaccine and drug development, nsp13 is a messenger RNA capping methyl transferase, and nsp16 is a uridine 2'-OH ribosomal RNA large subunit methyltransferase E.[5-8] Due to mutations, deletions, and insertions, the spread and death potential of the coronavirus changed from time to time, generating many variants of concern (VOC). In the United States, the Wuhan D614G variant first peak occurred between March and August 2020, the Alpha (B.1.1.7) second peak between January and June 2021, followed by a third peak of Delta (B.1.617.2, AY.X) between June and December 2021. From the last week of December 2022, the spread of the fourth peak of the Omicron BA.1 variant (B.1.1.519) with about 30 new mutations in the spike protein occurred, followed by a similar BA.2 variant (no 69HV deletion in spike) spread in April 2022.[9-11] From June to July 2022, the Omicron BA.4 and BA.5 variants with spike 24LPP and 69HV deletions increased worldwide. However, from November 2022, there was a spread of BQ.1 subvariants, followed by a spread of the XBB.1 lineage from March 2023.[12] In August 2023, a spread of more than 448 of the 249RWMD spike insertion sequences was detected in the United States and Europe. However, this lineage was not prominent at the end of 2023. Instead, during November to December 2023, a wave of new sub-subvariants, such as XBB.1.16, XBB.1.5, EG.5.1, HV.1, FL.1.5, BA.2.86, JN.1, and JD.1.1, dominated the Omicron coronavirus sequences deposited in the National Center for Biotechnology Information (NCBI) Virus database. Notably, more than 29 mutations in the spike protein of Omicron coronaviruses, along with concurrent D614G and N501Y mutations, caused antibody escape while causing mostly mild disease outcomes. These mutations included A67V (V67), T95I (I93), N211I (I206), L212V (V207), V215P (P210), R216E (E211), G341D (D336), S373L (L368), S375P (P370), S377F (F372), K419N (N414), N442K (K437), G448S (S443), S479N (N474), E486A (A481), Q495R (R490), G498S (S493), Q500R (R495), Y507H (H502), T549K (K544), H657Y (Y652), P683H (H678), N766K (K761), D798Y (Y793), N858K (K853), Q956H (H951), N971K (K966), and L983F (F978) (residue positions are adjusted for Omicron sequence numbering to account for deletions and insertions; alternate reference positions are indicated in parentheses where applicable).[13] The next major set of spike mutations occurred in the JN.1 variant toward the end of 2023.[14]

The JN.1 variant also contained the 2375SGF deletion in ORF1ab; deletions at positions 24LPP, 69HV, 145Y, 211N (corresponding to 208N in BA.2), and 483V (V480 in BA.2) in the spike protein, a 31ERS deletion in the N protein, and a 26-nucleotide deletion in the 3'-untranslated region (UTR) (based on NC_045512.2 coordinates). Many unique JN.1 spike mutations (H249N [242N], A268D [261D], K360T [352T], R407K [400K], P449H [442H], L456W [449W], L455S [L452], N485K [474K], A488K [480K], and A574V [566V]) were reported. Among these, the L455S mutation has been suggested as a key driver of increased transmissibility and immune escape.[15] Antibody evasion by JN.1 and related XBB.1-associated subvariants has been clearly demonstrated, raising concerns over reduced vaccine effectiveness. As a result, there is an urgent need to prioritize vaccine development targeting this lineage. By January 2024, JN.1 was estimated to account for approximately 80–90% of recent global SARS-CoV-2 transmissions.[16]

Human seasonal coronaviruses exhibit recombination rates of approximately 1×10^{-5} per site and year, contributing to their pathogenic potential. Among recent subvariants, KP.3.1.1 was reported as the most prevalent (>50%), followed by KP.2.3, KP.3.3, and LB.1.7 (>10%), with lower frequencies observed for JN.1.11.1.2, JN.1.16.1, and KS.1.1 (<3%)[1]. The KP.3.1.1 subvariant carried an extra 31S spike deletion, along with the F456L, Q493E, and V1104L point mutations found in KP.3. The LB.1.7 subvariant contained the core JN.1 mutations, along with LB.1-specific Q183H, R346T, and F456L, and additionally featured the new 31S deletion.[17,18] The XEC variant shared JN.1-associated spike mutations, including T22N, F59S, F456L, Q493E, and V1104L, but lacked the 31S deletion.[19] SWISS-MODEL analysis indicated that the PCov_GX spike (PDB: 7cn8.1) provided a suitable template for the XEC spike protein. However, the JN.1 spike (PDB: 8y5j.1.A) template produced a more compact trimeric three-dimensional (3D) model with higher similarity (99.08%) compared to 88.72% for the PCov_GX template[2]. In this study, new deletions and mutations in the JN.1, LB.1, XEC.1, and MC.1 variants were identified, and dominant, sustained point mutations were characterized in key recent Omicron VOCs.[15,19]

[1] Refer to the following website: https://www.idsociety.org/covid-19-real-time-learning-network/diagnostics/covid-19-variant-update/#/+/0/publishedDate_na_dt/desc/)

[2] Research Square, 2024; Doi: https://doi.org/10.21203/rs.3.rs-3830998/v1

2. Methods

Multiple sequence alignment and phylogenetic analysis were performed using the SARS-CoV-2 NCBI Database. The sequences were compared using the CLUSTAL-Omega software.[20] Individual sequences were retrieved from the database (www.ncbi.nlm.nih.gov/nucleotide or protein). BLASTX analysis was performed to identify peptide sequences translated from mutated DNA regions.[21] A BLASTP search was conducted to assess the prevalence of these mutated regions within existing protein databases.[22] For structural analysis, the SWISS-MODEL server was used to generate 3D models of the mutated proteins.[23,24] To identify sustained mutations, multi-alignment of genomes and proteins of important VOCs was conducted. This allowed the detection of clusters of recurrent mutations, which were termed as probable dominant mutations—mutations consistently retained across several VOCs, including the recent variants such as XEC.1, JN.1.11.1, KP.3.1.1, LB.1.7, and MC.1. The SARS-CoV-2 Database, which deposits data of newly isolated coronavirus as early as within 15 days, was used. However, given that approximately 80% of genomes deposited in the SARS-CoV-2 Database were partial sequences, complete sequences were prioritized, particularly those deposited by Howard *et al.*[3]

3. Results and discussion

The JN.1 Omicron coronaviruses have a unique 16MPLF spike insertion compensating 24LPP, 31S, 69HV, 145Y, 211N, and 483V deletions in the spike. A 30N mutation was found in the spike of 31 sequences in the database from November 2023 to December 2024 (Figure 1A and 1B). The 16MPLF insertion was found in 95–99% isolates, whereas a few groups described that JN.1 viruses had no such insertion. Opentrons Labworks Inc., deposited a significant number of JN.1 variant sequences from New York, most of which lacked the 16MPLF spike insertion. In contrast, one of the leading coronavirus sequencing groups reported that 1–5% of such variants may carry the 16MPLF insertion, although not consistently[4]. Data from scientists from the United Kingdom often contained ambiguous base calls (NNNN) at the 16MPLF insertion site; however, the Scotland-based United Kingdom group explicitly confirmed the presence of 16MPLF spike insertion in most JN.1 lineages. This issue has been a topic of the ongoing investigation, and several papers addressing it have been published.[15-17] The skepticism observed in certain circles, such as from Opentrons Labworks Inc., echoes what has been termed the "Duesberg Phenomenon"—named after the retrovirologist Peter H. Duesberg of the University of California, Berkeley. On March 15, 2024, Bajwa *et al.*[5] deposited variant sequences with and without the 16MPLF insertion (PV290532 vs. PV290537). Similarly, on March 14, 2024, Taki *et al.*[6] reported both forms (PV289262 vs. PV289272), suggesting the debate remains unresolved. In addition, more LP.8.1 subvariants of the JN lineage were identified, with Blankship *et al.*[7] reporting LP.8.1 coronaviruses containing the 16MPLF insertion (PV630987) and those without it (PV630992).

Figure 1A shows the initial multiple sequence alignment performed through the NCBI Virus Portal. Near the 31S deletion site, a secondary deletion was observed at two nearby positions, extending the gap (green arrows). To further validate these observations, a BLASTP-2 alignment was conducted between the Wuhan strain (2019) and the new 30N-deleted spike variant (2024) to confirm the deletion, insertion, and several point mutations at the NH_2 terminus of the JN.1 spike protein (Figure 1B). Next, a BLASTP search was performed using the N-terminal 51 amino acids, yielding 28 sequences with 100% similarity. The 30N deletion likely first appeared in November 2023, possibly in the JN.1 or BA.2.86.1 variants (Accession no: OR977133). 30N-deleted spike sequences were deposited by several groups, including (https://www.ncbi.nlm.nih.gov/nucleotide):

(i) Howard *et al.* Accession nos.: PQ206778, PP382191, PP129145, PP957308, PP716664, PQ333598, OR977133, PP973284, and OR985318)
(ii) Smith *et al.* (Accession nos.: PP418957, PP418958, PP494457, PQ210087, PP418956, and PP418953)
(iii) Matzinger *et al.* (Accession nos.: PQ422439, PQ589479, PQ464492, and PQ589518)
(iv) Anderson (Accession nos.: PQ168708, PQ168687, and PQ168624)
(v) Linares-Perdomo (Accession nos.: PQ199720 and PP490873)
(vi) Lauring (Accession nos.: PP777597 and PQ612710)
(vii) Young *et al.* (Accession nos.: PQ790692 and PQ790728)
(viii) Parrott *et al.* (Accession nos.: PP995192)
(ix) Prokop *et al.* (Accession nos.: PP43598t4).

This confirms the authenticity of the 30N deletion, which may disrupt critical N-glycosylation sites in the spike protein.[25] To determine the variant classification of these sequences, the virus database was reverse-searched,

[3] Accession nos.: PQ206778, PP382191, PP129145, PP957308, PP716664, PQ333598, OR977133, PP973284, and OR985318
[4] Accession nos.: PQ206778, PP382191, PP129145, PP957308, PP716664, PQ333598, OR977133, PP973284, and OR985318
[5] Accession nos.: PV290532 and PV290537
[6] Accession nos.: PV289262 and PV289272
[7] Accession nos.: PV630987 and PV630992

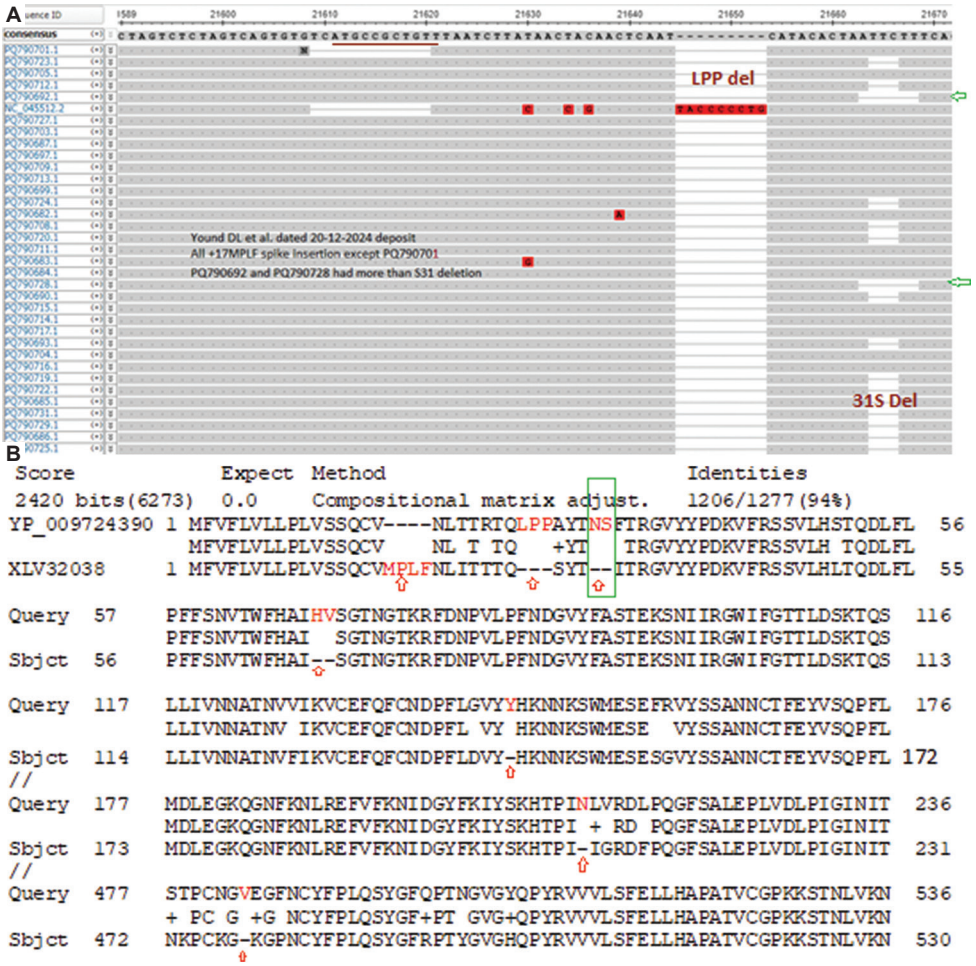

Figure 1. Sequences of coronavirus lineages. (A) First detection of 30N deletion near the 31S deletion in the JN.1 coronavirus lineage (green arrow). (B) BLASTP2 sequence homology of the spike sequence of Wuhan and a new JN.1 30NS spike deleted coronavirus. The new 30N deletion near the 31S deletion is represented by a green rectangular box. All deletions and insertions in the spike protein are also shown by arrows (red). The 16MPLF insertion was not detected by a few scientists but is likely due to the usage of the wrong sequencing primers.

which is quite challenging and time-consuming. The following variant assignments were made: (i) PQ790692 = XDK.3, (ii) PQ790728 = KP.2, (iii) PQ206778 = LB.1.7, (iv) PQ612710 = KP.2.3, (v) PQ333598 = XDC.1.9.1, and (vi) PP973284 = JN.1.15.1. Most of these are likely JN.1 derivatives; and notably, the XEC variant lacks the 31S spike mutation. Recently, an increasing number of XEC.1 and KP.3.1.1 sequences have been reported, indicating these are more infectious than other variants such as LB.1.7. Meanwhile, MC.1 subvariants (MC.10, MC.16, MC.19, and MC.22) display rapid mutation and selection rates. Globally, over 1,500 Omicron MC.1 sequences have been identified, with ~250 such sequences found in the United States. The MC.1 lineage is a descendant of the highly transmissible KP.3.1.1 subvariant (>40% current cases), which is derived from the JN.1 or BA.2.86.1 lineage.[26] According to recent surveillance data, KP.3.1.1 accounts for 39%, XEC for 25%, and MC.1, MC.10, and MC.13 subvariants individually represent 5–7% of all current Omicron infections[8]. No report was available on MC.1 variant coronaviruses in the PubMed as of January 4, 2025.

The XEC variant and subvariants were then compared, as XEC lacked the 31S deletion in the spike, nor the F60S mutation. Notably, the XEC subvariants also lacked the 30N deletion (Figure 2). However, several important point mutations were detected: A68V in XEC.2, H144Q in XEC.3, and G71R in XEC.5, located at the NH_2 terminus of the spike protein. In contrast, the K180R mutation in XEC.1 may not be as significant, given that lysine (K) and arginine (R) are both basic amino acids. In the 3D structure

[8] Refer to the website (https://www.publichealthontario.ca/-/media/documents/ncov/epi/covid-19-sars-cov2-whole-genome-sequencing-epi-summary.pdf obtained dated 4.1.2025

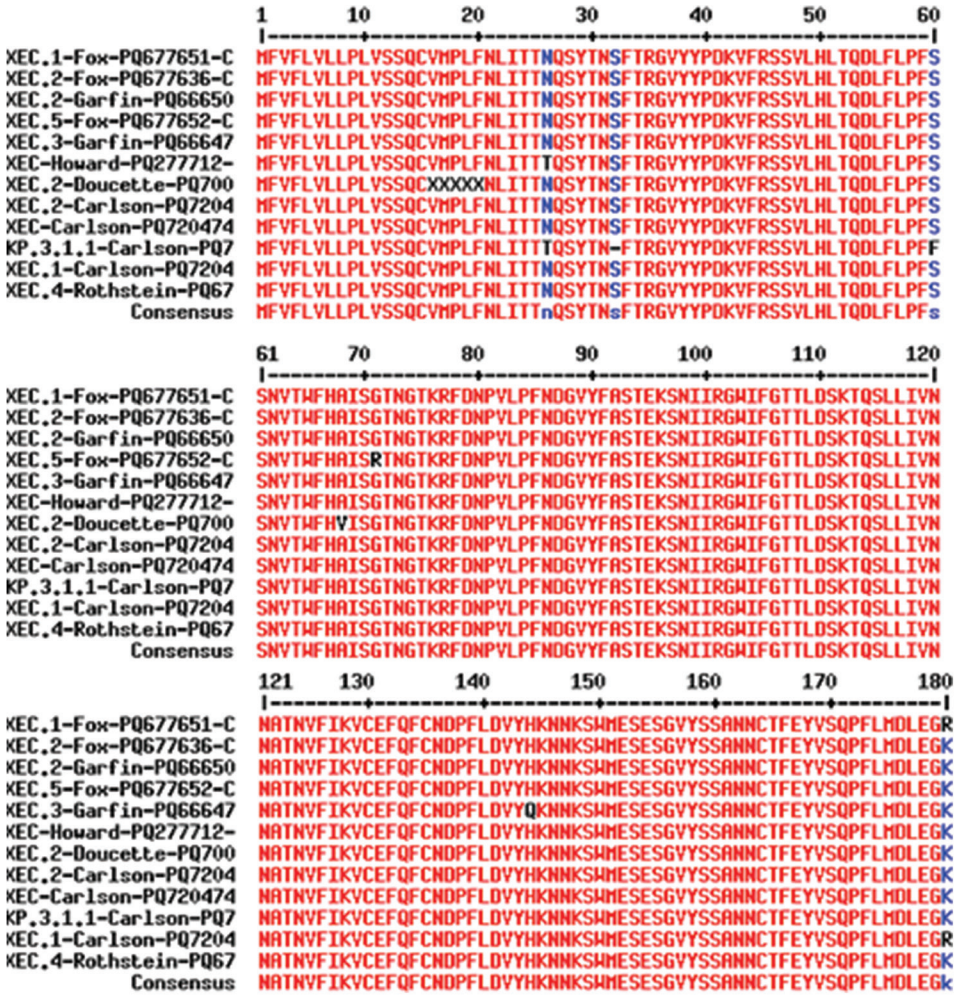

Figure 2. The spike multi-alignment of new XEC variants demonstrates mutations and proves that the SEC variant lacks the 31S deletion and the 30N deletion in the spike. The K180R mutation in the XEC.1, the A68V mutation in the XEC.2, the H144Q mutation in the XEC.3, and the G71R mutation in the XEC.5 were found to be important. The KP.3.1.1 (dominant Omicron variant) has a 31S deletion and F60S mutation in the NH_2-terminus of the spike.

of the proteins, the long side chain of lysine allows it to form hydrogen bonds with oxygen or nitrogen atoms of other amino acids located several angstroms away.

Furthermore, the spike N-terminus of Alpha, Beta, Delta, and Omicron BA.1 were compared with several new subvariants, JN.1, KP.3.1.1, MB.1.1.1, and XEC. It appears that in JN.1 lineages mutations such as threonine to isoleucine (T23I and T19I in Wuhan), serine to leucine (S51L and S50L in Wuhan), and valine to phenylalanine (V126F and V127F in Wuhan) at the NH_2-terminus of the spike protein may negatively impact spike biology by eliminating key phosphorylation sites (Figure 3 and Table 1). Although the substitution of one hydrophobic amino acid (valine) with another (phenylalanine) may seem conservative, the large aromatic ring and delocalized π-electrons of phenylalanine likely induce significant structural and functional changes at that site.[27] Similarly, deletion of asparagine (N) at position 483 in JN.1 lineages may be detrimental by removing a potential site for ionic interaction due to the loss of a positively charged side chain (Figure 3).

Multi-alignment of the receptor-binding domain (RBD) of the spike protein from recent JN.1 lineages was performed and compared with earlier variants, including Alpha (B.1.1.7) and Delta (B.1.617.2 and AY.100) variants (Figure 4). At position 349, a glycine in B.0 and early Omicron was replaced by aspartic acid, and in JN.1 lineages, it was further mutated to histidine. Arginine at position 356 was mutated to threonine (important for phosphorylation) in several JN.1 lineages, such as JN.1.16, KP.2, XDK, and were also noted in XBB.1.5 and BA.4.6 subvariants. Notably, threonine is important, and

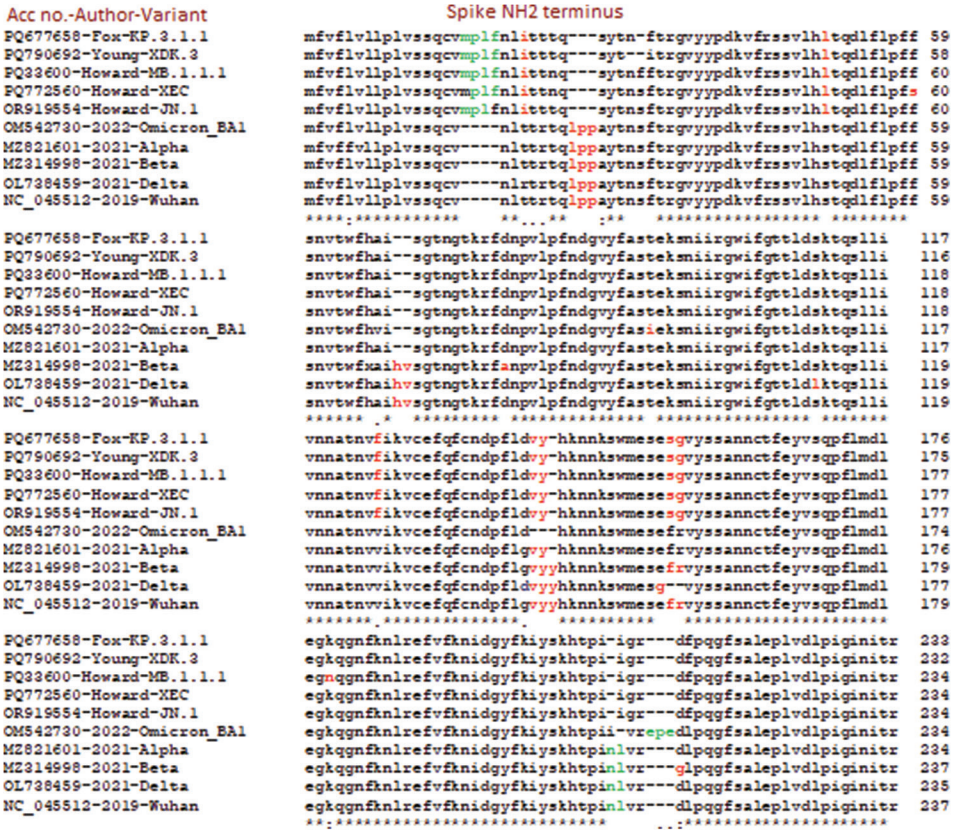

Figure 3. Point mutations, deletions, and insertions at the NH_2-terminus of spike protein of Wuhan, Alpha, Beta, Delta, and Omicron (BA.1, JN.1, KP.3.1.1, MB.1.1.1, and XEC subvariants) coronaviruses

at position 366, a mutation (K356T, Wuhan position) was observed in JN.1 lineages, including KP.2, XEC, XDK, and KP.3.1.1.[26,27] Interestingly, three serine amino acids at positions 381, 383, and 385 (S371, S373, and S375 in Wuhan, respectively) were mutated to phenylalanine, proline, and phenylalanine, respectively. This suggests a compensatory regeneration of phosphorylatable residues elsewhere in the spike (Figure 4A). Previously, it was shown that although Omicron variants carry 30 spike mutations, the overall acidic and basic amino acid proportions remain similar to Wuhan coronavirus.[4] In Figure 4B, important changes in spike can be observed, such as R413K (R403K), R418S (R408S), K427N (K417N), N450K (N440K), V455H (V445H), G456S (G446S), L462W (L452W), L465S (L455S), and N470K (N460K)—notably reintroducing serine residues lost elsewhere. Figure 4C reveals additional mutations in the RBD domain such as S487N (S477N), N491K (N481K), V496P (V486P), and Y515H (Y505H). Of particular interest is the Q503E (Q493) mutation (glutamine to glutamic acid) in JN.11.1.1, KP.3.1.1, and XEC, which may enhance transmission. Similarly, S487N (S477N) disrupts phosphorylation and hydrogen bonding with the oxygen atom or the hydrogen atom of the -OH group, while K488T (K478T) in XDV.1.9.1 restores these features, warranting further database tracking for its epidemiological impact. Mutation positions and their respective variants are detailed in Table 1. Readers are advised to distinguish carefully between multi-alignment and Wuhan reference positions. Numerous studies have addressed spike mutations and ACE2 receptor 3D interactions.[28-30]

Point mutations in the ORF1ab polyprotein were found to be less prevalent and less conserved compared to those in the spike protein. The P4715L mutation in RNA-dependent RNA polymerase (RdRp; P323L; 4401–5324aa) first appeared in 2020 and has been retained in all variants up to January 5, 2025. The analysis detected several additional mutations: Y4662H in BQ.1 and BQ.1.1.1; D4486N in EG.5.1.1; and G5063S in Delta, BA.2.75, FL.1.5.1, and EG.5.1.1 subvariants. However, persistent and defining RdRp mutations appear to be less common in JN.1 lineages (data not shown). However, several synonymous RdRP mutations such as 14676C>T (P412P), 14697C>T (F419F), 15096T>C (N552N), 15240C>T (N600N), and 15279C>T (H613H) were reported through *in silico* in genome

Table 1. Variation of dominant new mutation positions in different JN.1 lineage due to deletion and insertion compared to the multi-alignment position

Multi-alignment position in this article	Based on the Wuhan position (NC_045512.2)	JN.1 position with 16MPLF insertion but no 30NS deletion	KP. 3.1.1 position with 16MPLF insertion and 31S deletion	XEC position with 16MPLF insertion but no 30NS deletion	XDK.3 position with 16MPLF insertion and 30NS deletion
T23I	T19I	T23I	T23I	T23I	T23I
S50L	S50L	S51L	S50L	S51L	S49L
V127F	V127F	V126F	V125F	V126F	V124F
G349H	G339H	G336H	G335H	G336H	G334H
K366T	K356T	K353T	K352T	K353T	K351T
S381F	S371F	S368F	S367F	S368F	S366F
S383P	S373P	S370P	S369P	S370P	S368P
S385F	S375F	S372F	S371F	S372F	S370F
R418S	R403S	R405S	R404S	R405S	R403S
K427N	K417N	K414N	K413N	K414N	K412N
V455H	V445H	V442H	V441H	V442H	V440H
G456S	G446S	G443S	G442S	G443S	G441S
N470K	N460K	N457K	N456K	N457K	N455K
S487K	S477N	S474N	S473N	S474N	S472N
Q503E	Q493E	Q489Q?	Q488E	Q489E	Q487Q?
Y515H	Y505H	Y501H	Y500H	Y501H	Y499H
S949F	S939F	S935F	S934F	S935F	S933F

sequences analysis deposited in the Global Initiative on Sharing All Influenza Data repository.[31,32]

The nsp2 RNA topoisomerase (181–818aa) A211D mutation has been stable in JN.1 lineages (JN.1, KP.1.1, KP.3.3, LQ.1, LY.1, KS.1.1, MA.1, LP.1, KW.1.1, MC.10, and LP.8.1). This mutation may hold functional significance comparable to P4715L in RdRP or D614G and N501Y in the spike protein. Many nsp2 new point mutations (Figure 5) were also detected in KP.3.1.1 (R207C), MC.10 (H374Y), and FL.1.5.1 (K518E) subvariants of JN.1 lineages.[6]

The nsp3 papain-like protease is a multifunctional enzyme (819–2763aa), and due to its complex structure, naturally, many mutations were expected.[33] The T2283I mutation (threonine to isoleucine) was detected in many JN.1 lineages such as JN.1.11.1, KP.1.1, KP3.3, KP.3.1.1, MC.1, MC.10, MC.22, LP.1, and KW.1.1 (Figure 6). Similar dominant mutations such as K1973R (lysine to arginine), N2526S (asparagine to serine), and A2710T (alanine to threonine) were also found in the nsp3 protein (Figures 6 and 7). Individual mutations might be significant but hard to pinpoint in all subvariant classes. Still, several important mutations were identified: P885S and T2007I in the LQ.1 subvariant, G1093S, H1112Y, and S2022P in FL.1.5.1, K1855E in the KS.1.1 subvariant, as well as G1819S in EG.5.1.1. Interestingly, the G1307S mutation was found to be stable in most Omicron variants except BA.1, suggesting that it may play an important role in protease biology.[33,34] The N40A or N40D mutation in the Mac1 domain (206–386aa of nsp3; the mutable N40 amino acid [lowercase letter] is within the ORF1ab protein region, e.g., residues 1056–1067: VVVNAAnVYLKH) substantially reduced protease activity (papain-like protease region: 812–1076aa of nsp3), and lowered the replication efficiency of the virus in human airway organoid.[35] Mac1 (1023–1358aa of ORF1ab) is an adenosine diphosphate (ADP)-ribosylhydrolase that binds and hydrolyses mono-ADP-ribose from target proteins. Further study showed that the alteration of conserved leucine in loop 5 increased the ADP-ribose binding.[36] However, the roles of C-terminal N2526S and A2710T mutations have not yet been characterized. The amino acid mutations into serine, threonine, and tyrosine are essential in protein biology due to their phosphorylation and conjugation abilities and hydrogen bonding. Similarly, the nsp5 protease P3395H mutation was found in all Omicron coronaviruses (BA.1 [B.1.1.529.1], BA.2, BA.4, BA.5, BQ.1, and XBB.1), including newly identified JN.1, XEC, KP.3.1.1, and MC.1 subvariants. This mutation was not detected in Wuhan (B.0), Alpha (B.1.1.7), Beta (B.316.2), Gamma (P.1; B.1.1.28.1), Iota (B.1.526), Zeta (P.2; B.1.1.28), and Delta (B.1.617.2) variants (Figure 8). The other mutations that

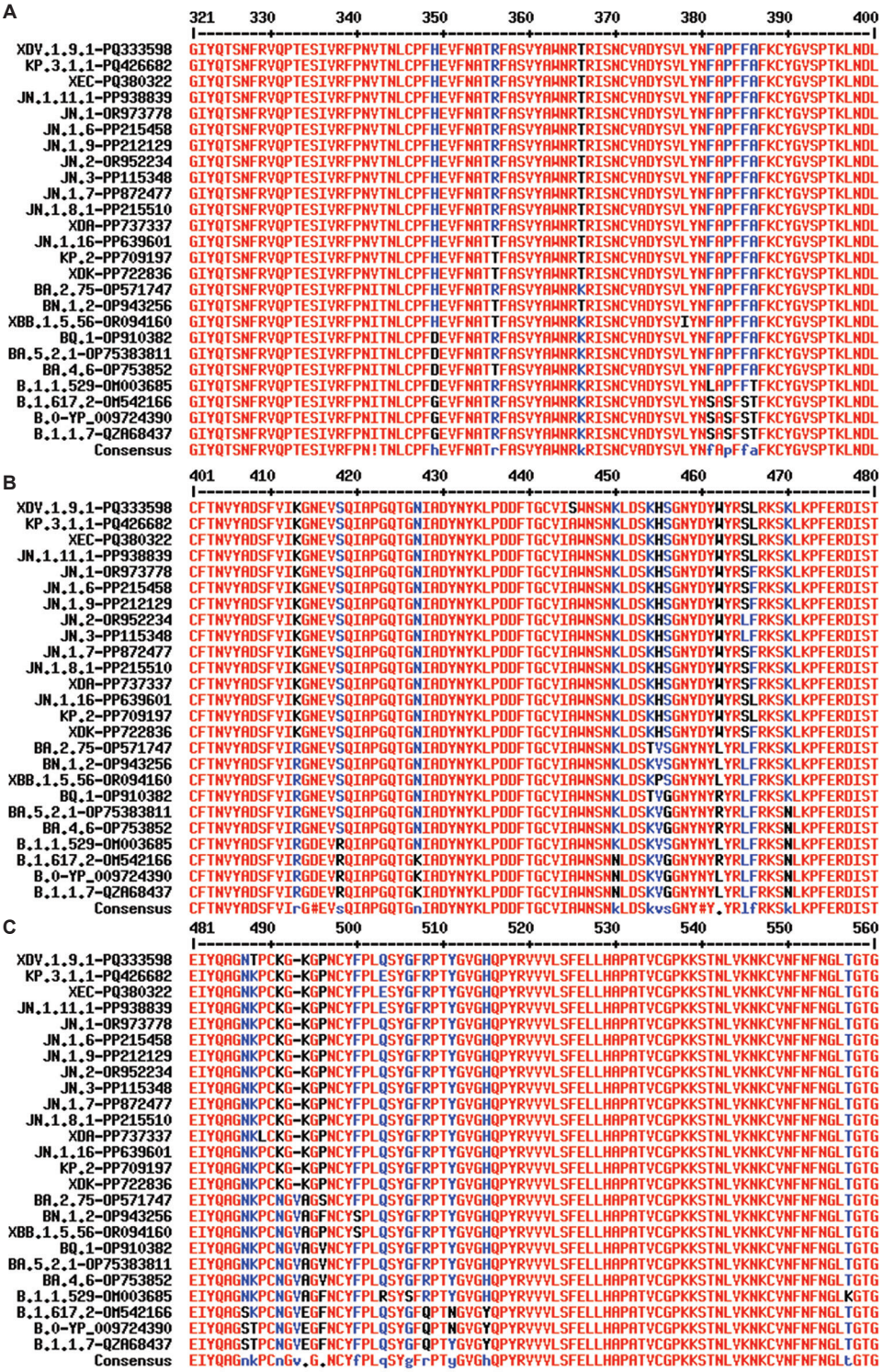

Figure 4. (A-C) Multi-alignment of the receptor binding domain (RBD) of the spike protein of Omicron JN.1-lineage coronaviruses compared to the Alpha and Delta variants. Wuhan variant spike (protein ID. YP_009724390) was used as the standard. The RBD amino acid sequences of the spike are greatly varied in the Omicron variants. The G349H, K366T, S381F, S383P, S385F, R418S, K427N, V455H, G456S, N470K, S487K, and Y515H mutations were considered important. Only 483V (one amino acid deletion) is shown in the JN.1 lineage.

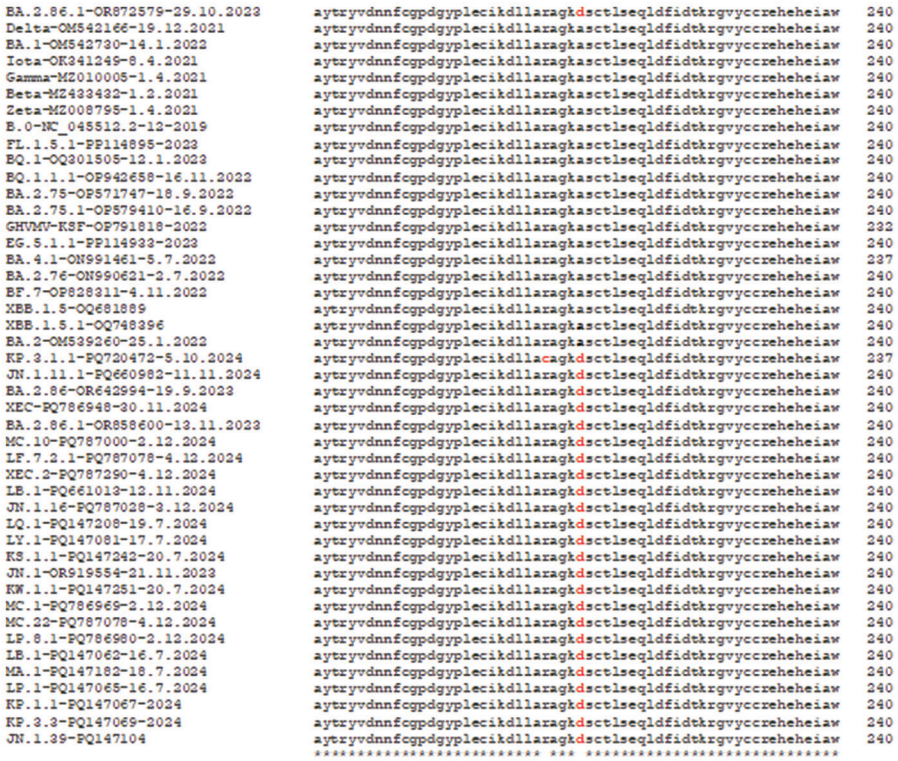

Figure 5. Important A211D (alanine to aspartic acid) mutation in nsp2 RNA topoisomerase (open reading frame 1ab polyprotein 181–818 amino acid position) of the JN.1 lineage Omicron coronaviruses

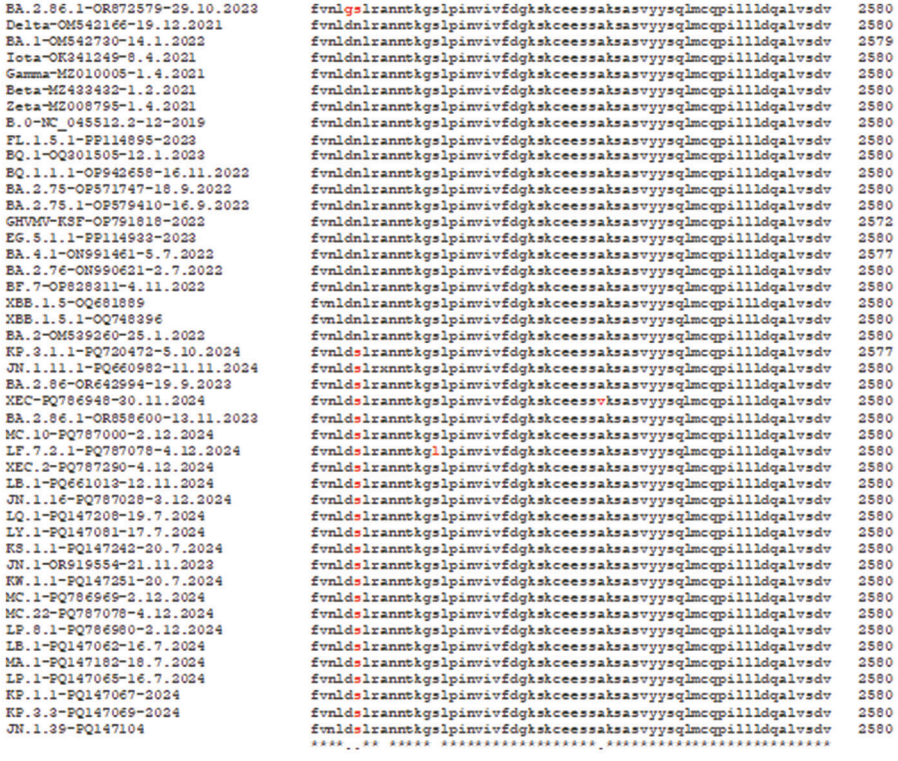

Figure 6. The multi-alignment of open reading frame (ORF)1ab polyprotein to demonstrate important N2526S mutation in nsp3 MLpro protease (ORF1ab 819–2763aa) in JN.1 lineage Omicron coronaviruses

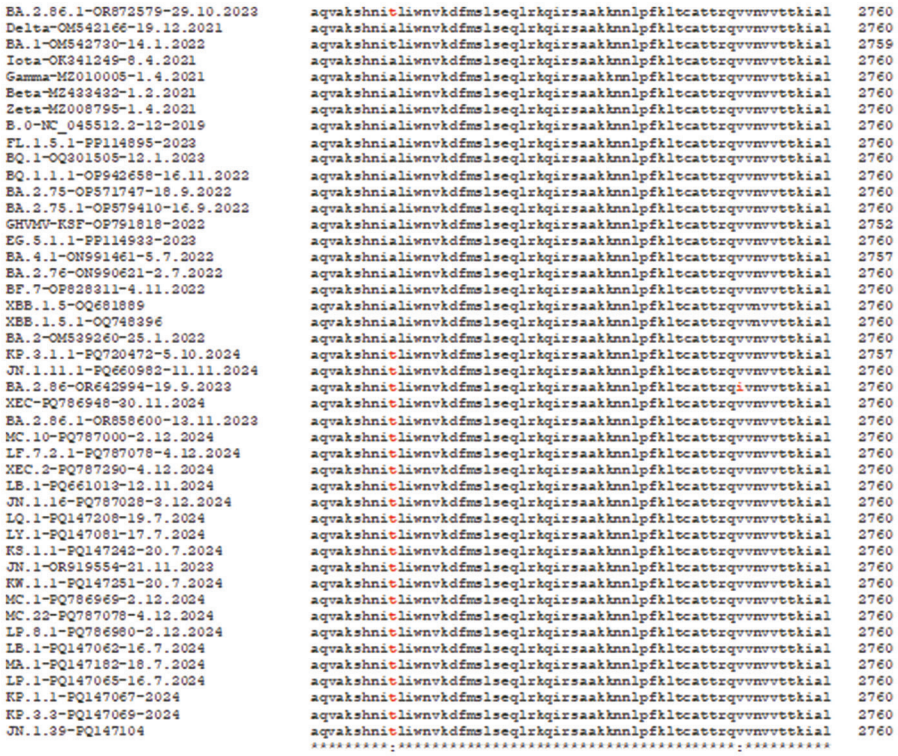

Figure 7. The multi-alignment of open reading frame (ORF) 1ab polyprotein to demonstrate important A2710T mutation (alanine to threonine) in the nsp3 MLpro protease (ORF1ab 819–2763 amino acid) in many JN.1 lineage of Omicron coronaviruses (amino acids in red)

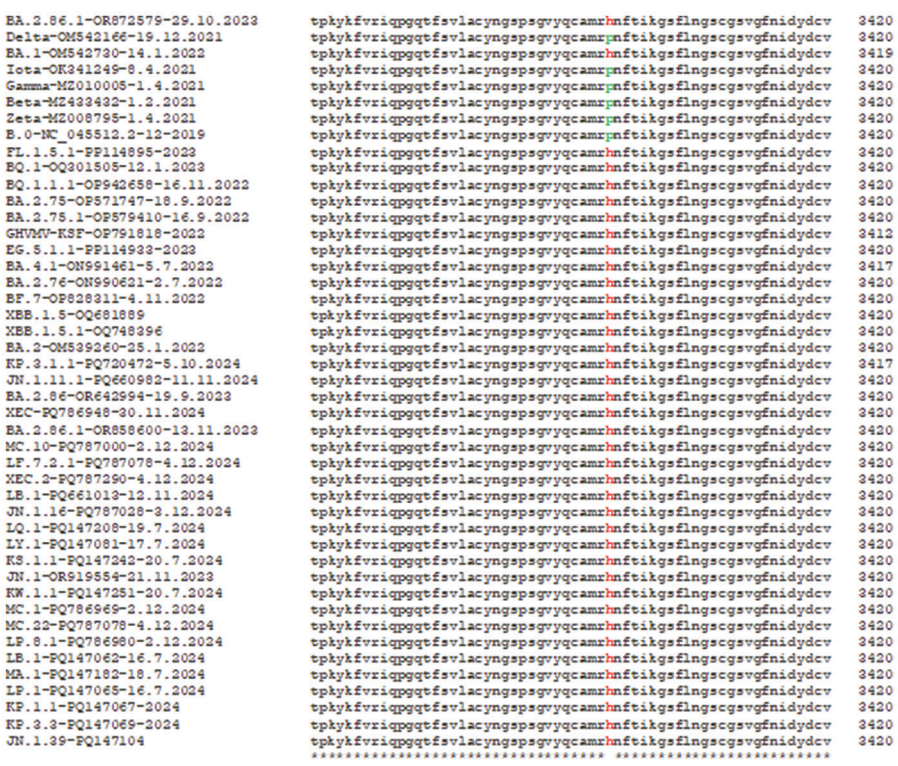

Figure 8. The multi-alignment of open reading frame 1ab polyprotein to demonstrate nsp5 protease P3395H mutation in all Omicron coronaviruses (BA.1, BA.2, BA.4, BA.5, BQ.1, and XBB.1), including the newly identified JN.1, XEC, KP.3.1.1, and MC.1 subvariants. This mutation was not detected in 2019–2021.

are immediately downstream of the P3395H site (ORF1ab residues 3391–3440: CAMRPNFTIK GSFLNGSCGS VGFNIDYDCV SFCYMHHmel PTGVhAGTDL EGNFYGPFVD RQTAqAAGTD) caused drug resistance to nirmatrelvir (amino acid changes are noted as lowercase letters).[37] The mutable amino acid region is given, as amino acid positions in the region vary across domains and peptides, making precise localization challenging. For example, the 3576SGF deletion changes the positional numbering.

A sustained amino acid change in the capping methyl transferase-RNA helicase (nsp13) was not found. However, R5713C (arginine to cysteine) mutation might be important to create a new S–S bond, stabilizing the 3D structure in many JN.1 coronaviruses (Figure 9).[38] Similarly, the single N5589S mutation in the BQ.1.1.1 subvariant, Y5936L in the KS.1.1 subvariant, T5535I in the MC.10 subvariant, and S5357P in the XBB.1.1 subvariant altered the number of important amino acid residues involved in phosphorylation. Interestingly, the A336V mutation in the nsp13 helicase impaired the helicase unwinding and adenosine triphosphatase activity but retained the ability to associate with the core replication proteins nsp7, nsp8, and nsp12.[39] Due to the homology search, a capping-methyltransferase activity was postulated in nsp13.[40] Notably, a recent paper by Grimes and Denison[41] accepted the hypothesis that nsp13 indeed had RNA capping activities.

There was no cluster of amino acid changes in nsp16 2'-O-ribose uridine methyl transferase.[8] However, several mutations were observed in the Delta variants (G7036H and E6945D), supporting the hypothesis that the higher mortality rate of Delta might be due to potential methylation of human rRNAs inhibiting protein synthesis in the ribosome. The role of inactivating nsp16 D130A and K170A mutations was recently explained.[42] However, single point mutation was detected in nsp15 ribonuclease (6453–6798aa) of various coronaviruses including XEC variant (G6735Y), KP.3.1.1 subvariant (S6737F), BA.2.86 subvariant (V6518M), BQ.1 variant (P6719L), BA.2.75.1 subvariant (L6616S), and FL.1.5.1 subvariant (S6596I) (data not shown).

The major mutations and deletions in the N protein involved in viral replication and cellular inflammation

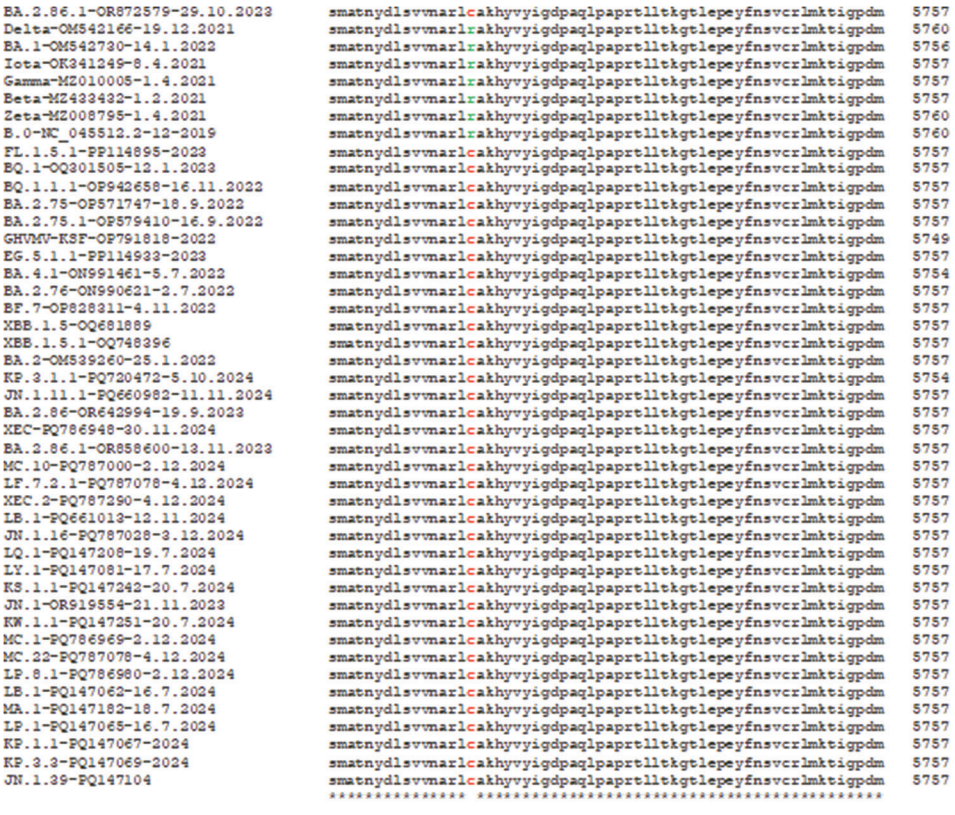

Figure 9. The multi-alignment of open reading frame 1ab polyprotein to demonstrate the important R5713C (arginine to cysteine) mutation in capping methyltransferase-RNA helicase (nsp13) of BA.2.75, BF.7, BA.4.1, XBB.1.5.1, KS.1.1, JN.1, LB.1, KP.1.1, KP.3.3, KW.1.1, KP.3.1.1, MC.1, MC.10, MC.22, and XEC variants. This mutation was not detected in Wuhan (B.0), Alpha, Beta, Gamma, Iota, and Delta variants, including the Omicron BA.1 variant.

were also studied.[43] The SARS-CoV-2 N protein spans 419 amino acids and encompasses three intrinsically disordered regions (IDRs), along with two conserved structural regions (CSRs). IDRs consist of an N-terminal disordered structure (N-arm), a central serine/arginine-rich flexible linker region positioned in the middle, and a C-terminal disordered structure (C-tail), whereas CSRs consist of two N-terminal and C-terminal domains to form multimeric protein complexes.[44] The results are shown in Figure 10. No 31ERS deletion was observed in the Alpha and Delta variants in 2021. However, the deletion appeared in early Omicron variants BA.2, BA.2.75, BQ.1, BA.5.2.1, BF.7, XBB1.5, XBB.1.5.9, XBB.1.5.69, XBB.1.16.6, FL.5.1.1, and EG.5.1 and in JN.1 lineages (JN.1.11.1, JN.1.16, KP.2, MV.1, KP.3.1.1, KP.3.3, XEC, LP.8.1, MC.1, MC.22, and LB.1.2.1) (Figure 10). Thus, the 31ERS deletion was stable in Omicron coronaviruses, including the P13L point mutation (Figure 10A). Mainly, the R204P mutation appeared newly in XEC, XEC.1, XEC.2, and XEK, while the G204R mutation was still maintained in most JN.1 lineages (MC.1, JN.1.16, JN.1.11.1, LB.1, and LP.8.1), including XBB.1.5 lineages (Figure 10B). The Q229K mutation was found in XEC and JN.1 lineages but not in BA.2, BA.5, and XBB.1.5 lineages, including EG.5.1 and FL.5.1.1 (Figure 10C). Similarly, the S413R mutation occurred early and was found in all Omicron coronaviruses, including JN.1 and XEC lineages. They were compared with Wuhan (B.0), Alpha (B.1.1.7), Beta (B.1.351), and Delta (B.1.617.2) variants, which were standard coronaviruses between 2019 and 2020.

The mutations of the ORF3a regulatory protein were characterized, and only the T223I dominant mutation was found in all BA.5, BQ.1, XBB.1, and JN.1 lineages. This mutation is critical for the stabilization of the ORF3a 3D structure to interact with cellular proteins, facilitating the life cycle of COVID-19 in the host (Figure 11). The new mutations were always dispersed in many JN.1 lineages. For example, D27H in the MC.22 subvariant, T89I in the MV.1 subvariant, K67N in the KP.2.3.12 subvariant, W149C in the LB.1.7 subvariant, T175K in the MC.10 subvariant, and P178L in the LP.8.1 subvariant may be important. The S171L mutation was detected in LB.1.7 and MV.1 new subvariants as well as in the EG.5.1.1 and Beta variants. Thus, the S171L and T223I mutations were favored in the ORF3a protein; however, the loss of amino acids such as serine and threonine could be detrimental due to the lack of a possible phosphorylation site that likely stabilized its 3D structure.[45] The recently reported cryo-electron microscopic structures of SARS-CoV-2 ORF3a revealed that it had the capacity to form dimers and functioned as a non-selective cation-permeable viroporin.[46] Hence, modeling was performed for the ORF3a protein of LB.1.7 subvariant (accession no.: PQ661028; protein ID: XKU01502) that had both detrimental mutations, the MV.1 subvariant (accession no.: PQ661072; protein ID: XKU02030) that carried one detrimental T223I and one extra T89I mutation, and the MC.1 subvariant (accession no. PQ786969; protein id. XLV20073) that carried T223I mutation only. Azad and Khan[46] reported that among the 12 important mutations, three mutations (Y160H, D210Y, and S171L) lead to alterations in secondary structure and protein disorder parameters of the ORF3a protein.

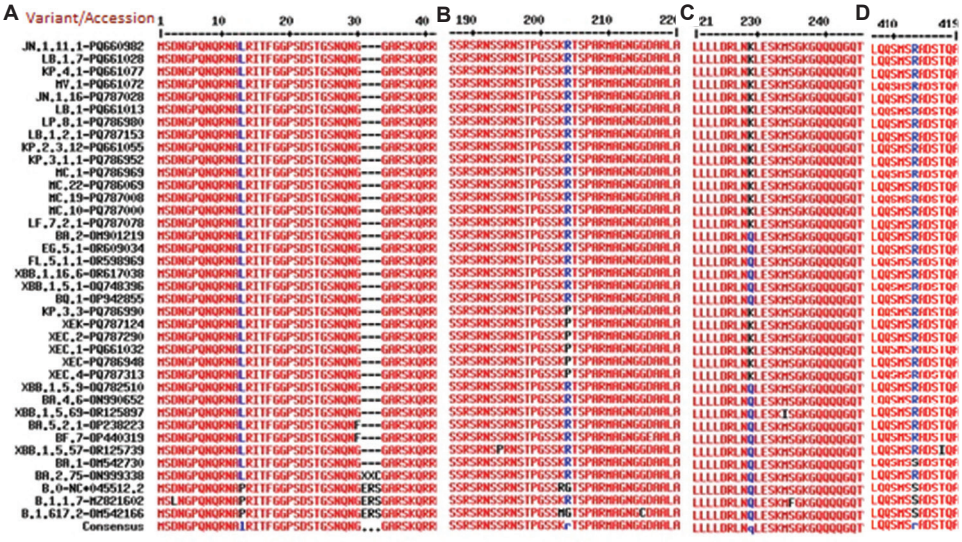

Figure 10. (A-D) The multi-alignment of nucleocapsid protein (n = 419 amino acid) to demonstrate important mutations (P13L, Q229K, and S413R) in important variants of coronaviruses, including MC.1, JN.1, MV.1, KP.3.1.1, and XEC.1 subvariants, with respect to time. The new R204P mutation was found only in the XEC lineage, which lacks the 30N and 31S deletions in the spike protein.

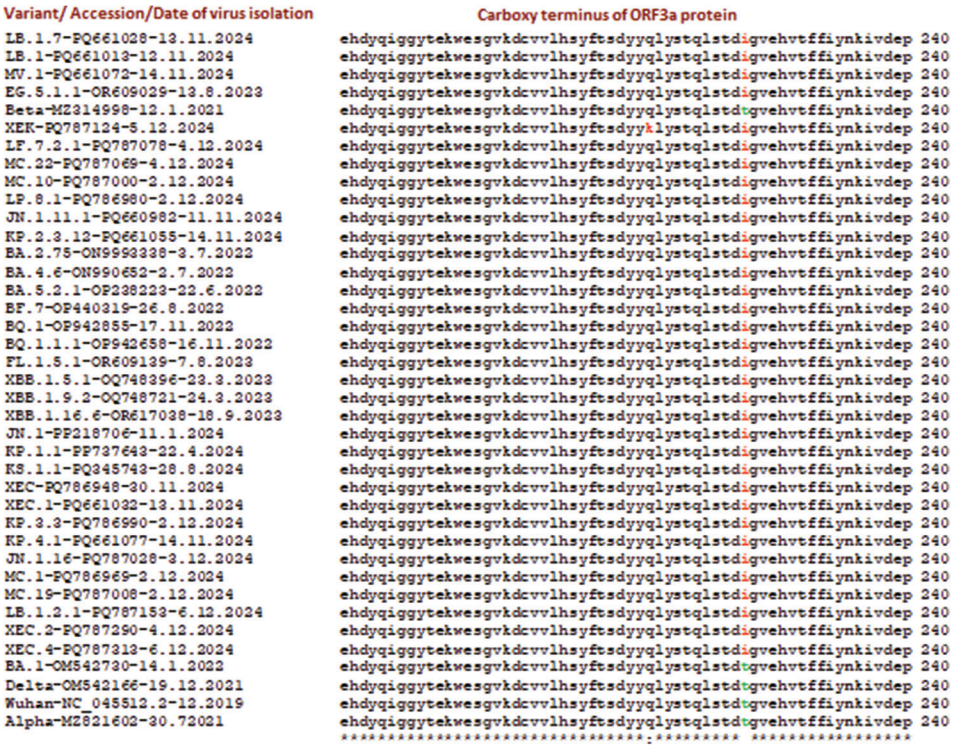

Figure 11. The multi-alignment of the open reading frame a (ORF3a) regulatory protein to demonstrate dominant T223I (threonine to isoleucine) mutation that first appeared in BA.2 lineages and was identified in JN.1 lineages, including JN.1, LB.1, KP.3.3, XEC.1, and MC.1 subvariants

The membrane protein (M) of BA.1 Omicron coronavirus had D3G, Q19E, and A63T mutations.[15,47,48] The A104V mutation in the JN.1 variant was previously detected, and the SWISS-MODEL analysis showed no gross changes in the 3D structure of M protein compared to the published SARS-CoV-2 M-protein 3D models (PDB ID: 8CTK; 7VGR; 7Y96). A T30A new mutation was mostly found in JN.1 lineages, but the A63T mutation was detected in all Omicron coronaviruses, including JN.1 lineages such as KP.3.3, MC.1, MC.22, LB.1.7, LP.1, XEC.2, and XEK (Figure 12).

Finally, the penetration of different mutations was checked by BLASTP search using oligonucleotides at the mutation or deletion boundary, as shown in Table 2. The 30N spike deletion was new, with only 31 sequences deposited in GenBank, whereas the 31S deletion had more than 5,000 sequences in the database. Similarly, the R405S and K414N mutations had only 150 entries, whereas the Q489E/Y501H and N436K/G442S mutations had high penetration, suggesting that the XEC and KP.3.1.1 subvariants, although they appeared only a few months ago, generated a high volume of data within a short period due to higher transmission.[49] The ORF1ab mutations are well-established; hence, greater than 5,000 sequences were available, but the exact figure was not available as the NCBI Server had a 5,000 limit. The ORF3a W149C and S179L mutations were less prevalent and were mostly found in the LB.1.7 subvariant, similar to the F19L mutation in the ORF7b of the XEC.2 variant (Table 2).

The SARS-CoV-2 small transactivator proteins such as ORF7a and ORF7b were implicated as modulators of cellular genes such as *STAT1/2*, *Tom70*, and *IRF3* to downregulate production of interferon gamma, interleukin 6, and immunoglobulin G. Genetic loci of these genes were frequently deleted and mutated with no expression of the small proteins, with an easier virus clearance by the host immune response.[41] Multi-alignment found ORF7a 60–63 nucleotide deletions in the carboxy-terminus, in which the TAG termination codon of ORF7a and the ATG initiation codon of the *ORF7b* gene can be deleted, with no production of both functional proteins. In some situations, a chimera ORF7a protein may be formed due to an inactivation of the TGA codon. More surprisingly, the ORF7a/b deletion mutants are also associated with the creation of a downstream TAA termination codon in the *ORF8* gene, which was shown as a potential hotspot of at least a dozen mutations. For example, 96-nucleotide *ORF7a* gene deletions were found in B.1 (MW309829), B.1.1.7 (MZ780448), BA.2 (ON729188), and BA.4 (OP138059) coronaviruses.

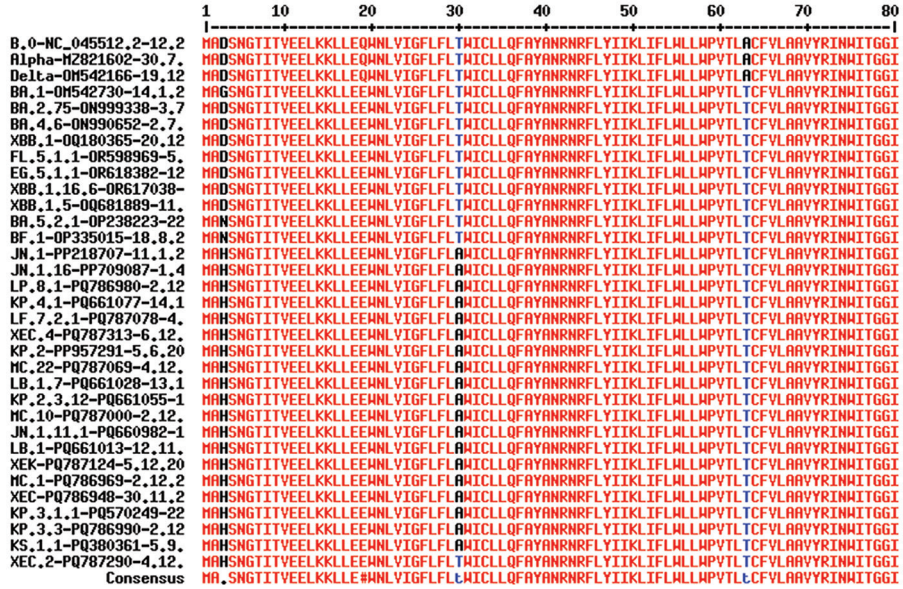

Figure 12. Multi-alignment of the membrane protein of COVID-19 to demonstrate the prevalence of the D3N, T30A, and A63T mutations in JN.1 new lineages. D3N did not appear in early variants including XBB.1, XBB.1.5EG.5.1.1, and FL.5.1.1. The new T30A mutation was mostly found in JN.1 lineages, but the A63T mutation was detected in all Omicron coronaviruses, including JN.1 lineages such as KP.3.3, MC.1, LB.1.7, LP.1, XEC.2, and XEK.

Table 2. Penetration of spike and other protein mutations in the JN.1 coronavirus lineages

Variant	Mutation	Sequences of the mutated region used for BLASTP	100% homology (limit=5,000)
XDK.3	30NS deletion	MPLFNLITTTQSYTITRGVYYPDKVFRSSVLHLT	31
KP. 3.1.1	30S deletion	MPLFNLITTTQSYTNFTRGVYYPDKVFRSSVLH	>5,000
Nil	Forced N30I mutation	MPLFNLITTTQSYTIFTRGVYYPDKVFRSSVLH	0
XEC	T26N, with no 30NS deletion	MPLFNLITTNQSYTNSFTRGVYYPDKVFRSSVLH	>800
JN.1	R405S	GVSPTKLNDLCFTNVYADSFVIKGNEVSQIAPGQTG	>150
Omicron and JN.1	S468F, S470L, and S472F	RISNCVADYSVLYNFAPFFAFKCYGVSPTKLNDLCF	>5,000
Omicron and JN.1	R405S and K414N	DSFVIKGNEVSQIAPGQTGNIADYNYKLPDDFT	>150
Omicron and JN.1	Y501H	NCYFPLQSYGFRPTYGVGHQPYRVVVLSFELLHAPATVCGP	>800
Omicron and JN.1	S935F	KLIANQFNSAIGKIQDSLFSTASALGKLQDVVNHNA	>5,000
KP. 3.1.1	N436K, G442S, etc.	VIAWNSNKLDSKHSGNYDYWYRSLRKSKLKPFE	>5,000
XEC	Q489E and Y501H	KGPNCYFPLESYGFRPTYGVGHQPYRVVVLSFELLHA	>5,000
ORF3A mutation penetration of LB.1.7			
LB.1.7	W149C and S179L	DANYFLCCHTNCYDYCIPYNSVTSSIVITLGDGTTSPIS	2
LB.1.7	S179L only	HTNCYDYCIPYNSVTSSIVITLGDGTTSPIS	>850
LB.1.7	W149C	WLCWKCRSKNPLLYDANYFLCCHTNCYDY	70
ORF7b protein (43 amino acids only) mutation penetration of LB.1 and XEC.2			
XEC.2 and LB.1	F19L	LIDFYLCFLAFLLLLVLIMLIIFWFSLEL	80
ORF1ab mutation penetration of JN.1 lineages			
JN.1	A211D	GPDGYPLECIKDLLARAGKDSCTLSEQLDFIDTKRG	>5,000
JN.1	N2526S	RHSLSHFVNLDSLRANNTKGSLPINVIVFDGKSK	>5,000

Preliminary 3D graphics interactive studies indicated a few dozen proteins such as poliovirus receptor, interferon regulatory factor 3, activating transcription factor 6, Beclin 1, FK506-binding protein 10, endoplasmic reticulum degradation-enhancing α-mannosidase-such as protein, vitronectin, OPJ94, SEC62, 36 kDa vesicular integral

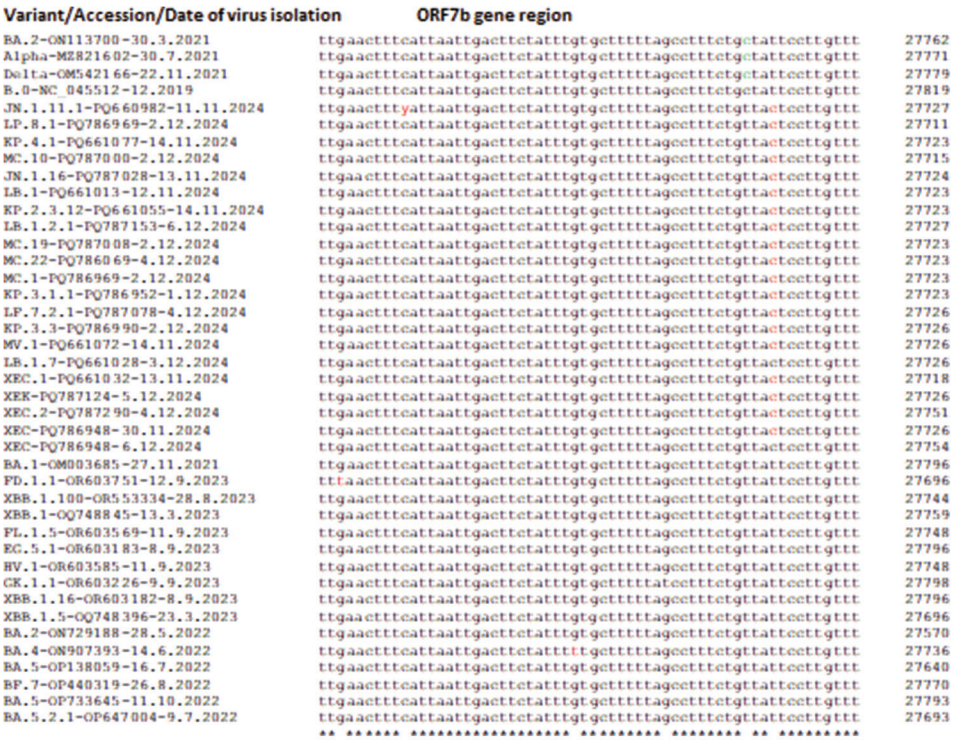

Figure 13. Genomic multi-alignment to demonstrate the important T27810C mutation (F19L amino acid change) in the *ORF7b* gene of JN.1 lineages

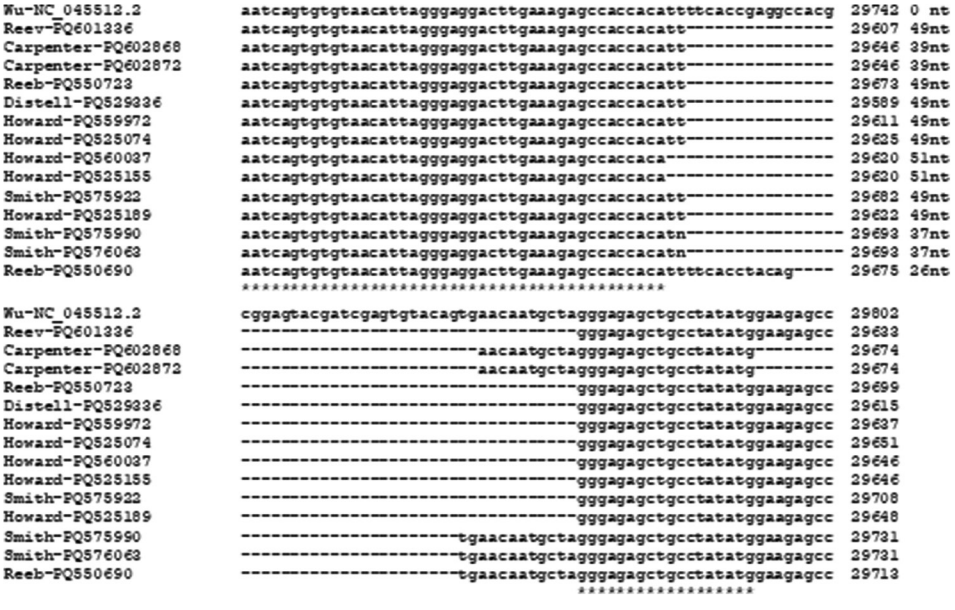

Figure 14. The 3'-untranslated region (UTR) has greater than 26-nucleotide deletions in several JN.1 lineage of coronaviruses. The 26-nucleotide 3'-UTR deletion was found to be 99% in the database. Note that the sequences were derived from 2022 and correspond to the BA.1 variant. The sequences lack the 16MPLF spike insertion but have the 69HV and 143VYY spike deletions, 215EPE spike insertion, and no 24LPP deletion (data not shown).

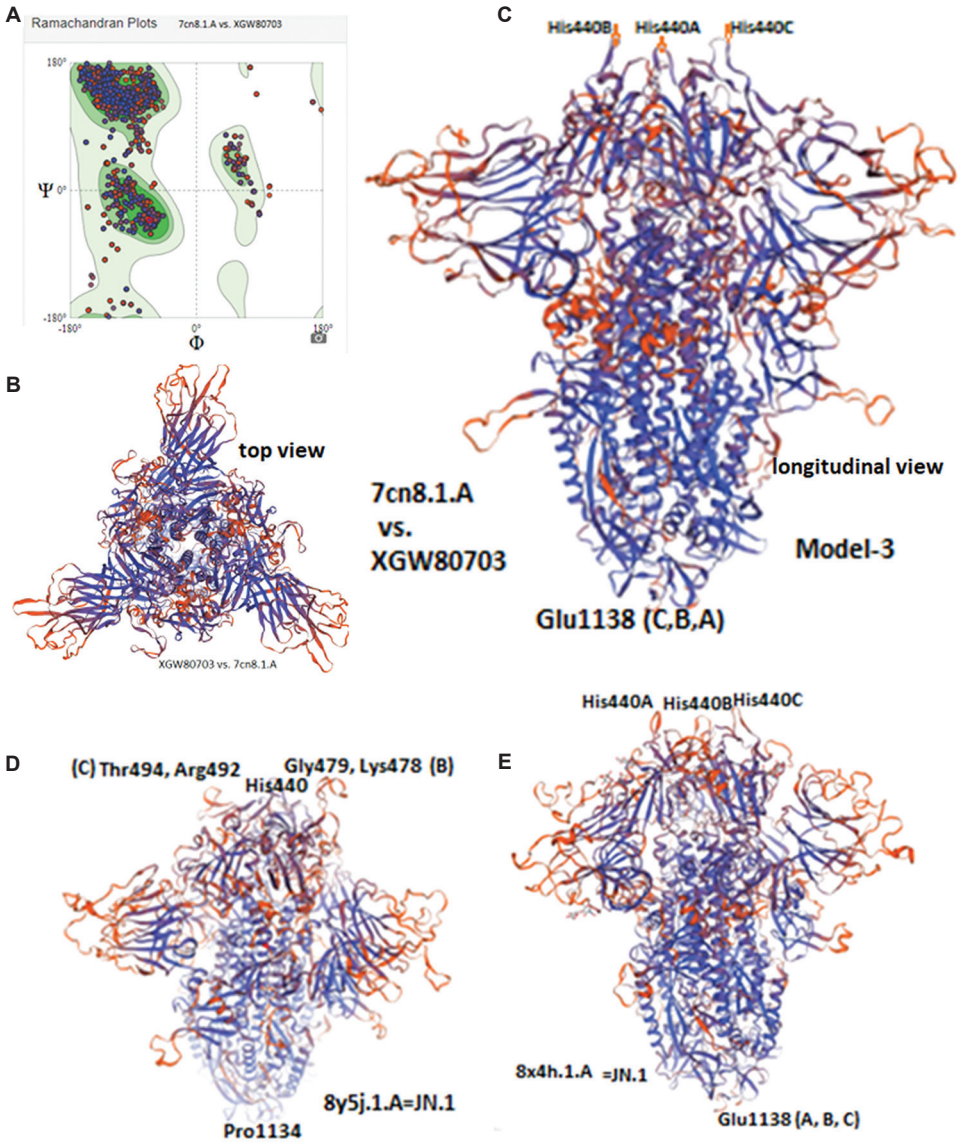

Figure 15. The SWISSMODEL three-dimensional (3D) structure of the spike of the 30NS deletion mutant of JN.1 coronavirus using different templates. (A) Ramachandran plot. (B) A good 3D model of spike top view using 7cn8.1.A template, (C) same longitudinal view with His440 as the first amino acid to interact with angiotensin-converting enzyme 2 (ACE2) receptor, (D) longitudinal flattened view using 8y5j.1.A (JN.1) template with protruding Lys478, Gly479, Pro480, and Asn481, as well as Arg492 plus Thr494 to interact first with ACE2 receptor, and (E) a longitudinal good 3D view of trimeric spike using 8x5h.1.A (JN.1) template and His 440 is the top amino acid to interact similar to 7cn8.1.A template. Note that 7cn8.1.A and 8x4h.1.A had 88% and 99% similarities to the modeled spike (protein ID: XGW80703).

membrane protein, TBP-related factor 3, and polycystin-1, lipoxygenase, alpha-toxin domain interacted with the ORF8 protein, regulating protein folding, apoptosis, and interferon production.[50] This interaction likely favored COVID-19 survival in host cells, inhibiting immune control mechanisms. It is reported that the ORF8 protein (121 aa) deregulation was due to the creation of a termination codon (CAA=TAA; AAA=TAA) with or without S24L mutation, but with no L84S mutation (accession nos.: MZ213478, OK234981, ON113700, and OP711844). One ORF8 mutant is in the BA.2 variant (OW221449), and the other is in the Omicron BA.5 variant (OP733645 and OP671680). One termination codon mutant also had a 63-nucleotide *ORF7a* gene deletion (OP711842).[51] Similarly, highly infectious, less pathogenic, and antibody-resistant Omicron XBB.1, XBB.1.5, XBB.1.9.1, and XBB.1.5.1–XBB.1.5.100 subvariants (accession no.: OQ783588) did not produce an ORF8 protein due to a termination codon mutation in the eighth codon (GGA=TGA).[52] Surprisingly, the ORF7b deletion or ORF8 termination codon mutations were not

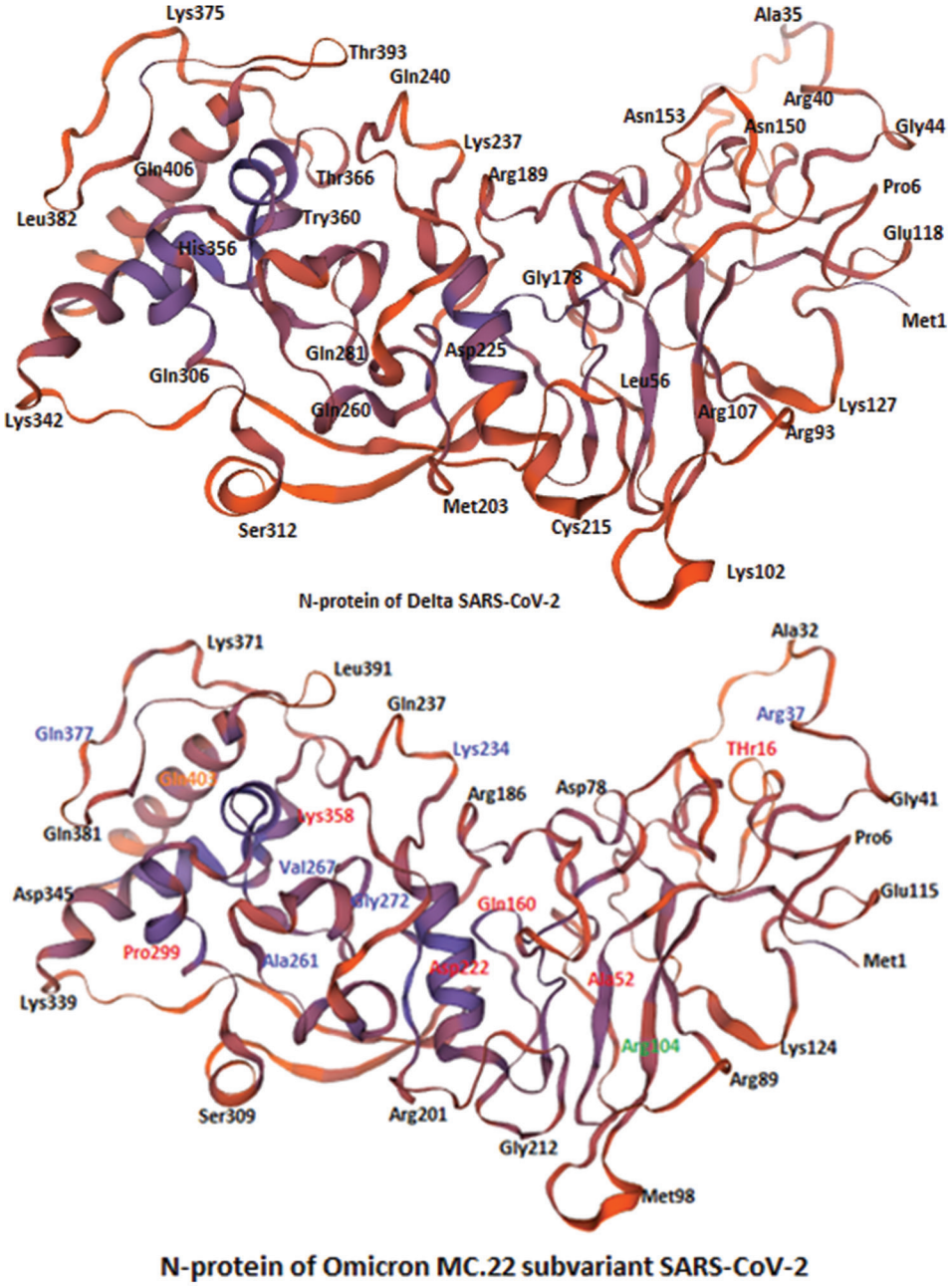

Figure 16. The three-dimensional structure of nucleocapsid protein (N) of Delta (B.1.617.2) coronavirus (2021) compared with the three amino acid-deleted new MC.22 subvariant Omicron coronavirus (2024)

found in the KP.3.3, JN.1, XEC.1, MC.1, and LB.1 variants. However, the ORF7a/b and ORF8 regions were shown to be very mutation- and deletion-prone in Omicron coronaviruses.[53,54] Instead, a dominant and sustainable F19L mutation was found in the *ORF7b* gene but not in the *ORF7a* gene (Figure 13). The 26-nucleotide 3'-UTR deletions of Omicron coronaviruses were overwhelming,[55] but the vigorous search method found larger deletions in that region, as demonstrated in Figure 14.

The SWISS-MODEL analysis of 3D structures is important to know if mutations affect the overall tertiary structure of the protein (Figure 15A to 15D). SWISS-MODEL analysis of the spike protein indicated a more compact symmetrical 3D structure of 30NS deletion mutants with His440 as the first amino acid to interact with the ACE2 receptor using 7nc8.1.A (88.8% similarity) and 8x4h.1.A (99.07% similarity) templates (Figure 15C). However, using the JN.1-derived 8y5j.1.A template, the

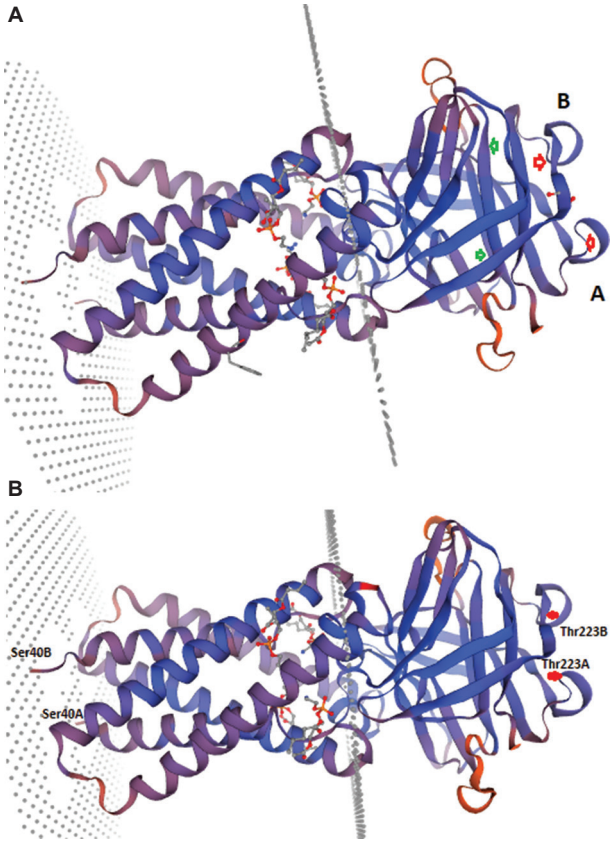

Figure 17. Swiss-model analysis of the three-dimensional longitudinal view of the open reading frame a (ORF3a) protein dimer with the (A) S171L and T223I mutations (upper panel) and (B) Wuhan ORF3a. The red arrow indicates the T223I mutation position, and the green arrow indicates the S171L mutation position.

trimeric spike 3D structure was flattened or shorter and had protruding amino acids (Lys478, Gly479, Prp480, and Asn481), with Thr494 and Arg492 encountering the receptor first (Figure 15D). Feng *et al.*[26] using cryo-electron microscopy (PDB=8Y5J) technology demonstrated that residues on the receptor-binding site of KP.3.1.1 RBD are highly conserved with JN.1 and form extensive electrostatic interactions with ACE2: E493 and R498 form salt-bridges with K31 and D38, respectively, the main-chain of P486, F490, S494, and G502 form hydrogen bonds with the side-chains of Y83, K31, H34, and K353, respectively, N477 and Y489 form hydrogen bonds with S19 and Y83, respectively. Moreover, Y449 form hydrogen bonds with D38 and N42, N487 with M82 and Y83 and T500 with Y41 and N330.[25]

The 3D structure of the nucleocapsid protein (N) of Delta (B.1.617.2) coronavirus was modeled and compared with the new MC.22 subvariant Omicron, which has three amino acid deletions and Q229K and S413R mutations, using the 8fd5.1.A template (Figure 16). The Global Model Quality Estimate value was the same (0.92), but the MolProbity score changed from 0.90 to 0.95. The bad bonds also increased from 15 to 21, suggesting that mutations did affect the 3D structure.

The mutations did not affect the 3D structure of ORF3a regulatory protein using the 8eqj.1.A template for S171L and T223I mutations (Figure 17). The overall symmetry was maintained, but the SWISS-MODEL clash score increased from 1.67 (Wuhan) to 2.73 (LB.1.7), indicating that mutations were not favored.[56,57]

4. Conclusion

The dominant mutations, deletions, and insertions in different JN.1 coronavirus lineages were documented in the context of sustained dominant mutations, mostly appearing first in BA.1 or BA.2 Omicron coronaviruses. The silent genetic changes were not focused on here, nor the amino acid changes with similar amino acids, like lysine to arginine or serine to threonine. The main goal was to characterize the sustained coronavirus mutations similar to the D614G spike mutations that may help elucidate the functions of viral proteins interacting with human regulatory proteins, increasing disease pathogenesis, such as cytokine storm, respiratory problems, immune deficiencies, convulsions, and deaths. The disease severity in the Alpha, Beta, and, specifically, the Delta variants was not associated with Omicron coronaviruses with 30 new mutations in the spike. The important 30NS deletion in the spike over earlier 24LPP, 69HV, 145Y, 211N, and 483V deletions and the spike 16MPLF insertion were reported. However, higher transmission with the JN.1.11, JN.1.16, LB.1.7, and KP.2.3 variants and more recent in the XEC, KP.3.1.1, and MC.1 variants casts doubt on the elimination of coronaviruses with time. The deleterious mutations caused the elimination of the virus, whereas sustained mutations such as spike D614G and N501N increased transmission. Meanwhile, the E484A, T478K, L452R, and K417N/T immune regulatory mutations caused vaccine resistance among the Omicron coronaviruses such as the BQ.1, XBB.1, EG.1, and FL.1 variants. XBB.1.5.8 had three mutations in the spike protein (P463S, E554K, and P1162S). The P2045S, T2137A, A3697V, T5941I, H5951Y, and P6376S mutations in the ORF1ab of XBB.1.5.30, including *ORF8* gene deletion, coupled with 3'-UTR and 31ERS N protein deletions, highlight the importance of studying this variant. However, the variant was eliminated in time, similar to the BQ.1.1.1 subvariants, which were dominant for some time. Thus, important mutations such as T19I, S50L, V127F, G339H, K356T, S371F, S373P, S375F, R403S, K417N, V455H, G446S, N460K, S477K, Q493E, and Y505H (Wuhan position) in the spike protein, and the A211D mutation in nsp2, P3395H, N2526S, and A2710T in nsp3 protease, P3395H in nsp5 protease, R5713C in

nsp13, P13L, Q229K, and S413R in the N protein, A63T in the M protein, T223I in ORF3a, and F19L in the ORF7b protein are sustained and dominant in COVID-19 biology and host-virus interactions. Therefore, such mutations should be studied further in the new JN.1 linages such as KP.3.1.1, LB.1.7, MV.1.1, XEC.1, and MC.1 subvariants. SWISS-MODEL analysis suggested that the mutations caused deleterious effects on the 3D structure, although this cannot be seen with the naked eye. Hence, it is vital to improve spike-based vaccine development similar to Covishield, while remdesivir (RdRP inhibitor) and lopinavir (protease inhibitor) drugs may still be effective to control the JN.1 coronavirus infection. Unfortunately, the LP.8.1 subvariant infections increased worldwide, and a few deaths were reported, with patients having severe comorbidity.

Acknowledgments

The author would like to acknowledge the NCBI SARS-CoV-2 database (NIH, USA), the free Swiss-Dock Server, and the free CLUSTAL-Omega and MultAlin software for the analyses conducted in this study.

Funding

None.

Conflict of interest

The author declares no conflicts of interest.

Author contributions

This is a single-authored article.

Ethics approval and consent to participate

Not applicable.

Consent for publication

Not applicable.

Availability of data

The raw data are available from the corresponding author upon reasonable request.

References

1. Lu R, Zhao X, Li J, *et al*. Genomic characterisation and epidemiology of 2019 novel coronavirus: Implications for virus origins and receptor binding. *Lancet*. 2020;395: 565-574.

   doi: 10.1016/S0140-6736(20)30251-8

2. Zhu C, Pang S, Liu J, Duan Q. Current progress, challenges and prospects in the development of COVID-19 vaccines. *Drugs*. 2024;84(4):403-423.

   doi: 10.1007/s40265-024-02013-8

3. Kesheh MM, Hosseini P, Soltani S, Zandi M. An overview on the seven pathogenic human coronaviruses. *Rev Med Virol*. 2022;32(2):e2282.

   doi: 10.1002/rmv.2282

4. Chakraborty AK. Hyper-variable spike protein of omicron corona virus and its differences with Alpha and Delta variants: Prospects of RT-PCR and new vaccine. *J Emerg Dis Virol*. 2022;7(1):166.

   doi: 10.16966/2473-1846.166

5. Kandeel M, Mohamed MEM, Abd El-Lateef HM, Venugopala KN, El-Beltagi HS. Omicron variant genome evolution and phylogenetics. *J Med Virol*. 2022;94(4):1627-1632.

   doi: 10.1002/jmv.27515

6. Chakraborty AK. Coronavirus Nsp2 protein homologies to the bacterial DNA topoisomerase I and IV suggest Nsp2 protein is a unique RNA topoisomerase with novel target for drug and vaccine development. *Virol Mycol*. 2020;9:185.

   doi: 10.31219/osf.io/tc9us

7. Chakraborty AK. Multi-alignment comparison of coronavirus non-structural proteins Nsp13-16 with ribosomal proteins and other DNA/RNA modifying enzymes suggested their roles in the regulation of host protein synthesis. *Int J Clin Med Inform*. 2020;3:7-19.

   doi: 10.35543/osf.io/qrxc5

8. Chakraborty AK. Clinical, diagnostic and therapeutic implications of coronavirus ORFab polyprotein associated Nsp16 protein-a bioinformatics approach. *Acta Sci Med Sci*. 2020;4(5):97-103.

   doi: 10.31080/ASMS.2020.04.0629

9. Wang Q, Guo Y, Iketani S, *et al*. Antibody evasion by SARS-CoV-2 Omicron subvariants BA.2.12.1, BA.4 and BA.5. *Nature*. 2022;608(7923):603-608.

   doi: 10.1038/s41586-022-05053-w

10. Xu C, Wang Y, Liu C, *et al*. Conformational dynamics of SARS-CoV-2 trimeric spike glycoprotein in complex with receptor ACE2 revealed by cryo-EM. *Sci Adv*. 2021;7(1):eabe5575.

    doi: 10.1126/sciadv.abe5575

11. Korber B, Fischer WM, Gnanakaran S, *et al*. Tracking changes in SARS-CoV-2 spike: Evidence that D614G increases infectivity of the COVID-19 virus. *Cell*. 2020;182:812-827.e19

    doi: 10.1016/j.cell.2020.06.043

12. Liu Y, Liu J, Plante KS, *et al*. The N501Y spike substitution enhances SARS-CoV-2 infection and transmission. *Nature*.

2022;602(7896):294-299.

doi: 10.1038/s41586-021-04245-0

13. Chakraborty AK. Coronaviruses have reached at pre-elimination stage with nine amino acid spike deletions and forty-nine nucleotide 3'-UTR deletions. *Int J Clin Virol*. 2024;8(2):31-44.

doi: 10.29328/journal.ijcv.1001060

14. Planas D, Staropoli I, Michel V, *et al*. *Distinct Evolution of SARS-CoV-2 Omicron and BA.2.86 Lineages Combining Increased Fitness and Antibody Evasion*. *bioRxiv*. [Preprint]; 2023.

doi: 10.1101/2023.11.20.567873

15. Chakraborty AK. Higher Omicron JN.1 and BA.2.86.1 coronavirus transmission due to unique 17MPLF spike insertion compensating 24LPP, 69HV, 145Y, 211N and 483V deletions in the spike. *J Future Med Healthc Innov.* 2024;2(1):1-20.

16. Chakraborty AK. The G36S, M147I, G265S, T568I, N852S new mutations in the spike of Omicron JN.1 subvariants: New subvariants JN.1.1 to JN.1.5 nomenclature and oligonucleotides design for JN.1 subvariants detection. *J Emerg Virol Infect Dis.* 2024;1(1):1-21.

doi: 10.21203/rs.3.rs-3879032/v1

17. Chakraborty AK. *Higher Omicron JN.1 Coronavirus Transmission Due to Unique 17MPLF Spike Insertion Compensating 24LPP, 69HV, 145Y, 211N and 483V Deletions in the Spike*. United States: Research Square; 2024.

doi: 10.21203/rs.3.rs-3830998/v1

18. Roemer C, Sheward DJ, Hisner R, *et al*. SARS-CoV-2 evolution in the Omicron era. *Nat Microbiol.* 2023;8(11):1952-1959.

doi: 10.1038/s41564-023-01504-w

19. Chakraborty AK. Genesis of recombinant XEC variant and comparable SWISS-modelling of spike of LB.1.7 and KP.3.1.1 subvariants coronaviruses. *SunText Rev Virol.* 2024;5(1):152.

doi: 10.51737/2766-5003.2024.052

20. Sievers F, Wilm A, Dineen DG, *et al*. Fast, scalable generation of high-quality protein multiple sequence alignments using Clustal Omega. *Mol Syst Biol.* 2011;7:539.

doi: 10.1038/msb.2011.75

21. Yang Y, Jiang XT, Zhang T. Evaluation of a hybrid approach using UBLAST and BLASTX for metagenomic sequences annotation of specific functional genes. *PLoS One.* 2014;9(10):e110947.

doi: 10.1371/journal.pone.0110947

22. Studer G, Tauriello G, Bienert S, Biasini M, Johner N, Schwede T. ProMod3-A versatile homology modelling toolbox. *PLoS Comput Biol.* 2021;17(1):e1008667.

doi: 10.1371/journal.pcbi.1008667

23. Bienert S, Waterhouse A, De Beer TAP, *et al*. The SWISS-MODEL repository-new features and functionality. *Nucleic Acids Res.* 2017;45:D313-D319.

doi: 10.1093/nar/gkw1132

24. Varadi M, Anyango S, Deshpande M, *et al*. AlphaFold protein structure database: Massively expanding the structural coverage of protein-sequence space with high accuracy models. *Nucleic Acids Res.* 2022;50:D439-D444.

doi: 10.1093/nar/gkab1061

25. Liu J, Yu Y, Jian F, *et al*. Enhanced immune evasion of SARS-CoV-2 variants KP.3.1.1 and XEC through N-terminal domain mutations. *Lancet Infect Dis.* 2025;25(1):e6-e7.

doi: 10.1016/S1473-3099(24)00738-2

26. Feng Z, Huang J, Baboo S, *et al*. *Structural and Functional Insights into the Evolution of SARS-CoV-2 KP.3.1.1 Spike Protein*. bioRxiv [Preprint]; 2024.

doi: 10.1101/2024.12.10.627775

27. Li P, Faraone JN, Hsu CC, *et al*. *Immune Evasion, Cell-Cell Fusion, and Spike Stability of the SARS-CoV-2 XEC Variant: Role of Glycosylation Mutations at the N-Terminal Domain*. bioRxiv [Preprint]; 2024.

doi: 10.1101/2024.11.12.623078

28. Barton MI, MacGowan SA, Kutuzov MA, Dushek O, Barton GJ, Van Der Merwe PA. Effects of common mutations in the SARS-CoV-2 spike RBD and its ligand, the human ACE2 receptor on binding affinity and kinetics. *ELife.* 2021;10:e70658.

doi: 10.7554/eLife.70658

29. Ghoula M, Deyawe Kongmeneck A, Eid R, Camproux AC, Moroy G. Comparative study of the mutations observed in the SARS-CoV-2 RBD variants of concern and their impact on the interaction with the ACE2 protein. *J Phys Chem B.* 2023;127(40):8586-8602.

doi: 10.1021/acs.jpcb.3c01467

30. Xue S, Han Y, Wu F, Wang Q. Mutations in the SARS-CoV-2 spike receptor binding domain and their delicate balance between ACE2 affinity and antibody evasion. *Protein Cell.* 2024;15(6):403-418.

doi: 10.1093/procel/pwae007

31. Majchrzak M, Madej Ł, Łysek-Gładysińska M, *et al*. The RdRp genotyping of SARS-CoV-2 isolated from patients with different clinical spectrum of COVID-19. *BMC Infect Dis.* 2024;24(1):281.

doi: 10.1186/s12879-024-09146-x

32. Stevens LJ, Pruijssers AJ, Lee HW, *et al*. Mutations in the SARS-CoV-2 RNA-dependent RNA polymerase confer resistance to remdesivir by distinct mechanisms. *Sci Transl*

Med. 2022;14:eabo0718.

doi: 10.1126/scitranslmed.abo0718

33. Li X, Song Y. Targeting SARS-CoV-2 nonstructural protein 3: Function, structure, inhibition, and perspective in drug discovery. *Drug Discov Today.* 2024;29(1):103832.

doi: 10.1016/j.drudis.2023.103832

34. Abbasian MH, Mahmanzar M, Rahimian K, *et al*. Global landscape of SARS-CoV-2 mutations and conserved regions. *J Transl Med.* 2023;21:152.

doi: 10.1186/s12967-023-03996-w

35. Taha TY, Suryawanshi RK, Chen IP, *et al*. A single inactivating amino acid change in the SARS-CoV-2 NSP3 Mac1 domain attenuates viral replication *in vivo*. *PLoS Pathog.* 2023;19(8):e1011614.

doi: 10.1371/journal.ppat.1011614

36. Kerr CM, Pfannenstiel JJ, Alhammad YM, *et al*. Mutation of a highly conserved isoleucine residue in loop 2 of several β-coronavirus macrodomains indicates that enhanced ADP-ribose binding is detrimental for replication. *J Virol.* 2024;98(11):e0131324.

doi: 10.1128/jvi.01313-24

37. Zhou Y, Gammeltoft KA, Ryberg LA, *et al*. Nirmatrelvir-resistant SARS-CoV-2 variants with high fitness in an infectious cell culture system. *Sci Adv.* 2022;8(51):eadd7197.

doi: 10.1126/sciadv.add7197

38. Inniss NL, Rzhetskaya M, Ling-Hu T, *et al*. Activity and inhibition of the SARS-CoV-2 Omicron nsp13 R392C variant using RNA duplex unwinding assays. *SLAS Discov.* 2024;29(3):100145.

doi: 10.1016/j.slasd.2024.01.006

39. Grimes SL, Choi YJ, Banerjee A, *et al*. A mutation in the coronavirus nsp13-helicase impairs enzymatic activity and confers partial remdesivir resistance. *mBio.* 2023;14(4):e0106023.

doi: 10.1128/mbio.01060-23

40. Chakraborty AK. Multi-alignment comparison of Coronavirus non-structural proteins Nsp13-Nsp16 with ribosomal proteins and other DNA/RNA modifying enzymes suggested their roles in the regulation of host protein synthesis. *Int J Clin Med Inform.* 2020;3(1):7-19.

doi: 10.46619/ijcmi.2020.1024

41. Grimes SL, Denison MR. The coronavirus helicase in replication. *Virus Res.* 2024;346:199401.

doi: 10.1016/j.virusres.2024.199401

42. Russ A, Wittmann S, Tsukamoto Y, *et al*. Nsp16 shields SARS-CoV-2 from efficient MDA5 sensing and IFIT1-mediated restriction. *EMBO Rep.* 2022;23:e55648.

doi: 10.15252/embr.202255648

43. Wang Z, Wang J, Jia Y, *et al*. SARS-CoV-2 N protein promotes NLRP3 inflammasome activation to induce hyperinflammation. *Nat Commun.* 2021;12:4664.

doi: 10.1038/s41467-021-25015-6

44. Huang Y, Chen J, Chen S, *et al*. Molecular characterization of SARS-CoV-2 nucleocapsid protein. *Front Cell Infect Microbiol.* 2024;14:1415885.

doi: 10.3389/fcimb.2024.1415885

45. Walia K, Sharma A, Paul S, *et al*. SARS-CoV-2 virulence factor ORF3a blocks lysosome function by modulating TBC1D5-dependent Rab7GTPase cycle. *Nat Commun.* 2024;15:2053.

doi: 10.1038/s41467.024-46417-2

46. Azad GK, Khan PK. Variations in Orf3a protein of SARS-CoV-2 alter its structure and function. *Biochem Biophys Rep.* 2021;26:100933.

doi: 10.1016/j.bbrep.2021.100933

47. Zhang Z, Nomura N, Muramoto Y, *et al*. Structure of SARS-CoV-2 membrane protein essential for virus assembly. *Nat Commun.* 2022;13:4399.

doi: 10.1038/s41467-022-32019-3

48. Mahtarin R, Islam S, Isla MJ, Ullah MO, Ali MA, Halim MA. Structure and dynamics of membrane protein in SARS-CoV-2. *J Biomol Struct Dyn.* 2020;40:4725-4738.

doi: 10.1080/07391102.2020.1861983

49. Abulsoud AI, El-Husseiny HM, El-Husseiny AA, *et al*. Mutations in SARS-CoV-2: Insights on structure, variants, vaccine and biomedical interventions. *Biomed Pharmacother.* 2023;157:113977.

doi: 10.1016/j.biopha.2022.113977

50. Chakraborty AK. Dynamics of SARS-CoV-2 ORF7a gene deletions and fate of downstream ORF7b and ORF8 genes expression. *SunText Rev Biotechnol.* 2022;3(1):142.

doi: 10.51737/2766-5097.2022.042

51. Chakraborty AK. *Highly Infectious, Less Pathogenic and Antibody Resistant Omicron XBB.1, XBB.1.5 and XBB.1.5.1-XBB.1.5.39 Subvariant Coronaviruses do not Produce ORF8 Protein due to 8th Codon GGA=TGA Termination Codon Mutation*. Research Square, [Preprint]; 2023.

doi: 10.21203/rs.3.rs-2990675/v1

52. Chakraborty AK. SARS-CoV-2 ORF8 gene CAA=TAA and AAA=TAA termination codon mutations found mostly in B.1.1.7 variant was independent of popular L84S mutations. *Int J Clin Med Educ Res.* 2022;1(6):192-208.

doi: 10.33140/IJCMER.01.06.01

53. Cecchetto R, Tonon E, Medaina N, *et al*. Detection of SARS-CoV-2 Δ426 ORF8 deletion mutant cluster in NGS screening. *Microorganisms.* 2023;11(10):2378.

doi: 10.3390/microorganisms11102378

54. Wagner C, Kistler KE, Perchetti GA, *et al*. Positive selection underlies repeated knockout of ORF8 in SARS-CoV-2 evolution. *Nat Commun*. 2024;15:3207.

doi: 10.1038/s41467-024-47599-5

55. Suharsono H, Mahardika BK, Sudipa PH, Sari TK, Suardana IBK, Mahardika GN. Consensus insertion/deletions and amino acid variations of all coding and noncoding regions of the SARS-CoV-2 Omicron clades, including the XBB and BQ.1 lineages. *Arch Virol*. 2023;168:156.

doi: 10.1007/s00705-023-05787-6

56. Baggen J, Jacquemyn M, Persoons L, *et al*. TMEM106B is a receptor mediating ACE2-independent SARS-CoV-2 cell entry. *Cell*. 2023;186(16):3427-3442.e22.

doi: 10.1016/j.cell.2023.06.005

57. Zhao Z, Zhou J, Tian M, *et al*. Omicron SARS-CoV-2 mutations stabilize spike up-RBD conformation and lead to a non-RBM-binding monoclonal antibody escape. *Nat Commun*. 2022;13(1):4958.

doi: 10.1038/s41467-022-32665-7

ACCSCIENCE PUBLISHING

Innovative Medicines & Omics

ORIGINAL RESEARCH ARTICLE

Antidiarrheal activity assessment of *Operculina turpethum* stem extract and *in silico* analysis of its compounds

Md. Abdullah Al Fahad*, Md. Fahim Hasan, Md. Arman Islam, Nusrat Jahan, and Md. Iqbal Ahmed*

Pharmacy Discipline, Khulna University, Khulna, Bangladesh

Abstract

Operculina turpethum is widely known for its use in traditional treatment practices to heal several diseases, such as bronchitis, pectoralgia, arthralgia, diarrhea, obesity, helminthiasis, gastropathy, ascites, sporadic fever, leucoderma, inflammation, pruritis, ulcers, erysipelas, tumors, jaundice, hemorrhoids, and ophthalmia. In this study, the antidiarrheal potential of the ethanolic extract of *O. turpethum* stem was assessed in an animal model, and molecular docking of previously reported stem-derived compounds was performed to determine the possible mechanism of action. The *in vivo* antidiarrheal effect was assessed using a castor oil-induced mouse model. *In silico* molecular docking analysis was performed using the 'Vina Wizard' program in PyRx 0.8. The stem extracts at 250 and 500 mg/kg produced significant, dose-dependent antidiarrheal activity. Among the four previously isolated compounds, three (22,23-dihydro-α-spinosterol-ß-D-glucoside, paprazine, and sitogluside) showed satisfactory binding affinity against the target M3 muscarinic acetylcholine receptor, comparable to the reference standard drug loperamide. These findings suggest that the *O. turpethum* stem has significant potential to prevent diarrhea that warrants further phytochemical, pharmacological, and mechanistic investigations.

Keywords: Anti-diarrheal; Plant extract; Molecular docking; ADME

***Corresponding authors:**
Md Abdullah Al Fahad
(saykat0047@gmail.com)
Md. Iqbal Ahmed
(i.ahmed@pharm.ku.ac.bd)

Citation: Al Fahad MA, Hasan MF, Islam MA, Jahan N, Ahmed MI. Antidiarrheal activity assessment of *Operculina turpethum* stem extract and *in silico* analysis of its compounds. *Innov Med Omics*. 2025;2(4):64-73.
doi: 10.36922/IMO025260028

Received: June 25, 2025

Revised: August 7, 2025

Accepted: August 13, 2025

Published online: September 22, 2025

1. Background

Diarrheal diseases pose a significant challenge in developing nations and are responsible for millions of deaths each year.[1] Diarrhea can be described as a change in typical bowel movement and is attributed to an increase in water content, volume, or stool frequency.[2] Globally, one in ten deaths among children under the age of five is attributed to diarrhea, making up to approximately 8,00,000 deaths per year.[3] There are a total of 2.8 billion incidents of diarrhea in children (>5 years of age), adults, and adolescents.[4] Multiple influential factors are implicated in its pathophysiology, including poor intestinal absorption, altered gut motility, gastric hypersensitivity, microbial infection, metabolic insufficiency, genetic pre-disposition, chemical irritation, a weak immune system, and a plethora of secretory stimuli, such as bacterial enterotoxins, hormones, dihydroxy bile acids, hydroxylated fatty acids, and inflammatory cytokines.[5] Effective strategies for treatment and prevention include continued breastfeeding, oral rehydration therapy, improved hygiene, zinc supplementation, immunization programs, and the use of antibiotics.[6]

Plant-derived substances have long been used as a reliable source of biologically active metabolites with diverse pharmacological activity. Nearly 80% of the population, especially those from developing and underdeveloped countries, rely directly or indirectly on plant-based medications. Natural compounds have advantages over synthetic molecules, such as better drug-likeness and compatibility with the body's biological system, making them attractive candidates for research and drug development. A myriad of plant species are still being investigated for their medicinal constituents and therapeutic plants continue to represent a promising source of antidiarrheal agents.[7] Plant-derived compounds, such as 1,8-cineole, friedelin, Stachysrosane (1), Stachysrosane (2), and apigenin have potent antidiarrheal activity.[8] For this reason, the World Health Organization (WHO) has encouraged studies on the prevention and treatment of diarrheal diseases using traditional medical practices.[9,10]

Operculina turpethum (L.) Silva Manso, a member of the Convolvulaceae family, is an important therapeutic plant widely used in both Unani and Ayurvedic practices. This indigenous Asian plant resides in Bangladesh, India, Nepal, Sri Lanka, Pakistan, China, Taiwan, and Myanmar.[11] In traditional Unani practice, *O. turpethum* roots are prescribed for conditions, such as colic, constipation, paralysis, helminthiasis, gastropathy, ascites, leucoderma, pruritis, ulcers, and hemorrhoids.[12] The stems are rich in phenols, flavonoids, phytosterols, terpenoids, and cardiac glycosides.[13] To date, four natural metabolites have been isolated from the chloroform extract of the stem, namely, β-sitosterol-β-D-glucoside, 22,23-dihydro-α-spinosterol-β-D-glucoside, salicylic acid,[14,15] and (2E)-3-(4-Hydroxyphenyl)-N-^{2}-(4-hydroxyphenyl)-ethyl]-acrylamide.[16] Although originally identified from chloroform fractions, the structural and pharmacological relevance of these compounds, particularly sterol glucosides and phenolic derivatives, supports their presence in other solvent extracts, including ethanol. According to our literature review, no study investigated the antidiarrheal activity of *O. turpethum* stems until recently. This knowledge gap provides the rationale for conducting the present study, involving *in vivo* and *in silico* assessments of the ethanolic extract of the stem.

2. Materials and methods

2.1. Drugs and chemicals

Ethanol was acquired from Merck (Germany), and Tween 80 from BDH Chemicals (UK). The standard drug loperamide (Square Pharmaceuticals, Bangladesh) was obtained from a local pharmacy, and castor oil was procured from a neighboring chemical supplier (WELL'S Castor Oil, Spain). All the chemicals and drugs employed in this study were of analytical grade.

2.2. Plant collection, identification, and preparation of the ethanolic extract

O. turpethum stems were collected from Khulna University and its surrounding area. The plant was identified by experts at the Bangladesh National Herbarium, Mirpur, Dhaka, and a voucher specimen (no. 46484 DACB) was deposited for future reference. A total of 210 g of dried powdered stem was placed in a properly cleaned flat-bottomed glass container and soaked in 800 mL of 96% ethanol. The container was then sealed and stored for 14 days with occasional shaking and stirring. The extract was first filtered through clean cotton cloth and then through Whatman no. 1 filter paper (Whatman™, UK). Eventually, the filtrate was evaporated through a rotary evaporator (LabTech, Italy) to yield the ethanolic extract of the *O. turpethum* stem, with a yield of 3.58%. The extract was stored at 4°C for further analysis.

2.3. Experimental animals

Swiss albino mice, which were aged approximately 4–6 weeks old and weighed approximately 22–28 g, were procured from the animal research branch of the International Centre for Diarrheal Disease and Research, Bangladesh (ICDDRB). Mice were acclimatized under standard laboratory conditions for 1 week. All the experimental animals were given standard laboratory food and clean tap water and maintained under a natural light–dark cycle. All experiments were performed in a noise-free and isolated pharmacological laboratory at the Pharmacy Discipline, Khulna University. The experiment was approved by the Animal Ethics Committee of Khulna University [Ref: KUAEC-2018-01-08].

2.4. Antidiarrheal activity assessment in castor oil-induced diarrhea

The antidiarrheal activity was evaluated using the castor oil-induced diarrhea model, as previously described.[1] Initially, all the mice were monitored by administering 0.5 mL of castor oil; only those exhibiting diarrhea were included in the subsequent experiment. The animals were divided into four groups (n = 5 per group) receiving different interventions orally: Negative control (1% Tween 80 in water, 10 mL/kg body weight), positive control (loperamide, 3 mg/kg body weight), test-I (*O. turpethum* extract, 250 mg/kg body weight), and test-II (*O. turpethum* extract, 500 mg/kg body weight). Each mouse was housed individually in a cage lined with blotting paper, which was replaced hourly. Thirty minutes after treatment, diarrhea

was induced by oral administration of 0.5 mL of castor oil. The animals were then observed for 4 h, during which the total number of fecal outputs and diarrheal feces were recorded. The percentage inhibition of diarrhea was calculated using the following equation: [(TD control – TD test groups)/TD control] × 100, where TD control represents the total number of diarrheal feces in the negative control group, and TD test groups represents the total number of diarrheal feces of the positive control or test groups.

2.5. Molecular docking study

Four compounds were selected for molecular docking studies: paprazine [(E)-3-(4-hydroxyphenyl)-N-^{2}-(4-hydroxyphenyl)ethyl]prop-2-enamide; PubChem CID: 5372945], loperamide (PubChem CID: 3955), salicylic acid (PubChem CID: 338), and sitogluside [β-sitosterol-β-D-glucoside; PubChem CID: 5742590]. The chemical structures of the compounds were downloaded from PubChem (https://pubchem.ncbi.nlm.nih.gov/) (Figure 1).[17] Since the 3D structure of 22,23-dihydro-a-spinosterol-β-D-glucoside (designated as "spinosterol" in this paper for simplicity) was unavailable, it was manually drawn in Avogadro (version 1.2.0; http://avogadro.cc/), based on its reported 2D structure (Figure 1).[15] All ligands were optimized using Avogadro with the Universal Force Field (UFF), and then saved in Protein Data Bank (.pdb) format for docking.

The M3 muscarinic acetylcholine receptor (MAChR; PDB ID: 4U14)[18] was obtained from the Protein Data Bank (http://www.rcsb.org/).[19] The structure was cleaned using PyMOL Molecular Graphics System (version 2.0, Schrödinger, US) and optimized with Swiss-PdbViewer (version 4.1; Swiss-PdbViewer/DeepView, by Nicolas Guex, Alexandre Diemand, Manuel C. Peitsch, and Torsten Schwede, https://spdbv.unil.ch/). Ramachandran plots were generated using the VADAR server to validate the predicted protein structures, based on criteria, such as preferred, allowed, and disallowed amino acid residue locations.

Molecular docking of the receptor with each ligand was performed using the Vina Wizard program in PyRx – Python Prescription 0.8.[20] The ligands and the receptor were loaded into the program with the appropriate designation as ligand or macromolecule. The docked complexes were subsequently visualized in PyMOL. For further interaction analysis, the complexes were imported into Discovery Studio Visualizer (version 4.5.0.15071, BIOVIA, Dassault Systèmes, France). The ligand–receptor interactions were observed, and snapshots of the best docking poses were obtained.

2.6. Pharmacokinetic parameters

Basic pharmacokinetic parameters were analyzed using the SwissADME web server (http://www.swissadme.ch/).[21] The input was provided in the form of SMILES or chemical structures.

2.7. Statistical analysis

GraphPad Prism software (version 8, GraphPad Software Inc., USA) was used to analyze all the experimental data. Results are presented as the mean ± standard error of the mean (SEM). A $p<0.05$ was considered statistically significant.

3. Results

3.1. Castor oil-induced diarrhea

The ethanolic extract of *O. turpethum* stem demonstrated dose-dependently antidiarrheal activity, with the most

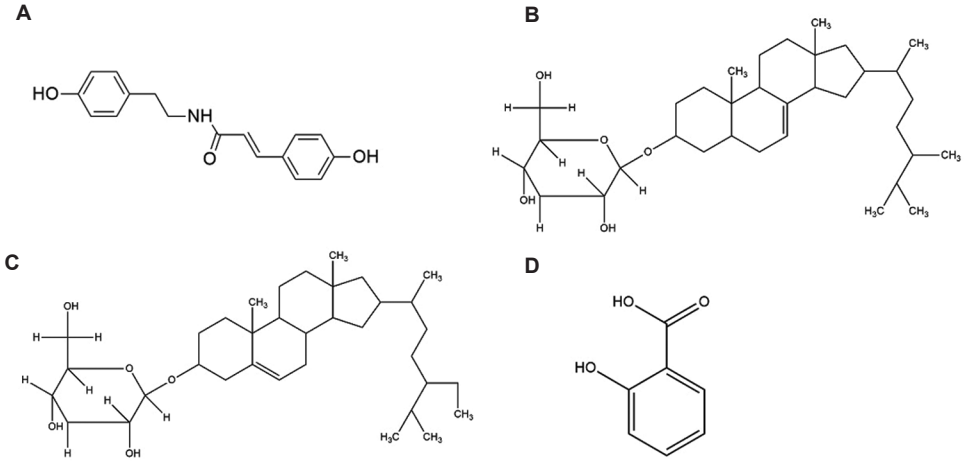

Figure 1. Previously isolated compounds from *O. turpethum*. (A) Paprazine. (B) Spinosterol. (C) Sitogluside. (D) Salicylic acid.

pronounced effect observed at 500 mg/kg (Table 1). At this dose, the mean latency period was 134 ± 3.71 min (Figure 2A), while defecation was inhibited by approximately 51% (Figure 2B). These results were comparable to those of the standard drug loperamide, which resulted in 89% inhibition with a mean latency period of 153 ± 3.11 min. Similarly, a 250 mg/kg dose demonstrated approximately 31% inhibition, with a mean latency period of 80 ± 2.07 min.

3.2. Molecular docking study

Loperamide was used as the standard compound for the docking study. The Ramachandran plot (Figure 3A) of the M3 MAChR (PDB ID: 4U14) showed 86% amino acids in the favored region, 11% in the allowed region, and 3% in the generously allowed or disallowed region (Figure 3B), indicating the suitability of the protein for molecular docking studies. The docking was carried out with a maximized grid box dimension (Table 2).

Table 1. Effect of *Operculina turpethum* stem extract on fecal output of castor oil-induced diarrhea mouse models

Treatment	Mean latent period (min)	Mean number of feces	Inhibition of defecation (%)
Negative control	35.2±2.63	18.6±1.86	-
Positive control	153±3.11	2±0.32*	89.24
Extract (250 mg/kg)	80±2.07*	12.8±0.37*	31.18
Extract (500 mg/kg)	134±3.70*	9.2±0.37*	50.53

Notes: Values are expressed as mean±standard error of the mean (n=5). *p<0.05 compared with the negative control.

Table 2. Grid box parameters used for molecular docking

Parameter	X	Y	Z
Centre coordinates	7.9825	20.6062	367.0162
Dimensions (Å)	60.9444	60.2098	86.2207

The binding energies of the best-docked complexes and their interacting amino acids are summarized in Table 3. Loperamide exhibited a binding energy of −8.3 kcal/mol with the receptor. All ligands, except salicylic acid, demonstrated satisfactory binding interactions with the receptor and thus were predicted to inhibit M3 MAChR activity. Ranking the ligands by binding affinity revealed the following order: spinosterol >paprazine >loperamide >sitogluside >salicylic acid.

The binding energies of the best-docked complexes and their interacting amino acids are summarized in Table 3. Loperamide exhibited a binding energy of −8.3 kcal/mol with the receptor. All ligands, except salicylic acid, demonstrated satisfactory binding interactions with the receptor and thus were predicted to inhibit M3 MAChR activity. Ranking the ligands by binding affinity revealed the following order: spinosterol >paprazine >loperamide >sitogluside >salicylic acid.

Among the tested ligands, 22,23-dihydro-α-spinosterol-ß-D-glucoside showed the strongest binding and emerged as the best candidate. Paprazine exhibited slightly lower affinity but outperformed the standard drug loperamide. β-Sitosterol-β-D-glucoside performed marginally less than the standard, although the binding affinities of both compounds were similar. In contrast, salicylic acid exhibited considerably lower affinity and is unlikely to serve as a potential antidiarrheal agent. Figures 4 and 5 show the 2D and 3D interactions between the ligands and the receptor, respectively. Table 4 explains the bonding categories and subcategories.

3.3. Pharmacokinetic analysis

The drug-like potential of the three ligand molecules was assessed based on absorption, distribution, metabolism, and elimination (ADME) parameters (Table 5). The evaluated

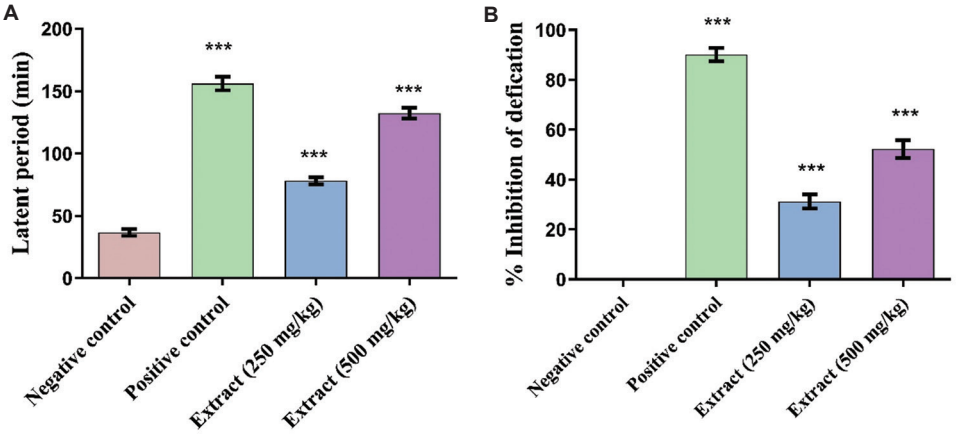

Figure 2. *In vivo* antidiarrheal activity of *O. turpethum* stem extract. (A) Effect of stem extract on prolongation of the latent period in castor oil-induced diarrheal episodes in mice. (B) Effect of stem extract based on inhibition of defecation in castor oil-induced diarrheal episodes in mice.

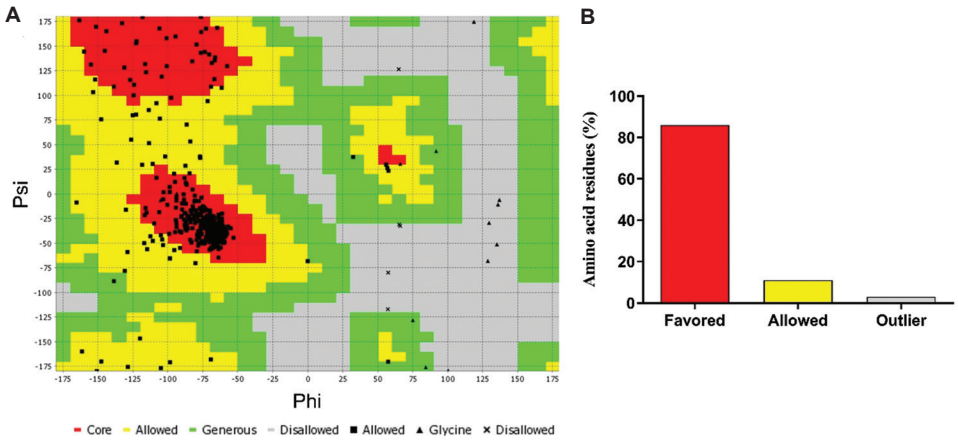

Figure 3. Structural validation of M3 muscarinic acetylcholine receptor. (A) Ramachandran plot of the receptor showing amino acids in the favored and allowed regions. (B) Percentage of amino acids in different regions.

Table 3. Docking results along with interacting amino acids

Ligand name	Binding affinity (kcal/mol)	RMSD/ub	RMSD/lb	Interacting amino acids
Paprazine	−8.9	0	0	TYR254, THR257, GLU258, LEU482, LYS487, ALA1093, VAL1094, and TRP1158
Spinosterol	−9.4	0	0	PHE124, TYR127, TRP143, LEU144, TYR148, ILE222, LEU225, ASN513, ASP517, LYS522, TRP525, and TYR529
Salicylic acid	−5.7	0	0	TYR148 and CYS532
Sitogluside	−8	0	0	LEU198, TRP199, PRO201, ALA202, PHE205, TRP206, PHE209, PHE224, ILE230, ALA237, and ALA238
Loperamide	−8.3	0	0	TYR104, SER108, CYS111, ILE146, VAL149, ILE188, TRP192, PHE196, and ALA200

Abbreviations: Rmsd/lb: Root mean square deviation lower bound; Rmsd/ub: Root mean square deviation upper bound.

Table 4. Types of bonds observed in the 2D diagram

Interaction category	Interaction type	Sub-type	Specific interaction
Favorable	Hydrogen bonds	Classical	Conventional hydrogen bond
		Non-classical	Carbon–hydrogen bond
	Hydrophobic	Pi hydrophobic (same color)	Pi–pi stacked
			Pi–pi T-shaped
			Amide-pi stacked
		Alkyl Hydrophobic	Alkyl[a]
		Mixed pi/alkyl hydrophobic	Pi-alkyl[a]
			Pi-sigma
	Miscellaneous	Sulfur	Pi-sulfur
Unfavorable	Acceptor/Donor clash	-	Unfavorable donor–donor

Note: [a]Both alkyl groups are represented in the same color.

parameters influence the cell permeation, bioavailability, and metabolic properties of the ligands. Notably, paprazine satisfied Lipinski's rule of five, suggesting it as a potentially drug-like compound.

4. Discussion

The ethanolic stem extract of *O. turpethum* was evaluated for its possible antidiarrheal effect in mice, and the results showed that the extract significantly attenuated castor oil-induced diarrhea in comparison with the standard drug loperamide. The phytochemicals that are present in *O. turpethum* stems, such as phenols, flavonoids, phytosterols, terpenoids, and cardiac glycosides,[13] are well known for their antidiarrheal properties.[25,26] Flavonoids, tannins, and saponins have been implicated in calcium channel-blocking activity, which might explain the therapeutic effect of *O. turpethum*.[27,28] Although our study focused on the stem extract, further comparative phytochemical analyses across different plant parts (i.e., root, stem, leaves) are warranted to better understand variations in active compound concentrations and their potential pharmacological implications.

Hydrolysis of castor oil results in the formation of ricinolic acid in the gastrointestinal tract, which induces

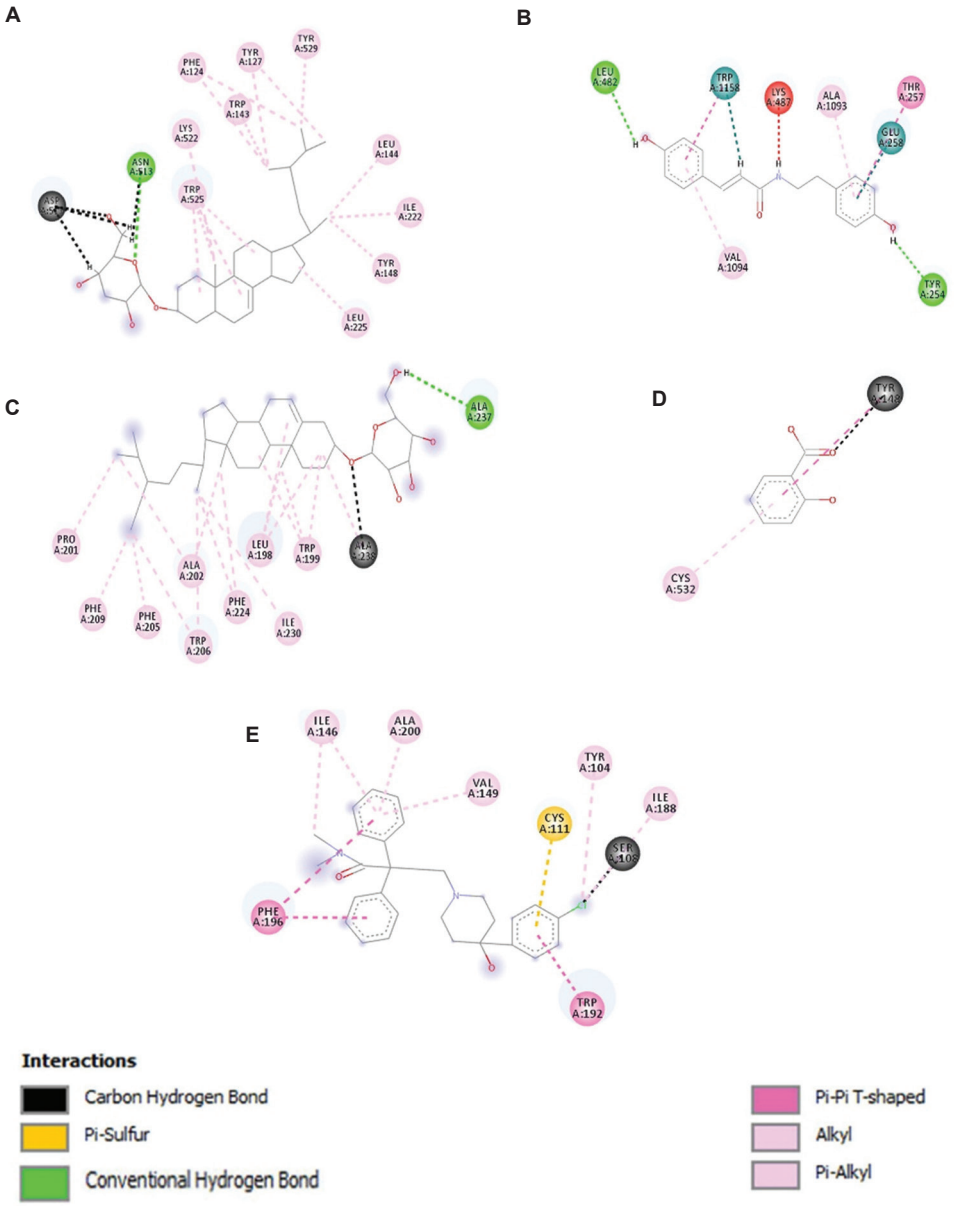

Figure 4. 2D interaction diagrams of the best binding poses for ligands docked to the M3 muscarinic acetylcholine receptor (PDB ID: 4U14). (A) Spinosterol. (B) Paprazine. (C) Sitogluside. (D) Salicylic acid. (E) Loperamide. Different bond types are represented in distinct colors and illustrated as dotted lines, showing the interactions between ligands and protein residues. Detailed interaction information is summarized in Table 4.

diarrhea by altering water and electrolyte transport, triggering a hypersecretory response, and stimulating massive contraction of the intestine.[29] Thus, phytochemicals present in *O. turpethum* likely counteracted these effects by hindering gut motility and electrolyte outflux. While the efficacy of *O. turpethum* was somewhat lower than that of loperamide, the results suggest that the extract possessed an acceptable inhibitory effect on gut motility and electrolyte outflux. To further confirm the possible inhibitory effect of the extract on gut motility, four previously isolated compounds—spinosterol, paprazine, sitogluside, and salicylic acid—were subjected to *in silico* molecular docking.

Gut motility is strongly associated with the activity of the M3 MAChR,[30] which is primarily regulated by the parasympathetic nervous system. Anticholinergic drugs, which antagonize M3 receptors, reduce smooth muscle spasms and relieve gastrointestinal disorders.[31] As a G protein–coupled receptor, the M3 MAChR mediates acetylcholine-induced increases in intracellular calcium,

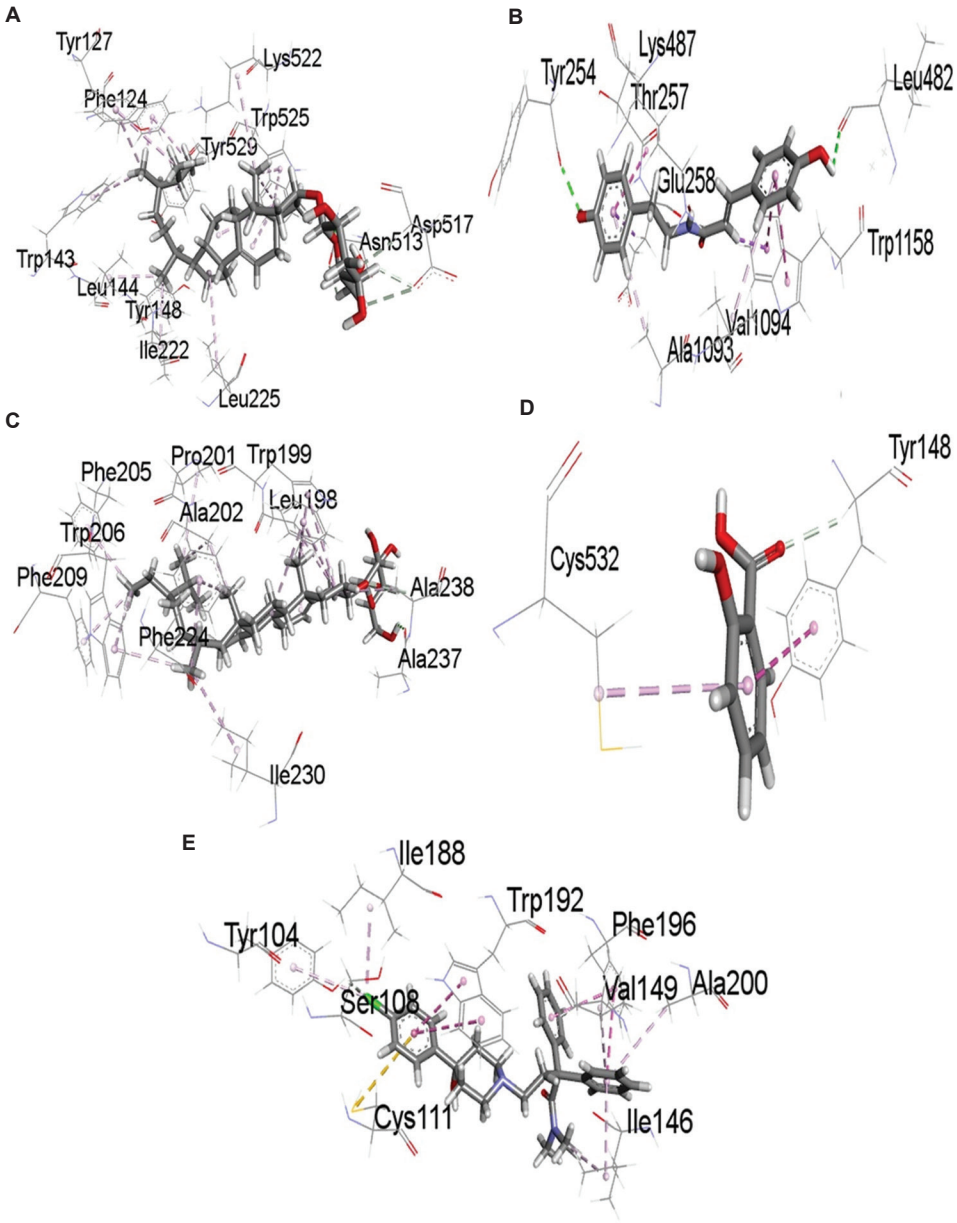

Figure 5. 3D interaction diagrams of the best-ranked binding poses for ligands docked to the M3 muscarinic acetylcholine receptor (PDB ID: 4U14). (A) Spinosterol. (B) Paprazine (C) Sitogluside. (D) Salicylic acid. (E) Loperamide.

leading to smooth muscle contraction.[32] Blocking this receptor reduces calcium influx, thereby decreasing gut constriction and providing antidiarrheal effects.[33] With this rationale, the four compounds and the standard drug loperamide were docked to the M3 MAChR. Among them, spinosterol, paprazine, and sitogluside exhibited excellent binding affinity with M3 MAChR, suggesting their potential to inhibit the receptor and block free calcium ion reflux in the cytoplasm, thereby contributing to the antidiarrheal effect of *O. turpethum*. Conversely, salicylic acid may not be a potential inhibitor of the receptor, but its presence in the stem may play a synergistic role because it can competitively inhibit prostaglandin formation.[34] Prostaglandins promote intestinal contractions and cause a range of gastrointestinal disorders, including diarrhea.[35]

ADME analysis of the four compounds further revealed that only paprazine satisfied Lipinski's rule of five as well as the Ghose, Veber, Egan, and Muegge criteria, suggesting that it is a potential drug-like molecule with favorable GI absorption and relatively easier synthesis.

Table 5. Pharmacokinetic properties of the ligands with good binding affinity

Properties	Paprazine	Sitogluside	Spinosterol
Molecular formula	$C_{17}H_{17}NO_3$	$C_{35}H_{60}O_6$	$C_{33}H_{56}O_5$
MW (g/mol)	283.32	576.85	532.79
TPSA (Å²)	69.56	99.38	79.15
Consensus Log $P_{o/w}$ (Lipophilicity)	2.46	5.51	5.65
Water solubility	Soluble or moderately soluble	Poorly soluble or moderately soluble	Poorly soluble or moderately soluble
GI absorption	High	Low	High
BBB permeant	Yes	No	No
P-gp substrate	No	No	No
CYP2D6 inhibitor	Yes	No	No
CYP3A4 inhibitor	Yes	No	No
Log Kp (skin permeation)	−6.10 cm/s	−4.32 cm/s	−4.21 cm/s
Drug-likeness			
Lipinski	Yes; no violations	Yes; 1 violation: MW > 500	No; 2 violations: MW > 500, MLOGP > 4.15
Ghose	Yes	No; 4 violations: MW > 480, WLOGP > 5.6, MR > 130, #atoms > 70	No; 4 violations: MW > 480, WLOGP > 5.6, MR > 130, #atom s > 70
Veber	Yes	Yes	Yes
Egan	Yes	Yes	No; 1 violation: WLOGP > 5.88
Muegge	Yes	No; 1 violation: XLOGP3 > 5	No; 1 violation: XLOGP3 > 5
Bioavailability score	0.55	0.55	0.17
Lead-likeness	Yes	No; 3 violations: MW > 350, Rotors > 7, XLOGP3 > 3.5	No; 3 violations: MW > 350, Rotors > 7, XLOGP3 > 3.5
Synthetic accessibility	2.28 (easy)	8.02 (difficult)	7.49 (difficult)

Notes: XLOGP3: Atomistic and knowledge-based method for calculating Log $P_{o/w}$ (XLOGP version 3.2.2, CCBG, Shanghai Institute of Organic Chemistry). WLOGP: Atomistic method for calculating Log $P_{o/w}$ (Wildman and Crippen).[22] MLOGP: Topological method for calculating Log $P_{o/w}$ (Moriguchi *et al*. and Lipinski *et al.*).[23,24]
Abbreviations: MR: Molar refractivity, MW: Molecular weight; TPSA: Topological Polar Surface Area.

This work has certain limitations. Although the extract was stored at 4°C to preserve its constituents, no formal stability analysis was performed to confirm the chemical integrity of the bioactive compounds during storage. In addition, while higher doses of the extract may improve efficacy, toxicity profiling will be essential before exploring dose escalation. Future investigations should address these limitations through stability studies, toxicity assessments, and mechanistic validation.

5. Conclusion

The ethanolic extract of *O. turpethum* stem demonstrated significant dose-dependent antidiarrheal activity in a castor oil-induced mouse model, although its efficacy was lower than that of the standard drug loperamide. *In silico* molecular docking studies revealed that three of the four previously reported stem-derived compounds—spinosterol, paprazine, and sitogluside—exhibited favorable binding affinities toward the M3 MAChR, supporting their potential contribution to the observed pharmacological effects of *O. turpethum*. While these findings suggest that *O. turpethum* contains promising bioactive constituents with antidiarrheal potential, future studies are necessary to perform detailed phytochemical profiling of the ethanolic extract using liquid chromatography with tandem mass spectrometry or nuclear magnetic resonance, evaluate the toxicity and safety of higher extract doses, assess synergistic interactions among isolated compounds, and investigate the mechanisms of action through *in vitro* and *ex vivo* models.

Acknowledgments

None.

Funding

None.

Conflict of interest

The authors declare that they have no competing interests.

Author contributions

Conceptualization: Md. Abdullah Al Fahad, Iqbal Ahmed
Investigation: Md. Abdullah Al Fahad, Iqbal Ahmed
Methodology: Md. Abdullah Al Fahad, Md. Fahim Hasan, Iqbal Ahmed
Writing – original draft: Md. Abdullah Al Fahad, Nusrat Jahan, Md. Fahim Hasan, Md. Arman Islam
Writing – review & editing: Iqbal Ahmed, Md. Abdullah Al Fahad

Ethics approval and consent to participate

The experiment was approved by the Animal Ethics Committee of Khulna University (Ref: KUAEC-2018-01-08).

Consent for publication

Not applicable.

Availability of data

Data are available from the corresponding author upon reasonable request.

References

1. Shoba FG, Thomas M. Study of antidiarrhoeal activity of four medicinal plants in castor-oil induced diarrhoea. *J Ethnopharmacol*. 2001;76(1):73-76.

   doi: 10.1016/s0378-8741(00)00379-2

2. Guerrant RL, Van Gilder T, Steiner TS, *et al.* Practice guidelines for the management of infectious diarrhea. *Clin Infect Dis*. 2001;32(3):331-351.

   doi: 10.1086/318514

3. Kotloff KL, Nataro JP, Blackwelder WC, *et al.* Burden and aetiology of diarrhoeal disease in infants and young children in developing countries (the Global Enteric Multicenter Study, GEMS): A prospective, case-control study. *Lancet*. 2013;382(9888):209-222.

   doi: 10.1016/S0140-6736(13)60844-2

4. Walker CF, Black RE. Diarrhoea morbidity and mortality in older children, adolescents, and adults. *Epidemiol Infect*. 2010;138(9):1215-1226.

   doi: 10.1017/S0950268810000592

5. Bouma G, Strober W. The immunological and genetic basis of inflammatory bowel disease. *Nat Rev Immunol*. 2003;3(7):521-533.

   doi: 10.1038/nri1132

6. Shah D, Choudhury P, Gupta P, *et al.* Promoting appropriate management of diarrhea: A systematic review of literature for advocacy and action: UNICEF-PHFI series on newborn and child health, India. *Indian Pediatr*. 2012;49(8):627-649.

   doi: 10.1007/s13312-012-0134-1

7. Maikere-Faniyo R, Van Puyvelde L, Mutwewingabo A, Habiyaremye F. Study of Rwandese medicinal plants used in the treatment of diarrhoea I. *J Ethnopharmacol*. 1989;26(2):101-109.

   doi: 10.1016/0378-8741(89)90057-3

8. Rawat P, Singh PK, Kumar V. Evidence based traditional anti-diarrheal medicinal plants and their phytocompounds. *Biomed Pharmacother*. 2017;96:1453-1464.

   doi: 10.1016/j.biopha.2017.11.147

9. Snyder JD, Merson MH. The magnitude of the global problem of acute diarrhoeal disease: A review of active surveillance data. *Bull World Health Organ*. 1982;60(4):605-613.

10. Lutterodt GD. Inhibition of gastrointestinal release of acetylchoune byquercetin as a possible mode of action of *Psidium guajava* leaf extracts in the treatment of acute diarrhoeal disease. *J Ethnopharmacol*. 1989;25(3):235-247.

    doi: 10.1016/0378-8741(89)90030-5

11. Ahmad T, Husain MK, Tariq M, *et al.* A Review on *Operculina turpethum*: A potent herb of Unani system of medicine. *J Pharmacogn Phytochem*. 2017;6(1):23-26.

12. Aswal B, Bhakuni D, Goel A, Mehrotra B, Mukherjee K. Screening of Indian plants for biological activity: Part X. *Indian J Exp Biol*. 1984;22:312-332.

13. Anju V, Radhamany P. Pharmacognostic and phytochemical studies on *Operculina turpethum* (L) Silva Manso stem. *World J Pharma Pharm Sci*. 2015;4(7):1920-1927.

14. Harun-or-Rashid H, Gafur M, Golam S, Aziz A. Antibacterial and cytotoxic activities of extracts and isolated compounds of *Ipomoea turpethum*. *Pak J Biol Sci*. 2002;5:597-9.

15. Gupta S, Ved A. *Operculina turpethum* (Linn.) Silva Manso as a medicinal plant species: A review on bioactive components and pharmacological properties. *Pharmacogn Rev*. 2017;11(22):158-166.

    doi: 10.4103/phrev.phrev_6_17

16. Rashid M, Rahman A, Sadik M, Gafur M. Biological activities of a novel acrylamide derivative from *Ipomoea turpethum*. *Pak J Biol Sci*. 2002;5:968-969.

    doi: 10.3923/pjbs.2002.968.969

17. Kim S, Chen J, Cheng T, *et al.* PubChem 2019 update: Improved access to chemical data. *Nucleic Acids Res*. 2018;47(D1):D1102-D1109.

    doi: 10.1093/nar/gky1033

18. Thorsen TS, Matt R, Weis WI, Kobilka BK. Modified T4

lysozyme fusion proteins facilitate G protein-coupled receptor crystallogenesis. *Structure*. 2014;22(11):1657-1664.

doi: 10.1016/j.str.2014.08.022

19. Berman HM, Westbrook J, Feng Z, *et al.* The protein data bank. *Nucleic Acids Res*. 2000;28(1):235-242.

doi: 10.1093/nar/28.1.235

20. Dallakyan S, Olson AJ. Small-molecule library screening by docking with PyRx. *Methods Mol Biol*. 2015;1263:243-250.

doi: 10.1007/978-1-4939-2269-7_19

21. Daina A, Michielin O, Zoete V. SwissADME: A free web tool to evaluate pharmacokinetics, drug-likeness and medicinal chemistry friendliness of small molecules. *Sci Rep.* 2017;7:42717.

doi: 10.1038/srep42717

22. Wildman SA, Crippen GM. Evaluation of ligand overlap by atomic parameters. *J Chem Inform Comput Sci*. 2001;41(2):446-450.

doi: 10.1021/ci0000880

23. Moriguchi I, Hirono S, Nakagome I, Hirano H. Comparison of reliability of log P values for drugs calculated by several methods. *Chem Pharm Bull*. 1994;42(4):976-978.

24. Lipinski CA, Lombardo F, Dominy BW, Feeney PJ. Experimental and computational approaches to estimate solubility and permeability in drug discovery and development settings. *Adv Drug Deliv Rev*. 1997;23(1-3):3-26.

doi: 10.1016/s0169-409x(00)00129-0

25. Prabhu AK, Devadas SM, Lobo R, Udupa P, Chawla K, Ballal M. Antidiarrheal activity and phytochemical analysis of carica papaya fruit extract. *J Pharm Sci Res*. 2017;9(7):1151.

26. Galvez J, Zarzuelo A, Crespo M, Lorente M, Ocete M, Jimenez J. Antidiarrhoeic activity of *Euphorbia hirta* extract and isolation of an active flavonoid constituent. *Planta Med*. 1993;59(4):333-336.

doi: 10.1055/s-2006-959694

27. Fu Z, Bo H, Chun-Yan H, *et al*. Effects of total flavonoids of *Hippophae rhamnoides* L. on intracellular free calcium in cultured vascular smooth muscle cells of spontaneously hypertensive rats and Wistar-Kyoto rats. *Chin J Integr Med*. 2005;11(4):287-292.

doi: 10.1007/BF02835791

28. Kai L, Wang Z, Xiao J. L-type calcium channel blockade mechanisms of panaxadiol saponins against anoxic damage of cerebral cortical neurons isolated from rats. *Zhongguo Yao Li Xue Bao Acta Pharmacol Sinica*. 1998;19(5):455-458.

29. NU R, Aslam K, Urooj F, *et al.* Presence of laxative and antidiarrheal activities in *Periploca aphylla*: A Saudi medicinal plant. *Int J Pharmacol*. 2013;9(3):190.

30. Grover M, Camilleri M. Ramosetron in irritable bowel syndrome with diarrhea: new hope or the same old story? *Clin Gastroenterol Hepatol*. 2014;12(6):960-962.

doi: 10.1016/j.cgh.2013.12.025

31. Memon AH, Tan MH, Khan MSS, *et al.* Toxicological, antidiarrhoeal and antispasmodic activities of Syzygium myrtifolium. *Revista Brasileira de Farmacognosia.* 2020;30(3):397-405.

doi: 10.1007/s43450-020-00054-0

32. Goodman LS. Goodman and Gilman's the pharmacological basis of therapeutics. vol 1549. McGraw-Hill New York; 1996.

33. Karaki H, Weiss GB. Calcium release in smooth muscle. *Life Sci*. 1988;42(2):111-122.

doi: 10.1016/0024-3205(88)90674-1

34. Peterson DA, Gerrard J, Rao G, White J. Salicylic acid inhibition of the irreversible effect of acetylsalicylic acid on prostaglandin synthetase may be due to competition for the enzyme cationic binding site. *Prostaglandins Med*. 1981;6(2):161-164.

doi: 10.1016/0161-4630(81)90087-2

35. Robert A, Nezamis J, Lancaster C, Hanchar A, Klepper M. Enteropooling assay: A test for diarrhea produced by prostaglandins. *Prostaglandins*. 1976;11(5):809-828.

doi: 10.1016/0090-6980(76)90189-1

ACCSCIENCE PUBLISHING

Innovative Medicines & Omics

ORIGINAL RESEARCH ARTICLE

In silico evaluation of ursodeoxycholic acid from *Janja rubens* and its analogs as potential anti-Alzheimer's agents

Oluwafemi S. Aina[1,2*], Owoyemi W. Elegbeleye[3], Nafisat O. Babamusa[1], Mujeeb O. Rofiu[1], Kafayat A. Owoseni-Fagbenro[1], Olubusayo F. Semire[1], Olasupo A. Idris[1], Luqman A. Adams[1], and Oluwole B. Familoni[1]

[1]Department of Chemistry, Faculty of Science, University of Lagos, Lagos, Nigeria

[2]Department of Biological Sciences, Faculty of Basic Medical and Applied Sciences, Trinity University, Lagos, Nigeria

[3]Department of Marine Sciences, Faculty of Science, University of Lagos, Lagos, Nigeria

(This article belongs to the *Special Issue: Alzheimer's Disease and Other Forms of Dementias - Current Research Progress and Drug Development*)

Abstract

Alzheimer's disease (AD), one of the neurodegenerative disorders, is marked by the gradual degeneration of nerve cells in the brain or peripheral nervous system, along with abnormal protein aggregation. While significant efforts have been made to manage AD, a dearth of data remains on candidate phytochemicals and analogs in its treatment. Herein, we present alkaloids derived from the marine algae *Janja rubens* as potential inhibitors of human acetylcholinesterase (AChE) relevant to AD therapy. Using *in silico* tools, such as Protox II and SwissADME, 40 isolates were screened for toxicity and absorption, distribution, metabolism, and excretion properties. Molecular docking simulations were performed using PyRx 0.8, AutoDock Vina Wizard, and Discovery Studio 2020. A 50-nanosecond molecular dynamics simulation was performed using the Groningen Molecular Simulation in the LINUX environment and bio-organic molecules force field simulation (CHARMM 36). Ursodeoxycholic acid (AL20), an isolate from *J. rubens*, exhibited strong inhibitory activity against AChE with a binding energy of −8.5 kcal/mol, surpassing standard anti-Alzheimer drugs donepezil (−8.3 kcal/mol), galantamine (−7.7 kcal/mol), and rivastigmine (−6.4 kcal/mol). However, *in silico* data revealed a 73% probability of hepatotoxicity for AL20. Thereafter, seven derivatives (AL20A–G) were designed to improve properties for drug likeness. The amide analog, AL20E, showed superior inhibitory activity (−9.0 kcal/mol) and non-toxicity compared to AL20 and the standard drugs. This derivative also demonstrated strong interactions with the AChE enzyme, forming three hydrogen bonds with amino acid residues Pro290, Ser293, and Leu289. The brain or intestinal estimated permeation model predicted favorable gastrointestinal absorption and blood–brain barrier penetration for AL20E, indicating its potential as a central nervous system-active drug. Density functional theory and molecular dynamics analyses confirmed the chemical stability of AL20E, making it a promising candidate for the development of an anti-Alzheimer drug. This study highlights AL20E ([4R]-4-[{3S,7S,8R,9S,10S,13R,14S,17R}-3,7-dihydroxy-10,13-dimethylhexadecahydro-1H cyclopenta{a}phenanthren-17-yl]pentanamide) as a non-toxic, AchE inhibitor with enhanced drug-likeness. This study thereby presents AL20E for consideration as a lead compound in the development of novel Alzheimer's therapeutics.

Keywords: *Janja rubens*; *In silico* analysis; Ursodeoxycholic acid; Acetylcholinesterase; Anti-Alzheimer drug

***Corresponding author:**
Oluwafemi S. Aina
(oluwafemi.aina@trinityuniversity.edu.ng)

Citation: Aina OS, Elegbeleye OW, Babamusa NO, *et al. In silico* evaluation of ursodeoxycholic acid from *Janja rubens* and its analogs as potential anti-Alzheimer's agents. *Innov Med Omics*. 2025;2(4):74-92. doi: 10.36922/IMO025260027

Received: June 24, 2025

Revised: August 25, 2025

Accepted: September 2, 2025

Published online: October 14, 2025

1. Introduction

Neurodegenerative diseases, especially Alzheimer's disease (AD) and Parkinson's disease, are leading causes of death worldwide and are identified by a progressive loss of specific neuronal cell populations due to abnormal protein aggregation within neurons. AD is the most common cause of dementia in people over 65 years, affecting 55 million people and increasing at an alarming rate of 10 million cases/year worldwide.[1,2] Based on the cholinergic hypothesis of the pathogenesis of AD, the clinical features of dementia observed in this disease are ascribed to decreased levels of acetylcholinesterase (AChE), a neurotransmitter involved in memory and learning, in the hippocampus and cortex.[3] Notably, Food and Drug Administration (FDA)-approved drugs (donepezil, galantamine, memantine, and rivastigmine) only temporarily improve symptoms by increasing the number of neurotransmitters in the brain.

Ursodeoxycholic acid prevents the degradation of inhibitor of kappa B alpha, thereby leading to the inhibition of nuclear factor kappa B-dependent gene expression in microglia. The expression of these genes is associated with inflammation, a significant factor in neurodegenerative diseases, such as AD.[4] AChE inhibitors are commonly employed to partially alleviate symptoms in mild to moderate AD. They are also used to manage various other forms of dementia and central nervous system disorders, including Parkinson's disease, Lewy body-related dementia, mild cognitive impairment, Down syndrome, Korsakov disease, and vascular dementia.[5]

Researchers are currently actively designing, synthesizing, and evaluating new bioactive compounds for Alzheimer's treatment with minimal side effects.[6] For instance, ursodeoxycholic acid has been found to reduce neuronal loss in prion-infected cerebellar slice cultures.[7] In addition, in models of acute bilirubin encephalopathy, ursodeoxycholic acid treatment has been demonstrated to prevent apoptosis induced by unconjugated bilirubin in astrocytes and fetal neurons isolated from rats.[8] Alkaloids of marine algae are rare and mostly belong to the indole and phenylethylamine groups. In addition, the biological properties of these alkaloids remain under investigation.[9,10] While current treatments for neurodegenerative diseases exist, a critical gap remains in the availability of diverse, non-toxic, and highly effective phytochemical and synthetic drug candidates discoverable through a rapid and cost-effective computational approach. Therefore, this study aims to develop a potent, non-toxic, and anti-neurodegenerative compound from *Jania rubens* alkaloids, specifically by optimizing ursodeoxycholic acid derivatives using a multi-stage *in silico* methodology to identify a potential lead compound with a favorable toxicity profile and enhanced drug-likeness.

2. Materials and methods

2.1. Isolates from red seaweed *Jania rubens*

Phytochemicals were extracted and analyzed from the red seaweed *J. rubens* as described by El-Din and El-Ahwany.[11] The chemical names and structures of the 40 isolates investigated herein are presented in Table 1 and Figure 1, respectively.

2.2. Toxicity analysis of phytochemicals from *Jania rubens*

The target phytochemicals were screened for toxicity by screening using the Protox II web server (https://tox.charite.de/protox3/). We generated the Simplified Molecular Input Line Entry System (SMILES) representation of each phytochemical compound from *J. rubens* drawn using ChemDraw (Version 14.0, PerkinElmer Informatics, United States of America) and saved it in.sdf format on the server. The retrieved toxicity information included hepatotoxicity, carcinogenicity, immunotoxicity, mutagenicity, and cytotoxicity.

2.3. Preparation of enzymes and docking study

Protein structures used were initially cleaned by removing all solvent molecules and the co-crystallized ligands before docking. Molecular docking calculations for the 40 compounds against the Alzheimer protein, AChE (PDB ID: 4EY6), were undertaken using PyRx (Version 0.8, The Scripps Research Institute, United States of America) and Discovery Studio (Version 2020, BIOVIA, France), with a sphere (15 Å radius) that can accommodate the cavity centered on the binding sites of the protein structure. This approach ensured alignment in their conformations.[12] Standard protonation states of the protein based on neutral pH were used in the docking studies. The isolated structures were built using ChemDraw. Variable orientations of each ligand were searched and ranked based on their re-rank score. For each docking simulation, the maximum number of iterations for the docking algorithm was set to 9, with a maximum population size of 9 mode runs per ligand. The root mean square deviation (RMSD) threshold for multiple poses was set to 1.00 Å.[13]

2.4. Structural modification of lead compound AL20

Compound AL20, as the lead candidate with the highest binding energy of −8.5 kcal/mol, was selected for derivatization due to unfavorable toxicity profiles. Consequently, seven hypothetical compounds (AL20A–AL20G) were generated using ChemDraw. The structures were saved in the.sdf format, and their corresponding

Table 1. Structural information of phytochemicals (AL1–AL40) investigated from red seaweed *Jania rubens*[11]

Compound	Chemical name	Molecular formula	Molecular weight (g/mol)
AL1	2-Imidazolidinone	$C_3H_6N_2O$	86.0940
AL2	2-Cyclohexylpiperidine	$C_{11}H_{21}N$	167.2960
AL3	Methylene chloride	CH_2C_{l2}	84.9270
AL4	6-Methyl-4-([4-methylphenyl] sulfonyl)-5-heptenoic acid	$C_{15}H_{20}O_4S$	296.3810
AL5	3-(3-Hydroxybutyl)-2,4,4trimethyl-2-cyclohexen-1-one	$C_{13}H_{22}O_2$	210.3170
AL6	3-Ethyl-5-(2-ethylbutyl)-octadecane	$C_{26}H_{54}$	366.7180
AL7	Heptadecane	$C_{17}H_{36}$	240.4750
AL8	Hexadecanal	$C_{16}H_{32}O$	240.4310
AL9	Tetradecanoic acid	$C_{14}H_{28}O_2$	228.3760
AL10	9-hexadecenoic acid	$C_{16}H_{30}O_2$	254.4140
AL11	Pentadecanoic acid	$C_{15}H_{30}O_2$	242.4030
AL12	3,7,11,15-Tetramethyl-2-hexadecen-1-ol	$C_{20}H_{40}O$	296.5390
AL13	6,10,14-Trimethyl-2-pentadecanone	$C_{18}H_{36}O$	268.4850
AL14	Pentadecanal	$C_{15}H_{30}O$	226.4040
AL15	3-Eicosyne	$C_{20}H_{38}$	278.5240
AL16	Hexadecenoic acid	$C_{16}H_{30}O_2$	254.4140
AL17	9-Oximino-2,7-diethoxyfluorene	$C_{17}H_{17}NO_3$	283.3270
AL18	Hexadecanoic acid methyl ester	$C_{17}H_{34}O_2$	270.4570
AL19	L-(+)-Ascorbic acid 2,6-dihexadecanoate	$C_{38}H_{68}O_8$	652.9540
AL20	Ursodeoxycholic acid	$C_{24}H_{40}O_4$	392.5800
AL21	Methyl 13-octadecenoate	$C_{19}H_{36}O_2$	296.4950
AL22	Phytol	$C_{20}H_{40}O$	296.5390
AL23	Trans-13-octadecenoic acid	$C_{18}H_{34}O_2$	282.4680
AL24	Octadecanoic acid	$C_{18}H_{36}O_2$	284.4840
AL25	Heptasiloxane	$H_{16}O_6Si_7$	308.7170
AL26	Octanoic acid	$C_8H_{16}O_2$	144.2140
AL27	Octasiloxane	$H_{18}O_7Si_8$	354.8170
AL28	Squalene	$C_{30}H_{50}$	410.7300
AL29	9,12,15-Octadecatrienoic acid	$C_{18}H_{30}O_2$	278.4360
AL30	Oleic acid	$C_{18}H_{34}O_2$	282.4680
AL31	17-Pentatriacontene	$C_{35}H_{70}$	490.9450
AL32	Propanoic acid	$C_3H_6O_2$	74.0790
AL33	Rhodopsin	$C_{40}H_{58}O$	554.9030
AL34	Stigmasterol	$C_{29}H_{52}O$	416.7340
AL35	Withaferin A	$C_{28}H_{38}O_6$	470.6060
AL36	Cholest-5-en-3-one	$C_{27}H_{44}O$	384.6480
AL37	Cyclopropanebutanoic acid	$C_7H_{12}O_2$	128.0837
AL38	Pregn-5-ene-3,20-dione	$C_{21}H_{30}O_2$	314.4690
AL39	2,4,6-Decatrienoic acid	$C_{10}H_{14}O_2$	166.2200
AL40	Demecolcine	$C_{21}H_{25}NO_5$	371.4330

SMILES notations were uploaded onto the Protox II web server as outlined in Section 2.2 to evaluate their toxicity profiles against necessary compliance with drug-likeness rules.[14]

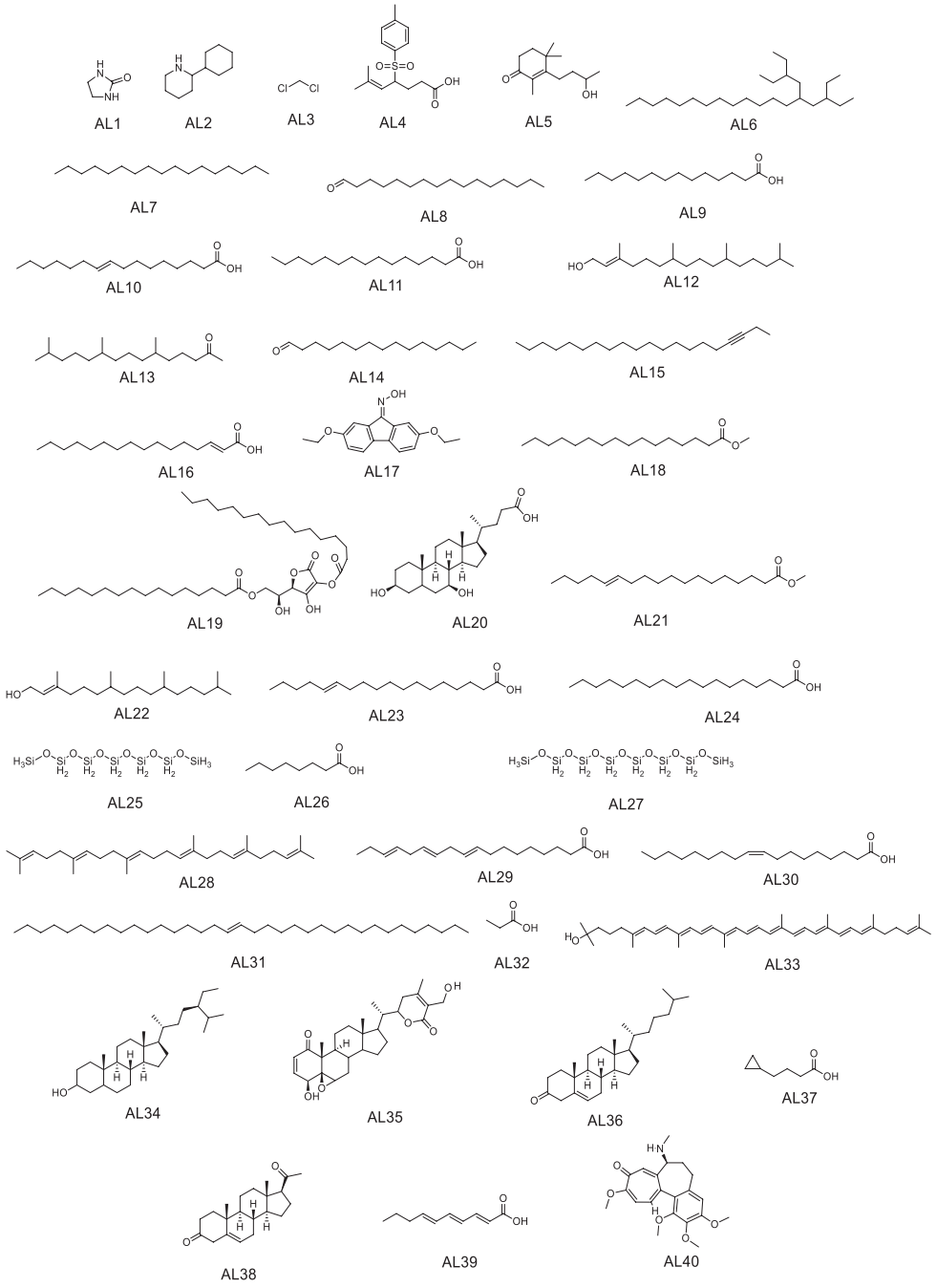

Figure 1. Molecular structures of isolated compounds from red seaweed *Jania rubens*

2.5. Drug-likeness and bioactivity

The seven derivative test compounds (AL20A–AL20G) were investigated using their SMILES representations on the admetSAR2 web server (lmmd.ecust.edu.cn/admetsar2) to predict absorption, distribution, metabolism, and excretion (ADME) parameters. Furthermore, bioactivity assessment using the Molinspiration web server was conducted to determine their potential as candidates for further drug development. Gastrointestinal (GI) and blood–brain barrier characteristics (brain or intestinal estimated permeation method [BOILED-Egg]) of the top three lead compounds obtained from AL20 were also obtained and analyzed.

2.6. Density functional theory studies

The geometry optimization of the lead AL20 and the top three derivative compounds, AL20B, AL20D, and AL20E, was carried out using the Gaussian 09W (Gaussian, Inc., United States of America) program.[15] Becke's three-parameter hybrid model with the Lee, Yang, and Parr's (B3LYP) correlation functional[16] was employed in combination with the Pople's standard, split-valence triple-zeta basis set (6–311++G[d,p])[17] for the calculations of density functional theory (DFT). The investigation of each compound's structural electronic data, chemical reactivity, molecular electrostatic potential map, molecular atomic charges, and molecular orbital properties was conducted. The simulated results were analyzed using GaussView software (Version 6.0, Gaussian, Inc., United States of America).[18]

2.7. Molecular dynamics simulation by Groningen Molecular Simulation

The molecular dynamics (MD) simulations of the lead compounds (AL20, AL20E) and reference drug (donepezil) were investigated against AChE, assessing protein (flexible)–ligand interactions stability and flexibility during binding.[19] Groningen Molecular Simulation (GROMACS) via the LINUX environment was employed to simulate the conformations, and the CHARMM 36 force field was used to generate the topological data for the complex. Small molecule topology and coordinate information were obtained from the CHARMM general force field (https://cgenff.com/). The macromolecular system was solvated in an aqueous phase using the simple point charge-216 water model and neutralized using a 0.15 M sodium chloride solution. A dodecahedron box was used to encapsulate the system, and 5,000 iterations of the steepest descent strategy were used to minimize energy. The equilibrium of ion molecules around the macromolecule was achieved at 310 K and 1.0 bar using the setup of constant number of particles, system pressure, and temperature, as well as constant number of particles, system volume, and temperature. A 50-nanosecond MD simulation was performed to generate structural trajectories for the analysis. Key parameters assessed include the RMSD, the root mean-square fluctuation (RMSF), the solvent-accessible surface area (SASA), hydrogen bonds (HBs), and the radius of gyration (Rg).

3. Results and Discussions

3.1. Toxicity analysis, druglikeness, and binding energy of lead phytochemicals from *Janiа rubens*

Toxicity evaluation is crucial in the identification and development of drugs. Lead compounds from *J. rubens* investigated using the Protox II web server are presented in Table 2. The toxicity profiles of the reference drugs are shown in Table 3. The summary of their binding energies is given in Table 4.

The isolated AL20 (ursodeoxycholic acid), alongside seven others, has exhibited high inhibitory activity against the human AChE protein (4EY6) crystal (Figure 2). The three standard reference drugs considered in this study are also included in Figure 2.

Druglikeness of five isolates with the good binding energy was analyzed using the SwissADME web server (http://www.swissadme.ch/index.php) and presented in Figure 3. Their compliance (or non-violation) with standard drug-likeness rules is presented in Table 5.

Out of the 40 isolates investigated, seven (AL1, AL4, AL5, AL26, AL32, AL37, and AL39) are non-toxic relative to the reference standard drugs (Table 3), whereas isolates AL17, AL20, AL35, AL38, and AL40 (Table 2) flouted one or more toxicity limitations. Interestingly, the isolates AL20, AL36, AL17, and AL35 demonstrated superior performance as anti-Alzheimer drug candidates based on their binding energy against human AChE enzyme (4EY6) (Table 4) compared to donepezil, galantamine, and rivastigmine (anti-Alzheimer standard drugs). Isolate AL20 (ursodeoxycholic acid) was therefore selected as the target moiety for further investigation through derivatization (Figure 4).

The isolate AL20 (ursodeoxycholic acid) exhibited the highest inhibitory activity against the human AChE

Table 2. Toxicity profiles of the *Janiа rubens* lead compounds

Toxicity profiles	Prediction (probability)											
	AL1	AL4	AL5	AL17	AL20	AL26	AL32	AL35	AL37	AL38	AL39	AL40
Hepatotoxicity	No (0.85)	No (0.54)	No (0.61)	No (0.64)	Yes (0.73)	No (0.52)	No (0.69)	No (0.93)	No (0.59)	No (0.67)	No (0.59)	No (0.68)
Carcinogenicity	No (0.88)	No (0.75)	No (0.68)	Yes (0.56)	No (0.79)	No (0.63)	No (0.76)	No (0.55)	No (0.66)	Yes (0.56)	No (0.69)	No (0.59)
Immunotoxicity	No (0.99)	No (0.99)	No (0.99)	No (0.72)	No (0.78)	No (0.99)	No (0.99)	Yes (0.99)	No (0.99)	Yes (0.96)	No (0.99)	Yes (0.99)
Mutagenicity	No (0.52)	No (0.68)	No (0.61)	Yes (0.59)	No (0.56)	No (100)	No (0.93)	No (0.79)	No (0.72)	No (0.99)	No (0.68)	No (0.87)
Cytotoxicity	No (0.80)	No (0.71)	No (0.95)	No (0.74)	No (0.76)	No (0.74)	No (0.75)	Yes (0.87)	No (0.76)	No (0.79)	No (0.75)	Yes (0.66)

Table 3. Toxicity compliance of standard drugs for Alzheimer's disease

Target	Prediction (probability)		
	Donepezil	Galantamine	Rivastigmine
Hepatotoxicity	No (0.98)	No (0.93)	No (0.93)
Carcinogenicity	Yes (0.50)	No (0.65)	No (0.74)
Immunotoxicity	Yes (0.95)	Yes (0.98)	Yes (0.69)
Mutagenicity	No (0.53)	No (0.76)	No (0.70)
Cytotoxicity	Yes (0.63)	Yes (0.50)	No (0.66)

Table 4. Complex binding scores of human acetylcholinesterase (4EY6) isolate from *Jania rubens*

4EY6-isolate complex	Binding energy
4EY6_AL20	−8.5
4EY6_AL36	−8.4
4EY6_AL17	−8.3
4EY6_AL35	−8.3
4EY6_donepezil	−8.3
4EY6_AL28	−8.1
4EY6_AL38	−8.1
4EY6_AL40	−8.0
4EY6_galantamine	−7.7
4EY6_AL34	−7.3
4EY6_AL39	−7.1
4EY6_AL4	−6.9
4EY6_rivastigmine	−6.4
4EY6_AL26	−5.7
4EY6_AL5	−5.5
4EY6_AL37	−5.3
4EY6_AL1	−4.0
4EY6_AL32	−3.7

protein crystal (4EY6), as presented in Table 4, along with other high-binding bioactive isolates. The three standard reference drugs considered in this study are shown in Figure 4. The drug-likeness of the high-binding energy isolates was analyzed using the SwissADME web server (http://www.swissadme.ch/index.php). We observed that five of the isolates (AL17, AL20, AL35, AL38, and AL40) fall within the optimal physicochemical space for bioavailability. All five isolates exhibited high GI absorption capability, while AL17, AL38, and AL40 showed blood–brain barrier permeability (Table 5). However, isolated AL35 violated one of the Ghose rules, suggestive of poor oral bioavailability.

3.2. Toxicity probability and bioavailability of the derivatives of AL20 (the highest binding isolate)

Despite its strong AChE inhibition and favorable drug-likeness, isolate AL20 exhibited high hepatotoxicity (73%), prompting the desire for new derivatives of the moiety. Guided by structure-activity relationship principles, seven new derivatives of AL20 (AL20A, AL20B, AL20C, AL20D, AL20E, AL20F, AL20G) were designed to reduce the toxicity properties. AL20 was modified at the carboxylic functional group to carry a methyl group (AL20A), ketone (AL20B), aldehyde (AL20G), acid chloride (AL20C), amides (AL20E), and ester (AL20F). In addition, the butanoic acid side chain was removed, and one of the hydroxyl groups was hypothetically oxidized to a ketone (AL20D). These modifications aimed to improve their biocompatibilities. Figure 5 presents the structures of the new derivatives, while Table 6 shows their toxicity compliance investigated using the Protox 3 web server. Figure 4 depicts the bioavailability of the three best derivatives compared to the standard drug for AD.

Virtual toxicity screening of AL20 derivatives using the Protox II web server showed that AL20B, AL20D, and AL20E (Table 6) were non-toxic, unlike AL20C, AL20F, and AL20G, which showed a high probability of being hepatotoxic (57–63%), while AL20A and AL20G exhibited a probability of 60–69% of being immunotoxic. Notably, the non-toxic derivatives of AL20 isolate were more biocompatible than the standard Alzheimer's drugs, which displayed varying degrees of toxicity, including carcinogenicity, immunogenicity, and cytotoxicity (Table 3). Donepezil, galantamine, and rivastigmine are prescription drugs used in early- to mid-stage AD. However, their inherent toxicity remains a concern. Interestingly, the bioavailability results (Figure 4) of all AL20 non-toxic derivatives (AL20B, AL20D, and AL20E) showed superior drug-likeness properties compared to the three standard drugs. Thus, the non-toxic derivatives were subjected to further analysis.

3.3. Bioactivity score of lead derivatives

The bioactivity scores of the three best lead derivatives, AL20B, AL20D, and AL20E, the isolate AL20, and the reference drug donepezil are presented in Figure 6. The bioactivity scores were evaluated using several parameters, including G-protein-coupled receptor (GPCR) ligands, ion channel modulators, kinase inhibitors, nuclear receptor ligands, protease inhibitors, and enzyme inhibitors.

Compounds with bioactivity scores higher than 0.00 are defined as active, those between −0.50 and 0.0 are

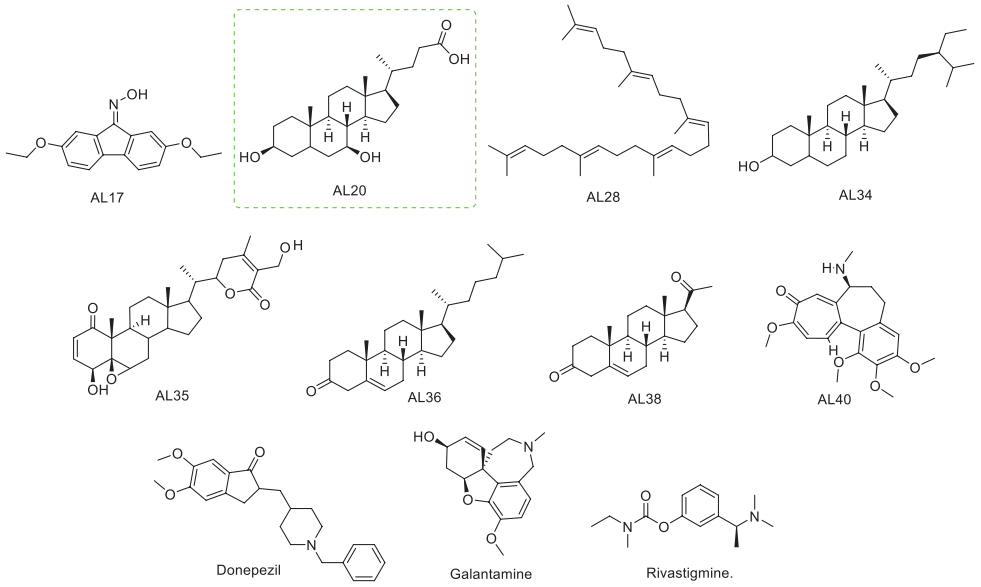

Figure 2. Structures of lead compounds of *Jania rubens* against human acetylcholinesterase and commonly used Alzheimer's drugs, donepezil, galantamine, and rivastigmine

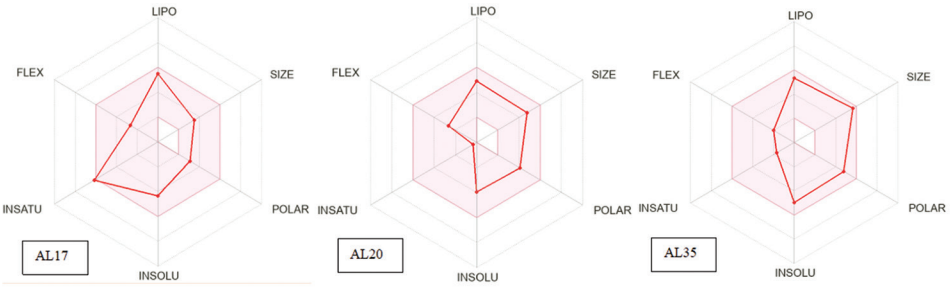

Figure 3. Lead compounds AL17, AL20, and AL35 with excellent binding energy and bioavailability (compliant physicochemical space)
Abbreviations: FLEX: Flexibility; INSATU: Saturation; INSOLU: Solubility; LIPO: Lipophilicity; POLAR: Polarity; SIZE: Molecular size.

Table 5. Compliance of active isolates with drug-likeness rules

Isolate	Lipinski	Ghose	Veber	Egan	Muegge	GI abs	BBB perm
AL17	0	0	0	0	0	High	Yes
AL20	0	0	0	0	0	High	No
AL35	0	1	0	0	0	High	No
AL38	0	0	0	0	0	High	Yes
AL40	0	0	0	0	0	High	Yes

Note: 0: No violation; 1: One violation.
Abbreviations: abs: Absorption; BBB: Blood–brain barrier; GI: Gastrointestinal; perm: Permeability.

moderately active, and scores below −0.50 are considered inactive.[20] They exhibited superior performance compared to donepezil in several bioactivity scores, including ion-channel modulator (0.2–0.4), protease inhibitor (0.1–0.4), enzyme inhibitor (0.6–0.8), nuclear receptor ligand (0.6–1.0), and GCPR ligands (0.0–0.4). However, derivatives AL20B and AL20D were inactive as kinase inhibitors (KI) (−0.8–−0.6).

3.4. Brain or intestinal estimated permeation model for blood–brain barrier permeability and GI absorption

The BOILED-Egg method predicts human GI absorption and blood–brain barrier (BBB) penetration using the SMILE string of the compounds. The algorithm utilizes two physicochemical models: lipophilicity (Wildman–Crippen LogP method [WLOGP]) and polarity (topological polar surface area), while estimating physicochemical descriptors, such as brain access and GI absorption for compounds AL20, AL20B, AL20D, and AL20E (Figure 7).

The analysis identifies the substrate of P-glycoproteins (PGP), which are detected as positive or negative in the BOILED-Egg method.[21,22] The statistical robustness, graphical nature, and speed of this method enable efficient

Figure 4. Bioavailability suitable physicochemical space of the standard drugs for Alzheimer's disease (donepezil, galantamine, and rivastigmine), AL20, and its lead derivatives (AL20B, AL20D, and AL20E)
Abbreviations: FLEX: Flexibility; INSATU: Saturation; INSOLU: Solubility; LIPO: Lipophilicity; POLAR: Polarity; SIZE: Molecular size.

Table 6. Toxicity compliance of AL20 designed derivatives, AL20A–AL20G

Target	Prediction (probability)							
	AL20	AL20A	AL20B	AL20C	AL20D	AL20E	AL20F	AL20G
Hepatotoxicity	Yes (0.73)	No (0.66)	No (0.63)	Yes (0.57)	No (0.53)	No (0.67)	Yes (0.62)	Yes (0.63)
Carcinogenicity	No (0.79)	No (0.80)	No (0.72)	No (0.66)	No (0.78)	No (0.63)	No (0.80)	No (0.72)
Immunotoxicity	No (0.78)	Yes (0.60)	No (0.83)	No (0.72)	No (0.53)	No (0.79)	No (0.53)	Yes (0.69)
Mutagenicity	No (0.56)	No (0.87)	No (0.78)	No (0.74)	No (0.94)	No (0.83)	No (0.63)	No (0.78)
Cytotoxicity	No (0.76)	No (0.89)	No (0.88)	No (0.77)	No (0.81)	No (0.74)	No (0.67)	No (0.88)

translation of molecular design in drug discovery and medicinal chemistry.[21] Drug-likeness models and methods, such as in-house physics-based LogP model, generalized born/surface area model, atom-additive method, WLOGP, Moriguchi LogP method, and Silicos-IT fragment- and topology-based model, as well as drug-likeness rules, such as Lipinski, Veber, Muegge, Ghost, and Egan, are incorporated in the BOILED-EGG tool. The SwissADME tool facilitates pharmacokinetics predictions, especially for ADME, bioavailability, and medicinal chemistry.[22,23]

More than 98% of small molecules are unable to cross the blood–brain barrier (BBB),[24] making the BBB an essential factor in the drug design process, particularly for central nervous system (CNS) disorders. The quantity of drug candidates absorbed by the intestinal system is a significant factor in assessing oral bioavailability,[25] thereby underlining the importance of the GI absorption of the molecules. PGP is a member of the ATP-binding cassette family (ABC) and an ABC transporter.[26] It acts as a biological barrier, pumping out toxins and xenobiotics

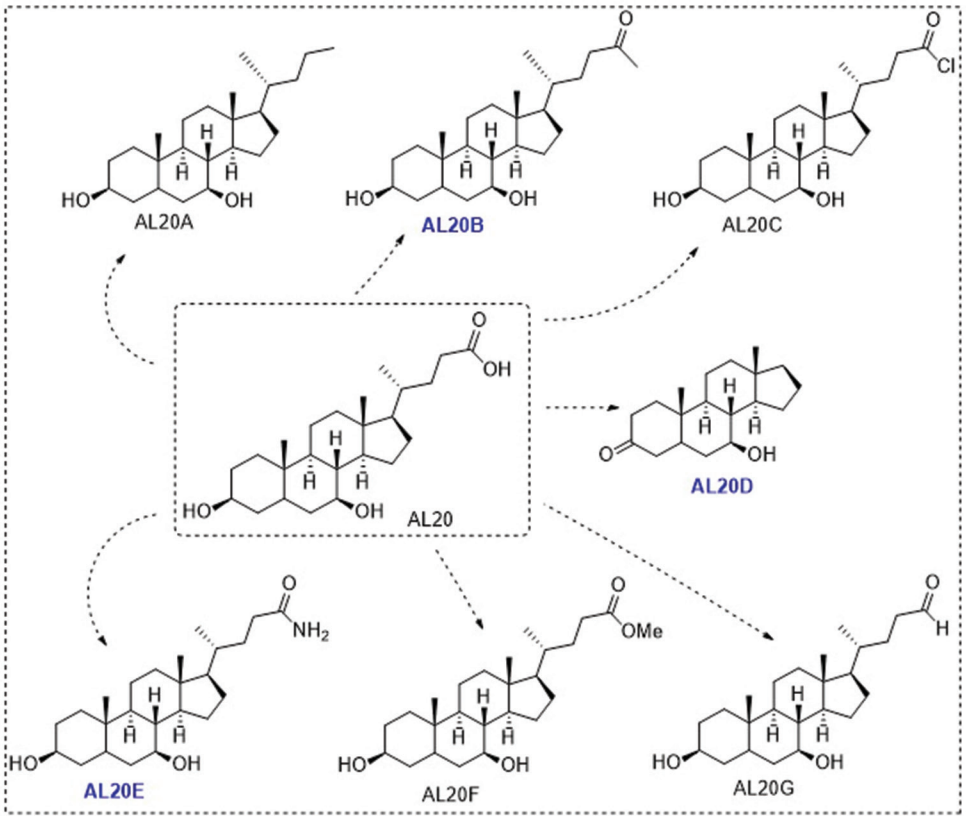

Figure 5. Structure of AL20 isolated from *Jania rubens* and its modified derivatives obtained through a structure-activity relationship study

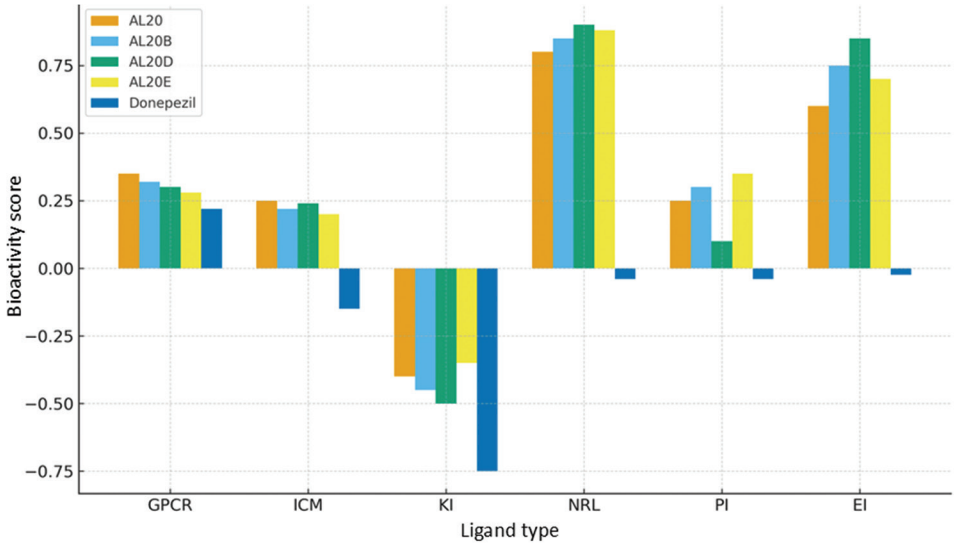

Figure 6. Bioactivity scores of *Jania rubens* phytochemical (AL20), its lead derivatives (AL20B, AL20D, and AL20E), and donepezil (Alzheimer reference drug)
Abbreviations: EI: Enzyme inhibitor; GPCR: G protein-coupled receptor ligand; ICM: Ion channel modulator; KI: Kinase inhibitor; NRL: Nuclear receptor ligand; PI: Protease inhibitor.

from cells while also contributing to the absorption of drugs.[27] The overexpression of ABC transporters causes multidrug resistance and is linked to the failure of disease treatments, such as cancer.[28]

The yellow region in Figure 7 represents a zone of compound having good permeation and absorption ability in both the BBB and GI. However, the white region defines good GI absorption but not BBB penetration. Molecules

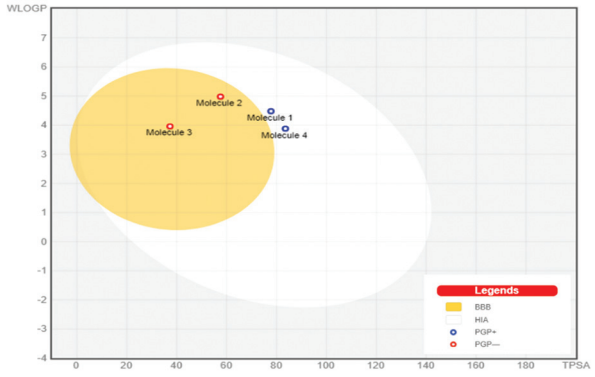

Figure 7. Brain or intestinal estimated permeation model of AL20 and its structurally modified non-toxic derivatives using the SwissADME web server (AL20, AL20B, AL20D, and AL20E are represented as molecules 1, 2, 3, and 4, respectively)
Abbreviations: BBB: Blood–brain barrier; HIA: Human intestinal absorption; PGP: P-glycoprotein; TPSA: Topological polar surface area; WLOGP: Wildman–Crippen LogP.

1 (AL20) and 4 (AL20E), marked with blue dots, and molecules 2 (AL20) and 3 (AL20D), marked with red dots, indicate that the former are predicted to be effluxed from the CNS by PGP, while the latter are predicted to escape PGP efflux. Notably, compounds expected to undergo PGP efflux still display good permeation and absorption ability. In contrast, compounds depicted in red dots (AL20 and AL20D), although they exhibit good permeation and absorption in the BBB, their CNS availability may still be negatively impacted by PGP.

3.5. Density functional theory measurements of target compounds

The molecular geometry optimization for the lead compound AL20's non-toxic derivatives (AL20B, AL20D, and AL20E) was performed using DFT/B3LYP level theory with 6–311+G (d,p) basis set. The optimized molecular geometry of the AL20s is shown in Figure 8, and the chemical reactivity parameters are listed in Table 7. The molecular electrostatic potential (MEP) map of AL20E is shown in Figure 9.

The chemical characteristics of the designed compounds AL20B, AL20D, and AL20E were analyzed using the highest occupied molecular orbital (HOMO) and lowest unoccupied molecular orbital (LUMO) energy levels.[29] This provides insights into the atomic orbital and electron density around the atomic surfaces to define the chemical stability in molecules based on the conceptual-DFT indices,[30] such as hardness, softness, electrophilicity index, and chemical potential. The global chemical hardness and softness measure the resistance and susceptibility of a molecule to exchange electrons with other molecules, respectively.[31] The electrophilicity index indicates the overall electrophilicity and nucleophilicity of a molecule. Furthermore, the feasibility of intermolecular electron transfer in the ground state is defined by the chemical potential.[32] The chemical reactivity descriptors were summarized in Table 7.

The band gaps of the designed compounds are in the increasing order of AL20D < AL20B < AL20E (Table 7). As shown by the frontier HOMO and LUMO molecular orbitals distribution (Figure 9), the carbonyl substituents likely enhanced the electrophilicity, leading to a lower energy gap as indicated in the smaller band gaps in AL20B and AL20D. The larger band gap in AL20E can be attributed to the amide substituent, which has a smaller electron-withdrawing effect compared to the carbonyl group. Compound AL20E also has the highest chemical potential (−0.136). The electrophilicity index value of 0.076 for AL20E demonstrates a stronger nucleophilic character compared to AL20B and AL20D, in the order of AL20D < AL20B < AL20E. AL20E utilizes the nature of conventional HBs with Ser293, Leu289, and Pro290 in interaction with the target receptor. Overall, it can be concluded that the designed compounds can be potential drug candidates for AD.

The MEP map provides information on molecular interactions and the chemical behavior of molecules with other molecular species.[33] The color gradient ranges from red (high electron density, negative electrostatic potential) to blue (low electron density, positive electrostatic potential), with green representing neutral regions. The MEP map for the AL20E derivatives was computed using DFT/B3LYP level of theory with 6–311++G (d,p) basis set (Figure 9). The red regions indicate sites for electrophilic attack, while the blue regions highlight areas susceptible to nucleophilic interactions. Consistent with the DFT-concept reactivity indices, the blue regions, such as the amino group in AL20E, align with nucleophilic interactions, supporting conventional HBs with Ser293, Leu289, and Pro290. In conclusion, the maps revealed possible surfaces of interactions between drugs and proteins.

The transition of electrons from HOMO to LUMO energy levels is represented by the electronic distribution on the HOMO and LUMO surfaces (Figure 9). It is inferred from the surfaces that the lower energy gaps for AL20D and AL20B may be well indicated by the localization of the electron density on the carbonyl or the aliphatic moiety, both in the HOMO and LUMO, after the transition. That is, the transition is occurring within the same regions or very close regions on the molecular surface. In AL20E, the transition from HOMO to LUMO will result in the transfer

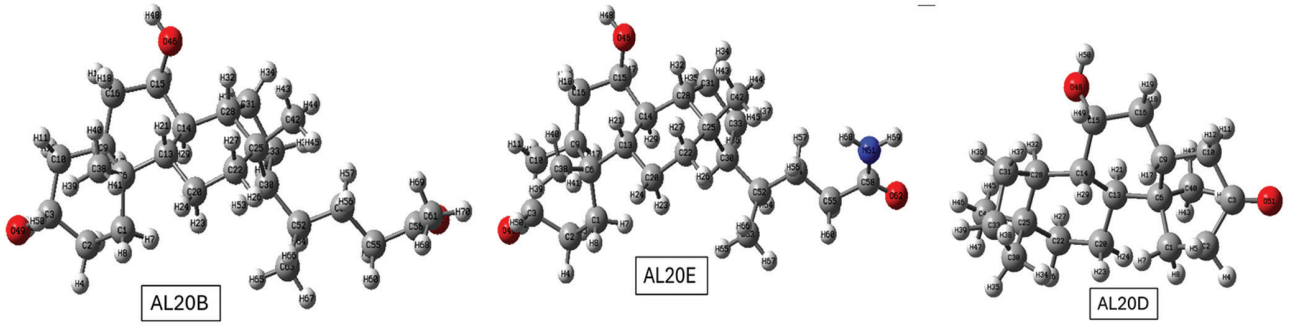

Figure 8. Geometry optimization of AL20 lead derivatives (AL20B, AL20D, and AL20E)

Table 7. Chemical reactivity parameters of the three AL20 lead derivatives

Derivatives	E_{HOMO}	E_{LUMO}	ΔE	IE	EA	H	S	ω	M
AL20B	−0.251	−0.026	0.225	0.251	0.026	0.1125	8.889	0.085	−0.139
AL20D	−0.248	−0.03	0.218	0.248	0.03	0.109	9.174	0.089	−0.139
AL20E	−0.256	−0.015	0.241	0.256	0.015	0.1205	8.299	0.076	−0.136

Abbreviations: ΔE: Energy gap; ω: Electrophilicity index; E_{HOMO}: Energy of the highest occupied molecular orbital; E_{LUMO}: Energy of the lowest unoccupied molecular orbital; EA: Electron affinity; H: Hardness; IE: Ionization energy; M: Chemical potential; S: Softness.

Table 8. Summary of docking results for AL20 hypothetical derivatives

Ligand	Binding affinity	RMSD/UB	RMSD/LB
4EY6_AL20E	−9.0	0	0
4EY6_AL20	−8.5	0	0
4EY6_donepezil	−8.3	0	0
4EY6_AL20B	−8.2	0	0
4EY6_AL20D	−8.1	0	0
4EY6_AL20C	−7.8	0	0
4EY6_AL20A	−7.8	0	0
4EY6_galantamine	−7.7	0	0
4EY6_AL20F	−7.6	0	0
4EY6_AL20G	−7.3	0	0
4EY6_rivastigmine	−6.4	0	0

Abbreviations: LB: Lower bound; RMSD: Root mean square deviation; UB: Upper bound.

of the electron distribution from the carbonyl or aliphatic region to the alicyclic region of the compound (Figure 9). This might explain the higher energy gap in the HOMO-LUMO transition.

3.6. Binding potentials of AL20 derivatives

It was necessary to dock the non-toxic derivatives of AL20 (AL20B, AL20D, and AL20E) to confirm their binding affinity (Table 8). Extracted three-dimensional (3D) structures of the interactions are presented in Figures 10-12.

It was necessary to dock these derivatives, expecting that any of those non-toxic derivatives would also provide excellent binding, and it was noteworthy that derivative AL20E performed better than phytochemical AL20 and all the reference drugs (Table 8) as a potential inhibitor of human AChE (4EY6), a significant target for therapeutic drugs.

The comparative analysis of AL20, AL20E, and donepezil binding to AChE (PDB: 4EY6) reveals distinct inhibitory mechanisms (Figures 11-13), despite all three ligands sharing a common anchor point: Trp_{286}. This residue is part of the peripheral anionic site (PAS) at the gorge entrance. In every complex, the ligand's aromatic core forms a stabilizing hydrophobic π–π stacking interaction with it. Beyond this initial binding, their strategies diverge the reference drug donepezil and the ligand AL20 primarily occupies the PAS, blocking the entrance. However, AL20 achieves a potentially more stable fit by utilizing an additional hydrogen bond with the polar residue Thr_{175}, differentiating its mechanism from the solely aromatic interactions of Donepezil.

The most unique binding profile belongs to AL20E (Figure 11), which acts as a deep-gorge binder. Its extended flexible aliphatic chain enables it to span the entire active site. While still anchored by Trp_{286} at the PAS, the ligand's tail reaches a deeper sub-site, forming a key hydrogen bond with Val_{340}. This strategy of dual-site occupancy is characteristic of potent inhibitors designed to maximize contact area, making AL20E's inhibitory mechanism the

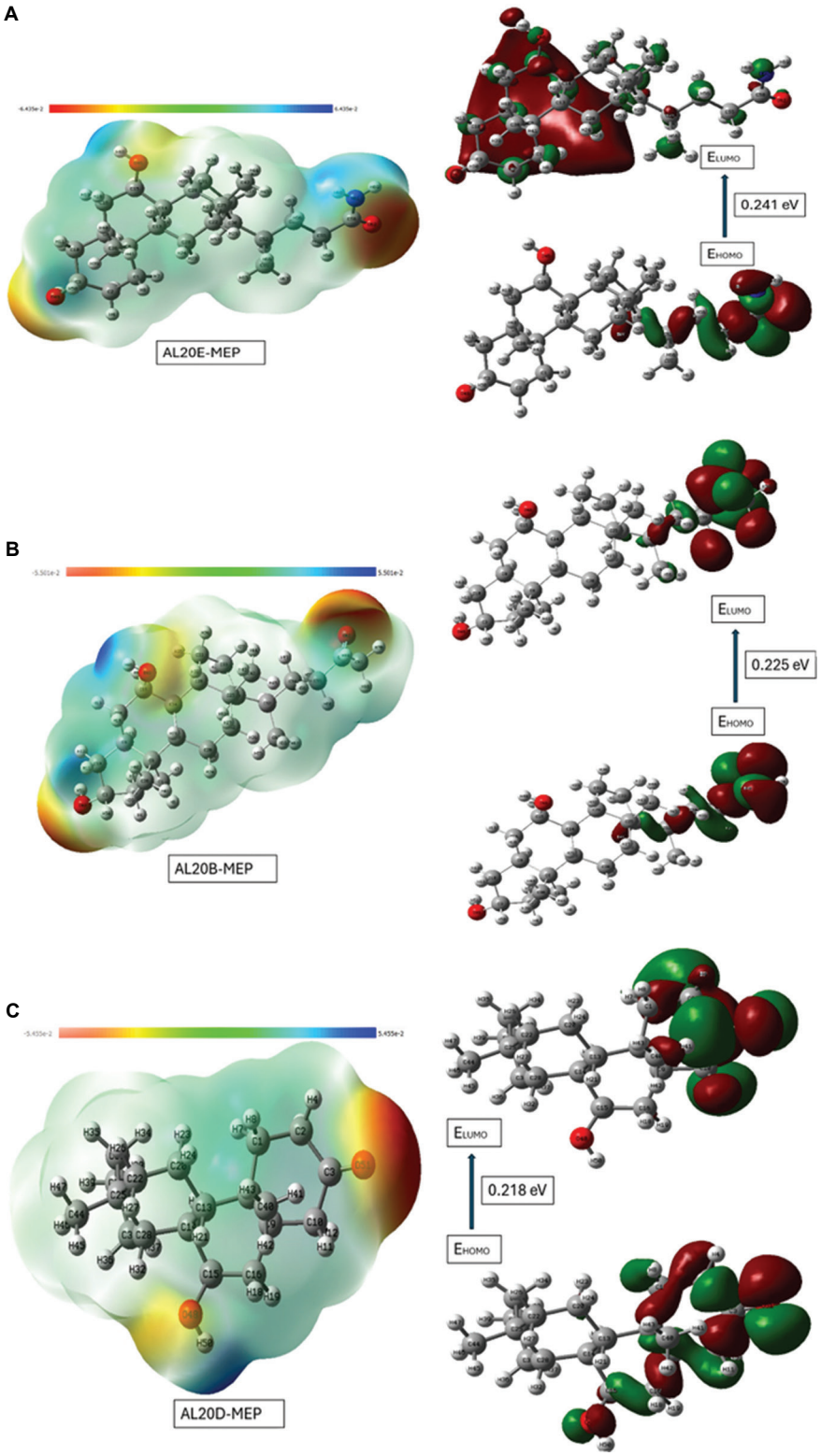

Figure 9. The MEP and HOMO–LUMO transitions of AL20 derivatives. (A) AL20E. (B) AL20B. (C) AL20D.
Abbreviations: E: Energy; HOMO: Highest occupied molecular orbital; LUMO: Lowest unoccupied molecular orbital; MEP: Molecular electrostatic potential.

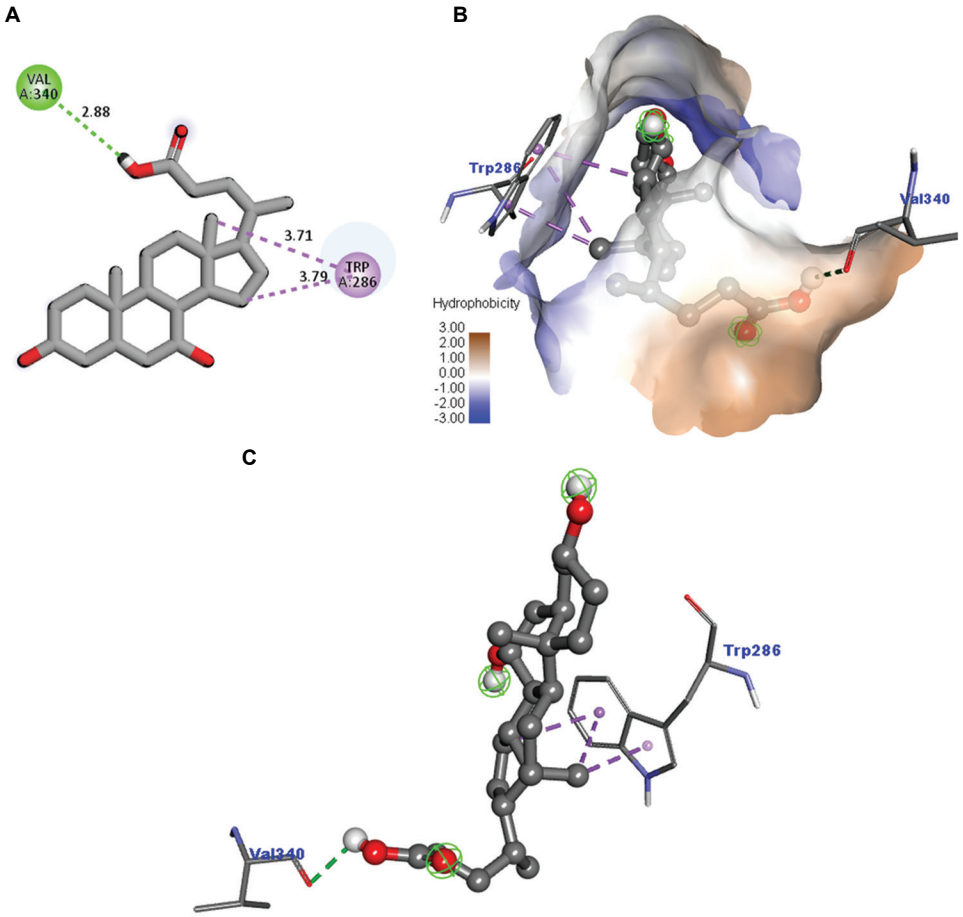

Figure 10. Two- and three-dimensional structures of the 4EY6_AL20 complex. (A) Bonding amino acids in a two-dimensional view. (B) Hydrophobic interactions. (C) Binding residues in a three-dimensional view.

most structurally complex and potentially more effective than AL20 and donepezil.

3.7. Molecular dynamics of lead derivatives and reference drug

The backbone of AChE (4EY6) and the RMSD values of 4EY6_AL20, 4EY6_AL20E, and 4EY6_donepezil complexes are shown in Figure 13, while the RMSF plot to determine the flexibility of each residue over a 50-nanosecond simulation is presented in Figure 14.

Figure 15 depicts the hydrogen bond plots for complexes 4EY6_AL20, 4EY6_AL20E, and 4EY6_donepezil measured in nanoseconds. The thermodynamic stability and energy profiles of 4EY6_AL20, 4EY6_AL20E, and 4EY6_donepezil complexes in terms of temperature, pressure, and density, with minimal fluctuations measured in picoseconds are presented in Figure 16. The SASA and Rg energy plots for complexes 4EY6_AL20, 4EY6_AL20E, and 4EY6_donepezil are illustrated in Figure 17.

Molecular dynamics simulations offer insights into the dynamic behavior of protein-ligand complexes, including structural stability, interaction strength, and thermodynamic properties.[34] In this molecular dynamics study, we compared the complexes formed from two non-toxic derivatives of AL20: 4EY6_AL20 and 4EY6_AL20E with the complex formed with the reference drug, 4EY6_donepezil. Donepezil was chosen to serve as a reference ligand due to its established efficacy as an AChE inhibitor.[35]

3.7.1. Stability analysis of the AChE_AL20 complex

The RMSD values of 4EY6_AL20, 4EY6_AL20E, and 4EY6_donepezil for the backbone of AChE (4EY6) were fluctuating between 0.12 and 0.24 nm, 0.10 and 0.18 nm, and 0.12 and 0.23 nm, with average RMSD values of 0.180 nm, 0.140 nm, and 0.175 nm, respectively. This indicated that the compound, AL20E, having the lowest RSMD value of 0.140 nm, is more stable across the 50-nanosecond simulations compared to AL20 and donepezil (Figure 13A).

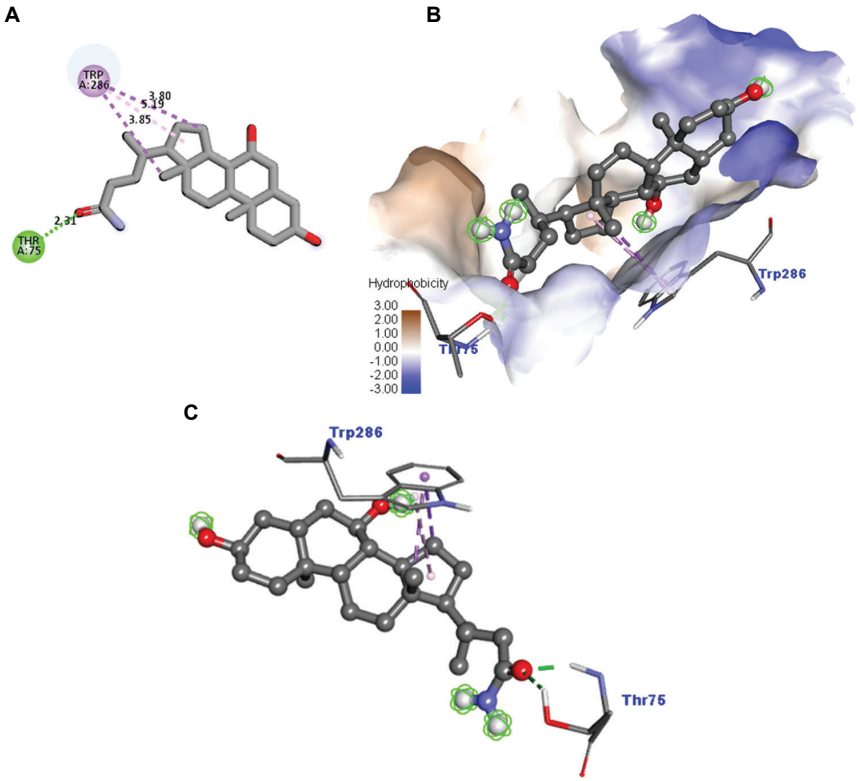

Figure 11. Two- and three-dimensional structures of 4EY6_AL20E complex. (A) Bonding amino acids in a two-dimensional view. (B) Hydrophobic interactions. (C) Binding residues in a three-dimensional view.

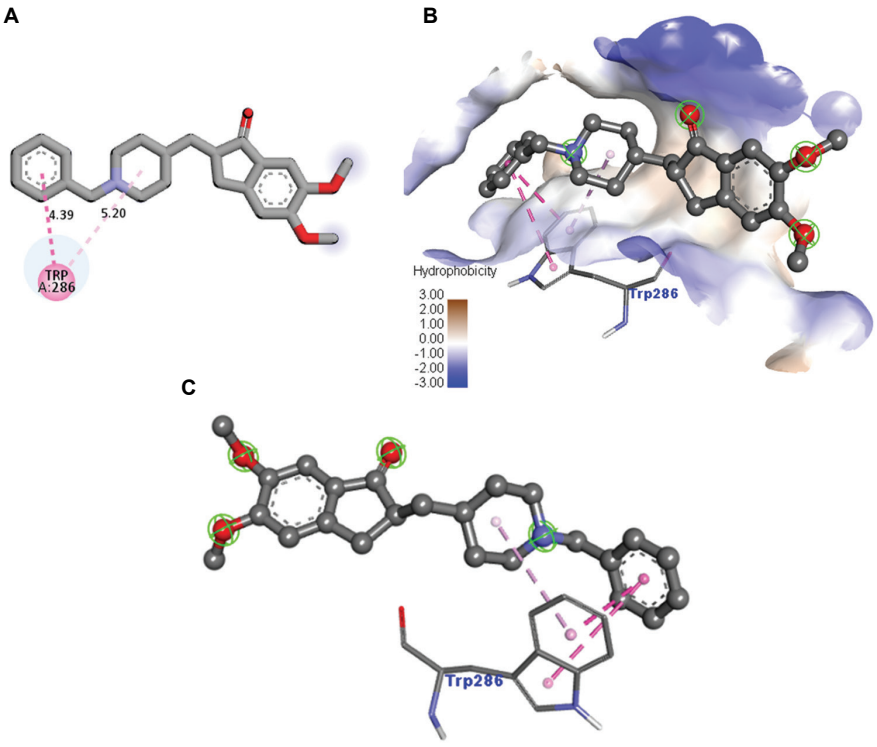

Figure 12. Two- and three-dimensional structures of 4EY6_donepezil complex. (A) Bonding amino acids in a two-dimensional view. (B) Hydrophobic interactions. (C) Binding residues in a three-dimensional view.

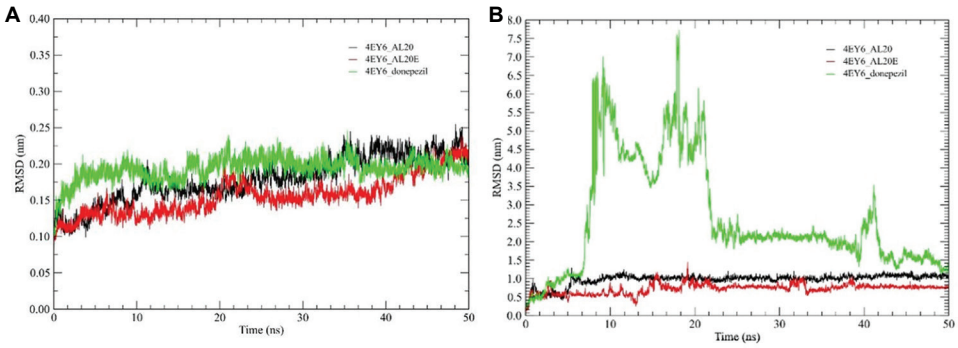

Figure 13. Root mean square deviation (RMSD) plots for complexes 4EY6_AL20, 4EY6_AL20E, and 4EY6_donepezil. (A) Backbone. (B) Ligand.

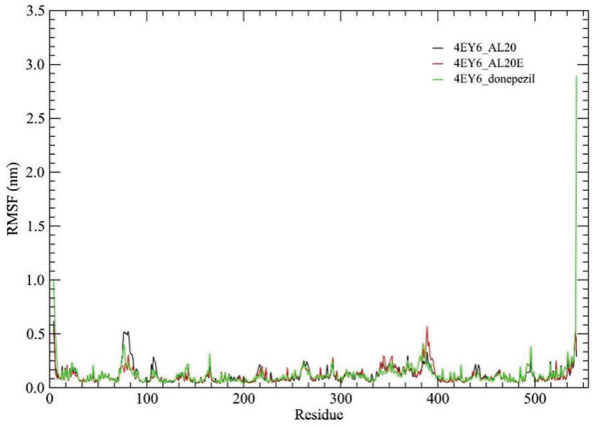

Figure 14. Root mean square fluctuation for complexes 4EY6_AL20, 4EY6_AL20E, and 4EY6_donepezil.

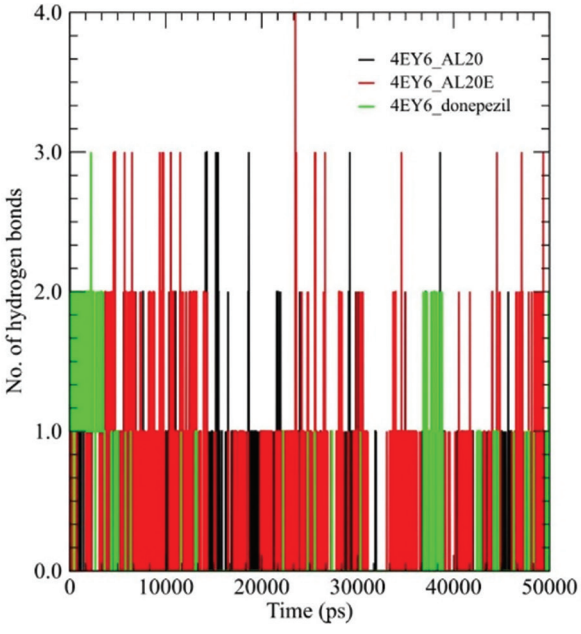

Figure 15. Stability analysis measured in nanoseconds for complexes 4EY6_AL20, 4EY6_AL20E, and 4EY6_donepezil.

The RMSD values of the ligands of AL20, AL20E, and donepezil were predicted, with AL20 starting at approximately 0.4 nm and fluctuating between 0.6 and 1.0 nm. Similarly, AL20E started at approximately 0.00 nm and fluctuated slightly between 0.5 and 0.8 nm. In contrast, donepezil started at approximately 0.2 nm but spiked drastically after 5 ns, showing multiple peaks at 6.0 to 7.5 nm, after which it stabilized to around 1.5 to 2.5 nm after 22 ns (Figure 13B). The average RMSD values of AL20, AL20E, and donepezil are 0.70 nm, 0.40 nm, and 3.85 nm, respectively. This indicates that AL20E binds the strongest to AChE as it exhibits the most stable interaction, as shown in Figure 13.

Hydrogen bonding analysis of the 4EY6_AL20 complex showed stable interactions, with 1–2 HBs throughout the simulation and a transient increase to 3 bonds at 15–18 ns (Figure 15). In comparison, 4EY6_AL20E exhibited stronger interactions, fluctuating between one and three HBs and peaking at four bonds around 20 ns. The reference complex, 4EY6_donepezil, showed the least fluctuation, maintaining 1–2 HBs with a single increase to 3 HBs at 2 ns. Overall, 4EY6_AL20E exhibited the highest and most consistent HB count, consistent with its strong binding capacity.

3.7.2. Flexibility analysis of the AChE_AL20 complex

The RMSF plot shows the flexibility of each residue over a 50-nanosecond simulation (Figure 14). 4EY6_AL20 fluctuated mostly below 0.5 nm, with a peak at residue 80 (0.5 nm), suggesting flexibility. Similarly, peaks of 4EY6_AL20E are minimal, with most residues below 0.4 nm, but exhibit a peak near residue 400 (0.5 nm), suggesting flexibility in that region. In contrast, 4EY6_donepezil fluctuates more than 4EY6_AL20 and 4EY6_AL20E, with a small peak near residue 400 (0.5 nm) and a large peak at the C-terminal (2.9 nm). The high fluctuation at the C-terminal of 4EY6_donepezil suggests flexibility or unfolding, making it the least stable, while 4EY6_AL20E is the most stable complex with the least fluctuation, as

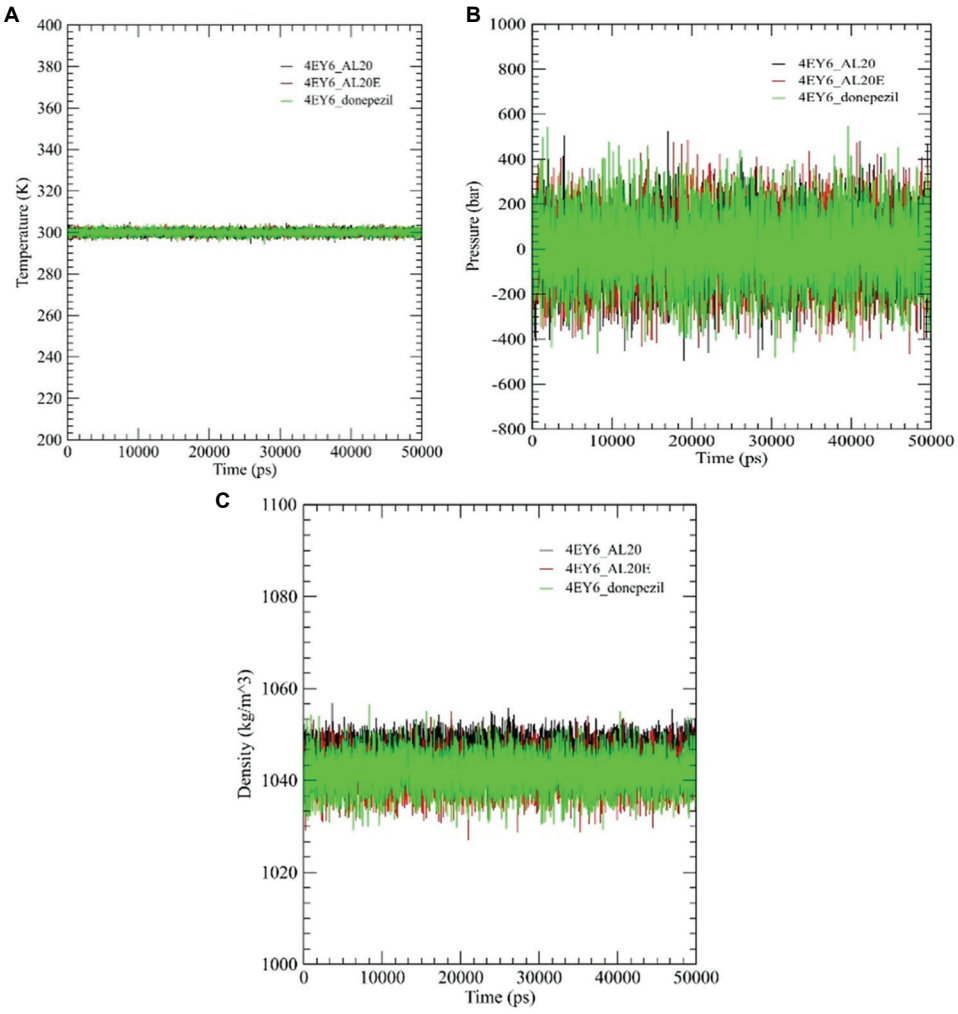

Figure 16. Gromacs energy measured in picoseconds for complexes 4EY6_AL20, 4EY6_AL20E, and 4EY6_donepezil. (A) Temperature. (B) Pressure. (C) Density.

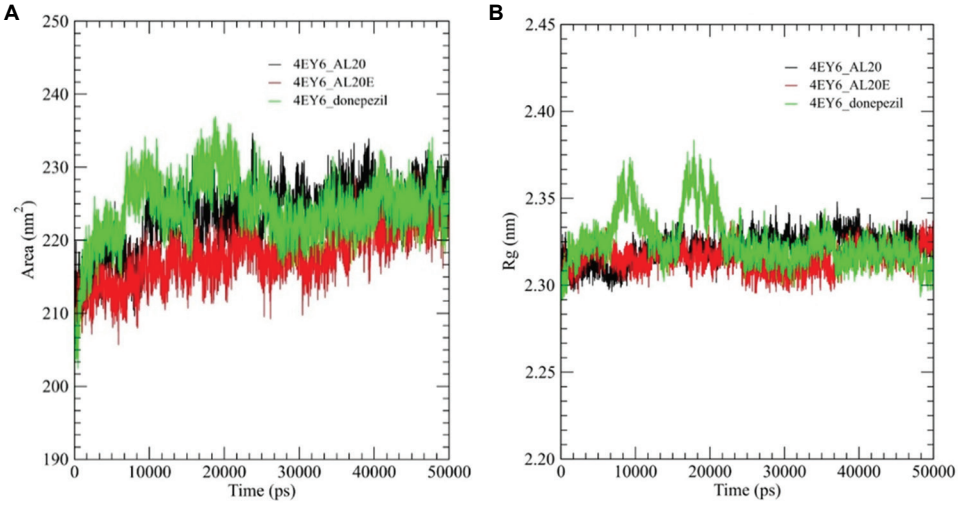

Figure 17. Structural flexibility and compactness measured in nanoseconds for complexes 4EY6_AL20, 4EY6_AL20E, and 4EY6_donepezil (A) Solvent-accessible surface area (B) Radius of gyration.

shown in Figure 14.

3.7.3. Compactness analysis of the AChE_AL20 complex

Radius of gyration value (Figure 17B) for both 4EY6_AL20 and 4EY6_AL20E ranged from 2.30 to 2.34 nm with minimal fluctuations. In contrast, 4EY6_donepezil started around 2.30 nm and exhibited significant fluctuations between 2.30 and 2.37 nm at around 10,000–20,000 ps (10–20 ns). The fluctuation stabilized toward the end of the simulation. 4EY6_AL20E displayed similar Rg values to 4EY6_AL20 but with slightly reduced fluctuations, suggesting improved structural integrity. In conclusion, 4EY6_AL20E is more compact and stable compared to 4EY6_AL20 and 4EY6_donepezil (Figure 17B).

Solvent accessible surface area reflects the extent of the protein's surface exposure to solvent. As shown in Figure 17, 4EY6_AL20 and 4EY6_AL20E showed a similar trend of fluctuating between 215 and 230 nm^2 and 210 and 225 nm^2, respectively. In contrast, 4EY6_donepezil increased from 202 nm^2 to 234 nm^2 for the first 20 ns and became stable for the rest of the simulation. Overall, 4EY6_AL20 and 4EY6_AL20E displayed relatively stable SASA values, whereas 4EY6_donepezil exhibited greater variation, suggesting higher solvent exposure and lower structural stability (Figure 17).

3.7.4. Thermodynamic stability and energy profiles of the AChE_AL20 complex

Regarding the Gromacs energies, the temperature (Figure 16A) of 4EY6_AL20, 4EY6_AL20E, and 4EY6_donepezil exhibited a stable trend with minimal fluctuations around 300 K throughout the 50-nanosecond simulation, indicating proper temperature coupling and stable thermal conditions. The pressure plot (Figure 16B) shows significant fluctuations between −400 bar and 400 bar for all complexes. The density plot for all complexes exhibits a similar trend to the temperature plot, which remains stable around 1044 kg/m^3 throughout the 50-nanosecond simulation (Figure 16C). Overall, the results indicate that the system remains stable throughout the 50-nanosecond simulations, with a slight fluctuation in pressure.

In conclusion, based on the MD results, 4EY6_AL20E exhibits the highest stability, as well as higher hydrogen bond counts and compactness, with reduced flexibility and optimal energy levels, reaffirming its effectiveness as an AChE inhibitor.

4. Conclusion

This study investigated the potential of alkaloids from the marine red seaweed *J. rubens* as inhibitors of human AChE, a key target for treating neurodegenerative diseases, such as AD. Using *in silico* methods, including molecular docking, MD, and DFT studies, we identified seven novel analogs of ursodeoxycholic acid (AL20A–AL20G). Among these, the AL20E derivative, (4R)-4-([3S,7S,8R,9S,10S,13R,14S,17R]-3,7-dihydroxy-10,13-dimethylhexadecahydro-1H-cyclopenta[a]phenanthren-17-yl)pentanamide, demonstrated superior characteristics. It exhibited a favorable toxicity profile and improved drug-likeness compared to both the parent compound (AL20) and the FDA-approved drug, donepezil. MD simulations confirmed the stability of AL20E's binding, showing three strong HBs with key amino acid residues in the protein's hydrophobic region. The BOILED-Egg model also predicted good GI absorption for AL20E. These findings strongly recommend AL20E as a promising candidate for further research and development as an anti-Alzheimer's drug.

Acknowledgments

The authors wish to appreciate the Royal Society of Chemistry, Computer Laboratory at the D. K. Olukoya Central Research & Reference Laboratories, University of Lagos, for supporting this research.

Funding

None.

Conflict of interest

The authors declare that they have no competing of interests.

Author contributions

Conceptualization: Owoyemi W. Elegbeleye, Luqman A. Adams, Oluwole B. Familoni
Data curation: Oluwafemi S. Aina, Mujeeb O. Rofiu, Nafisat O. Babamusa
Formal analysis: Oluwafemi S. Aina
Investigation: Oluwafemi S. Aina, Luqman A. Adams
Methodology: Oluwafemi S. Aina, Mujeeb O. Rofiu, Nafisat O. Babamusa
Supervision: Luqman A. Adams, Oluwole B. Familoni
Writing–original draft: Oluwafemi S. Aina, Owoyemi W. Elegbeleye
Writing–review & editing: Oluwafemi S. Aina, Kafayat A. Owoseni-Fagbenro, Olubusayo F. Semire, Olasupo A. Idris, Nafisat O. Babamusa, Luqman A. Adams

Ethics approval and consent to participate

Not applicable.

Consent for publication

Not applicable.

Availability of data

All data generated in this study are included in the manuscript.

References

1. Li B, He DJ, Li XJ, Guo XY. Modeling neurodegenerative diseases using non-human primates: Advances and challenges. *Ageing Neurodegener Dis*. 2022;2(3):12.

   doi: 10.20517/and.2022.14

2. Kumar A, Sudevan ST, Nair AS, *et al*. Current and future nano-carrier-based approaches in the treatment of Alzheimer's disease. *Brain Sci*. 2023;13(2):213.

   doi: 10.3390/brainsci13020213

3. Martorana A, Esposito Z, Koch G. Beyond the cholinergic hypothesis: Do current drugs work in Alzheimer's disease? *CNS Neurosci Ther*. 2010;16(4):235-245.

   doi: 10.1111/j.1755-5949.2010.00175.x

4. Joo SS, Won TJ, Lee DI. Potential role of ursodeoxycholic acid in suppression of nuclear factor kappa B in microglial cell line (BV-2). *Arch Pharm Res*. 2004;27(9):954-960.

   doi: 10.1007/bf02975850

5. Giacobini E. Cholinesterase inhibitors: New roles and therapeutic alternatives. *Pharmacol Res*. 2004;50(4):433-440.

   doi: 10.1016/j.phrs.2003.11.017

6. Bores GM, Huger FP, Petko W, *et al*. Pharmacological evaluation of novel Alzheimer's disease therapeutics: Acetylcholinesterase inhibitors related to galanthamine. *J Pharmacol Exp Ther*. 1996;277(2):728-738.

7. Cortez LM, Campeau J, Norman G, *et al*. Bile acids reduce prion conversion, reduce neuronal loss, and prolong male survival in models of prion disease. *J Virol.* 2015;89(15): 7660-7672.

   doi: 10.1128/JVI.01165-15

8. Silva RF, Rodrigues CM, Brites D. Bilirubin-induced apoptosis in cultured rat neural cells is aggravated by chenodeoxycholic acid but prevented by ursodeoxycholic acid. *J Hepatol.* 2001;34(3):402-408.

   doi: 10.1016/S0168-8278(01)00015-0

9. Guven KC, Percot A, Sezik E. Alkaloids in marine algae. *Mar Drugs*. 2010;8(2):269-284.

   doi: 10.3390/md8020269

10. Souza CR, Bezerra WP, Souto JT. Marine alkaloids with anti-inflammatory activity: Current knowledge and future perspectives. *Mar Drugs*. 2020;18(3):147.

    doi: 10.3390/md18030147

11. El-Din SMM, El-Ahwany AM. Bioactivity and phytochemical constituents of marine red seaweeds (*Jania rubens*, *Corallina mediterranea* and *Pterocladia capillacea*). *J Taibah Univ Sci*. 2016;10(4):471–484.

    doi: 10.1016/j.jtusci.2015.06.004

12. Trott O, Olson AJ. AutoDock Vina: Improving the speed and accuracy of docking with a new scoring function, efficient optimization, and multithreading. *J Comput Chem*. 2010;31(2):455-461.

    doi: 10.1002/jcc.21334

13. Morris GM, Goodsell DS, Halliday RS, *et al*. Automated docking using a Lamarckian genetic algorithm and an empirical binding free energy function. *J Comput Chem*. 1998;19(14):1639-1662.

    doi: 10.1002/(sici)1096-987x(19981115)19:14%3c1639:aid-jcc10%3e3.0.co;2-b

14. Lipinski B, Herzog H, Kops ER, Oberschelp W, Müller-Gärtner HW. Expectation maximization reconstruction of positron emission tomography images using anatomical magnetic resonance information. *IEEE Trans Med Imaging*. 1997;16(2):129-136.

    doi: 10.1109/42.563658

15. Frisch MJ, Trucks GW, Schlegel HB, *et al*. *Gaussian 09, Revision B.01*. Connecticut: Gaussian Inc., 2010. Available from: https://cir.nii.ac.jp/crid/1370298757422456580 [Last accessed on 2023 Mar 12].

16. Rivero P, Moreira IDP, Illas F, Scuseria GE. Reliability of range-separated hybrid functionals for describing magnetic coupling in molecular systems. *J Chem Phys*. 2008;129(18):184110.

    doi: 10.1063/1.3006419

17. Bielecki J, Lipiec E. Basis set dependence using DFT/B3LYP calculations to model the Raman spectrum of thymine. *J Bioinform Comput Biol*. 2016;14(1):1650002.

    doi: 10.1142/s0219720016500025

18. García-Valverde M, Cordero NA, De la Cal ES. Gaussview (R) as a tool for learning organic chemistry. In: *Edulearn15: 7th International Conference on Education and New Learning Technologies*; 2015. p. 4366-4370.

19. Chitra L, Kumar CR, Basha HM, Ponne S, Boopathy R. Interaction of metal chelators with different molecular forms of acetylcholinesterase and its significance in Alzheimer's disease treatment. *Proteins*. 2013;81(7):1179-1191.

    doi: 10.1002/prot.24267

20. Murugesan B, Somasundram B, Samykannu G, *et al*. Exploring lichen-derived compounds as potential anti-cervical cancer agents: An DFT and MD simulation analysis. *In-Silico Pharmacol*. 2025;13(2):114.

    doi: 10.1007/s40203-025-00380-y

21. Daina A, Zoete V. A BOILED-Egg to predict gastrointestinal absorption and brain penetration of small molecules.

ChemMedChem. 2016;11(11):1117-1121.

doi: 10.1002/cmdc.201600182

22. Daina A, Michielin O, Zoete V. iLOGP: A simple, robust, and efficient description of n-octanol/water partition coefficient for drug design using the GB/SA approach. *J Chem Inf Model*. 2014;54(12):3284-3301.

doi: 10.1021/ci500467k

23. Lipinski CA, Lombardo F, Dominy BW, Feeney PJ. Experimental and computational approaches to estimate solubility and permeability in drug discovery and development settings. *Adv Drug Deliv Rev*. 2001;46(1):3-26.

doi: 10.1016/S0169-409X(00)00129-0

24. Pardridge WM. The blood-brain barrier: Bottleneck in brain drug development. *Neurotherapeutics*. 2005;2(1):3-14.

doi: 10.1602/neurorx.2.1.3

25. Barthe L, Woodley J, Houin G. Gastrointestinal absorption of drugs: Methods and studies. *Fundam Clin Pharmacol.* 1999;13(2):154-168.

doi: 10.1111/j.1472-8206.1999.tb00334.x

26. Mollazadeh S, Sahebkar A, Hadizadeh F, Behravan J, Arabzadeh S. Structural and functional aspects of P-glycoprotein and its inhibitors. *Life Sci.* 2018;214:118-123.

doi: 10.1016/j.lfs.2018.10.048

27. Lin JH, Yamazaki M. Role of P-glycoprotein in pharmacokinetics: Clinical implications. *Clin Pharmacokinet.* 2003;42(1):59-98.

doi: 10.2165/00003088-200342010-00003

28. Dong J, Qin Z, Zhang WD, *et al*. Medicinal chemistry strategies to discover P-glycoprotein inhibitors: An update. *Drug Resist Update.* 2020;49:100681.

doi: 10.1016/j.drup.2020.100681

29. Aina OS, Rofiu MO, Oloba-Whenu OA, Olasupo IA, Adams LA, Familoni OB. Drug design and *in-silico* study of 2-alkoxylated quinoline-3-carbaldehyde compounds: Inhibitors of *Mycobacterium tuberculosis*. *Sci Afr.* 2024;23:e01985.

doi: 10.1016/j.sciaf.2023.e01985

30. Geerlings P, Chamorro E, Chattaraj PK, *et al*. Conceptual density functional theory: Status, prospects, issues. *Theor Chem Acc*. 2020;139(2):36.

doi: 10.1007/s00214-020-2546-7

31. Pal R, Chattaraj PK. Electrophilicity index revisited. *J Comput Chem*. 2023;44(3):278-297.

doi: 10.1002/jcc.26886

32. Galabov B, Ilieva S, Koleva G, Allen WD, Schaefer HF 3rd, Schleyer PVR. Structure-reactivity relationships for aromatic molecules: Electrostatic potentials at nuclei and electrophile affinity indices. *Wiley Interdiscip Rev Comput Mol Sci*. 2013;3(1):37-55.

doi: 10.1002/wcms.1112

33. Dos Santos MAB, De Oliveira LFS, De Figueiredo AF, *et al.* Molecular electrostatic potential and chemometric techniques as tools to design bioactive compounds. *In: Cheminformatics and its Applications*. London: IntechOpen; 2019.

doi: 10.5772/intechopen.89113

34. Berendsen HJC, Van der Spoel D, Van Drunen R. GROMACS: A message-passing parallel molecular dynamics implementation. *Comput Phys Commun*. 1995;91(1-3):43-56.

doi: 10.1016/0010-4655(95)00042-e

35. Shintani EY, Uchida KM. Donepezil: An anticholinesterase inhibitor for Alzheimer's disease. *Am J Health Syst Pharm*. 1997;54(24):2805-2810.

doi: 10.1093/ajhp/54.24.2805

ACCSCIENCE PUBLISHING

Innovative Medicines & Omics

ORIGINAL RESEARCH ARTICLE

Intramuscular progesterone and frozen embryo transfer outcomes: A multicenter prospective evaluation of the clinical relevance of serum progesterone monitoring

Vipin Chandra[1], Matheus Roque[2], Kshitiz Murdia[3], Nitiz Murdia[4], Shashank V. Sanagoudar[3]*, Nagadeepti Naik[5], Shipra Nigam[6], Anjali Gahlan[7], Walmik Mistari[8], Isha Suwalka[9], Nihar Ranjan Bhoi[3], Ankita Saha[10,11], Korhan Cengiz[12], and Saurav Mallik[13,14]*

[1]Department of Clinical and Lab Operations, Indira IVF Hospital Pvt Ltd., Udaipur, Rajasthan, India
[2]Department of Reproductive Medicine, Huntington, São Paulo, Brazil
[3]Department of Reproductive Medicine, Indira IVF Hospital Pvt Ltd., Udaipur, Rajasthan, India
[4]Department of Embryology, Indira IVF Hospital Pvt Ltd, Udaipur, Rajasthan, India
[5]Department of Reproductive Medicine, Indira IVF Hospital Pvt Ltd., Vashi, Maharashtra, India
[6]Department of Reproductive Medicine, Indira IVF Hospital Pvt Ltd., Shahdara, Delhi, India
[7]Department of Reproductive Medicine, Indira IVF Hospital Pvt Ltd., Allahabad, Uttar Pradesh, India
[8]Indira IVF Hospital Pvt Ltd, Udaipur, Rajasthan, India
[9]Research and Publications, Indira IVF Hospital Pvt Ltd., Udaipur, Rajasthan, India
[10]Department of Computer Science, Swami Vivekananda University, Barrackpore, West Bengal, India
[11]Department of Management and Technology, ABS Academy of Science, Technology and Management, Durgapur, West Bengal, India
[12]Department of Electrical Engineering, College of Engineering, Prince Mohammad Bin Fahd University, Al Khobar, Eastern Province, Saudi Arabia
[13]Department of Environmental Health, Harvard T. H. Chan School of Public Health, Harvard University, Boston, Massachusetts, United States of America
[14]Department of Pharmacology and Toxicology, University of Arizona, Tucson, Arizona, United States of America

***Corresponding authors:**
Shashank V. Sanagoudar (drsanagoudar@gmail.com)
Saurav Mallik (smallik@arizona.edu)

Citation: Chandra V, Roque M, Murdia K, *et al.* Intramuscular progesterone and frozen embryo transfer outcomes: A multicenter prospective evaluation of the clinical relevance of serum progesterone monitoring. *Innov Med Omics*. 2025;2(4):93-101. doi: 10.36922/IMO025310037

Received: August 1, 2025

Revised: September 2, 2025

Accepted: October 10, 2025

Published online: November 14, 2025

Abstract

The progesterone concentration in endometrial tissue after using vaginal progesterone supplementation is significantly higher than that with IM progesterone administration, whereas; serum progesterone levels are approximately four times higher with IM progesterone compared with vaginal administration. Therefore, serum progesterone cut-off points will differ according to the route of progesterone administration. This study aims to assess the association between serum progesterone levels on the day of frozen embryo transfer (FET) and pregnancy outcomes in artificial FET cycles. This multicenter prospective cohort study, conducted at different centers of Indira IVF Hospitals across India, included 353 women aged 21–40 years who underwent hormone replacement therapy-based FET cycles with intramuscular (IM) progesterone administered up to the day of embryo transfer. The mean serum progesterone level was 31.36 ± 13.78 ng/mL. Participants were categorized into quartiles based on serum progesterone levels: Q1 (<21.7 ng/mL), Q2 (21.7–28.1 ng/mL), Q3 (28.2–40.0 ng/mL), and Q4 (≥40.0 ng/mL). No significant differences in ongoing pregnancy rate (OPR), clinical pregnancy rate (CPR), first-trimester miscarriage rates, or live birth rate (LBR) were observed across the quartiles. Binary logistic regression revealed no statistically significant differences in OPR among the

quartiles. Our findings suggest that serum progesterone levels do not significantly influence clinical outcomes, including OPR, CPR, and LBR, in patients undergoing artificial FET cycles with IM progesterone support.

Keywords: Serum progesterone; Frozen embryo transfer; *In vitro* fertilization; Ongoing pregnancy; Live birth rate

1. Introduction

Assisted reproductive technology (ART) has significantly evolved over the past decades, with frozen-thawed embryo transfer (FET) emerging as a key technique to enhance pregnancy outcomes. Increasing evidence highlights a concerning association between *in vitro* fertilization (IVF)/embryo transfer (ET) and adverse obstetric outcomes, including ectopic pregnancy, twin gestation, and placenta accreta spectrum (PAS) disorders.

Ectopic pregnancy, defined as the implantation of an embryo outside the uterine cavity, occurs in approximately 1.4–5.4% of IVF cycles, significantly higher than the 1–2% rate observed in spontaneous conceptions.[1] This elevated risk is influenced by factors such as tubal damage, multiple ETs, and embryo quality. Moreover, the incidence of twin pregnancies in IVF cycles remains disproportionately high—up to 32.1% compared to 1.5% in natural conceptions—primarily due to the transfer of multiple embryos.[2] Twin gestations are associated with increased maternal and neonatal complications, including preterm birth, hypertensive disorders, and cesarean delivery. Another critical concern is the rising prevalence of PAS disorders in IVF pregnancies. PAS encompasses a range of conditions characterized by abnormal placental adherence and invasion into the uterine wall, often leading to massive postpartum hemorrhage, organ injury, and hysterectomy. These findings underscore the importance of individualized risk assessment, judicious frozen ET practices, and multidisciplinary prenatal care in ART-conceived pregnancies. As fertility preservation and ART become more integrated into oncologic and reproductive medicine, understanding and mitigating these risks is essential for optimizing maternal and neonatal outcomes.

The success of FET largely depends on optimal endometrial receptivity, which is intricately regulated by the hormonal environment, particularly progesterone.[3] Progesterone plays a critical role in facilitating implantation by preparing the endometrium to support the embryo, thereby creating a conducive environment for implantation and pregnancy progression.[4,5]

Recent advancements have emphasized the importance of monitoring serum progesterone levels to predict the success of ART cycles. Studies have shown that suboptimal progesterone levels on the day of ET can negatively impact pregnancy outcomes.[6-8] Specifically, in cycles utilizing vaginal micronized progesterone, serum progesterone levels below a certain threshold have been linked to reduced clinical pregnancy rates (CPR) and ongoing pregnancy rates (OPR).[9,10]

Intramuscular (IM) progesterone has been used as an alternative to vaginal administration because it can achieve higher serum progesterone levels. The pharmacokinetics of IM progesterone differs from those of the vaginal route, potentially influencing its efficacy and clinical outcomes. While vaginal progesterone directly affects the endometrial tissue with lower systemic levels, IM progesterone results in higher systemic levels; however, its impact on endometrial receptivity and subsequent pregnancy outcomes remains unclear.[11,12]

Despite widespread use of IM progesterone in FET cycles, there is limited data on the association between luteal serum progesterone levels and FET outcomes when IM progesterone is used for luteal phase support. Existing literature primarily focuses on vaginal routes, leaving a knowledge gap regarding the predictive value of serum progesterone levels in cycles utilizing IM administration. This gap underscores the need for studies that specifically address whether serum progesterone levels on the day of FET correlate with clinical outcomes when using IM progesterone.[13-18]

This prospective cohort study aims to address this knowledge gap by investigating the relationship between serum progesterone levels on the day of ET and pregnancy outcomes in FET cycles utilizing IM progesterone. By categorizing participants based on their serum progesterone levels, this study seeks to identify if there is a threshold or optimal range that predicts better clinical outcomes. The findings could significantly impact clinical practice, potentially simplifying protocols and improving patient management in ART.

2. Materials and methods

2.1. Study design and participants

This prospective multicenter cohort study included 353 women aged 21–40 years undergoing FET under hormone

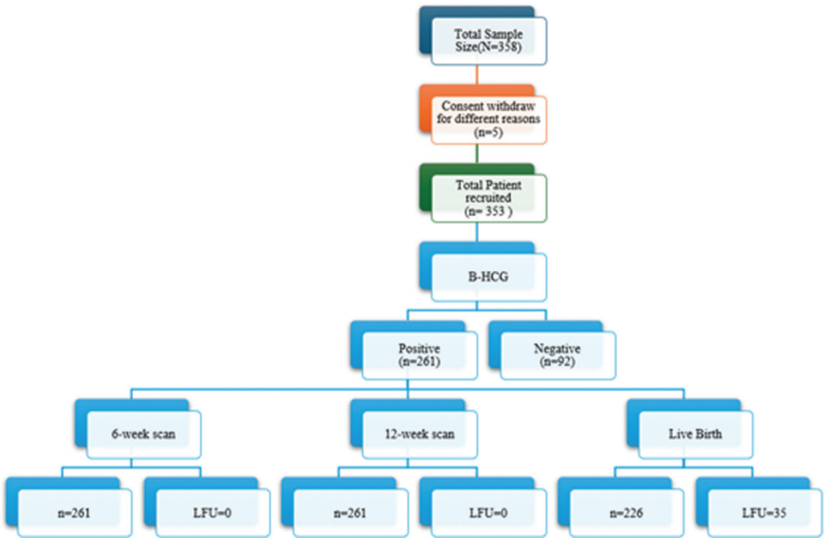

Figure 1. Patient flowchart from screening to the end of follow-up
Abbreviations: B_HCG: Beta-human chorionic gonadotropin; LFU: Luteinized unruptured follicles.

replacement therapy (HRT) cycles between February and December 2022. Participants were considered eligible if they had a triple-layer endometrium >7 mm and at least two high-quality embryos (Gardner's grade 3/4/5/AA/AB/BA/BB) available for transfer. Exclusion criteria included significant comorbidities such as uncontrolled diabetes, hypertension, heart disease, autoimmune disorders, uterine infertility factors, severe male factor infertility (total sperm count <5 million/mL), and cases requiring surgically retrieved sperm for intracytoplasmic sperm injection. All participants provided written informed consent before participating in the study. The patient flowchart from screening to the end of study follow-up is presented in Figure 1.

2.2. Ethical approval

The study was conducted in accordance with the ethical principles outlined in the Declaration of Helsinki. Ethical approval was obtained from the Institutional Ethics Committee at Indira IVF Hospital Private Limited under approval number ECR/1614/lns/RJ/2021, and the trial registration number is CTRI/2022/11/046995. All participants were informed of the study's objectives, procedures, potential risks, and benefits, and written consent was obtained before their participation. Data confidentiality was strictly maintained, with personal identifiers removed and data stored securely in compliance with data protection regulations.

2.3. Endometrial preparation and hormone administration

Endometrial preparation commenced with oral estradiol valerate (2 mg, twice or thrice daily) starting either on the 2nd day of the menstrual cycle or within 21 days of gonadotropin-releasing hormone agonist depot administration for downregulated cycles. Endometrial thickness was evaluated after 14 days of estradiol treatment. Progesterone supplementation was initiated if the endometrial thickness was ≥7 mm and the serum progesterone level was <1 ng/mL. IM progesterone was administered at a dose of 100 mg daily for 6 days before ET. Luteal phase support included oral estradiol valerate (6 mg daily), vaginal progesterone gel (Crinone 8%®) twice daily, and oral dydrogesterone (10 mg, twice daily) starting from the day of ET. A serum pregnancy test was performed 14 days after ET to confirm pregnancy.[19-21]

2.4. Embryo transfer procedure

Embryo transfer was conducted on the 6th day of progesterone administration. On the day of transfer, embryos were assessed for viability, expansion, and degeneration. Viable day-5 or day-6 blastocysts with good expansion were selected for transfer. The decision to perform a single or double ET was based on patient characteristics and clinical discretion. ETs were performed under ultrasound guidance using a soft catheter to ensure precision and reduce variability.[23]

2.5. Serum hormonal measurements

Serum progesterone levels were measured on the day of ET, approximately 20 h after the previous progesterone dose. Blood samples were processed within 8 h, and serum progesterone was quantified using a quantitative electrochemiluminescence immunoassay. The assay's reportable range for progesterone was 0.030–60.00 ng/mL.

Participants were stratified into quartiles based on their serum progesterone levels for subsequent analysis. Serum beta-human chorionic gonadotropin levels were determined by quantitative electrochemiluminescence immunoassay on day 14 post-ET; values ≥100 IU were considered positive for biochemical pregnancy.

2.6. Outcome measures

The primary outcome measure was the OPR. Secondary outcomes included CPR, miscarriage rate, and live birth rate (LBR). Clinical pregnancy was defined as the presence of one or more gestational sacs on ultrasound at 7 weeks of gestation or definitive clinical signs of pregnancy with fetal heart activity. Ongoing pregnancy was defined as a viable pregnancy beyond 12 weeks of gestation. First-trimester miscarriage was classified as a pregnancy loss occurring within the first 12 weeks.[23]

2.7. Statistical analysis

Statistical analysis was performed using the Statistical Package for the Social Sciences version 28.0. Continuous variables were presented as mean ± standard deviation (SD) or median (range), and categorical variables as frequencies and percentages. Serum progesterone levels were categorized into quartiles based on the 25th, 50th, and 75th percentiles. Comparisons between groups were performed using the unpaired *t*-test or Mann–Whitney U-test for continuous variables and the Chi-square test for categorical variables. Binary logistic regression analysis was conducted to evaluate the impact of serum progesterone levels on clinical pregnancy and ongoing pregnancy outcomes. $p<0.05$ was considered statistically significant.

3. Results

The mean age of the study population was 32.09 ± 4.19 years, and the mean body mass index was 24.70 ± 3.07 kg/m^2. The mean endometrial thickness was 8.87 ± 1.06 mm. The mean serum progesterone level on the day of ET was 31.36 ± 13.78 ng/mL (Table 1).

Participants were categorized into four groups based on serum progesterone levels as follows: Q1 (<21.7 ng/mL), Q2 (21.7–28.1 ng/mL), Q3 (28.2–40.0 ng/mL), and Q4 (≥40.0 ng/mL) (Table 2). The CPR, OPR, miscarriage rates, and LBR showed no significant differences across quartiles (Table 3 and Figure 2). To adjust for confounders, a binary logistic regression analysis was performed to compare IVF outcomes across different progesterone levels (ng/mL) on the day of ET, with Q1 as the reference (Table 4).

The OPRs by serum progesterone quartiles were as follows: Q1: 57.5%; Q2: 62.6%; Q3: 59.6%; and Q4: 62.8%. There were no statistically significant differences among these groups. Binary logistic regression analysis revealed no significant associations between progesterone quartiles and clinical outcomes.

Table 1. Baseline patient characteristics

Characteristic (*n*=353)	Mean	SD	Median	Range	Minimum	Maximum
Age (years)	32.09	4.19	32.00	19.00	21.00	40.00
BMI (kg/m^2)	24.70	3.07	24.80	18.50	18.50	30.00
Endometrial thickness (mm)	8.87	1.06	8.80	5.00	7.00	12.00
P4 level on the day of ET (ng/mL)	31.36	13.78	28.10	81.39	4.21	85.60

Abbreviations: BMI: Body mass index; ET: Embryo transfer; P4: Serum progesterone.

Table 2. Quartile-wise distribution of serum progesterone among patients receiving embryo transfers

Variables	Categories	Number of patients	Percentage
Serum progesterone level by quartile (ng/dL)	Q1 (<21.7)	87	24.6
	Q2 (21.7–28.1)	91	25.8
	Q3 (28.2–40.0)	89	25.2
	Q4 (>40)	86	24.4
Number of embryos transferred	Single embryo transfer	61	17.3
	Double embryo transfer	292	82.7

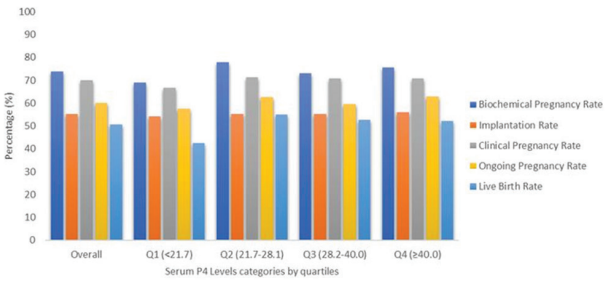

Figure 2. The *in vitro* fertilization outcomes among different quartiles

4. Discussion

Current evidence suggests that a minimum clinically significant serum luteal progesterone level is necessary to achieve optimal IVF clinical outcomes, and that lower progesterone levels on the day of ET may adversely affect these outcomes.[24] However, most of this data come from studies using vaginal progesterone for luteal phase support. There is limited evidence regarding patients undergoing artificial endometrial preparation

Table 3. Pregnancy and perinatal outcomes across serum progesterone quartiles

Characteristics	Total, *n* (%)	Q1	Q2	Q3	Q4	*p*-value
Biochemical pregnancy rate	261/353 (73.9%)	60/87 (69.0%)	71/91 (78.0%)	65/89 (73.0%)	65/86 (75.6%)	0.565
Biochemical loss rate	14/261 (5.4%)	2/60 (3.3%)	6/71 (8.5%)	2/65 (3.1%)	4/65 (6.1%)	0.382
Implantation rate	356/645 (55.2%)	85/157 (54.1%)	93/168 (55.3%)	89/161 (55.3%)	89/159 (55.9%)	0.402
Clinical pregnancy rate	247/353 (70.0%)	58/87 (66.7%)	65/91 (71.4%)	63/89 (70.8%)	61/86 (70.9%)	0.895
1st-trimester miscarriage rate	33/247 (13.4%)	8/58 (13.7%)	8/65 (12.3%)	10/63 (15.9%)	7/61 (11.5%)	0.908
Ongoing pregnancy rate	214/353 (60.6%)	50/87 (57.5%)	57/91 (62.6%)	53/89 (59.6%)	54/86 (62.8%)	0.869
2nd-trimester and perinatal loss rate	19/247 (7.7%)	6/58 (10.3%)	4/65 (6.2%)	3/63 (4.8%)	6/61 (9.8%)	0.613
Live birth rate	179/353 (50.7%)	37/87 (42.5%)	50/91 (54.9%)	47/89 (52.8%)	45/86 (52.3%)	0.551
Loss of follow-up	16/353 (4.53%)	7/87 (8.04%)	3/91 (3.29%)	3/89 (3.37%)	3/86 (3.48%)	NA

Table 4. Binary logistic regression for *in vitro* fertilization outcomes according to different progesterone levels on the day of embryo transfer

In vitro fertilization outcomes	Serum progesterone levels (ng/mL)	Odds ratios	95% confidence interval	*p*-values
Clinical pregnancy	21.7–28.1	1.25	(0.66, 2.36)	0.49
	28.2–40.0	1.21	(0.64, 2.29)	0.55
	>40	1.22	(0.64, 2.32)	0.54
Ongoing pregnancy	21.7–28.1	1.24	(0.68, 2.26)	0.48
	28.2–40.0	0.99	(0.54, 1.81)	0.98
	>40	1.18	(0.65, 2.18)	0.58
Live birth	21.7–28.1	1.52	(0.83, 2.81)	0.17
	28.2–40.0	1.40	(0.76, 2.58)	0.28
	>40	1.38	(0.74, 2.54)	0.31

using IM progesterone. In this prospective study, we found that when using IM progesterone until the day of ET in HRT-FET cycles, neither low nor high serum progesterone levels adversely impacted clinical outcomes. To the best of our knowledge, this is the first study to propose a protocol of just 6 days of IM progesterone until the day of ET, followed by vaginal gel progesterone and oral dydrogesterone.[25]

The evolving landscape of reproductive medicine and gynecologic oncology has brought forth significant advancements in fertility preservation, particularly for women diagnosed with early-stage endometrial and cervical cancers. A multidisciplinary approach integrating molecular diagnostics, minimally invasive techniques, and ARTs is reshaping clinical decision-making and patient outcomes. The debate between open and closed vitrification systems centers on biosafety and clinical outcomes. Closed systems, such as the Rapid-i device, offer superior protection against contamination from liquid nitrogen, addressing concerns about disease transmission.[26] While survival rates of oocytes and embryos are comparable across systems, the closed system is increasingly favored for its aseptic handling and reduced risk of cross-contamination.

Recent systematic reviews have expanded the scope of fertility-sparing treatment to include Grade 2 Stage IA endometrioid endometrial cancer, traditionally excluded from conservative protocols.[27] Hormonal therapies—particularly progestins such as medroxyprogesterone acetate and levonorgestrel intrauterine devices—combined with hysteroscopic resection, have shown promising oncologic and reproductive outcomes.[28] However, recurrence remains a concern, necessitating rigorous follow-up and molecular profiling.

The integration of molecular classification (e.g., *POLE*-mutated, *MMR*-deficient, and p53-abnormal) into fertility-sparing strategies marks a shift toward precision medicine. Biomarkers such as *PTEN*, *POLE*, and *SPAG9* have demonstrated predictive value for treatment response, enabling personalized therapeutic plans.[29] This approach not only improves oncologic safety but also enhances reproductive success rates.

Assisted reproductive technology, including IVF and intracytoplasmic sperm injection, has revolutionized fertility preservation but raises concerns about long-term child health. A critical appraisal of neuro-psycho-motor outcomes found no significant correlation between ART and cognitive or developmental disorders. However, data on cerebral palsy remain inconclusive due to confounding factors such as prematurity and multiple gestations.[30] In addition, sentinel lymph node biopsy is emerging as a less invasive alternative to pelvic lymphadenectomy in early-stage cervical cancer. Sentinel lymph node biopsy offers comparable diagnostic accuracy with reduced morbidity, although its long-term oncologic safety is still under investigation.[31] Its adoption could facilitate fertility-sparing surgeries by minimizing surgical trauma.

Children born from FET exhibit higher birth weights and increased rates of macrosomia and large-for-gestational-age status, with reduced incidence of low birth weight and small-for-gestational-age outcomes. While these findings suggest favorable perinatal outcomes, long-term developmental data remain limited, warranting further research. Circulating microRNAs are gaining traction as non-invasive biomarkers for early detection of endometrial cancer. Panels of microRNAs can potentially guide both diagnosis and fertility-sparing eligibility, offering a dual benefit of early intervention and personalized care.[32] Their integration into clinical practice could revolutionize screening protocols.

Transcriptomic tools like the microenvironment cell population-counter enable quantification of immune and stromal cell populations within the tumor microenvironment, providing insights into prognosis and therapeutic response.[33] Understanding the tumor microenvironment composition is critical for tailoring immunotherapies and predicting fertility-sparing treatment outcomes. Cell-free fetal DNA testing has become a cornerstone of non-invasive prenatal diagnosis, particularly for chromosomal aneuploidies and monogenic diseases.[34] Techniques such as next-generation sequencing and haplotype dosage analysis offer high accuracy, though ethical and legal considerations remain pivotal in clinical implementation.[1]

It is estimated that over 8 million newborns worldwide have been born as a result of IVF. Despite significant refinements and advancements in reproductive treatments over the past 20 years, including improved ovarian stimulation protocols and laboratory techniques, the LBR per initiated cycle remains relatively low, ranging between 25% and 30%.[35] These low success rates have a considerable psychological impact on couples struggling with infertility, often being the primary reason for discontinuing IVF treatments. After an initial failure, up to two-thirds of infertile couples do not seek further treatment, with many citing the intense psychological stress of IVF treatments as the main deterrent.

The optimal route of progesterone administration in FET cycles remains uncertain. A randomized controlled trial, involving 1125 women undergoing FET, randomly assigned participants to endometrial preparation using daily vaginal micronized progesterone, daily IM progesterone, or a combination of vaginal and IM routes. The study was prematurely terminated after an interim analysis showed lower LBRs in the vaginal route group. However, biases such as the relatively low dose of vaginal progesterone (200 mg twice daily) and the differing intervals between the start of progesterone supplementation and ET timing between groups might have influenced the results.[9]

Concerns have recently been raised about the impact of low serum progesterone levels on clinical outcomes in FET cycles, even in natural cycles[11] or those using IM progesterone. However, the detrimental threshold levels can vary depending on the method of luteal phase support administration. Recent studies, both prospective[14,16] and retrospective,[4,8,11,12,22] have shown that low progesterone levels on the day of or the day before ET, in both HRT and natural cycles, are negatively correlated with clinical outcomes. However, these studies mainly focused on cycles with vaginal progesterone. Conversely, a recent retrospective study found no association between progesterone levels and clinical outcomes,[24] although patients with progesterone levels below 8 ng/mL received additional doses, potentially influencing the results.

In a multicenter prospective cohort study, the association between serum progesterone levels on the day of FET and the probability of live birth was evaluated among different progesterone administration regimens. The study found that the relationship between serum progesterone levels and IVF clinical outcomes varied depending on the FET cycle regimen and the route of progesterone administration. For women undergoing HRT cycles with vaginal progesterone, the mean probability of live birth increased approximately linearly as serum progesterone levels rose. In contrast, when combining vaginal and subcutaneous progesterone, there was a slight variation in the likelihood of live birth according to different serum progesterone levels.[21] The study evaluated 402 FET cycles, with only 111 patients (27.6%) receiving luteal phase support with injectable progesterone. This distribution aligns with clinical practice, where vaginal progesterone is used alone as a single agent in approximately 77% of IVF cycles worldwide.[25]

This study adds to this body of knowledge by providing data supporting the notion that neither low nor high serum progesterone levels affects clinical outcomes when using IM progesterone in FET cycles.

This study has several strengths, including its prospective cohort design, standardized FET protocol, and consistent hormonal analysis timing. In addition, the same immunoassay was used for progesterone measurements, reducing variability. However, some limitations must be acknowledged. Despite being the largest prospective study evaluating the impact of IM progesterone on FET outcomes to date, the findings may be subject to bias. Future research with larger sample sizes and randomized clinical trials is warranted to confirm these results and explore the complex interactions between progesterone levels, administration routes, and patient characteristics.

5. Conclusion

The results of this study have important implications for clinical practice. They indicate that serum progesterone testing before ET in FET cycles using IM progesterone may not be necessary, potentially simplifying treatment protocols and reducing patient burden. Given that the success of ART largely hinges on individualized patient care, our findings could help refine FET protocols by avoiding unnecessary interventions and focusing on factors that truly influence reproductive outcomes. In conclusion, our study provides evidence that serum progesterone levels on the day of FET do not correlate with the likelihood of achieving pregnancy in artificial FET cycles using IM progesterone. These findings can inform clinical decision-making and streamline FET protocols, ultimately improving patient experiences and ART outcomes. Further research is warranted to continue optimizing treatment approaches for individuals undergoing assisted reproduction.

Acknowledgments

None.

Funding

None.

Conflict of interest

The authors declare that they have no competing interests.

Author contributions

Conceptualization: Vipin Chandra, Matheus Roque, Kshitiz Murdia, Nitiz Murdia
Data curation: Nagadeepti Naik, Shipra Nigam, Anjali Ghanlan
Formal analysis: Walmik Mistari, Ankita Saha, Korhan Cengiz, Saurav Mallik
Investigation: Kshitiz Murdia, Nitiz Murdia
Methodology: Nagadeepti Naik, Shipra Nigam, Anjali Gahlan
Supervision: Shashank V. Sanagoudar, Nihar Ranjan Bhoi
Validation: Shashank V. Sanagoudar, Ankita Saha, Korhan Cengiz, Saurav Mallik
Writing-original draft: Isha Suwalka
Writing-review & editing: Shashank V. Sanagoudar, Ankita Saha, Korhan Cengiz, Saurav Mallik

Ethics approval and consent to participate

This study was approved by the Institutional Ethics Committee at Indira IVF Hospital Private Limited (IIHPL-UDR/P/005_2021). This study was conducted with the patient's informed consent and in accordance with all ethical guidelines (ECR\1614\Inst\RJ\2021).

Consent for publication

Patients provided written consent for their data to be published.

Availability of data

Data from the study will be made available on request to the corresponding authors.

References

1. Benaglia L, Bermejo-Alvarez P, Brambillasca F, *et al*. Frozen embryo transfer and obstetric outcomes: A systematic review and meta-analysis. *Int J Gynaecol Obstet*. 2023;162(2):345-356.

   doi: 10.1002/ijgo.15220

2. Petitprez F, Vano YA, Becht E, *et al*. Transcriptomic analysis of the tumor microenvironment to guide prognosis and immunotherapies. *Cancer Immunol Immunother*. 2018;67(6):981-988.

   doi: 10.1007/s00262-017-2058-z

3. Adamson GD, de Mouzon J, Chambers GM, *et al*. International Committee for Monitoring Assisted Reproductive Technology: World report on assisted reproductive technology, 2011. *Fertil Steril*. 2018;110:1067-1080.

4. Alsbjerg B, Thomsen L, Elbaek HO, *et al*. Progesterone levels on pregnancy test day after hormone replacement therapy-cryopreserved embryo transfer cycles and related reproductive outcomes. *Reprod Biomed Online*. 2018;37:641-647.

   doi: 10.1016/j.rbmo.2018.08.022

5. Alsbjerg B, Thomsen L, Elbaek HO, *et al*. Can combining vaginal and rectal progesterone achieve the optimum progesterone range required for implantation in the HRT-FET model? *Reprod Biomed Online*. 2020;40:805-811.

   doi: 10.1016/j.rbmo.2020.02.007

6. Boynukalin FK, Gultomruk M, Turgut E, *et al*. Measuring the serum progesterone level on the day of transfer can be an additional tool to maximize ongoing pregnancies in single euploid frozen blastocyst transfers. *Reprod Biol Endocrinol*. 2019;17:102.

   doi: 10.1186/s12958-019-0549-9

7. Bulletti C, De Ziegler D, Flamigni C, *et al*. Targeted drug delivery in gynaecology: The first uterine pass effect. *Hum Reprod*. 1997;12:1073-1079.

   doi: 10.1093/humrep/12.5.1079

8. Cédrin-Durnerin I, Isnard T, Mahdjoub S, *et al*. Serum progesterone concentration and live birth rate in frozen-thawed embryo transfers with hormonally prepared endometrium. *Reprod Biomed Online*. 2019;38:472-480.

   doi: 10.1016/j.rbmo.2018.11.026

9. Devine K, Richter KS, Widra EA, McKeeby JL. Vitrified

blastocyst transfer cycles with the use of only vaginal progesterone replacement with Endometrin have inferior ongoing pregnancy rates: Results from the planned interim analysis of a three-arm randomized controlled noninferiority trial. *Fertil Steril*. 2018;109:266-275.

doi: 10.1016/j.fertnstert.2017.11.004

10. Domar AD, Rooney K, Hacker MR, Sakkas D, Dodge LE. Burden of care is the primary reason why insured women terminate *in vitro* fertilization treatment. *Fertil Steril*. 2018;109:1121-1126.

doi: 10.1016/j.fertnstert.2018.02.130

11. Gaggiotti-Marre S, Álvarez M, González-Foruria I, *et al*. Low progesterone levels on the day before natural cycle frozen embryo transfer are negatively associated with live birth rates. *Hum Reprod*. 2020;35:1623-1629.

doi: 10.1093/humrep/deaa092

12. Gaggiotti-Marre S, Martinez F, Coll L, *et al*. Low serum progesterone the day prior to frozen embryo transfer of euploid embryos is associated with significant reduction in live birth rates. *Gynecol Endocrinol*. 2019;35:439-442.

doi: 10.1080/09513590.2018.1534952

13. Gleicher N, Kushnir VA, Barad DH. Worldwide decline of IVF birth rates and its probable causes. *Hum Reprod Open*. 2019;2019(3):hoz017.

doi: 10.1093/hropen/hoz017

14. González-Foruria I, Gaggiotti-Marre S, Álvarez M, *et al*. Factors associated with serum progesterone concentrations the day before cryopreserved embryo transfer in artificial cycles. *Reprod Biomed Online*. 2020;40:797-804.

doi: 10.1016/j.rbmo.2020.03.001

15. Kofinas JD, Blakemore J, McCulloh DH, Grifo J. Serum progesterone levels greater than 20 ng/mL on day of embryo transfer are associated with lower live birth and higher pregnancy loss rates. *J Assist Reprod Genet*. 2015;32:1395-1399.

doi: 10.1007/s10815-015-0546-7

16. Labarta E, Mariani G, Holtmann N, Celada P, Remohí J, Bosch E. Low serum progesterone on the day of embryo transfer is associated with a diminished ongoing pregnancy rate in oocyte donation cycles after artificial endometrial preparation: A prospective study. *Hum Reprod*. 2017;32:2437-2442.

doi: 10.1093/humrep/dex316

17. Labarta E. Relationship between serum progesterone (P) levels and pregnancy outcome: Lessons from artificial cycles when using vaginal natural micronized progesterone. *J Assist Reprod Genet*. 2020;37:2047-2048.

doi: 10.1007/s10815-020-01862-y

18. Labarta E, Mariani G, Paolelli S, *et al*. Impact of low serum progesterone levels on the day of embryo transfer on pregnancy outcome: A prospective cohort study in artificial cycles with vaginal progesterone. *Hum Reprod*. 2021;36(3):683-692.

doi: 10.1093/humrep/deaa322

19. Melo P, Chung Y, Pickering O, *et al*. Serum luteal phase progesterone in women undergoing frozen embryo transfer in assisted conception: A systematic review and meta-analysis. *Fertil Steril*. 2021;116(6):1534-1556.

doi: 10.1016/j.fertnstert.2021.07.002

20. Melo P, Wood S, Petsas G, *et al*. The effect of frozen embryo transfer regimen on the association between serum progesterone and live birth: A multicentre prospective cohort study (ProFET). *Hum Reprod Open*. 2022;2022(4):hoac054.

doi: 10.1093/hropen/hoac054

21. Roque M, Simon C. Time to pregnancy: As important for patients as underestimated by doctors. *Fertil Steril*. 2020;113(3):522-523.

doi: 10.1016/j.fertnstert.2019.12.025

22. Vaisbuch E, de Ziegler D, Leong M, Weissman A, Shoham Z. Luteal-phase support in assisted reproduction treatment: Real-life practices reported worldwide by an updated website-based survey. *Reprod Biomed Online*. 2014;28(3):330-335.

doi: 10.1016/j.rbmo.2013.11.013

23. Volovsky M, Pakes C, Rozen G, Polyakov A. Do serum progesterone levels on day of embryo transfer influence pregnancy outcomes in artificial frozen-thaw cycles? *J Assist Reprod Genet*. 2020;37(5):1129-1135.

doi: 10.1007/s10815-020-01713-w

24. Yovich JL, Conceicao JL, Stanger JD, Hinchliffe PM, Keane KN. Mid-luteal serum progesterone concentrations govern implantation rates for cryopreserved embryo transfers conducted under hormone replacement. *Reprod Biomed Online*. 2015;31(2):180-191.

doi: 10.1016/j.rbmo.2015.05.005

25. Zegers-Hochschild F, Adamson GD, Dyer S, *et al*. The international glossary on infertility and fertility care, 2017. *Fertil Steril*. 2017;108(3):393-406.

doi: 10.1016/j.fertnstert.2017.06.005

26. Pujol A, Zamora MJ, Obradors A, Garcia D, Rodriguez A, Vassena R. Comparison of two different oocyte vitrification methods: A prospective, paired study on the same genetic background and stimulation protocol. *Hum Reprod*. 2019;34(6):989-997.

doi: 10.1093/humrep/dez045

27. Giampaolino P, Cafasso V, Boccia D, *et al*. Fertility-sparing approach in patients with endometrioid endometrial cancer grade 2 stage IA (FIGO): A qualitative systematic review. *Biomed Res Int*. 2022;2022:4070368.

doi: 10.1155/2022/4070368

28. Rodolakis A, Scambia G, Planchamp F, *et al*. ESGO/ESHRE/ESGE Guidelines for the fertility-sparing treatment of patients with endometrial carcinoma. *Hum Reprod Open*. 2023;2023(1):hoac057.

doi: 10.1093/hropen/hoac057

29. Ran X, Hu T, Li Z. Molecular classification in patients with endometrial cancer after fertility-preserving treatment: Application of ProMisE classifier and combination of prognostic evidence. *Front Oncol*. 2022;12:810631.

doi: 10.3389/fonc.2022.810631

30. Djuwantono T, Aviani JK, Permadi W, Halim D, Achmad TH, Dhamayanti M. Intelligence, motoric and psychological outcomes in children from different ART treatments: A systematic review and meta-analysis. *J Neurodev Disord*. 2023;15:26.

doi: 10.1186/s11689-023-09490-0

31. Margioula-Siarkou C, Almperis A, Gullo G, *et al*. Sentinel lymph node staging in early-stage cervical cancer: A comprehensive review. *J Clin Med*. 2024;13(1):27.

doi: 10.3390/jcm13010027

32. Gullo G, Scaglione M, Cucinella G, *et al*. Neonatal outcomes and long-term follow-up of children born from frozen embryo, a narrative review of latest research findings. *Medicina (Kaunas)*. 2022;58(9):1218.

doi: 10.3390/medicina58091218

33. Piergentili R, Gullo G, Basile G, *et al*. Circulating miRNAs as a tool for early diagnosis of endometrial cancer-implications for the fertility-sparing process: Clinical, biological, and legal aspects. *Int J Mol Sci*. 2023;24(14):11356.

doi: 10.3390/ijms241411356

34. Gullo G, Scaglione M, Buzzaccarini G, *et al*. Cell-free fetal DNA and non-invasive prenatal diagnosis of chromosomopathies and pediatric monogenic diseases: A critical appraisal and medicolegal remarks. *J Pers Med*. 2023;13(1):1.

doi: 10.3390/jpm13010001

35. Zhou Y, Wang J, Zhang H, Li X. Placenta accreta spectrum in assisted reproductive technology pregnancies: A retrospective cohort study. *J Minim Invasive Gynecol*. 2023;30(5):789-796.

doi: 10.1016/j.jmig.2023.03.021

Our Journals

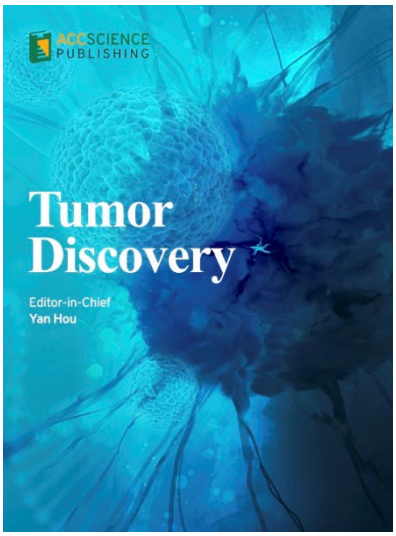

Tumor Discovery is a peer-reviewed and open-access journal that aims to present new cancer research with strong emphasis on fundamental and translational studies. *Tumor Discovery* covers topics, including but not limited to the following:

- Etiology and pathogenesis of cancer
- Mechanisms and molecular pathways underlying cancer initiation and progression
- Tumor metastasis
- Tumor evolution and heterogeneity
- Tumor microenvironment and tumor-host interactions
- Cancer genetics and genomics
- Cancer characterization using omics approaches
- Discovery and validation of cancer biomarker
- Discovery of new therapeutic targets
- New approaches of diagnostic and treatment modalities
- Statistical methods in cancer research

Artificial Intelligence in Health is an online open-access, multidisciplinary journal dedicated to publishing high-quality peer-reviewed research in all areas of Artificial Intelligence in health and medicine science. By publishing high-quality research papers, reviews, and case studies, the journal seeks to contribute to the scientific community's understanding of the potential, challenges, and impact of AI and its applications on health delivery, patient outcomes, and population health.

Artificial Intelligence in Health covers topics, including but not limited to the following: AI-based medical diagnosis and prognosis, AI clinical decision support systems, AI-driven drug discovery and development, AI-enabled healthcare operations and management, and the research and application in telemedicine, AI-assisted electronic health records and clinical informatics, AI-based research and application of wearable devices for diagnosis and treatment and social implications of AI in health.

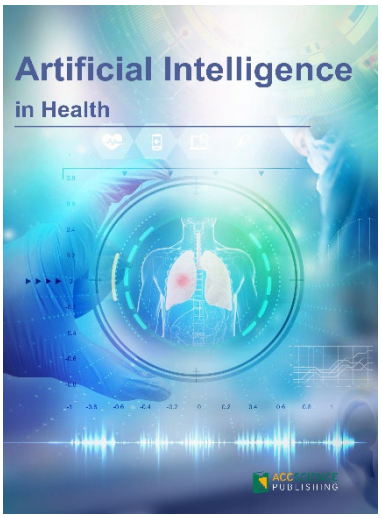

Start a new journal

Write to us via email if you are interested to start a new journal with AccScience Publishing. Please attach your CV, professional profile page and a brief pitch proposal in your email. We shall inform you of our decision whether we are interested to collaborate in starting a new journal.

Contact: info@accscience.com

https://accscience.com/journal/IMO

Access Science Without Barriers

Contact

www.accscience.com
9 Raffles Place, Republic Plaza 1 #06-00 Singapore 048619
Email: editorial@accscience.com
Phone: +65 8182 1586